Applications of calcium isotopes in marine carbonates in the Recent and Phanerozoic

Clara L. Blättler

University College

Trinity Term 2012

Thesis submitted for the degree of DPhil

Department of Earth Sciences

Mathematical, Physical, and Life Sciences Division

University of Oxford

Abstract

Applications of calcium isotopes in marine carbonates in the Recent and Phanerozoic

DPhil thesis, Department of Earth Sciences, University of Oxford

Clara L. Blättler, University College

Trinity Term 2012

The applications of calcium-isotope measurements in marine carbonates are explored in several different contexts within this thesis. As a record of global ion fluxes, seawater calcium-isotope ratios can be used as tracers for large weathering imbalances, which develop as a feedback system in response to intervals of climate change. This approach provides valuable constraints on the complex climatic and oceanographic phenomena known as the Oceanic Anoxic Events. Over much longer timescales, the calcium-isotope ratio of seawater is influenced by steady-state processes that reflect the evolution of seawater chemistry. To understand these influences, the modern calcium-isotope budget is assessed quantitatively using a compilation of marine carbonate samples, revealing several distinctive components of the carbonate burial sink that can affect the steady-state balance of the calcium cycle. Changes in the major ion composition of seawater and in the organisms that contribute to sedimentary carbonate burial are shown to contribute significantly to the geological record of seawater calcium-isotope ratios. The importance of skeletal carbonate in the calcium cycle leads to another application of calcium isotopes towards understanding biomineralization. This large and complex topic is approached with calcium-isotope data from two unique growth experiments that constrain some of the mechanisms by which biogenic aragonite acquires its geochemical signatures. This range of topics presents a diverse, but by no means exclusive, sample of the topics that are accessible for investigation through calcium-isotope analysis. The potential of this isotopic tool is demonstrated by the breadth of environments and timescales represented in this work.

Long Abstract

As an abundant element with crucial roles in sedimentary cycling, seawater chemistry, and carbonate skeletons, calcium contributes to many fundamental Earth system processes. In marine carbonates, calcium represents an important part of the sedimentary record of ancient environmental conditions. The stable isotopes of calcium provide a valuable tool for studying its geochemical cycle over both modern and geological timescales, but they have only proven their usefulness relatively recently due to technological advances in mass spectrometry. Natural calcium-isotope variation remains relatively small, but where resolvable, its application contributes new dimensions to many long-standing questions. A firm understanding of the calcium cycle and the nature of the archival phase is necessary for interpreting calcium-isotope data, and the content of this thesis works towards that goal.

Chapter 2 describes the methods that were developed and utilized throughout the calcium-isotope studies presented here. Sample preparation procedures are customized for the use of multi-collector inductively coupled plasma mass spectrometry, which analyzes samples as purified solutions of calcium and allows replicate measurements to be performed with little additional effort. Using the full potential of multiple replicate analyses, statistical precision for sample measurements are achieved that are sufficient to resolve calcium-isotope variation for the following applications.

Chapter 3 applies knowledge of the calcium cycle to investigate periods of abrupt climate change in the Mesozoic. Calcium-isotope ratios ($\delta^{44/42}$Ca) were measured in carbonate-rich sedimentary sections deposited during Oceanic Anoxic Events 1a (Early Aptian) and 2 (Cenomanian–Turonian). In sections from Resolution Guyot, Mid-Pacific Mountains; Coppitella, Italy; and the English Chalk at Eastbourne and South Ferriby, UK, a negative excursion in $\delta^{44/42}$Ca of ~0.20‰ and ~0.10‰ is observed for the two events. These $\delta^{44/42}$Ca excursions occur at the same stratigraphic level as the carbon-isotope excursions that define the events, but do not correlate with evidence for carbonate dissolution or lithological changes. Diagenetic and temperature effects on the calcium-isotope ratios can be discounted, leaving changes in global seawater composition as the

most probable explanation for $\delta^{44/42}$Ca changes in four different carbonate sections. An oceanic box model with coupled strontium- and calcium-isotope systems indicates that a global weathering increase is likely to be the dominant driver of transient excursions in calcium-isotope ratios. The model suggests that contributions from hydrothermal activity and carbonate dissolution are too small and short-lived to affect the oceanic calcium reservoir measurably. A modelled increase in weathering flux, on the order of three times the modern flux, combined with increased hydrothermal activity due to formation of the Ontong-Java Plateau (OAE1a) and Caribbean Plateau (OAE2), can produce trends in both calcium and strontium isotopes that match the signals recorded in the carbonate sections. This study presents the first major-element record of a weathering response to Oceanic Anoxic Events.

Chapter 4 considers the long-term, steady-state behaviour of the calcium cycle over the Phanerozoic. A new geochemical budget for the modern marine carbonate sink helps to explain the major features of the Phanerozoic calcium-isotope record. A large compilation of calcium-isotope ratios for modern carbonates, incorporating more than 50 new measurements, represents the quantitatively important components of the system. With this dataset, distinct calcium-isotope ratios are identified for different types of marine carbonate, the balance of which has changed over time with shifts between calcite and aragonite seas and with the development of pelagic calcification during the Mesozoic. It is suggested that large-scale changes in the calcium-isotope ratio of seawater, as exemplified by that in the Carboniferous, were no longer possible post-Jurassic because of the generation of a deep-sea calcite sink expressed by deposition of foraminiferal–coccolith ooze across the world ocean. This work demonstrates the close connection between isotopic cycling, carbonate sedimentation, seawater chemistry, and evolutionary trends.

Chapter 5 focuses on an application of calcium isotopes over a much smaller spatial and temporal scale. The process of biocalcification not only has a strong influence on the long-term calcium cycle, but also produces a record of skeletal carbonate which potentially contains valuable information about past marine conditions. Lacking direct measurements of ancient environments, interpretations of geochemical proxy records mea-

sured in skeletal archives are important for testing current understanding of the climate system. Two case studies are presented that provide specific constraints on the sources of calcium-isotope fractionation in marine aragonite. *Halimeda* algae and *Porites* corals represent two contrasting modes of aragonite precipitation, which can be compared with inorganic carbonate precipitation experiments to isolate particular biological influences on skeletal composition. The results from these example organisms support a new model for coral aragonite geochemistry, which incorporates multiple sources of cations and mechanisms for isotopic fractionation in order to explain the behaviour of proxy records.

These studies reflect only a small subset of the possible applications for calcium isotopes. As a major element in the Earth's crust, calcium is involved in many processes over the broadest range of environments and timescales. Not all of these are resolvable with calcium-isotope analysis, but the range of questions that can be resolved using measurements of marine carbonates alone show the great potential of this tool. Further extensions of these studies are proposed that will expand and refine the conclusions derived from this work, and will continue to explore the valuable applications of calcium isotopes.

Contents

1 Introduction **1**

1.1 Background and history of calcium-isotope analysis 2

1.2 Introduction to Oceanic Anoxic Events 7

1.3 Introduction to major cation seawater chemistry 10

1.4 Introduction to calcium isotopes in biomineralization 14

2 Methods **19**

2.1 Sample preparation 19

2.2 Ion-exchange chromatography 21

2.3 Mass spectrometry 23

2.4 External and stratigraphic reproducibility 27

3 Ca isotopes during OAE1a and OAE2 **29**

3.1 Introduction 29

3.2 Background 31

3.3 Samples 33

3.3.1 Oceanic Anoxic Event 1a: ODP Leg 143, Site 866, Resolution Guyot, Mid-Pacific Mountains 33

3.3.2 Oceanic Anoxic Event 1a: Coppitella, Gargano, Italy 34

3.3.3 Oceanic Anoxic Event 2: Eastbourne, UK 37

3.3.4 Oceanic Anoxic Event 2: South Ferriby, UK 39

3.3.5 Comments on the studied sections 40

3.4 Methods 40

3.5 Results . . . 41
3.6 Discussion . . . 44
3.6.1 Observed Ca-isotope variation attributed to changing seawater composition . . . 44
3.6.2 Modelling seawater calcium-isotope excursions . . . 47
3.6.3 Quantitatively exploring the weathering response to OAEs . . . 54
3.7 Conclusions . . . 56
3.A Appendix . . . 57

4 Ca isotopes of Phanerozoic seawater 75
4.1 Introduction . . . 75
4.2 Samples and methods . . . 77
4.3 Results . . . 78
4.4 Discussion . . . 79
4.4.1 Patterns of biocalcification . . . 79
4.4.2 The modern Ca-isotope budget . . . 82
4.4.3 The evolution of marine carbonate and Ca-isotope ratios . . . 83
4.5 Conclusions . . . 86
4.A Appendix . . . 87

5 Ca isotopes in biomineralization 127
5.1 Introduction . . . 127
5.2 Background to Ca-isotope fractionation . . . 129
5.2.1 Inorganic Ca-isotope fractionation . . . 129
5.2.2 Organic Ca-isotope fractionation . . . 130
5.3 Samples and methods . . . 132
5.3.1 *Halimeda* experiment . . . 132
5.3.2 Coral FOCE experiment . . . 133
5.3.3 Ca-isotope analysis . . . 135
5.4 Results . . . 136

5.5 Discussion 140
5.5.1 Ca isotopes in *Halimeda* 142
5.5.2 Ca isotopes in corals 144
5.6 Conclusions 148

6 Conclusions **151**

List of Figures

1.1 Phanerozoic seawater Ca-isotope ratios 6

1.2 OAE2 black shales 8

1.3 Phanerozoic Mg/Ca ratios of seawater 12

1.4 Pelagic vs cratonic carbonate accumulation 13

1.5 Sample *Halimeda* specimen 15

1.6 Sample *Porites* specimen 16

2.1 Belemnite sample preparation 20

2.2 Elution curves for column chromatography 22

2.3 Sr doping experiments 24

2.4 Ca triple-isotope plot 25

2.5 Ca-isotope reproducibility tests 27

3.1 Paleogeographic reconstructions 32

3.2 Resolution Guyot data 35

3.3 Coppitella data 36

3.4 Eastbourne data 38

3.5 South Ferriby data 39

3.6 Box model parameters 49

3.7 Model simulations 51

3.8 Resolution Guyot sample photographs 58

3.9 Eastbourne section photographs 61

3.10 South Ferriby section photographs 63

3.11 Raia del Pedale data 64

3.12 Yorkshire data 67
3.13 Junction Bed data 69
3.14 Forada data 72

4.1 Phanerozoic seawater Ca-isotope ratios 76
4.2 Ca-isotope ratios of modern carbonates 80
4.3 Modelling seawater Ca-isotope ratios in aragonite and calcite seas 85
4.4 Seawater Ca-isotope ratios, 0–40Ma 88
4.5 Raw Phanerozoic Ca-isotope data 89
4.6 Modern carbonate samples 125

5.1 XRD calibration curve 134
5.2 *Halimeda* sample photographs 137
5.3 *Halimeda* Ca-isotope data vs mineralogy 139
5.4 FOCE experiment data 140
5.5 Schematic of coral physiology 145

List of Tables

1.1 Elemental abundances 1

1.2 Isotopes of calcium 3

1.3 Mesozoic OAEs 8

2.1 Ion-exchange column chemistry 22

2.2 Ca-isotope standard values 26

3.1 Resolution Guyot Ca-isotope data 59

3.2 Coppitella Ca-isotope data 60

3.3 Eastbourne Ca-isotope data 61

3.4 South Ferriby Ca-isotope and C-isotope data 62

3.5 Raia del Pedale Ca-isotope data 65

3.6 Yorkshire Ca-isotope data 68

3.7 Junction Bed Ca-isotope and C-isotope data 70

3.8 Forada Ca-isotope data 73

4.1 Model for carbonate budget 90

4.2 Reconstructed seawater Ca-isotope data 91

4.3 Original Ca-isotope data for modern marine carbonates 110

4.4 Ca-isotope compilation of modern marine carbonates 113

5.1 *Halimeda* XRD and Ca-isotope data 138

5.2 FOCE Ca-isotope data 141

Acknowledgements

Gideon M. Henderson and Hugh C. Jenkyns supervised this work and contributed great improvements to every part of it. Their critical input and positive encouragement throughout my time at Oxford is very much appreciated. Guidance and training from Linda M. Reynard was invaluable for performing the calcium-isotope analyses in this project, and I thank her for the patience and generosity she showed me. The various members of the Climotope research group at Oxford have supported this work through helpful discussions, technical assistance, and friendly interactions. Departmental staff provided technical and institutional support, without which the work presented here would not have been possible. Finally, a large number of friends, family, and teachers have left their mark on this project and its author, and they also deserve much thanks.

I am very grateful for the funding of my studentship by the Rhodes Trust (Registered Charity No. 232492), as well as additional financial support from the Burdett-Coutts Fund of the Department of Earth Sciences, University of Oxford. This thesis was examined by Rosalind E. M. Rickaby and Anton Eisenhauer, and I thank them for their attention and suggestions for this work.

Chapter 1

Introduction

Calcium is a major element in the Earth's crust and a component of many globally important reactions and processes. It is the fifth most abundant element in the Earth's crust, in seawater solution, and in the human body (see Table 1.1), where it plays a central role in many geological, marine, and biological systems. The geochemical behaviour of calcium allows the study of major processes over a range of spatial and temporal scales that may otherwise be difficult to observe or constrain. The work presented here ranges from the global scale of the world ocean to the microscopic scale of mineral growth, and from multi-million year evolutionary trends, to abrupt historical climate change, to individual algal lifespans, with the purpose of exploring the calcium-isotope system and the insight it provides into geological questions.

As increased sensitivity and stability of mass spectrometers have allowed more precise and widespread measurement of isotope ratios, geochemists have been able to reach across the periodic table to investigate many isotopic systems beyond the traditional light

Table 1.1: The natural abundances of elements (Haynes, 2011).

Earth's crust (mass %)		Seawater (dissolved mg/L)		Human body (mass %)	
O	46.1	Cl	19400	O	61.0
Si	28.2	Na	10800	C	23.0
Al	8.23	Mg	1290	H	10.0
Fe	5.63	S	905	N	2.6
Ca	4.15	Ca	412	Ca	1.4
Na	2.36	K	399	P	1.1
Mg	2.33	Br	67	S	0.20
K	2.09	C	28	K	0.20

elements such as carbon and oxygen. The first natural variation in calcium-isotope ratios was identified by Russell et al. (1978), which has been followed by a greater range of studies within the last 15 years. The geological importance and abundance of calcium have led to applications as diverse as paleothermometry (e.g. Nägler et al., 2000) and nutrient cycling (e.g. Farkaš et al., 2011). An increased interest in climate processes also motivates understanding the calcium cycle, which is intimately linked to that of carbon on both short and long timescales through oceanic carbonate compensation and rock weathering reactions, in quantitative terms (Skulan et al., 1997; Zhu and Macdougall, 1998; Schmitt et al., 2003a; Caro et al., 2010; Tipper et al., 2010). This thesis presents several different applications of isotopic analysis of calcium in marine carbonate minerals. The following introductory chapter presents a summary of the systematics of calcium stable-isotope analysis as well as a broader overview of the various topics discussed in later chapters.

1.1 Background and history of calcium-isotope analysis

Calcium (Ca) has six naturally occurring stable, or extremely long-lived, isotopes (see Table 1.2). The radioactive (beta) decay of ^{40}K also produces a small radiogenic contribution to ^{40}Ca, the most abundant of the calcium isotopes. Depending on the analytical method and research goals, a variety of conventions have been used for reporting stable-isotope ratios of Ca. In some cases, interest in the abundance of radiogenic ^{40}Ca has justified normalization by the second most abundant isotope, ^{44}Ca, whereas studies concerned with stable-isotope fractionation use the inverse ratio, normalizing by ^{40}Ca. The technical approach for measuring stable-isotope fractionation also affects the convention for reporting isotope ratios. Analysis by TIMS (thermal ionization mass spectrometry) and a double-spiking technique, usually with the addition of ^{43}Ca–^{48}Ca (e.g. Heuser et al., 2005) or ^{42}Ca–^{48}Ca (e.g. De La Rocha and DePaolo, 2000) spikes, usually leads to reporting the ratio of the two most abundant isotopes, following the definition of Eisenhauer et al. (2004), as

$$\delta^{44/40}\mathrm{Ca} = \left[\frac{\left(^{44}\mathrm{Ca}/^{40}\mathrm{Ca}\right)_{sample}}{\left(^{44}\mathrm{Ca}/^{40}\mathrm{Ca}\right)_{standard}} - 1 \right] \cdot 1000.$$

Table 1.2: The natural abundances of the stable isotopes of Ca (de Laeter et al., 2003).

Mass number (A)	Atomic mass (u)	Abundance (mol %)
40	39.9625912	96.941
42	41.9586183	0.647
43	42.9587668	0.135
44	43.9554811	2.086
46	45.9536927	0.004
48	47.952533	0.187

An alternative analytical method uses MC-ICP-MS (multi-collector inductively coupled plasma mass spectrometry). The use of argon gas in the plasma introduces a large interference on ^{40}Ca (because ^{40}Ar = 99.6% of total Ar), so MC-ICP-MS measurements generally report ratios, as defined by Eisenhauer et al. (2004), as

$$\delta^{44/42}\mathrm{Ca} = \left[\frac{\left(^{44}\mathrm{Ca}/^{42}\mathrm{Ca}\right)_{sample}}{\left(^{44}\mathrm{Ca}/^{42}\mathrm{Ca}\right)_{standard}} - 1 \right] \cdot 1000.$$

This reporting convention avoids the potential inconsistency from radiogenic ^{40}Ca on the stable-isotope fractionation. The two different notations, $\delta^{44/42}$Ca and $\delta^{44/40}$Ca, can be converted to one another roughly by multiplying by two, or by applying a more precise formula based on the expected process generating isotopic fractionation, such as a linear fractionation law:

$$\begin{aligned} \delta^{44/42}\mathrm{Ca} &= \delta^{44/40}\mathrm{Ca} \cdot \frac{m_{42} - m_{44}}{m_{40} - m_{44}} \\ &= \delta^{44/40}\mathrm{Ca} \cdot 0.500105 \end{aligned}$$

or an equilibrium fractionation law:

$$\begin{aligned} \delta^{44/42}\mathrm{Ca} &= \delta^{44/40}\mathrm{Ca} \cdot \frac{1/m_{42} - 1/m_{44}}{1/m_{40} - 1/m_{44}} \\ &= \delta^{44/40}\mathrm{Ca} \cdot 0.476314 \end{aligned}$$

where m_x are precise atomic masses (Young et al., 2002; Hippler et al., 2003). Although it is possible to double-spike samples for analysis by MC-ICP-MS (e.g. Farkaš et al.,

2007b), straightforward sample–standard–sample bracketing can also be used to correct for instrumental mass bias, due to sample introduction as a pure Ca solution. The details of this method, as performed at Oxford, are described further in Chapter 2.

Other methods for analyzing Ca-isotope ratios include a 'cool-plasma' technique, which allows measurement of ^{40}Ca by MC-ICP-MS using a plasma with greatly reduced radio-frequency power and subsequently reduced argon ionization (Fietzke et al., 2004). Ion-microprobe analysis with SIMS (secondary ion mass spectrometry) has also been used to measure natural Ca-isotope fractionation (e.g. Rollion-Bard et al., 2007; Kasemann et al., 2008). Reviews of analytical procedures for Ca-isotope measurements can be found in DePaolo (2004) and Boulyga (2010).

The first measurements of natural variation in stable Ca-isotope ratios by Russell et al. (1978) introduced some of the possible applications and limits of this tool. Although modern instruments can reliably obtain 10-fold higher precision, these original analyses were able to demonstrate the mass-dependent behaviour of Ca and resolve the range of natural fractionation, as well as indicate possible mechanisms for Ca-isotope fractionation. Investigation of Ca-isotope variation has continued in wide-ranging samples and applications. In biologically oriented studies, Ca isotopes have been used to track trophic levels in food chains, variations in diet and bone mineralization, and the production or consumption of dairy (Skulan et al., 1997; Skulan and DePaolo, 1999; Chu et al., 2006; Hirata et al., 2008; Reynard et al., 2010). Weathering processes in different environments and on different substrates can be investigated through studies of rocks, soils, and river waters (Schmitt et al., 2003a; Tipper et al., 2006; Ewing et al., 2008; Cenki-Tok et al., 2009; Hindshaw et al., 2011). On an ecosystem scale, measurements of natural materials can elucidate elemental cycling and nutrient balances (Wiegand et al., 2005; Perakis et al., 2006; Page et al., 2008; Holmden and Bélanger, 2010; Cobert et al., 2011; Farkaš et al., 2011). Recent studies of bone mineral balance in humans using Ca-isotope analysis of urine (Skulan et al., 2007; Heuser and Eisenhauer, 2010) demonstrate the beginning of Ca-isotope applications in the biomedical sciences as well.

Ca-isotope analyses of marine carbonates have generated several additional applica-

tions in paleoclimate and paleoceanography. Initial interest in Ca-isotopes as a paleotemperature proxy led to intensive research on planktic foraminifera (Nägler et al., 2000; Gussone et al., 2003; Sime et al., 2005; Hippler et al., 2006; Sime et al., 2007; Griffith et al., 2008b; Gussone et al., 2009; Hippler et al., 2009; Kısakürek et al., 2011), which has since expanded to many other forms of biogenic calcite and aragonite (Gussone et al., 2005; Immenhauser et al., 2005; Böhm et al., 2006; Gussone et al., 2006; Steuber and Buhl, 2006; Gussone et al., 2007; Langer et al., 2007; Heinemann et al., 2008; von Allmen et al., 2010; Gussone et al., 2010; Gussone and Filipsson, 2010) as well as other mineral forms of carbonate (Gussone et al., 2005; Holmden, 2009; Böhm et al., 2011; Gussone et al., 2011). A cohesive explanation of how Ca isotopes are fractionated in different inorganic and biogenic systems remains to be described (see Chapter 5 for further discussion). Assuming that certain relationships between seawater and marine carbonate are constant through time, reconstructions of past seawater Ca-isotope values from fossil carbonate archives have been produced (De La Rocha and DePaolo, 2000; Fantle and DePaolo, 2005; Heuser et al., 2005; Fantle and DePaolo, 2007; Farkaš et al., 2007b,a; Sime et al., 2007; Griffith et al., 2008b), including abrupt events in geological history (Kasemann et al., 2005; Payne et al., 2010). Non-carbonate archives such as phosphate (Schmitt et al., 2003b; Soudry et al., 2006) and barite (Griffith et al., 2008a, 2011) have also been used for reconstructing the ancient Ca cycle. Understanding and interpreting these records has motivated further study of the present-day Ca-isotope system, with numerous studies trying to establish constraints on the important reservoirs and fluxes of Ca (Zhu and Macdougall, 1998; Chang et al., 2004; Tipper et al., 2006; Amini et al., 2008; Tipper et al., 2008, 2010; Caro et al., 2010). These contributions have allowed all the major oceanic inputs and outputs to be characterized to a reasonable degree.

Observations in both natural and laboratory environments as well as theoretical considerations have contributed progress towards explaining the source of Ca-isotope fractionation in certain carbonates. Significant uncertainty surrounds the theoretical, *ab initio* calculations for equilibrium Ca-isotope fractionation by Rustad et al. (2010), which suggest enrichment of the heavier Ca isotopes in the solid mineral phase, such as have never

been measured. The ionic nature of Ca^{2+} as bound in carbonates suggests that kinetic isotope fractionation, which would favor the lighter Ca isotopes in mineral precipitates, is more appropriate than models of equilibrium isotope fractionation based on covalent bonding (Gussone et al., 2003, 2005). Observations from beaker experiments (Gussone et al., 2003; Lemarchand et al., 2004; Marriott et al., 2004; Tang et al., 2008), drip experiments (Reynard et al., 2011), and natural systems (Fantle and DePaolo, 2007; Jacobson and Holmden, 2008) can be reconciled by a crystal surface growth model described by DePaolo (2011). This model, which extends beyond the limiting case of hydrated Ca^{2+}-ion dynamics suggested by Gussone et al. (2003), uses the relative balance of growth rate with diffusion into a surface boundary layer and the backwards dissolution reaction to explain a range of Ca-isotope fractionation observed in carbonates, from zero to approximately $-2‰$.

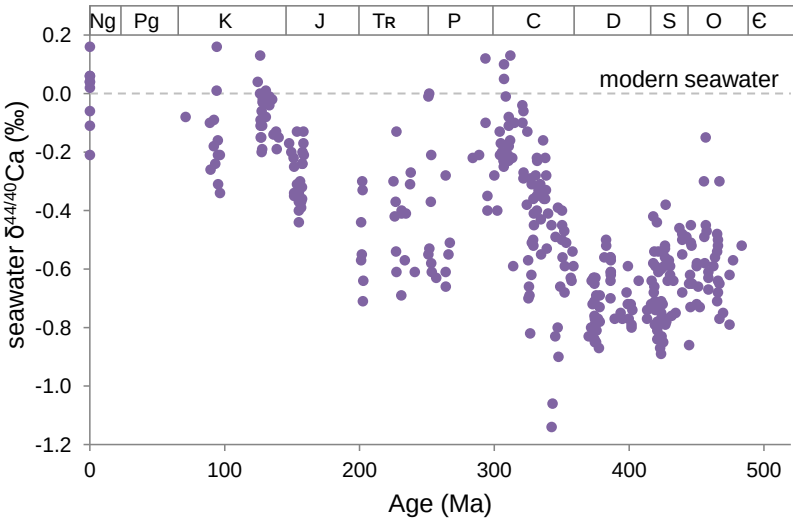

Figure 1.1: Reconstructed seawater Ca-isotope ratios, relative to modern seawater, using data from fossil belemnites and brachiopods (Farkaš et al., 2007a,b). For further discussion on this and other seawater $\delta^{44/40}$Ca datasets, see Chapter 4.

Ca-isotope measurements of carbonate minerals are applied to several different geochemical problems in the following chapters. A brief introduction to each of the disparate topics is presented in the following sections. Section 1.2 introduces some of the research concerning the Oceanic Anoxic Events (OAEs) of the Mesozoic, which are some of the most dramatic and well-studied climate perturbations of the Phanerozoic. Section 1.3

presents the investigation of changing seawater chemistry over the Phanerozoic, and the effect this may have had on the composition of the carbonate sink. Finally, Section 1.4 introduces the broad field of biomineralization studies, and how certain geochemical tests may increase the understanding of environmental proxies preserved in geological archives.

1.2 Introduction to Oceanic Anoxic Events

In Chapter 3, the Ca-isotope records of OAEs 1a and 2 are constructed from carbonate sediments in multiple stratigraphic sections, and a simple model evaluates the different possibilities for generating Ca-isotope variation in the context of OAEs. Many global processes were disrupted by these events, and changes in carbonate dissolution, weathering reactions, and hydrothermal activity are all expected to have had an effect on the marine Ca cycle. Tracing the effects on Ca in the geological record is one of the most direct ways to observe perturbations in these major processes. The behaviour of the Ca-isotope cycle complements information from several other geochemical proxies as well as other analytical approaches to studying the OAEs. An overview of the different types of questions and research surrounding the OAEs is presented below.

The OAEs were initially identified by the globally widespread, synchronous deposition of organic-rich black shales in sedimentary sections (Schlanger and Jenkyns, 1976), although they have come to be recognized and characterized by other geochemical signals as well. Several comprehensive reviews of the OAEs cover their effects on the carbon cycle (Jenkyns, 2003), their effect on oceanic oxygenation (Arthur and Sageman, 1994; Meyer and Kump, 2008), the biotic response (Erba, 2004), and wider geochemical implications (Jenkyns, 2010). The three major OAEs of the Mesozoic are the Toarcian OAE (~183 Ma), The Early Aptian OAE1a (~120 Ma), and the Cenomanian–Turonian OAE2 (~93.6 Ma), although several other shorter and possibly regional events have also been identified (see Table 1.3). Characteristic carbon-isotope profiles of the major events have been recognized in widespread and diverse settings, confirming their global extent. Stratigraphic studies continue to recognize OAE1a worldwide in the Tethys (Menegatti et al.,

Table 1.3: Names and ages of major (widespread across global ocean basins) and minor (extent of anoxia regionally limited) oceanic anoxic events (Jenkyns, 2010). Ages based on timescale of Ogg et al. (2008).

Major OAEs			
OAE2	Bonarelli Event	93.5 Ma	Cenomanian–Turonian
OAE1a	Selli Event	120 Ma	Early Aptian
T-OAE	Posidonienschiefer Event	183 Ma	Early Toarcian
Minor (regional) OAEs			
OAE3		86 Ma	Coniacian–Santonian
OAE1d	Breistoffer Event	100 Ma	Late Albian
OAE1b	Paquier Event	112 Ma	Early Albian
Faraoni Event		131 Ma	Latest Hauterivian
Weissert Event		135 Ma	Late Valanginian

1998; Weissert et al., 1998; Herrle et al., 2004; Vahrenkamp, 2010), Atlantic (Millán et al., 2009; Najarro et al., 2011), Pacific (Sliter, 1989; Jenkyns, 1995; Ando et al., 2008; Robinson et al., 2008), and terrestrial environments (Gröcke et al., 1999). OAE2 has likewise been described in the Tethys (Gale et al., 1993; Paul et al., 1999; Tsikos et al., 2004; Parente et al., 2008), Atlantic (Tsikos et al., 2004), Pacific (Schlanger et al., 1987), and North American Western Interior Seaway (Kennedy et al., 2005). The biological effects of the OAEs have also been well studied, with patterns of extinction and radiation identified in many plankton assemblages during these events (e.g. Premoli Silva et al., 1999; Leckie et al., 2002; Erba, 2004).

Figure 1.2: Sedimentological expressions of OAE2 (Cenomanian–Turonian). The Bonarelli Level of the Italian Apennines is exposed at Furlo Gorge (left) as an organic-rich black shale ~1.5 m thick. The Black Band represents the same stratigraphic level within the English Chalk, shown in the condensed stratigraphic section at South Ferriby (right). Photos by H.C. Jenkyns.

The causes of the OAEs are an actively debated topic, with an original focus on ex-

plaining the abundance of organic matter through increased productivity or preservation (Arthur and Sageman, 1994). Both factors likely contributed to the abundance of black shales during these events, although oceanographic models suggest that an active overturning circulation is required for generating widespread anoxia and therefore an increase only in preservation due to a stagnant ocean is not a realistic possibility (Sarmiento et al., 1988). Biogeochemical feedbacks also make the distinction between productivity and preservation less meaningful, since, for example, anoxic conditions increase organic matter preservation but selectively regenerate phosphorus, which can support further surface productivity (Mort et al., 2007; Tsandev and Slomp, 2009). Volcanic activity at large igneous provinces (LIPs) could be the external cause for initiating anoxia and organic matter burial, an idea that is supported by a variety of geochemical and geochronological data connecting the Ontong-Java Plateau and OAE1a, and the Caribbean-Colombian Plateau and OAE2 (Kerr, 1998; Larson and Erba, 1999; Snow et al., 2005; Kuroda et al., 2007; Turgeon and Creaser, 2008). LIP volcanism would have generated a greenhouse climate with high atmospheric carbon dioxide and possibly high methane (Jahren et al., 2001; Beerling et al., 2002; Misumi et al., 2009), which may have been the necessary trigger for increased weathering, nutrient availability, and primary productivity.

A variety of other geochemical data has contributed to understanding different aspects of these dramatic global events. Characterization of organic matter by Rock-Eval pyrolysis or biomarker analysis, for example, provides some indication about its source and the oceanographic conditions required for its preservation (e.g. Erbacher et al., 1996; Dumitrescu and Brassell, 2005; Méhay et al., 2009), and the identification of particular biomarkers derived from anaerobic photoautotrophs constrains the extent of anoxia to within the photic zone (Kuypers et al., 2002). Estimates of high sea-surface temperatures (SSTs) have been generated for OAE1a (Dumitrescu et al., 2006) and OAE2 (Forster et al., 2007; Sinninghe Damsté et al., 2010) from organic geochemical proxies, which are consistent with hypotheses about the influence of LIP volcanism on global climate. Volcanic influences have also been suggested by trace element analysis (e.g. Turgeon and Brumsack, 2006; Pearce et al., 2009; Hetzel et al., 2009) and radiogenic isotope systems

(e.g. Frijia and Parente, 2008; Tejada et al., 2009), providing multiple lines of evidence in both local and global oceanographic signals. Mo and U isotopes have been used in a different manner, to quantify global ocean anoxia during OAEs (Pearce et al., 2008; Montoya-Pino et al., 2010), although significant uncertainty surrounds these quantitative estimates.

The OAEs, as currently recognized and named, are all confined to the Mesozoic, although other events throughout the Phanerozoic show evidence of similar characteristics and might also be considered 'OAEs'. Many localities experienced anoxic conditions and carbonate crises at the Permo–Triassic boundary, in addition to the devastating mass extinction for which the interval is best known (Wignall and Hallam, 1992; Isozaki, 1997), and a Ca-isotope study of the interval reveals geochemical evidence of ocean acidification and accelerated weathering (Payne et al., 2010). The Paleocene–Eocene Thermal Maximum (PETM) has been represented as the closest analogue for modern rates of climate change and also shows characteristics of a proto-OAE (Cohen et al., 2007). Although anoxia was not as widespread during the PETM as during the true Mesozoic OAEs, the carbon cycle appears to have been perturbed in similar ways, with evidence for the occurrence of ocean acidification and methane hydrate release (Dickens et al., 1997; Ravizza et al., 2001; Zachos et al., 2005; Panchuk et al., 2008). These and other events during Earth history could be used as natural extensions of the work presented in Chapter 3, to confirm the response of the Ca cycle to other climate perturbations throughout geological time.

1.3 Introduction to major cation seawater chemistry

Chapter 4 investigates the Phanerozoic history of Ca-isotope ratios in seawater, using insights from a modern Ca-isotope budget. In particular, the suggestion that oceanic Ca isotopes may be linked to long-term trends in seawater chemistry and carbonate sedimentation generates testable hypotheses, given sufficient constraints on the Ca cycle and marine Ca-isotope fractionation, that are compared to arrive at an explanation for the published record of seawater Ca-isotope composition. Support for changes in the major

ion chemistry of seawater, especially the Mg/Ca ratio, comes from several different lines of evidence. To provide context for the history of Ca isotopes in seawater, the evidence for this and other long-term trends in Phanerozoic seawater and carbonate composition is discussed below.

The chemical composition of ancient oceans, and its geological controls, is a long-standing question in geochemistry. Several different approaches have been used to constrain the ionic balance of seawater, starting with simple mass balance considerations and progressing to thermodynamic equilibria, chemical kinetics, and evaporite chemistry (e.g. Mackenzie and Garrels, 1966; Broecker, 1971; Holland, 1972; Maynard, 1976). In addition to justifying the relative constancy of seawater composition (e.g. why the oceans are not infinitely salty, or completely depleted in certain ions), explanations were also required for observations of changing conditions through time. The mineralogy of nonskeletal carbonates and the composition of evaporites appear to have varied cyclically over the Phanerozoic, leading to the concept of 'aragonite seas' and 'calcite seas' (Sandberg, 1983; Hardie, 1996). According to this model, the Mg/Ca ratio of seawater and concentration of SO_4^{2-} control the preferred carbonate mineralogy of ooids, as well as the presence of KCl or $MgSO_4$ in evaporite sequences. The alternation between different seawater states is supported by other datasets (see Figure 1.3), such as the composition of fluid inclusions in evaporitic halite (Horita et al., 1996; Kovalevich et al., 1998; Lowenstein et al., 2001; Brennan and Lowenstein, 2002; Horita et al., 2002; Lowenstein et al., 2003), the mineralogy of major reef builders and sediment producers (Stanley and Hardie, 1998), and the Mg/Ca ratio of echinoderm skeletons (Dickson, 2002, 2004).

While the definitive cause of these cyclic trends remains unknown, models point to several processes that might exert control over oceanic Mg/Ca. Rough temporal correlation between changing sea level, icehouse/greenhouse intervals, and atmospheric carbon dioxide suggests a tectonic control (Sandberg, 1983). Coupled changes in Mg^{2+}, Ca^{2+}, and SO_4^{2-} could be produced by changes in the relative importance of hydrothermal exchange reactions, and a variable rate of dolomitization could also affect the Mg/Ca ratio of seawater (Wilkinson and Algeo, 1989; Holland et al., 1996; Horita et al., 2002; Holland,

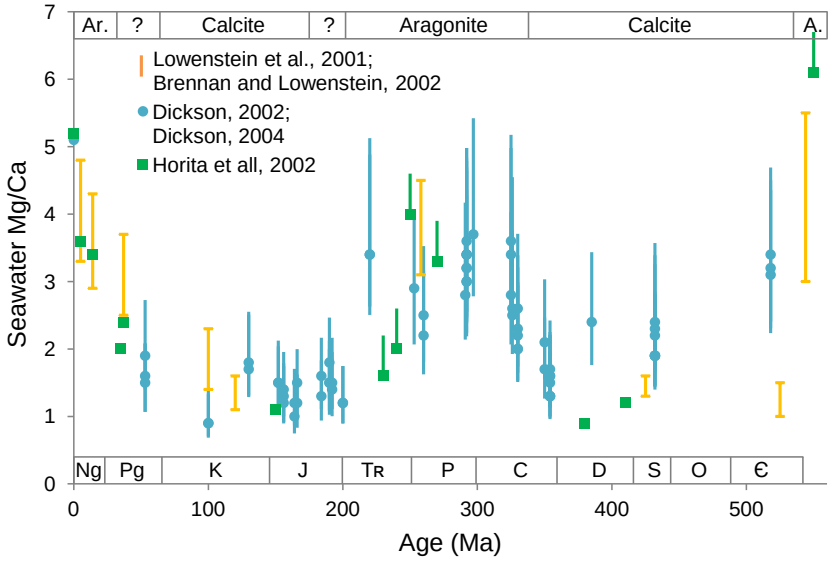

Figure 1.3: Seawater molar Mg/Ca ratio reconstructed from halite fluid inclusions (Lowenstein et al., 2001; Brennan and Lowenstein, 2002; Horita et al., 2002) and fossil echinoderm ossicles (Dickson, 2002, 2004), with aragonite and calcite sea intervals as defined by Sandberg (1983).

2005). Modifying the magnitude of these fluxes through time can result in Mg/Ca changes over the Phanerozoic from values as low as 1.0 to the modern high of 5.2. This variation is likely to have affected skeletal mineralogy and Mg content for a range of biomineralizers, potentially providing evolutionary pressure for certain calcifying taxa (Stanley, 2006) and possibly influencing the first advent of biocalcification (Brennan et al., 2004).

Patterns of carbonate sedimentation have also changed over the Phanerozoic, as evolutionary processes have modified both the organisms and the environments in which biocalcification occurs. In the modern oceans, carbonate burial is split approximately evenly between shallow-water and deep-water environments (Milliman, 1993; Milliman and Droxler, 1996), but this proportion has not always been constant. Over glacial/interglacial timescales, for example, the ratio of shelf to deep-sea carbonate may have changed with sea level, which the 'coral reef hypothesis' suggests may have been partially responsible for Pleistocene atmospheric carbon dioxide variations (Opdyke and Walker, 1992). A general shift from cratonic to pelagic carbonate deposition (see Figure 1.4) appears to have taken place throughout the Phanerozoic (Opdyke and Wilkinson, 1988; Wilkinson and Algeo, 1989; Wilkinson and Walker, 1989), especially as the planktic foraminifera and coccolithophores that dominate modern pelagic calcification diversified in the Meso-

zoic. The composition of carbonate reefs and sediment producers has also varied over time, according to the fossil record (Wood, 1995; Kiessling et al., 2003). These changes in the composition of the carbonate sink are important factors in the history of the Ca cycle and its isotopic evolution.

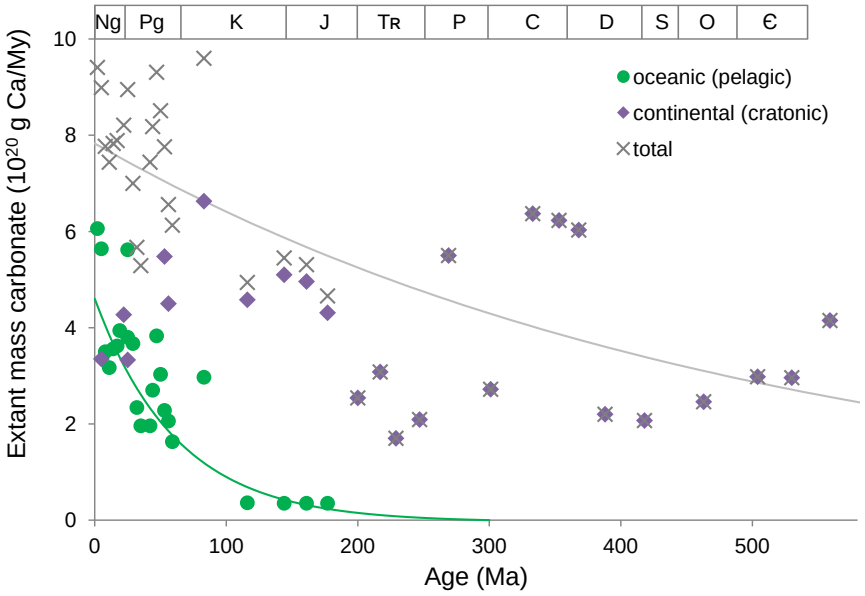

Figure 1.4: Estimates of global carbonate accumulation in pelagic and cratonic environments, converted to apparent rate of extant (remaining) mass of Ca (assuming 100% $CaCO_3$) per million years. Data and exponential decay lines are derived from Wilkinson and Walker (1989) and include processing and conversions of the original data (Ronov, 1982; Davies and Worsley, 1981; Hay, 1985).

The long history of marine carbonate sedimentation has been affected by many variables, both external forcings and internal evolution, and as the only major sink of oceanic Ca, the composition of this sink can have major consequences for the Ca cycle. Chapter 4 proposes an interpretation for the connection between the carbonate burial sink, the chemical composition of seawater, and the oceanic Ca-isotope ratio. This analysis explores the limits of the Ca-isotope system at steady state, in contrast to the non-steady state behaviour expected over the ~1 My timescales of the OAEs.

1.4 Introduction to calcium isotopes in biomineralization

Chapter 5 presents two unusual growth experiments using corals and green algae that provide insight into the mechanisms of Ca-isotope fractionation during biocalcification. Biomineralization is a complex and poorly understood subject, because although general strategies can be recognized that apply to many species, a hugh diversity of minerals, functions, and mechanisms are utilized by different organisms (Lowenstam and Weiner, 1989). Biominerals can be found across the entire tree of life and in many different forms, but some of the most important ones on a global scale are the calcium carbonate minerals. Calcium carbonate is a central part of the sedimentary rock cycle, and all the work presented in this thesis revolves around measurements in these minerals. As an abundant component of the geological record, carbonate holds the potential to archive past environmental conditions over a range of timescales. Environmental variables that are essential to understanding ancient climates, but impossible to measure directly in the past, can often be estimated using proxies, or measurable attributes that can be related to the desirable variable. Measuring proxies in biominerals often exposes 'vital effects', or deviations from the expected inorganic relationship. A mechanistic understanding of biomineralization processes could resolve some of these vital effects and make proxy measurements in skeletal archives much more useful for interpreting environmental conditions.

Ca isotopes offer particular promise for investigating mechanisms of biomineralization, due to the role of Ca as the major cation in carbonate. Whereas some familiar proxy measurements, such as $\delta^{13}C$ and $\delta^{18}O$, are hosted within the carbonate ion, metal cations are often incorporated in trace amounts relative to Ca and hold much potential as proxies if cation incorporation can be understood. Mg/Ca and Sr/Ca have been widely studied and used as recorders of paleotemperature (e.g. Elderfield and Ganssen, 2000; Cohen et al., 2001), although other ratios such as Ba/Ca, Cd/Ca, U/Ca, and Zn/Ca have also attracted attention (e.g. Boyle, 1981; Lea, 1993; Lynch-Stieglitz et al., 1996; Marchitto et al., 2000; Cardinal et al., 2001). The mechanisms by which these metals are transported to the calcifying regions and affected by skeletal growth kinetics are likely related to those for Ca. Some work has attempted to model Ca-isotope fractionation during biocalcification

(Böhm et al., 2006; Griffith et al., 2008b; Gussone et al., 2009; Kısakürek et al., 2011), but much more remains to be done in this field towards the goal of understanding vital effects.

Figure 1.5: A sample specimen of the calcareous green algae *Halimeda tuna* collected from Big Point, the Bahamas.

The experiments presented in Chapter 5 are concerned with biogenic aragonite in *Halimeda* algae and in scleractinian corals. *Halimeda* is a genus of calcifying green algae (see Figure 1.5) that can form large bioherm structures and may be a major sediment producer in tropical shelf regions (Wefer, 1980; Milliman, 1993). The algae's aragonitic skeleton disaggregates after death and contributes to lime mud accumulation, but as its components cannot be uniquely identified or separated, it does not provide a very useful geological archive. Nevertheless, *Halimeda* does present a useful system for studying biomineralization and some of the fundamental isotopic effects that occur in biogenic systems, due to the simplicity of its calcification mechanism. Imaging studies and microsensor analysis reveal minimal biological control over ion transport and aragonite precipitation, with seawater diffusing into an intercellular space and photosynthesis-induced pH changes causing growth of unoriented aragonite needles (Macintyre and Reid, 1995; de Beer and Larkum, 2001). This simple system bridges the gap between inorganic growth experiments controlled by physical chemistry and kinetics and a more complex system of biocalcification involving cellular transport, internal reservoirs, and organic

matrices.

Figure 1.6: A sample specimen of the scleractinian coral *Porites porites* collected from Castle Harbour Reef, Bermuda.

In contrast to the disaggregated components of *Halimeda* algae, understanding the biocalcification of scleractinian corals such as *Porites* has more useful geological applications. The composition of fossil aragonite skeletons is susceptible to modification from recrystallization, but samples recovered from the more recent past can provide high-resolution (annual and sub-annual) records of the marine environment. In addition, the incorporation of uranium from seawater allows coral samples to be dated radiometrically in absolute terms, providing good constraints on the timing of proxy records recovered from the skeleton. Hermatypic corals from reef environments (see Figure 1.6), which usually grow in a symbiotic relationship with photosynthetic zooxanthellae, can record conditions in the surface ocean; deep-sea corals, which are asymbiotic and ahermatypic, can provide valuable records from the deep ocean. Many different laboratory techniques have been applied to study coral physiology and biomineralization, including microscale imaging, radioactive tracers, fluorescent dyes, inhibiting drugs, and microsensor probes, under both natural and experimental conditions (Bénazet-Tambutté et al., 1996; Tambutté et al., 1996; de Beer et al., 2000; Clode and Marshall, 2002; Al-Horani et al., 2003a,b; Tambutté et al., 2012). These investigations provide a physiological basis for investigating geochemical signals in coral aragonite, which can in turn provide quantitative constraints on cellular processes, as well as recording information about environmental conditions (e.g. Cohen and McConnaughey, 2003; Allison et al., 2011). By comparing the response

of aragonite Ca-isotope ratios to experimental conditions in both *Halimeda* algae and *Porites* corals, a better understanding of Ca-isotope fractionation and other metal cation proxies can be established and used to interpret records of the marine environment.

Chapter 2

Methods

The majority of original data presented in this thesis are stable-isotope measurements of calcium. The range of different approaches for producing such measurements are described in Chapter 1, and this chapter contains the detailed methods for measuring $\delta^{44/42}$Ca by MC-ICP-MS, as performed at the University of Oxford, including verifications and tests of the analytical procedures. Previous Ca-isotope work at Oxford (e.g. Halicz et al., 1999; Chang et al., 2004; Marriott et al., 2004; Chu et al., 2006; Reynard et al., 2010) contributed to the development of the methods described below.

2.1 Sample preparation

Carbonate specimens, which constitute most $\delta^{44/42}$Ca measurements produced for this thesis, are sampled with a low-speed, handheld drill or powdered with a mortar and pestle. Samples with significant amounts of organic matter (especially *Halimeda* algae, see Chapter 5) are first bleached with 15% NaOCl for ~2 hours or until white. Fossil belemnite tests are cleaned thoroughly following the procedures in Jones et al. (1994), which include physically scraping or drilling to remove detrital matrix, sonicating in deionized water, etching in weak acid, and crushing and partially dissolving skeletal fragments to remove crack-filling secondary calcite (see Figure 2.1). Samples can then be visually inspected and drilled at clean, fresh surfaces. The chemical procedures described below have been calibrated for 0.5–3.0 mg (usually ~1 mg) of carbonate, corresponding to 0.2–

1.2 mg Ca. Measurements of pure Ca standard solutions, seawater, and seawater-like solutions are made using as little as 0.05 mg Ca (equivalent to ~0.12 mL of seawater at 412 ppm Ca). These solutions are evaporated to dryness and then treated in an identical manner to the carbonate samples.

Figure 2.1: Representative samples of Jurassic belemnite tests before (left) and after (right) the preparation procedure involving cleaning, etching, crushing, and partially dissolving the fossil calcite.

Samples are dissolved in 2N HCl in preparation for ion-exchange chromatography and, if necessary, centrifuged to separate any insoluble residue (clays or organic material). To minimize contamination, quartz-distilled acids and purified 18 MΩ water (MQ) are used at all times, and acid-cleaned Teflon beakers are used to collect and evaporate samples during chemical procedures. Once dissolved, samples are treated in a positive-pressure class-1000 clean laboratory environment and exposed only in laminar-flow hoods.

In fossil samples where diagenesis needs to be assessed, trace-metal analysis is useful for identifying possible alteration. For belemnite tests and other fossils of primary calcite, concentrations of >150 ppm Fe and >50 ppm Mn have been shown to be often, if not necessarily or exclusively, indicative of significant alteration (Jones et al., 1994). Such elevated levels of Fe or Mn signal possible calcite recrystallization or failure of the above methods to remove secondary calcite, and suggest that Ca-isotope ratios from those samples be interpreted cautiously, if not discarded entirely. In the case of bulk carbonate samples, trace-metal analysis is less useful due to the variable composition of carbonate micrite, although high levels of Mg can signal dolomitization, with an effect on Ca-isotope ratios of unknown but likely significant magnitude (Böhm et al., 2011). Theory, based on analysis of a representative carbonate-rich oceanic core, suggests that the relative rates of

carbonate sedimentation and recrystallization in deep-sea sediments could lead to positive $\delta^{44/40}$Ca offsets of <0.15‰ due to the high Ca-isotope ratio of seawater (Fantle and DePaolo, 2007). In general, diagenesis is expected to have only a small effect on Ca-isotope ratios due to the high concentration of Ca in carbonate fossils or sediment relative to meteoric fluids, and the similar isotopic composition of many natural Ca reservoirs.

2.2 Ion-exchange chromatography

To purify Ca from the rest of the sample matrix, ion-exchange chromatography is performed using a two-step column chemistry procedure described in Table 2.1. This purification is essential for reliable mass spectrometry, removing other cations that could alter plasma conditions, affect Ca ionization, or generate isobaric interferences. Particular attention must be given to remove Sr, whose double-charged ^{84}Sr, ^{86}Sr, and ^{88}Sr isotopes contribute direct interferences on the single-charged ^{42}Ca, ^{43}Ca, and ^{44}Ca ion beams. Methods for the analysis of bone, dairy, and vegetation described in Chu et al. (2006) with modification in Reynard et al. (2010) were adapted for geological samples for this work with slight adjustments. As a first step, Bio-Rad AG50W-X12 resin (200–400 μm particle size) is used to separate Ca^{2+} and Sr^{2+} from Na^+, K^+, Mg^{2+}, and other cations (see Figure 2.2). Following that process, Ca^{2+} is separated from Sr^{2+} with a second column of Triskem (Eichrom) Sr-specific resin (50–100 μm particle size). After each elution, samples are evaporated to dryness and treated with concentrated HNO_3 to oxidize organic molecules derived from the resins. The resulting purified Ca solutions are then redissolved in 2% HNO_3 to a concentration of 10 ppm Ca for mass spectrometry.

The effectiveness of the column elution for a typical carbonate sample was tested with a fossil belemnite, generating a calibration for separation of Ca and Sr from the calcite matrix (see Figure 2.2). Mg and Na are removed entirely within the first 10 mL of 2N HCl to pass through the columns, and Sr and Ca overlap in the 12–24 mL fraction. Complete collection of sample Ca must take place at this stage to ensure that no chemical fractionation is introduced during sample processing, since isotopic analysis of the fractions which yielded Ca show that the heavier isotopes are eluted first. Assuming 100% $CaCO_3$ in the

Table 2.1: Recipe for the isolation of Ca^{2+} from other cations through a two-step ion-chromatographic column separation.

Separation of Ca and Sr from other cations		
Load resin (to reuse)	1.6 mL	AG50W-X12
Prepare/clean resin	6.0 mL	6N HCl
	6.0 mL	2N HCl
Load sample	0.5 mL	2N HCl
Elute sample	0.5 mL	2N HCl
	10.0 mL	2N HCl
Collect Ca and Sr	2.0 mL	6N HCl
	10.0 mL	6N HCl
Clean resin	5.0 mL	6N HCl
	10.0 mL	MQ H_2O
Separation of Ca from Sr		
Load resin (to discard)	250 µL	Sr-specific resin
Prepare/clean resin	1000 µL	6N HCl
	1000 µL	MQ H_2O
	2000 µL	0.01N HNO_3
	1500 µL	3N HNO_3
	900 µL	3N HNO_3
Load sample/collect Ca	300 µL	3N HNO_3
Collect Ca	300 µL	3N HNO_3
	1500 µL	3N HNO_3
Elute Sr (optional)	200 µL	0.01N HNO_3
	800 µL	0.01N HNO_3
	800 µL	0.01N HNO_3

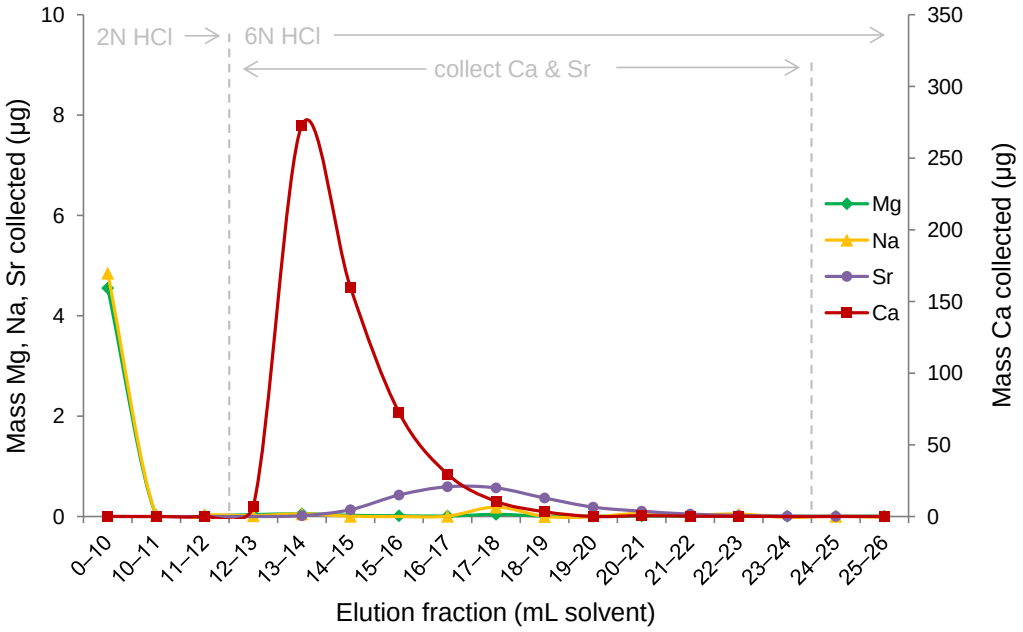

Figure 2.2: Elution curves for the first step of ion-exchange column chromatography for a matrix of fossil belemnite calcite. Note the clear separation of Mg and Na, but overlapping Sr and Ca, which necessitates a second column separation.

initial sample, concentration measurements of the eluted sample show complete collection of sample Ca, within the measurement accuracy of 1%. The Sr-specific resin used in the second columns has a very high affinity for Sr, which remains bound in the resin and is discarded after the sample Ca is eluted. After this step, Sr concentrations are below detection limit, and again, 100% collection of Ca takes place. Two standards of known isotopic composition are processed in parallel with every batch of samples to check for any systematic fractionation due to the ion chromatographic separations. The level of procedural blanks is ~5 ng Ca, which is negligible relative to sample sizes that are several orders of magnitude larger.

2.3 Mass spectrometry

Ca-isotope ratios are measured using a Nu Instruments multi-collector ICP-MS, whose original technical development and performance is described in Belshaw et al. (1998). This method of mass spectrometry offers the possibility of efficient sample preparation and high sample throughput, and therefore permits multiple replicates with little effort, yielding standard errors with comparable precision to TIMS measurements. Samples and standards are introduced through a Teflon sipper into the mass spectrometer as solutions of 10 ppm Ca in 2% HNO_3, with an uptake rate of 75 μL/min. The solution proceeds into a DSN-100 desolvator, which converts the sample into a dried aerosol to minimize molecular interferences from the fluid. The aerosol is carried into the plasma with a sample gas flow of ~3 L/min. The plasma is maintained with forward RF power at 1300 W. After being ionized in the plasma, the sample passes through nickel sampler and skimmer cones into the flight tube, where the ion beam is doubly focused by an electro-static analyzer and a magnetic sector. Ion optics are adjusted daily to maximize signal intensity and optimize peak alignment.

The voltage intensities of ion beams at mass 42, 43, and 44 are monitored simultaneously in Faraday collectors. A sample is measured for 120 one-second integrations, with automatic rejection of data whose internal standard deviations lie significantly outside the mean. Voltage spikes can sometimes occur due to discharge between the plasma

and sampler cone, but these are easily recognized and do not affect the integrated mean of the beam. A single measurement sequence lasts approximately 9 minutes, including multiple washes, a background/memory measurement (clean 2% HNO_3), and a sample uptake time of ~65 seconds. Beams at mass 41.5 through 45.5 are also measured, with the intensity of the mass 43.5 beam from double-charged ^{87}Sr (= 7.0% of total Sr), used to correct for direct interferences of double-charged ^{88}Sr (= 82.58%), ^{86}Sr (= 9.86%), and ^{84}Sr (= 0.56%) on the ^{44}Ca, ^{43}Ca, and ^{42}Ca beams, respectively. Before correction, Sr interferences tend to elevate $\delta^{44/42}Ca$ (as well as decrease $\delta^{44/43}Ca$ and increase $\delta^{43/42}Ca$) and can therefore be identified on a triple-isotope plot comparing two Ca-isotope ratios (see Figure 2.4). Doping experiments reveal that the correction using ^{87}Sr is sufficient for at least Sr/Ca ≤ 0.002 (see Figure 2.3, data from L.M. Reynard), which is easily achieved with ion chromatography. Background corrections due to the scatter of the large ^{40}Ca and ^{40}Ar beams were found to have negligible effect and were not applied. Intensity on the ^{44}Ca beam is 3–5 V, on average, giving a sensitivity of approximately 20 V/ppm ^{44}Ca.

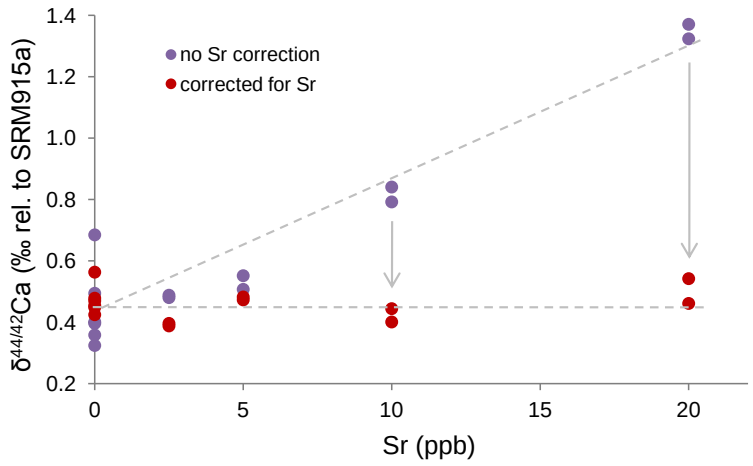

Figure 2.3: Doping 10 ppm Ca standard solutions with varying amounts of Sr shows the effect of the calculated Sr-interference correction using the mass 43.5 beam. The correction is effective for the entire range of Sr/Ca measured here. Data were collected by L.M. Reynard.

To correct for instrumental mass fractionation and calculate $\delta^{44/42}Ca$ (see formula in Section 1.1), samples are run in alternation with two standards, a reference and an internal standard. This sample–standard bracketing assumes an approximately linear fractionation over the small range between the reference standard and the sample. The ratio of

the reference standard is also used as a measure of stability, to monitor drift in machine mass bias. Using corrected intensities, values of $\delta^{44/42}$Ca are calculated for the samples and internal standard lying between subsequent measurements of the reference standard. Based on the standard deviation of the internal standard (usually ~50 analyses during a 24-hour run) and multiple (3–6) analyses of each sample, the average 2σ error on a sample $\delta^{44/42}$Ca value is 0.06‰. A triple-isotope plot of $\delta^{44/43}$Ca against $\delta^{44/42}$Ca verifies the mass-dependence of all the observed fractionation, with data falling around a line of slope 0.4875 as expected (see Figure 2.4). Sample data are discarded if deviations from mass-dependent fractionation (>2 standard deviations) are detected for either the sample $\delta^{44/42}$Ca or the paired internal standard measurement.

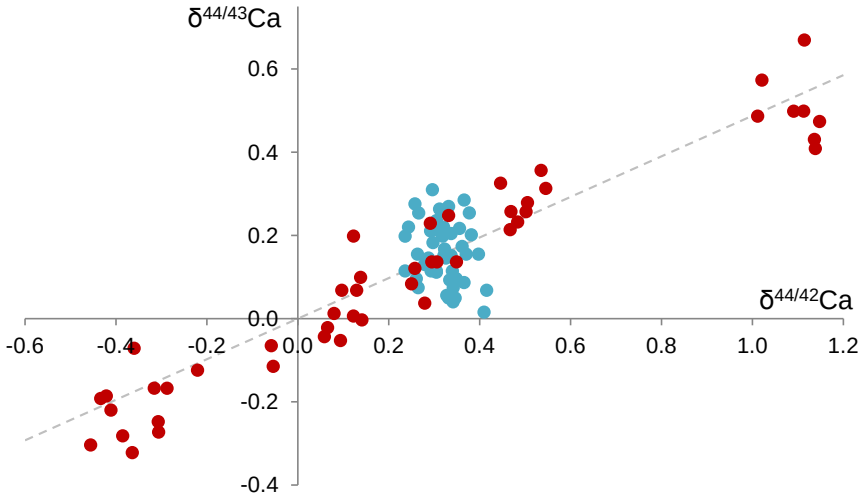

Figure 2.4: Triple-isotope plot showing mass-dependent fractionation (relative to an internal standard) over nearly the entire range of natural Ca-isotope variation. Red circles represent a variety of samples; blue circles are measurements of a second internal standard. All these data were collected on a single day (24/10/2010).

Values of $\delta^{44/42}$Ca are reported relative to the carbonate standard NIST SRM915a, although conversion to other reporting conventions is possible. A wide variety of standards have been used to report Ca-isotope ratios in the literature, including NIST SRM915a (currently used to depletion), NIST SRM915b, seawater, an internal fluorite standard (CaF_2), and a 'bulk earth' Ca-isotope value. Published values for these standards are shown in Table 2.2. The accuracy of measurements conducted at Oxford are confirmed by use of the reference standard SRM915a. The internal standard used at Oxford, 'HPS Ca', has a well established $\delta^{44/42}$Ca of +0.34‰ relative to SRM915a ($\delta^{44/40}$Ca = 0.71‰).

Table 2.2: A comparison of various calcium-isotope standards relative to the carbonate standard SRM915a, with original published and accepted values (converted from $\delta^{44/42}$Ca, where applicable). Accuracy in Ca-isotope analysis of samples for this thesis is confirmed by measurement of comparable values for seawater, SRM915b, and HPS Ca (see section 2.3).

Standard (phase)	$\delta^{44/40}$Ca	Published source
Seawater (solution)	1.88‰	Hippler et al. (2003)
laboratory CaF_2 (fluorite)	1.44‰	Hippler et al. (2003)
bulk silicate Earth (fluorite)	1.20‰	Fantle and DePaolo (2007)
Alfa Ca (solution)	0.84‰	Chu et al. (2006)
SRM915b (carbonate)*	0.72‰	Heuser and Eisenhauer (2008)
HPS Ca (solution)	0.65‰	Chu et al. (2006)
SRM1486 (phosphate)	−1.01‰	Heuser and Eisenhauer (2008)

*possible interferences from Sr

Measurements of seawater, having undergone ion-exchange chemical preparation identical to the treatment for carbonate samples, yield $\delta^{44/42}$Ca = +0.93‰ (n = 24, standard deviation = 0.07‰), agreeing well with the published value of $\delta^{44/40}$Ca = +1.88‰, or $\delta^{44/40}$Ca = +0.90‰ (Hippler et al., 2003), and confirming accuracy of the measurement methods described here. The reference standard SRM915b is measured to be +0.42‰ (n = 111, standard deviation = 0.06‰), slightly heavier than the published value of $\delta^{44/40}$Ca = +0.72‰, or $\delta^{44/42}$Ca = +0.34‰ (Heuser and Eisenhauer, 2008; Wombacher et al., 2009). However, the values measured at Oxford may be affected by significant interferences from Sr in this material, which can be identified by high intensities at mass 43.5 (^{87}Sr) and systematic deviation from mass-dependent fractionation. Analyses suggest that SRM915b carbonate contains 100 times as much Sr as samples treated with ion-exchange chromatography and 5–10 times as much as other Ca standards, and that the Sr-interference correction based on mass 43.5 is not effective at these concentrations (equivalent to ∼100 ppb Sr per 10 ppm Ca). The work of Heuser and Eisenhauer (2008) with the published reference value of $\delta^{44/40}$Ca = +0.72‰ is not susceptible to these interferences due to lack of Sr ionization during TIMS analysis, but the results of measurements presented here suggest that SRM915b should not be used as a reference material for analysis of Ca-isotope ratios by MC-ICP-MS without prior chemical purification.

2.4 External and stratigraphic reproducibility

Several tests were carried out to confirm the reproducibility of $\delta^{44/42}$Ca measurements during chemical preparation and analysis, and at a single point in time in the geological record. The statistics of repeat measurements of internal standards demonstrates the long-term precision of the mass spectrometer, with a standard deviation of 0.04‰ over 40 analytical sessions for 'HPS Ca' ($\delta^{44/42}$Ca = +0.34‰, n = 1744 total analyses) and a standard deviation of 0.02‰ over 16 analytical sessions for 'Fisher Ca' ($\delta^{44/42}$Ca = +0.56‰, n = 905 total analyses). The external precision of sample measurements is demonstrated by repeat analysis of a representative carbonate sample, which matches the average sample matrix and is treated with the complete chemical and analytical procedures. Analysis of a single Jurassic belemnite ($\delta^{44/42}$Ca = −0.04‰) confirms the reproducibility of sample treatment procedures with n = 19 separate treatments and a standard deviation of 0.04‰.

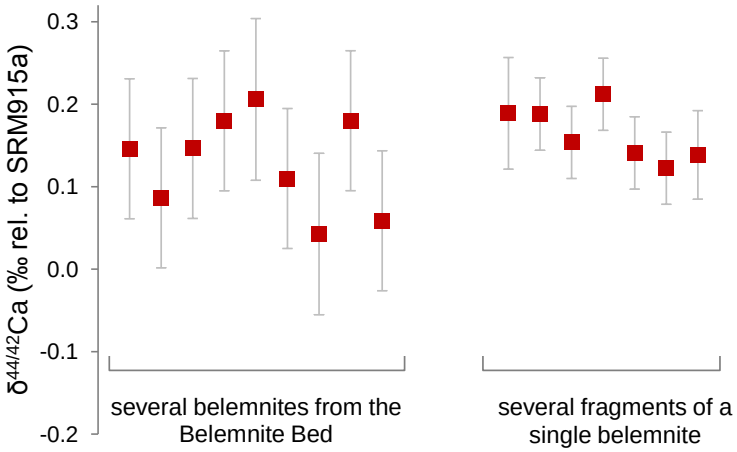

Figure 2.5: Multiple sample treatments of belemnites from a single bedding plane (n = 9) and from fragments of a single belemnite (n = 7), showing values within error of each other and confirming the usefulness of $\delta^{44/42}$Ca measurements on geological samples.

For practical application of Ca-isotope measurements to geological materials, the consistency of Ca-isotope ratios within an organism or fossil and across a single stratigraphic layer must also be tested. For the first case, samples across multiple fragments of a single belemnite confirmed that the entire fossil recorded identical Ca-isotope ratios, within error, ensuring that fragments of fossils can be used and that a typical ∼1 mg sample

sufficiently homogenizes any internal variability (see Figure 2.5). For the second case, several belemnites were sampled from a single bedding plane, the fossiliferous Belemnite Bed, exposed at Seatown, Dorset, UK. Assuming the length of time represented by this bed is much less than the residence time of Ca in the oceans (0.5–1.0 My), the Ca-isotope ratio of seawater should be uniform during that interval and individual fossils that express the same fractionation factor should all record the same value. The results of this test confirm that the natural variability in fossil carbonate over a bedding plane is within analytical precision, and that these methods can be used to reconstruct temporal changes in seawater Ca-isotope ratios.

Chapter 3

Significant increases in global weathering during Oceanic Anoxic Events 1a and 2 indicated by calcium isotopes

This chapter was published in very similar form in the journal *Earth and Planetary Science Letters* (Blättler et al., 2011). Supplementary information accompanying the published version is provided below as an appendix, along with some additional datasets and discussion.

3.1 Introduction

Oceanic Anoxic Events (OAEs) are among the largest climate perturbations of the Phanerozoic and offer an opportunity to observe the response of the Earth system to large and abrupt changes in the carbon cycle. Stratigraphy, sedimentology, macro- and micropaleontology, and organic- and inorganic geochemistry have all been used to study the interconnected processes involved during these periods of major environmental change. OAEs were initially recognized in the geological record by the widespread, synchronous deposition of marine black shales, interpreted as signals of global ocean anoxia (Schlanger

and Jenkyns, 1976). The events can also be recognized in diverse sedimentary sections (that may or may not have experienced local anoxia) using carbon-isotope stratigraphy, with a characteristic carbon-isotope curve associated with each event (Scholle and Arthur, 1980).

Many other processes are linked to the major changes in carbon cycling that occur during OAEs. There is evidence for volcanic activity at large igneous provinces (LIPs), high levels of greenhouse gases, increased temperature, bursts of primary productivity, widespread global ocean anoxia/euxinia, taxon-specific extinctions and radiations, seafloor carbonate dissolution, ocean acidification, and general ecosystem disruption (Erba, 2004; Jenkyns, 2010). A range of isotope proxies (e.g. Sr, Os, Mo, and U) has been measured across OAEs to assess aspects of these processes (e.g. Jones and Jenkyns, 2001; Cohen et al., 2004; Pearce et al., 2008; Montoya-Pino et al., 2010), and pulses of terrestrial weathering have been inferred from strontium- and osmium-isotope data (Frijia and Parente, 2008; Tejada et al., 2009). Calcium isotopes may also be useful in identifying and quantifying changes in geochemical cycles during OAEs, because the calcium-isotope ratio of seawater changes in response to large flux imbalances. Calcium is a key component in chemical weathering reactions, where its transfer from silicate to carbonate form actively draws down atmospheric CO_2 and stabilizes climate on long timescales (e.g. Walker et al., 1981). In this study, calcium-isotope ratios are reported from four sections spanning OAE1a (Early Aptian, ~123 Ma) and OAE2 (Cenomanian–Turonian, ~93.6 Ma). Two of these measured sections provide nearly pure carbonate records throughout these events. These sections do not strongly express conditions of organic carbon burial and local marine anoxia, which would lead to large changes in local sediment chemistry, but still clearly express the global changes in the carbon cycle in their carbon-isotope ratios, and are hence well suited to investigating the response of the calcium cycle to large climatic events.

Calcium is broadly conservative in seawater and its isotopic composition is uniform in the modern and presumably past oceans, due to its long residence time of ~0.5–1.0 My. Marine calcium-isotope histories have been reconstructed on geological timescales in a

variety of substrates (carbonate, apatite, and barite) and results are most often reported as

$$\delta^{44/40}\mathrm{Ca} = \left[\frac{\left(^{44}\mathrm{Ca}/^{40}\mathrm{Ca}\right)_{sample}}{\left(^{44}\mathrm{Ca}/^{40}\mathrm{Ca}\right)_{standard}} - 1 \right] \cdot 1000$$

with maximum measured temporal $\delta^{44/40}$Ca variation of ~1‰, for a given substrate, over the Phanerozoic (Schmitt et al., 2003b; Fantle and DePaolo, 2005; Heuser et al., 2005; Farkaš et al., 2007a; Sime et al., 2007; Griffith et al., 2008a). The marine calcium cycle is relatively simple with input from hydrothermal fluids at mid-ocean ridge systems and from dissolved riverine calcium produced by continental weathering (and small contributions from sediment diagenesis and groundwater fluxes), and output by seafloor calcium-carbonate deposition (DePaolo, 2004). Isotopic fractionation occurs during the removal of calcium from seawater, with the precipitation of isotopically light calcium carbonate maintaining relatively high seawater calcium-isotope ratios. This seawater ratio is expected to change due to variations in the fractionation factor (e.g. from changes in the dominant $CaCO_3$ mineralogy through time) or due to imbalances in the size or isotopic ratios of the input/output fluxes (Fantle, 2010). Despite its long oceanic residence time, the calcium-isotope composition of seawater may still respond to geologically short events if the forcing is large enough. A short calcium-isotope response has been reported in a Permo–Triassic boundary section from China, where $\delta^{44/40}$Ca variation of 0.2–0.3‰ was interpreted as a CO_2-acidification response (Payne et al., 2010). Four new high-resolution records of calcium isotopes during OAEs are presented in this study. These records show changes in the calcium cycle due to climatic perturbations, apparently due to changes in global weathering.

3.2 Background

Changes in global carbon-isotope ratios and paleotemperature proxies are well documented for OAE1a and OAE2 (Jenkyns, 2003). The Early Aptian (~123 Ma) OAE1a is classically known from its reference section in Italy, the Cismon Apticore, where a 5 m

thick black shale known as the Selli Level appears between pelagic carbonates and marls, a stark lithologic representation of the anoxic event (Erba et al., 1999). The defining carbon-isotope curve (see Figure 3.2, for example) has a sharp ~3‰ negative carbon-isotope excursion followed by a positive excursion and plateau (Menegatti et al., 1998; Weissert et al., 1998; Li et al., 2008). Negative excursions, common to many OAEs, may arise from sudden releases of ^{13}C-depleted carbon, either as a cause or effect (and amplifier) of environmental change. During OAE1a, the negative carbon-isotope excursion has been interpreted as the result of a release of methane hydrate, which could have induced global warming of 2.5–3.0 °C before subsequent CO_2 drawdown from organic-carbon burial (Jahren et al., 2001; Beerling et al., 2002; Dumitrescu et al., 2006). Positive carbon-isotope excursions often closely follow the negative excursions, and are generally interpreted as the result of increased global burial of organic, ^{13}C-depleted carbon (Scholle and Arthur, 1980). Orbital tuning of the Cismon core has produced estimates for the duration of the negative and subsequent positive carbon-isotope excursions of 1.0–1.3 My (Bralower et al., 1994; Li et al., 2008) and 1.1 My (Malinverno et al., 2010).

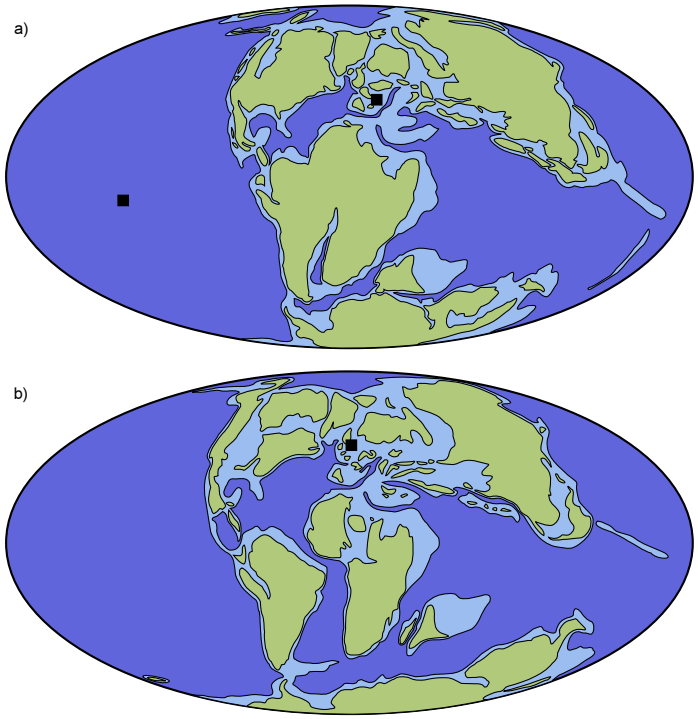

Figure 3.1: Paleogeographic reconstructions adapted from Blakey (2010) of: a) 120 Ma (Aptian), and b) 90 Ma (Turonian). Black squares show sample localities for this study.

OAE2 occurred at the Cenomanian–Turonian (C/T) boundary at ~93.6 Ma (Ogg et al., 2008). The global reference locality in Pueblo, CO, USA has produced a characteristic carbon-isotope curve that has been reproduced worldwide, with a broad ~2.5‰ positive excursion in carbonate carbon isotopes (Sageman et al., 2006). Orbitally derived estimates of the duration of the excursion range from 563–601 ky from analysis in the Western Interior Seaway (Sageman et al., 2006) to a shorter estimate of 430–445 ky from a locality in Northern Germany (Gale et al., 2005; Voigt et al., 2008). TEX_{86} and $\delta^{18}O$ paleotemperature data suggest that global sea-surface temperatures were high (> 33 °C) before a mid-event cooling of ~4 °C or 5–11 °C, depending on the locality, which again is attributed to CO_2 drawdown through organic-carbon burial (Forster et al., 2007; Sinninghe Damsté et al., 2010).

3.3 Samples

3.3.1 Oceanic Anoxic Event 1a: ODP Leg 143, Site 866, Resolution Guyot, Mid-Pacific Mountains

A carbonate record of OAE1a was sampled at Resolution Guyot (21°N, 174°E), drilled during Leg 143 of the Ocean Drilling Program. Hole 866A yielded a ~1620 m shallow-water carbonate record from the Hauterivian through the Albian (Jenkyns, 1995). Platform carbonate accumulation continued atop the extinct volcanic seamount from ~128 Ma until its drowning at ~99 Ma, during which time the guyot was located in the southern tropical Pacific (Wilson et al., 1998; Jenkyns and Wilson, 1999). Figure 3.1a shows the approximate paleogeographic location of Resolution Guyot during the Aptian (Blakey, 2010). Despite poor recovery (1.4% for the upper 300 m, 28–32% for deeper intervals, average of 15.4%), this core is remarkable in recording such a long-lived marine carbonate sequence from this time period, with sedimentation continuing through OAE1a. The carbonate in recovered core sections reflects shallow-water platform and lagoonal facies, dominated by oolitic/oncoidal/peloidal grainstone, cyanobacterial laminite, and mudstone-wackestone (Jenkyns and Strasser, 1995; Strasser et al., 1995). Skeletal frag-

ments of rudists, gastropods, and corals were also recovered throughout the core. The lower part of the core has undergone some dolomitization (1–5%, up to 35% $MgCO_3$ in a few samples), which may have occurred as recently as the Paleogene (Flood and Chivas, 1995); otherwise the core is nearly 100% calcite, interrupted only by an immature, ~10 cm thick, laminated 'black shale' corresponding to OAE1a (Arnaud et al., 1995; Jenkyns, 1995). This unit and a few accompanying organic carbon-rich clay layers characterize the onset of the event.

The initial stratigraphic correlation of Site 866 is based on benthic foraminiferal biostratigraphy (Arnaud-Vanneau and Sliter, 1995) as well as strontium- and carbon-isotope stratigraphies (Jenkyns, 1995; Jenkyns et al., 1995; Jenkyns and Wilson, 1999). Later comparison of the strontium-isotope curve to other records suggests that platform growth may have decreased in the upper core (Jenkyns and Wilson, 1999). The characteristic carbon-isotope curve of OAE1a from other worldwide sections, with a sharp negative excursion followed by a longer positive one, is robustly reproduced in the core samples (see Figure 3.2). Despite previous interpretations of subaerial exposure and karstification, others have argued that no evidence exists for meteoric-water diagenesis (Wilson et al., 1998; Jenkyns and Wilson, 1999). Such alteration, if it did occur, would likely have a minimal effect on carbon and calcium isotopes of calcite due to low concentrations of these elements in meteoric water. The excellent correlation of the OAE1a carbon-isotope curve with other global sections also suggests minimal diagenesis of this record. Dolomitized intervals, with a clear history of cation exchange, may contain altered calcium-isotope ratios, but these samples are easily identifiable by trace-element analysis and given separate consideration.

3.3.2 Oceanic Anoxic Event 1a: Coppitella, Gargano, Italy

Another carbonate-rich section spanning OAE1a was sampled from Coppitella, on the Gargano Peninsula in Italy (41.9°N, 16.2°E, see Figure 3.1a for paleogeography). The stratigraphy at Coppitella is described in Cobianchi et al. (1999) and Luciani et al. (2001). The marl–limestone couplets of the Marne a Fucoidi formation represent pelagic deposi-

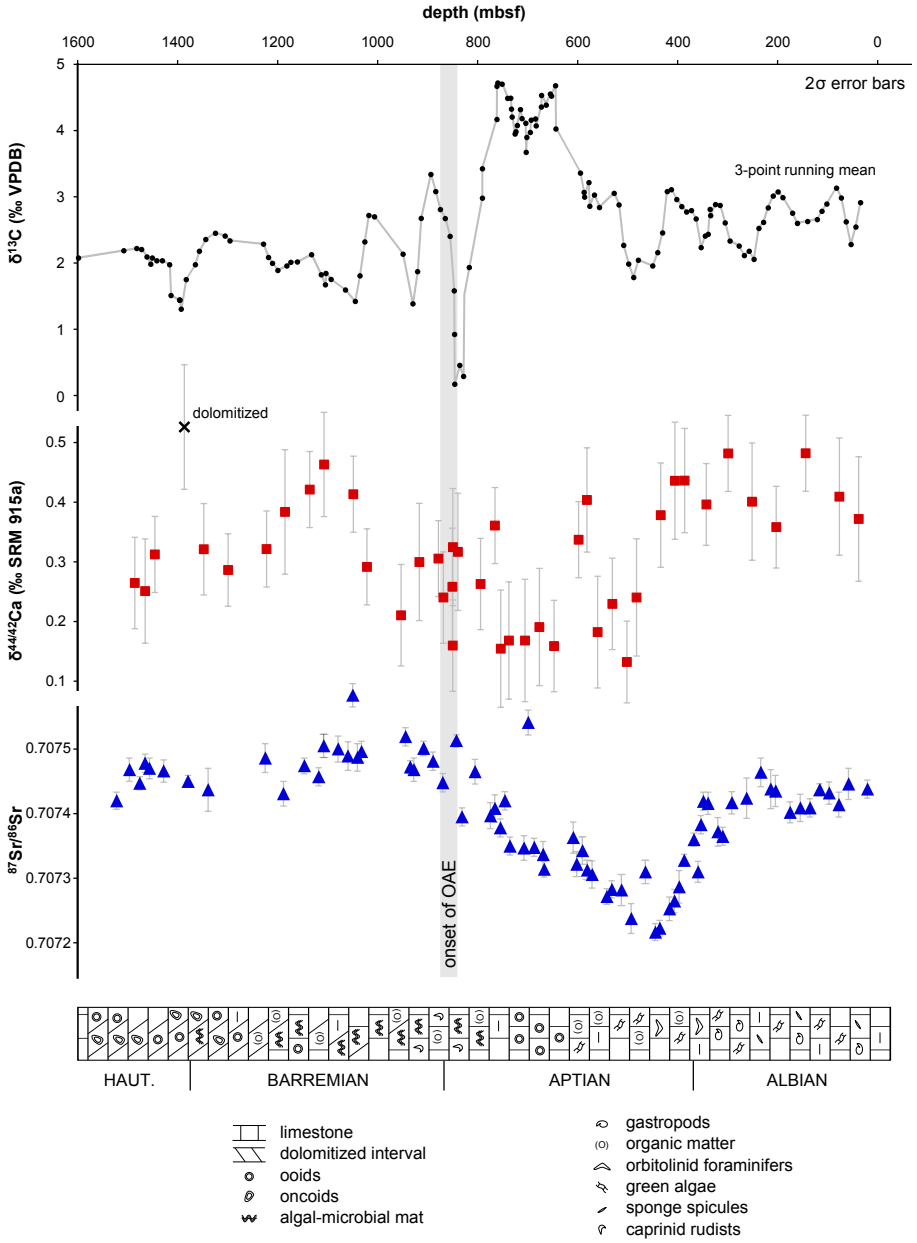

Figure 3.2: Calcium-, carbon-, and strontium-isotope ratios covering the OAE1a interval from ODP Site 866A, Resolution Guyot, Mid-Pacific Mountains. Carbon isotopes are from Jenkyns (1995). Strontium isotopes are from Jenkyns et al. (1995) and normalized to SRM987 $^{87}Sr/^{86}Sr$ = 0.710260. The symbolic stratigraphic log is modified from Strasser et al. (1995), where full descriptions of the units, sequences, and carbonate sedimentology can also be found.

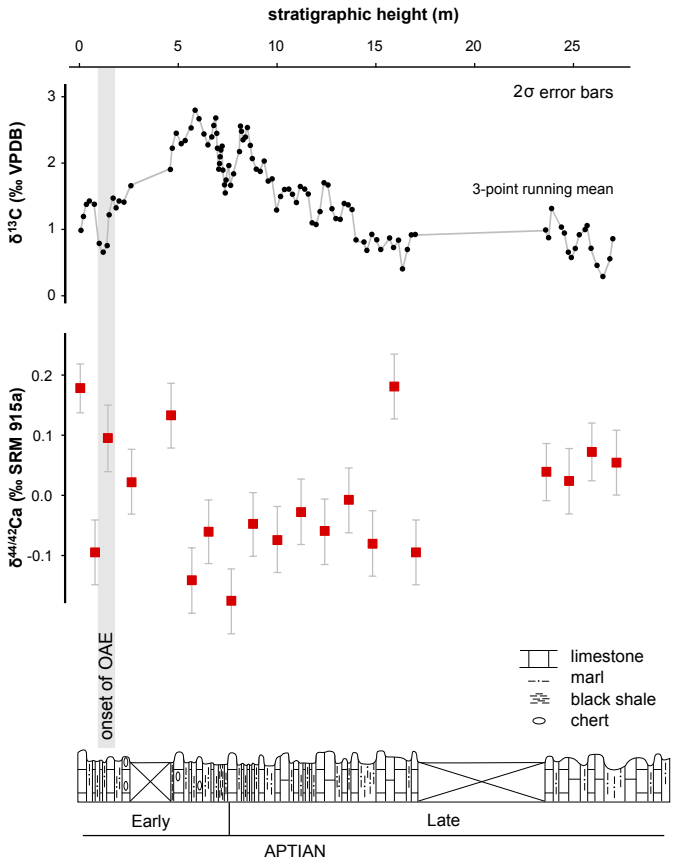

Figure 3.3: Calcium- and carbon-isotope ratios covering the OAE1a interval from Coppitella, near Vieste, Gargano, Italy. A subset of the carbon-isotope values shown are published in Luciani et al. (2001). Additional values as well as the stratigraphic log are from Luciani, Cobianchi, and Jenkyns (unpublished).

tion in the Ionian Basin. The samples are carbonate-rich, but with a significant percentage of clays in the marl intervals, and with a pair of thin black shale levels 5–10 cm thick. Correlation with OAE1a is based on calcareous nannofossil and planktonic foraminiferal biostratigraphy (Cobianchi et al., 1999; Luciani et al., 2001) as well as a high-resolution carbon-isotope curve (see Figure 3.3). The different depositional environment and distant location of this section compared to Resolution Guyot provide an opportunity to test for global calcium-isotope effects during OAE1a, as opposed to local effects influenced by the nature of the sediment at a single site.

3.3.3 Oceanic Anoxic Event 2: Eastbourne, UK

OAE2 is expressed in the Plenus Marls and lower White Chalk cropping out at Eastbourne, UK (50.7°N, 0.3°E), which has been proposed as a reference locality for the Cenomanian–Turonian boundary interval (Paul et al., 1999). This locality offers the thickest section of that interval in the Anglo–Paris basin (Gale et al., 1993; Jarvis et al., 2006). The marly (10–20% clay) carbonates of the Plenus Marls are overlain by the coccolith- and calcisphere-dominated nodular limestones of the Chalk (Paul et al., 1999; Gale et al., 2005). These units were deposited in the shallow epicontinental seas that covered northwestern Europe during the Cretaceous and can be considered as pelagic shelf-sea deposits (Figure 3.1b). The Eastbourne section (see Figure 3.4) is very well correlated with other global sections that cover OAE2 through extensive micro- and macro-fossil biostratigraphy (Gale et al., 1993; Paul et al., 1999; Tsikos et al., 2004; Gale et al., 2005) and high-resolution carbon-isotope profiles (Tsikos et al., 2004; Gale et al., 2005; Jarvis et al., 2006). The proposal to use the Eastbourne section as a European reference curve for the Cenomanian–Turonian boundary event is based on assumed stratigraphic completeness and an assessment of minimal diagenesis. Minor modification of oxygen-isotope ratios may have occurred, as well as slight smoothing of the carbon-isotope record from carbonate cementation, but carbon isotopes and other geochemical data remain robust (Jenkyns et al., 1994; Paul et al., 1999).

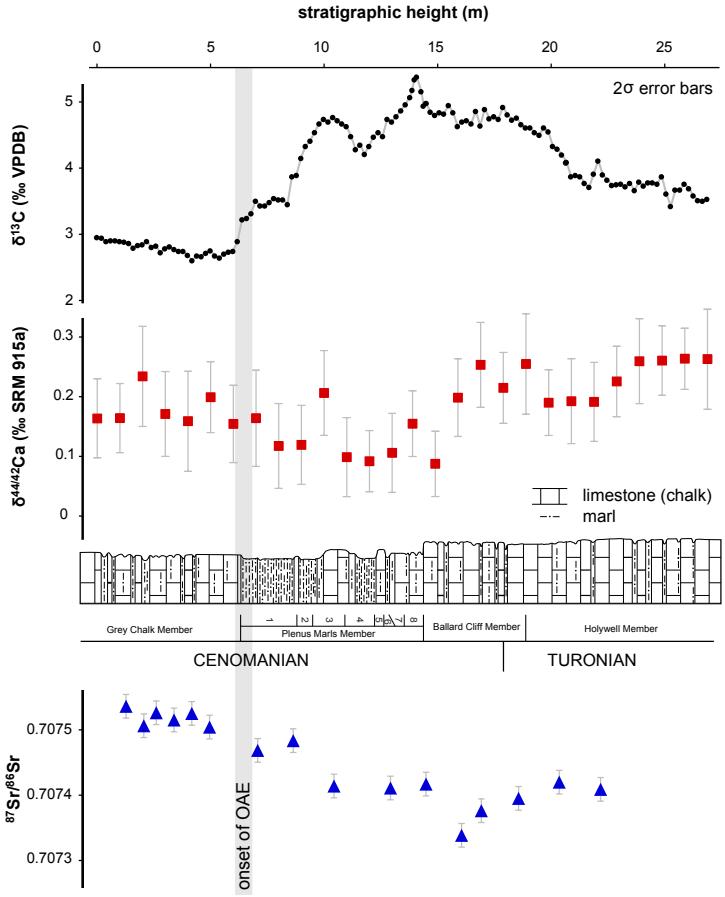

Figure 3.4: Calcium- and carbon-isotope ratios covering the OAE2 interval from Eastbourne, Sussex, England with strontium isotopes from the same time interval. Carbon isotopes are from Tsikos et al. (2004). The stratigraphic log, along with further biostratigraphic information, can be found in Erba (2004), Tsikos et al. (2004), and references therein. Strontium isotopes (normalized to SRM987 $^{87}Sr/^{86}Sr$ = 0.710260) are from McArthur et al. (1993) from the Trunch Borehole, Norfolk, England covering the same interval in the same facies, using carbon-isotope stratigraphy to correlate with Eastbourne.

3.3.4 Oceanic Anoxic Event 2: South Ferriby, UK

The South Ferriby quarry pit in Lincolnshire, UK (53.7°N, 0.5°W), yields a section of pelagic chalk interrupted by a 'Black Band' of organic-rich, laminated marls that is the lithological expression of OAE2 (Schlanger et al., 1987; Jenkyns et al., 2007). The section reflects the same chalk facies as at Eastbourne and has experienced a similar diagenetic history with good preservation of carbonate, although the South Ferriby section is condensed by a factor of about 20 relative to Eastbourne (Gale et al., 1993). A phosphatized chalk-pebble conglomerate below the Black Band and an abrupt shift in the carbon-isotope ratios of over 1‰ (see Figure 3.5) signal a long depositional hiatus (Hart et al., 1991). Despite this stratigraphic gap in the record, and the absence of a continuous chalk record, the partial overlap of this section with that from Eastbourne provides a good opportunity to reproduce globally significant signals at a second locality.

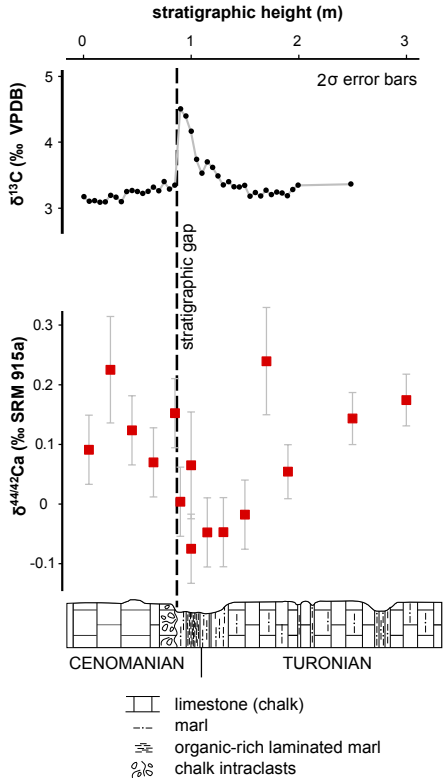

Figure 3.5: Calcium- and carbon-isotope ratios covering the OAE2 interval from South Ferriby, Lincolnshire, England. The stratigraphic log is modified from Gale et al. (1993) and Hart et al. (1991). Both $\delta^{44/42}$Ca and δ^{13}C values are new geochemical datasets, although the δ^{13}C record matches closely those in Hart et al. (1991) and Schlanger et al. (1987).

3.3.5 Comments on the studied sections

The dramatic changes in local redox conditions and lithology that occur in most sedimentary sequences during an OAE complicate geochemical analyses seeking to discern global conditions. The sample sections from Resolution Guyot and Eastbourne are unusual because of the uniformity and purity of the carbonate record throughout OAE1a and OAE2, respectively. The facies of those sections are little affected by the environmental changes that took place in the water column, so they provide excellent records for carbonate-based analyses of OAEs. Carbon-rich sequences, on the other hand, are typically low in carbonate and have a heavy diagenetic overprint, with secondary carbonate forming from oxidation of organic carbon. Calcium isotopes in carbonate are generally resistant to diagenesis, even during minor recrystallization, because of the strong buffering effect of calcium in the carbonate when exposed to fluids with low concentrations of this element. That duplicate sections are measured for each event also provides a test of signal reproducibility independent of any local diagenetic effects. Together, the four localities measured in this study provide important high-resolution and continuous records of the two major Cretaceous OAEs.

3.4 Methods

Samples were either powdered as a bulk hand sample, or drilled from the carbonate rock with a low-speed, hand-held drill, selecting the micritic portion of the carbonate and avoiding bioclasts and cements where visible. A total of 100 powders (~1–3 mg) from the various sites were dissolved directly in quartz-distilled acids, centrifuged to remove any insoluble clay content, and analyzed at Oxford. Elemental concentrations (for assessment of diagenesis) were measured on a Thermo Finnigan Element 2 ICP-MS (inductively coupled plasma mass spectrometer). For calcium-isotope analysis, samples were chemically processed using modifications of the method of Chu et al. (2006), as described in Reynard et al. (2010). Briefly, a two-step ion-exchange chromatographic separation is performed in a clean laboratory setting to isolate Ca^{2+}. Sample solutions are prepared at 10 ppm Ca and

^{42}Ca, ^{43}Ca, and ^{44}Ca beam intensities are measured on a Nu Instruments multi-collector ICP-MS, deriving

$$\delta^{44/42}\mathrm{Ca} = \left[\frac{\left(^{44}\mathrm{Ca}/^{42}\mathrm{Ca}\right)_{sample}}{\left(^{44}\mathrm{Ca}/^{42}\mathrm{Ca}\right)_{standard}} - 1 \right] \cdot 1000$$

using sample–standard bracketing with a reference material (NIST SRM915a). Every sample solution is measured multiple times. Data quality is assessed by checking for agreement with expected fractionation on a triple-isotope $\delta^{44/43}$Ca vs $\delta^{44/42}$Ca plot (following Reynard et al., 2010). An in-house standard solution ('HPSCa', $\delta^{44/42}$Ca = 0.34‰ relative to SRM915a) is analyzed between each sample bracket, and two aliquots of this pure calcium standard are also taken through the complete chemical procedure with every batch of samples to assess any isotopic fractionation introduced by the chemical and analytical procedures. Measurement uncertainty for $\delta^{44/42}$Ca is ±0.06‰ (2 SE), reflecting the external reproducibility of multiple measurements of the same solution. Five replicate treatments of a sample from Resolution Guyot confirm that this is an appropriate level of reproducibility for the entire analytical procedure. The use of ICP-MS does not allow analysis of ^{40}Ca, so measured calcium-isotope ratios in this study are reported as $\delta^{44/42}$Ca values relative to the reference solution SRM915a, instead of the alternative unit of $\delta^{44/40}$Ca. Values of $\delta^{44/42}$Ca can be approximately converted (within analytical error) to $\delta^{44/40}$Ca by simply multiplying by two.

3.5 Results

Calcium-isotope ($\delta^{44/42}$Ca) values from Resolution Guyot range from maxima of ~0.40‰ in the mid-Barremian and Albian, to a minimum of 0.15–0.20‰, with the lowest values all occurring in the Aptian (Figure 3.2). Variation within the Barremian and the Albian is on a similar scale to the analytical reproducibility (2σ = 0.04–0.08‰), while the difference of ~0.20‰ between these stages and the Aptian is greater than can be explained by analytical variability. The record of calcium isotopes within the Aptian stage is not smooth, but ranges from 0.15 to 0.35‰. It is noticeable that the excursion in calcium isotopes reaches its lowest values (800–650 mbsf) coincident with the negative carbon-

isotope excursion, and returns to higher values (400 mbsf) only as the carbon isotopes recover fully from their positive plateau. An analysis of variance shows that differences in calcium-isotope ratios between the three groups, (1) 1500–800 mbsf, (2) 800–450 mbsf, and (3) 450–0 mbsf, are statistically significant (ANOVA, $p = 1.1 \times 10^{-5}$; Tukey HSD, $p < 0.001$ between groups 1–3 and 2–3, $p = 0.07$ between groups 1–2). One sample from a dolomitized interval (1387 mbsf, within the Barremian) records a much heavier calcium-isotope ratio and stands out as an outlier at 0.53‰. The late-stage dolomitization in this sample (see Section 3.3.1) suggests that this outlier has no relation to the original calcium-isotope ratio at the time of deposition, and the high value from this sample is consistent with the predicted direction of fractionation for this process (Fantle and DePaolo, 2007). The samples measured here are the same as for the previously published carbon- and strontium-isotope curves, which are also shown in Figure 3.2 (Jenkyns, 1995; Jenkyns et al., 1995).

The calcium-isotope record from Coppitella shows a negative excursion of a similar magnitude to that from Resolution Guyot, despite the fact that the two records are from very different locations and settings. The absolute values are lower, ranging from −0.17 to −0.52‰, with a negative calcium-isotope excursion of ~0.2‰ occurring during the positive carbon-isotope excursion (see Figure 3.3). The more negative values in the middle of the section differ significantly from the background value (ANOVA, $p = 0.04$; Tukey HSD, $p = 0.05$ between groups of data before and during excursion).

Calcium-isotope values from Eastbourne show slightly less variation, with values ranging from 0.08 to 0.25‰ (Figure 3.4). The five-point mean of the data varies from 0.17‰ at the bottom of the section to a minimum of 0.10‰, and then rises to 0.24‰ at the top of the section. Again, this variation is greater than that during any one interval and must be explained by changes in the record, not by analytical uncertainty. The group of five measurements with the lowest $\delta^{44/42}$Ca values (mean = 0.10‰) clusters right at the apex of the positive carbon-isotope excursion. These five points are significantly different from the data above and below (ANOVA, $p = 4 \times 10^{-7}$; Tukey HSD, $p < 0.005$ for all pair-wise comparisons between groups). The carbon-isotope ratios were measured in

the same samples (Tsikos et al., 2004), but the strontium-isotope ratios at the bottom of Figure 3.4 are a representative curve of the event taken from a correlative section of the Chalk from Trunch, Norfolk, England (McArthur et al., 1993).

The calcium-isotope values at South Ferriby are slightly lower than those at Eastbourne, but show a similar trend when correlated by the carbon-isotope curve (Figure 3.5). At the bottom of the section, $\delta^{44/42}$Ca values average 0.13‰, with a drop to −0.02‰ (five-point mean) following the stratigraphic gap, simultaneous with the highest δ^{13}C values. At the top of the section, values recover to ~0.15‰ as the carbon-isotope ratios also return to pre-excursion levels. The data grouped into three sections (5 points pre-Black Band, 6 points in and after the Black Band, and 4 points towards the top of the section) are significantly different from each other (ANOVA, $p = 0.001$; Tukey HSD, $p < 0.004$ between the middle group of points and the other groups). Despite the condensed nature of the sequence and the existence of the laminated Black Band, the carbonate record of $\delta^{44/42}$Ca in this section reproduces the shape of the trend from the Eastbourne section over the same time interval.

Minor- and trace-element concentrations were also measured for all samples from Resolution Guyot and Eastbourne to check for samples/intervals that may have experienced more significant alteration and might generate artefacts in the calcium-isotope records. Iron and manganese concentrations are relatively uniform throughout the sections: Resolution Guyot samples have below 100 ppm Fe and below 50 ppm Mn, and Eastbourne samples contain higher values of 500–2000 ppm Fe and 200–500 ppm Mn. Strontium concentrations are approximately 150 ppm for Resolution Guyot samples and 300–600 ppm for Eastbourne samples. Magnesium concentrations are also quite uniform, around 0.1–0.5 wt.% in both sections, except for a few samples from Resolution Guyot with up to 8 wt.% Mg, a clear sign of dolomitization.

The magnitude of calcium-isotope variation in any single one of these sections is close to the limit of measurement precision, although replication of the observed trends in multiple stratigraphic sections leads to increased confidence in the existence of a shared signal recorded during these time periods. Statistical tests (ANOVA, Tukey HSD, performed us-

ing software by R Development Core Team, 2009) confirm the significance of variation among the groupings described above (pre-excursion, excursion, and post-excursion) in all of the measured sections. Variation over the entire stratigraphic section is in every case at least twice that of any such grouping of the data or the uncertainty on an individual measurement. These measures lead to the interpretation of the calcium-isotope records as displaying small but significant negative excursions during OAE1a and OAE2.

3.6 Discussion

3.6.1 Observed Ca-isotope variation attributed to changing seawater composition

The negative $\delta^{44/42}$Ca excursions of 0.1–0.2‰ measured in more than one section for both studied OAEs suggest a common process. Generally, changes in calcium-isotope ratios of marine precipitates originate from: a) changes in the fractionation factor between seawater and sample, such as from compositional (e.g. aragonite vs. calcite) or temperature effects; b) post-depositional alteration; or c) changes in the calcium-isotope composition of seawater from which the material precipitated. In the case of the samples measured here, changes in carbonate composition, precipitation temperature, and post-depositional diagenesis are all unlikely explanations for the data, so the sections are interpreted as recording real variation in seawater composition.

The continuity and homogeneity of the carbonate sediments from Resolution Guyot and Eastbourne suggest that a change in fractionation factor between seawater and substrate is not the major cause of $\delta^{44/42}$Ca variation at these locations. Although changes in fractionation factor due to local effects are difficult to rule out entirely in natural sequences where sediment varies over space and time, especially in a record spanning an OAE with changing environmental conditions, the duplication of the signals in additional sections suggests that the negative excursions are global phenomena. At Resolution Guyot, the texture of the bulk carbonate varies from radially structured calcitic ooids to peloids to cyanobacterial laminite, but these changes are not accompanied by any mineralogical

changes. Changes in calcium-isotope values also do not correlate with any particular carbonate lithology (e.g. oolite and microbial laminite). The section was sampled for non-skeletal phases, which allow limited opportunity for strong biological control over the fractionation factor. Unintentional sampling of a skeletal fragment rather than the surrounding limestone may lead to scattered $\delta^{44/42}$Ca values, but this does not explain entire intervals with average values that vary by up to 0.20‰. The Coppitella section has generally high nannofossil abundance and diversity, suggesting good preservation of the carbonate fraction (Luciani et al., 2001), and although carbonate percentage in the samples shows a bimodal distribution due to variation in clay content in the marl–limestone couplets, carbonate percentage is not well correlated with calcium isotopes ($R^2 = 0.12$). The carbonate of the Eastbourne Chalk is a very homogeneous, coccolith-rich facies. Samples have high carbonate content throughout (most samples > 90%), and carbonate percentage is again not well correlated with calcium isotopes ($R^2 = 0.44$). Changes in nannofloral assemblages take place throughout the section, with the largest change being the decline of *Biscutum* spp. that constitutes ~30% of the coccolith abundance, but many species that contribute a significant percentage to the total nannofossils do not vary in abundance during OAE2 (Linnert et al., 2011). If *Biscutum* were at one extreme of the range of fractionation factors measured in individual coccolith species by Gussone et al. (2007), and the remaining nannofossils lay at the other extreme, the 30% change in assemblage composition would still not account for the entire excursion. The similar excursion in the chalk of South Ferriby, which has different absolute $\delta^{44/42}$Ca values and likely a different nannofossil assemblage, as well as a lithological change at the Black Band, also suggests that assemblage changes are not responsible for the negative excursions.

Temperature effects on the fractionation factor are another possible source of global variation in calcium-isotope ratios, depending on the source of the carbonate, but the variation expected from such an effect is inconsistent with paleotemperature records from these OAEs. Although the planktonic foraminifera *Globigerinoides sacculifer* has been shown to exhibit a $\delta^{44/40}$Ca temperature dependence of +0.24‰ per °C (Nägler et al., 2000), a much weaker temperature dependence of < 0.02‰ per °C is found in other

carbonates, such as the foraminifera *Orbulina universa* and inorganic precipitates (Gussone et al., 2003; Marriott et al., 2004). No temperature relationship has been calibrated for lagoonal/shallow-water carbonates, such as those from Resolution Guyot, but if, as expected, these non-skeletal carbonates follow the inorganic calcite trend ($\delta^{44/40}$Ca varying by ~0.02‰ per °C), then the $\delta^{44/40}$Ca variation of −0.4‰ (converted from $\delta^{44/42}$Ca) in the measured section would require a > 20 °C drop in temperatures of the tropical Pacific surface oceans. A similar interpretation can be made for the nannofossil-rich Coppitella section, using the temperature calibrations for coccolithophores of ~0.02‰ per °C (Gussone et al., 2006, 2007; Langer et al., 2007). Not only would such conditions be climatically implausible, but it is unlikely that carbonate production would have continued at such temperatures. In fact, suggested temperature changes during OAE1a are towards warmer conditions and are therefore in the wrong direction to explain the observed calcium-isotope excursions.

Using the ~0.02‰ per °C relationship for the coccolith-dominated chalk records of OAE2, the $\delta^{44/40}$Ca shifts of −0.2 to −0.3‰ (converted) in the Eastbourne and South Ferriby sections could be explained by a drop in temperatures of 10–15 °C during the OAE. Some component of these records may therefore be explained by a temperature effect, since a cooling episode during the middle of OAE2 has been inferred from paleotemperature proxies in various locations, with a magnitude of 4 °C in the equatorial Atlantic (Forster et al., 2007) and 5–11 °C in the proto-North Atlantic (Sinninghe Damsté et al., 2010). It seems reasonable to attribute some of the calcium-isotope variation in the chalk records of OAE2 to temperature changes, but this is unlikely to explain more than half the observed variation in calcium isotopes.

Selection of carbonate-dominated sequences with minimal change in sediment type means that the samples will have been subjected to minimal diagenetic alteration, particularly of the type that could significantly alter their calcium-isotope composition. Early diagenesis through reaction with pore waters may increase $\delta^{44/40}$Ca values slightly, on the order of ~0.15‰ depending on sedimentation and recrystallization rates (Fantle and DePaolo, 2007), but this should affect each site relatively uniformly and would not generate

differential zones within a continuously deposited section. There is no evidence for partial dissolution at the sections studied, which may selectively dissolve components of the carbonate and affect the isotopic ratios in the remaining material. No value of minor- and trace-element concentrations (iron, manganese, strontium, and magnesium) suggests that any sample has been significantly altered, apart from a few easily identifiable dolomitized samples, which can be discarded (see Section 3.5).

Neither systematic changes in fractionation nor diagenetic alteration seems to be a viable explanation for the similar calcium-isotope signals measured in four different sections. To explain the consistency and reproducibility of these signals, changes in the calcium-isotope composition of seawater are proposed as the origin of the negative excursions during OAEs.

3.6.2 Modelling seawater calcium-isotope excursions

A simple one-box model of the oceanic calcium and strontium cycles was used to explore the possible variation in seawater calcium isotopes, assuming that a common process is driving the similar calcium-isotope responses to both OAEs. The model specifically tests the effects of submarine LIP eruption, ocean acidification, and increased continental weathering, three processes that have been shown to occur during these OAEs (see Section 3.1). To evaluate the extent of these processes, model results are compared with two targets defined by the general form of the data: a negative $\delta^{44/42}$Ca excursion of 0.1–0.2‰ (i.e. a $\delta^{44/40}$Ca excursion of 0.2–0.4‰) lasting ~1 My (see horizontal bars in Figure 3.7), and a decrease in $^{87}Sr/^{86}Sr$ of 0.0002–0.0003 toward non-radiogenic values over 3–5 My following both OAEs (data in Figures 3.2 and 3.4).

The calcium cycle is modelled with the mass-balance equation:

$$\frac{\mathrm{d}}{\mathrm{d}t}(N_{\mathrm{Ca}}) = F_{\mathrm{hyd}} + F_{\mathrm{riv}} - F_{\mathrm{carb}}$$

where N_{Ca} is the oceanic calcium reservoir and F_{x} is a flux of calcium to/from x. F_{hyd} and F_{riv} are hydrothermal and riverine sources, respectively, and F_{carb} is the net carbonate

burial sink (equal to total marine carbonate precipitation minus carbonate dissolution). The isotope-balance equation:

$$N_{\mathrm{Ca}} \cdot \frac{\mathrm{d}}{\mathrm{d}t}(\delta^{44/40}\mathrm{Ca_{SW}}) = (\delta^{44/40}\mathrm{Ca_{hyd}} - \delta^{44/40}\mathrm{Ca_{SW}}) \cdot F_{\mathrm{hyd}} + (\delta^{44/40}\mathrm{Ca_{riv}} - \delta^{44/40}\mathrm{Ca_{SW}}) \cdot F_{\mathrm{riv}} - (\delta^{44/40}\mathrm{Ca_{carb}} - \delta^{44/40}\mathrm{Ca_{SW}}) \cdot F_{\mathrm{carb}}$$

with

$$\delta^{44/40}\mathrm{Ca_{carb}} = \delta^{44/40}\mathrm{Ca_{SW}} + \Delta_{\mathrm{carb}}$$

describes the evolution of the seawater isotope ratio ($\delta^{44/40}\mathrm{Ca_{SW}}$), where Δ_{carb} is the difference, due to fractionation, between seawater and average bulk carbonate. All model isotope ratios are reported as $\delta^{44/40}$Ca relative to SRM915a. N_{Ca} is 2.5 times higher than the modern oceanic reservoir of calcium, to approach the modelled Cretaceous value (Stanley and Hardie, 1998; Lowenstein et al., 2003). Magnitudes and isotope ratios of calcium fluxes (see Figure 3.6) are taken from literature estimates of the modern calcium cycle (De La Rocha and DePaolo, 2000; Schmitt et al., 2003a; Heuser et al., 2005; Farkaš et al., 2007b). F_{carb} is treated as a first-order sink relative to N_{Ca}, and due to the increased size of the oceanic reservoir, the modelled residence time of calcium is 2.5 times that of the modern calcium cycle. The treatment of F_{carb} describes the long-timescale relationship between alkalinity and silicate weathering, where atmospheric carbon dioxide, rather than biocarbonate derived from weathering of limestones and dolomites, is necessarily involved in the removal of excess Ca^{2+} as marine carbonate precipitates. Limestone weathering and carbonate chemistry influence oceanic calcium, bicarbonate, and carbonate ion concentrations on the order of 10^4 years, and while marine carbonate compensation will prevent large changes in the size of the oceanic calcium reservoir, silicate weathering products must ultimately be removed by increased net carbonate deposition over long timescales (Archer et al., 1997; Gaillardet et al., 1999). Additional calcium that is mixed into the marine reservoir will have an isotopic effect similar to that derived from this simplified modelling strategy representing carbonate removal as a first-order sink for calcium,

making this approach an effective tool for investigating calcium-isotope variation.

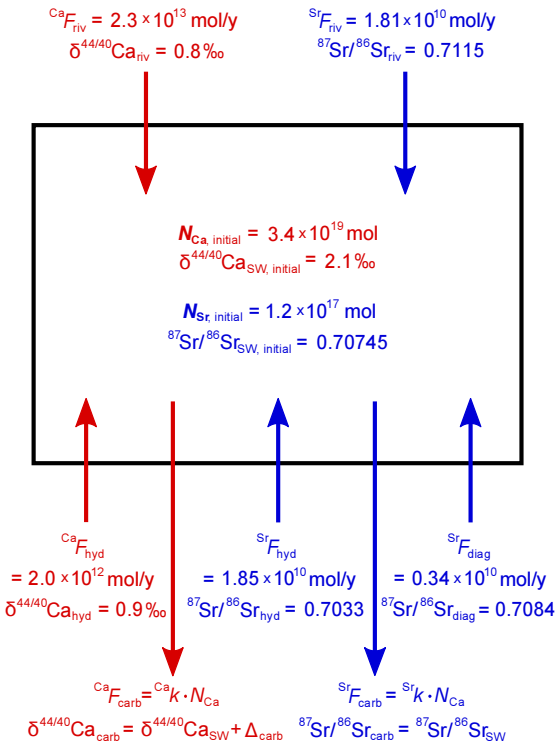

Figure 3.6: Schematic of the oceanic box model used in this study, including initial values for reservoir sizes, flux magnitudes, and isotope ratios. The calcium cycle is in red, with $\delta^{44/40}$Ca values relative to SRM915a; the strontium cycle is in blue, with isotope ratios normalized to SRM987 ^{87}Sr/^{86}Sr = 0.710260. Model parameters are derived from Palmer and Edmond (1989), De La Rocha and DePaolo (2000), Schmitt et al. (2003a), Heuser et al. (2005), and Farkaš et al. (2007b). The molar amounts and isotope ratios of seawater are initial steady-state values, derived using other model parameters to balance the calcium and strontium cycles. The relative proportions of riverine vs hydrothermal strontium are also derived from calculations to achieve an initial steady-state given seawater ^{87}Sr/^{86}Sr data. Seawater and output flux (F_{carb}) values respond to model forcing effects and change over time.

The model strontium cycle is linked to the calcium cycle through the common sources of both elements, riverine and hydrothermal fluxes. The mass balance equation for strontium is identical in form to that for calcium, except for the additional input term of a diagenetic (benthic carbonate recrystallization) flux. Strontium removal, by incorporation into carbonate, is proportional to the first-order calcium sink, F_{carb}, and does not affect strontium-isotope ratios. Isotope ratios (^{87}Sr/^{86}Sr) of input fluxes are taken from published values (Palmer and Edmond, 1989) and determine the initial steady-state balance prior to the OAE excursion (see Figure 3.6). The oceanic strontium-isotope ratio then evolves as the balance of the input fluxes changes through the model run.

The steady-state balance of the system is perturbed by changing source and sink fluxes linked to the relevant processes (i.e. LIP emplacement), or by changing their isotopic ratios, or by changing Δ_{carb} (reflecting a change in the dominant species or mineralogy of carbonate output) or F_{carb} (reflecting a change in the precipitation/dissolution balance of seafloor carbonate, such as from ocean acidification). The equations are solved numerically to calculate the time-dependent ocean calcium- and strontium-isotope compositions. The magnitudes of the modelled excursions are sensitive to the residence times of calcium, which is increased relative to the modern, and strontium, and therefore suggests the possibility of greater calcium-isotope excursions or less extreme required forcing effects (either less intense or of a shorter duration) than those indicated by model results. Limiting changes in the size of the oceanic calcium reservoir, rather than permitting variation due to the treatment of carbonate precipitation as a first-order sink, increases the magnitude of modelled calcium-isotope excursions by approximately 30%. Due to the large oceanic calcium reservoir and the similar isotopic composition of the two input fluxes, only large changes to the magnitude of the input fluxes displace the model seawater calcium-isotope ratio. Such a large change will cause an initial isotope excursion, but if the perturbation is maintained for much longer than the residence time of calcium in the oceans, the ratio will return to its initial value (see Figure 3.7a). This behaviour arises because the precipitation of calcium carbonate is the only source of significant fractionation in the system, leaving seawater isotopically heavy; because carbonate burial is the only major calcium sink, the calcium-isotope ratio of seawater and the carbonate sink adjust in parallel (separated by Δ_{carb}) until establishment of a new steady-state where the isotope ratios of the output and input are equal. In this model configuration, which is likely to capture the major features of the oceanic calcium-isotope cycle, isotope excursions and concentration changes are therefore only recorded as transient phenomena until the seawater concentration and output flux adjust to a new steady-state. Persistent shifts to the seawater calcium-isotope ratio are generated only by changes to Δ_{carb} or to the isotope ratios of source fluxes (see Figure 3.7b).

Model results from perturbing the system by an increase in hydrothermal activity

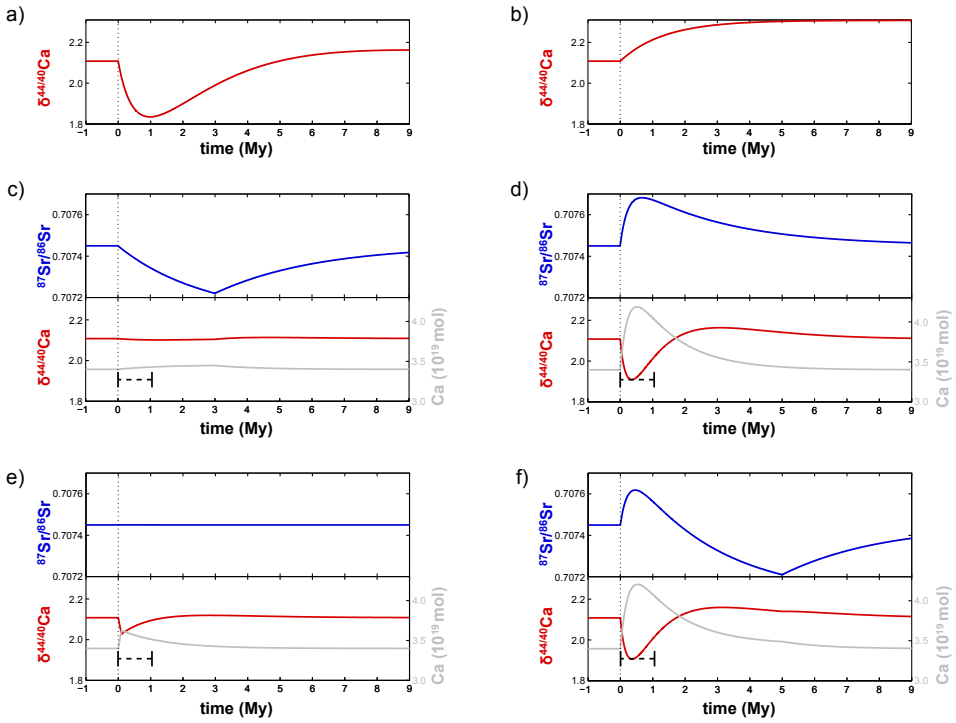

Figure 3.7: Model results for six particular forcing arrangements, showing strontium-isotope ratios (plots c–f only, upper plots), calcium-isotope ratios (red lines, lower plots), and the molar calcium reservoir of the oceans (grey lines, lower plots). Vertical dotted lines show the onset of forced perturbations; short, horizontal dashed bars show the target calcium-isotope response. The time axis marks millions of years from the onset of the perturbation. a) Hypothetical forcing arrangement to show the behaviour of calcium isotopes to flux imbalances. The weathering input flux is doubled at time t = 0 and remains elevated. Note that the calcium-isotope ratio exhibits a negative excursion, then returns to a new steady-state value even while the input flux remains high. b) Hypothetical forcing arrangement to show the shift of calcium isotopes due to changes in the fractionation factor. The fractionation factor between seawater and average bulk carbonate changes at time t = 0 from –1.3‰ to –1.5‰ (e.g. from precipitating a larger proportion of aragonite, which is isotopically lighter than calcite). Note that the calcium-isotope ratios remain permanently displaced from initial values. c) The effect of increasing hydrothermal input of calcium and strontium, such as from the emplacement of the Ontong-Java or Caribbean Plateau. d) The effect of increasing weathering inputs of calcium and strontium, such as from a period of global warming, then allowing them to decay back to initial values. e) The effect of ocean acidification, modelled as a decrease of the net carbonate burial sink. f) Best-fit model results for the data describing OAEs 1a and 2, resulting in a negative calcium-isotope excursion and a short-lived radiogenic (positive) strontium-isotope excursion followed by a larger nonradiogenic (negative) strontium-isotope excursion. This result is effectively a combination of c and d. See text for further details.

(F_{hyd}) are presented in Figure 3.7c. OAEs 1a and 2 were synchronous, within dating errors, with the formation of the Ontong–Java and the Caribbean Plateaus, respectively, and the volcanic plateaus likely had significant, if not causal, effects on the environmental response (e.g. Kerr, 1998; Larson and Erba, 1999; Jones and Jenkyns, 2001; Snow et al., 2005; Turgeon and Creaser, 2008; Tejada et al., 2009). The effect of emplacing these LIPs was modelled by increasing hydrothermal fluxes of both strontium and calcium ions by 20% for 3–5 My. This duration reflects the hypothetical timescale of increased delivery of ions from fresh underwater basalt, which may be longer than the duration of actual volcanic activity (Tarduno et al., 1991). With a 3 My hydrothermal forcing, strontium-isotope ratios match the target response, falling by 0.00023, but calcium-isotope ratios only fall by an immeasurable 0.007‰. For hydrothermal activity to produce a calcium-isotope signal that matches the data, the flux would have to increase by an implausible 500%, which would drive model strontium-isotope ratios down by 0.00250. Such a large strontium-isotope response is not a feature of OAEs 1 or 2, nor anywhere else in the Phanerozoic (McArthur et al., 2001). These results suggest that hydrothermal activity does not drive oceanic calcium-isotope ratios.

The model results from increasing the riverine input flux (F_{riv}) while keeping its isotope ratio constant are shown in Figure 3.7d. Global warming associated with both OAEs (see Section 3.2) would have resulted in an intensified continental weathering regime (see Section 3.6.3 for further discussion). Forcing a threefold increase in the model riverine flux, which then exponentially decays back to its initial value with an *e*-folding time of 250 ky, generates both a negative calcium-isotope excursion with a maximum $\delta^{44/40}Ca$ amplitude of 0.28‰, and a positive (radiogenic) excursion in $^{87}Sr/^{86}Sr$ of 0.00027. These results indicate that weathering flux changes can drive oceanic calcium isotopes. The model target of producing a longer lasting, non-radiogenic strontium-isotope excursion is not met in this instance, so another factor must be involved during OAEs besides weathering alone. Section 3.6.3 discusses the evidence that short-lived excursions in strontium isotopes to radiogenic values are indeed a feature of the strontium-isotope records of these OAEs.

Ocean acidification will affect the oceanic calcium-isotope budget through seafloor carbonate dissolution and temporary shutdown of the carbonate sink, but model results imply that this is not capable of producing large (measurable) calcium-isotope variation. The net effect of carbonate dissolution and reduced carbonate precipitation is modelled as a 90% reduction in the carbonate sink flux (F_{carb}) for 100 ky, which displaces oceanic calcium-isotope ratios by only 0.08‰ (see Figure 3.7e). The sizable oceanic calcium reservoir effectively damps the impact of even near-total disruption to the carbonate burial system. Payne et al. (2010) invoke ocean acidification as a partial explanation for the calcium-isotope perturbation at the Permo–Triassic boundary. The 'acidification scenario' described in that study includes, however, both a carbonate sink disruption and a weathering flux increase, and it is the weathering flux increase that produces the majority of the target calcium-isotope excursion. In isolation, a 17.7% perturbation to carbonate burial, as assumed in the Payne et al. (2010) study, produces a negligible (0.02‰) calcium-isotope excursion in the simple model configuration used in this study. A greater effect from a longer or larger disruption to F_{carb} is limited by the short recovery timescale (~10 ky) of the exogenic carbon cycle and by the finite amount of seafloor carbonate (1600 Gt C, or 130×10^9 mol Ca) that can be dissolved (Archer, 1996; Archer et al., 1997). The global calcium reservoir is on the order of 10^{19} mol, so dissolution of seafloor carbonate from ocean acidification, without the terrestrial weathering effects associated with increased atmospheric carbon, does not affect oceanic calcium isotopes to a measurable degree.

The model result that best fits the observations for both calcium and strontium isotopes is a short-term weathering flux increase and a longer-term hydrothermal flux increase (Figure 3.7f). This combination of forcing mechanisms fits with the geological evidence for global warming and LIP emplacement during the two OAEs. Given that the continental riverine input of calcium is ~90% of the total input flux, changes to weathering emerge as the primary driver for negative calcium-isotope excursions on the short timescales of OAEs. Hydrothermal activity is implicated by the non-radiogenic trends in strontium-isotope ratios. A tripling of weathering inputs (e.g. Figure 3.7d), combined with increased hydrothermal activity equal to 20% of global mid-ocean ridge activity for

5 My, produces model curves that closely fit the observations (see Figure 3.7f).

3.6.3 Quantitatively exploring the weathering response to OAEs

While model results show that variations in the magnitude of the weathering flux can affect seawater calcium-isotope ratios, the results presented above (and in Figure 3.7) do not explore the possible effects of changing isotope ratios of weathered material. The measured range in $\delta^{44/40}$Ca of dissolved river loads is as large as the total variation measured in Phanerozoic marine carbonates, ~1.0‰ (Zhu and Macdougall, 1998; Schmitt et al., 2003a; Tipper et al., 2008). Integrated over a regional scale, however, rivers are more homogeneous, showing half as much variation, and more importantly, calcium-isotope variation is not correlated with lithology or climate of the watershed (Schmitt et al., 2003a; Tipper et al., 2010). Schmitt et al. (2003a) conclude that the isotopic value of river calcium input should be stable over time, and that variation in past oceanic calcium-isotope ratios would be due to changes in flux magnitudes rather than changes in their isotope ratios. Little to no fractionation has been measured for rock-weathering reactions, although soils, groundwater, and small rivers have been shown to contain fractionated calcium isotopes due to removal of light calcium by biological activity and by secondary calcite precipitation (Schmitt et al., 2003a; Tipper et al., 2006, 2010). Measurement of an isotopically heavy groundwater reservoir led to the suggestion that oceanic calcium isotopes could be influenced by the variable storage time of calcium in such terrestrial reservoirs (Tipper et al., 2006), but this effect is likely to be small. Although changing the isotope ratio of input fluxes is one possible mechanism for modelling changes in seawater calcium-isotope ratios, these published studies suggest that the isotopic ratio of weathering inputs to the oceans does not change greatly with time, much less over the ~1 My timescales of OAEs, and support the interpretation that the measured OAE anomalies are due to a large flux imbalance.

Evidence from radiogenic isotopes supports the model results invoking increased weathering fluxes as the driver behind oceanic calcium-isotope variations during OAEs. Strontium- and osmium-isotope ratios in the ocean effectively resolve a balance between

a continental, radiogenic source (weathering input) and a mantle-derived, non-radiogenic source (hydrothermal input). Osmium-isotope ratios through a section recording OAE1a show two consecutive sharp decreases in $^{187}Os/^{188}Os$ during the OAE, which are interpreted as increases in mantle-derived osmium from the Ontong-Java Plateau (Tejada et al., 2009). The authors explain the reversal in $^{187}Os/^{188}Os$ between these two pulses as a transient weathering pulse due to higher global temperatures, an increased hydrological cycle, and subsequently increased chemical weathering rates. An increase in $^{187}Os/^{188}Os$ of this magnitude (0.3 to 0.7) suggests a large weathering increase, although the true contribution of the continental end-member may be masked by the effect of the hydrothermal end-member. For this reason, quantifying the magnitude of a weathering pulse from this osmium-isotope record is not straightforward. During OAE2, records of osmium isotopes from Demerara Rise in the Atlantic Ocean and Furlo, in the central Apennines, Italy, do not show any positive radiogenic enrichment, although the signal may be overridden by the strong, non-radiogenic influence of volcanic activity at the Caribbean–Colombian plateau or lost in a depositional gap (Turgeon and Creaser, 2008; Jenkyns, 2010). There is, however, evidence for a positive, radiogenic pulse in $^{87}Sr/^{86}Sr$ at the onset of OAE2, measured in foraminifera and rudist fossils, in the middle of a trend towards lower strontium-isotope ratios (Bralower et al., 1997; Frijia and Parente, 2008). The size of the pulse agrees with model results (e.g. Figure 3.7f) produced by forcing a short-lived threefold increase in weathering. In this manner, a radiogenic spike in $^{87}Sr/^{86}Sr$ can be produced without evoking a stratified ocean or a reduced residence time for strontium, as some previous studies, e.g. Frijia and Parente (2008), suggest. Oceanic strontium-isotope ratios are also being pulled in two directions by different sources and, in this case, the negative calcium-isotope excursion clarifies the balance of those two sources better than the strontium record itself, because calcium isotopes are so much less influenced by hydrothermal activity. Calcium is a major crustal ion and a key component in weathering reactions, and this new evidence agrees with, and furthers, trace-element isotope records (e.g. osmium and strontium) in describing an intense weathering response to OAEs.

The size and duration of the calcium-isotope excursions, if they are attributed solely

to weathering flux changes, can constrain the magnitude of the weathering response and its contribution to atmospheric CO_2 drawdown. The riverine calcium load includes silicate and carbonate weathering products, which are indistinguishable in their effects on the global calcium budget when they reach the ocean. Only silicate weathering has a long-term effect on the global carbon cycle, and as silicate weathering increases with temperature, a negative feedback mechanism is thought to maintain the climate balance on long timescales (Walker et al., 1981). Identifying a pulse of calcium delivery to the oceans is one of the most direct measurements of this active feedback. Modern calcium discharge is estimated to be one quarter derived from silicate weathering (Meybeck, 1987; Gaillardet et al., 1999). If this fraction is maintained proportionally during a weathering pulse, a tripling of delivered calcium to the oceans could increase the calcium flux from silicate weathering from 0.6×10^{13} mol/year to 1.8×10^{13} mol/year, which could sequester approximately ~0.2 Gt/year carbon during the most intense weathering periods. Over long timescales, this is an effective sink for large mass releases of atmospheric carbon and would have helped to stabilize climate after OAEs.

3.7 Conclusions

Four new high-resolution calcium-isotope records spanning OAE1a and OAE2 exhibit decreases in $\delta^{44/42}$Ca of 0.1–0.2‰ lasting 0.5–1.0 My. These data indicate a change in the ocean calcium-isotope composition, and a significant change to the global calcium cycle. A simple box model of ocean strontium and calcium isotopes demonstrates that the isotope history of these two OAEs is best explained by a threefold increase in continental weathering during the OAE, coupled to a longer-lived but less extreme change in hydrothermal activity. These calcium-isotope data support indications from strontium and osmium isotopes for a change in weathering during OAEs, but the fact that calcium is particularly responsive to riverine inputs, and that it is a major crustal component (unlike strontium and osmium) means that these calcium-isotope records provide more confidence in weathering changes as well as an ability to quantify the weathering flux increase during an OAE. Given that carbonate is a ubiquitous component of the sed-

imentary record, it is expected that similar variation in calcium isotopes will be found in carbonate records during other periods of major environmental change.

Acknowledgements

Thanks are due to Andrew Mason, Nick Belshaw, and Norman Charnley for assistance with mass spectrometry at Oxford. Samples from Resolution Guyot were obtained courtesy of the Ocean Drilling Program. Samples from the Coppitella section were collected by Valeria Luciani and Miriam Cobianchi. Harilaos Tsikos and Ken Amor helped in collecting the samples from Eastbourne and South Ferriby, respectively. The manuscript was improved by the suggestions of M.S. Fantle and two anonymous reviewers. Research funding was provided by a UK-IODP grant award from NERC (NE/G001316/1).

3.A Appendix

Table 3.1, Table 3.2, Table 3.3, and Table 3.4 were made available as Supplemental Data to Blättler et al. (2011). Additional photos of the samples and field localities are also presented here (Figure 3.8, Figure 3.9).

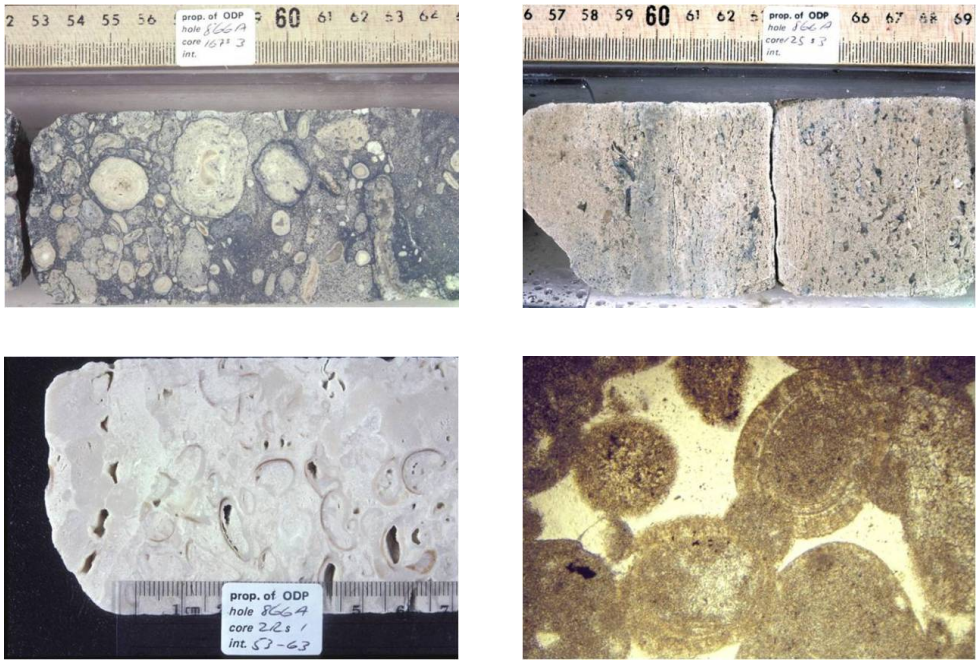

Figure 3.8: Photos of samples from Resolution Guyot (ODP Site 866A). Lower right image of ooids is approximately 1.5 mm across. Photos by H.C. Jenkyns.

Table 3.1: Resolution Guyot calcium-isotope data. Values of $\delta^{44/42}$Ca are relative to the carbonate standard NIST SRM915a.

Resolution Guyot, Mid-Pacific Mountains, ODP Leg 143, Hole 866A					
Core section		Interval	Depth (mbsf)	$\delta^{44/42}$Ca (‰)	2 SE
6R	CC	9–10	38.49	0.37	0.10
10R	CC	11–13	77.01	0.41	0.10
17R	CC	2–3	144.42	0.48	0.06
23R	CC	3–4	203.43	0.36	0.07
28R	CC	9–11	251.69	0.40	0.10
33R	CC	12–13	299.62	0.48	0.06
38R	01	53–54	343.23	0.40	0.07
43R	CC	21–22	386.51	0.44	0.09
45R	CC	38–40	405.98	0.44	0.10
48R	01	3–5	434.43	0.38	0.09
53R	01	1–5	482.71	0.24	0.10
55R	CC	18–19	502.08	0.13	0.07
58R	01	12–13	531.12	0.23	0.08
61R	01	68–69	560.58	0.18	0.09
63R	02	113–115	581.93	0.40	0.09
65R	01	3–6	598.63	0.34	0.06
70R	01	78–80	647.68	0.16	0.08
73R	01	120–122	677.00	0.19	0.10
76R	01	114–118	705.84	0.17	0.10
79R	03	141–143	738.06	0.17	0.10
82R	03	19–20	765.87	0.36	0.06
85R	02	145–149	794.70	0.26	0.08
89R	01	43–44	831.03	0.15	0.10
90R	CC	13–14	840.03	0.32	0.10
91R	01	65–66	850.15	0.32	0.10
91R	01	98–99	850.48	0.16	0.08
91R	02	26–27	851.02	0.26	0.10
93R	01	36–38	869.06	0.24	0.08
94R	01	57–60	878.97	0.31	0.06
98R	01	20–23	917.20	0.30	0.10
102R	01	97–98	953.67	0.21	0.09
109R	02	89–91	1021.93	0.29	0.06
112R	01	19–21	1049.09	0.41	0.06
118R	01	94–96	1107.74	0.46	0.09
121R	01	73–75	1136.43	0.42	0.06
126R	02	62–63	1185.91	0.38	0.10
130R	01	5–7	1222.65	0.32	0.06
138R	01	14–17	1299.64	0.29	0.06
143R	01	34–36	1348.24	0.32	0.08
147R	01	108–109	1387.18	0.53	0.10
153R	02	54–55	1446.06	0.31	0.06
155R	02	58–62	1465.49	0.25	0.09
157R	03	41–43	1486.17	0.26	0.08

Table 3.2: Coppitella calcium-isotope data. Stratigraphic heights are relative to the base of the section. Values of $\delta^{44/42}$Ca are relative to the carbonate standard NIST SRM915a.

Coppitella, Gargano, Italy		
Height (m)	$\delta^{44/42}$Ca (‰)	2 SE
27.15	−0.29	0.05
25.90	−0.28	0.05
24.75	−0.32	0.05
23.60	−0.31	0.05
17.00	−0.44	0.05
15.90	−0.17	0.05
14.80	−0.43	0.05
13.60	−0.35	0.05
12.38	−0.41	0.05
11.18	−0.38	0.05
9.98	−0.42	0.05
8.75	−0.39	0.05
7.65	−0.52	0.05
6.50	−0.41	0.05
5.65	−0.49	0.05
4.60	−0.21	0.05
2.60	−0.33	0.05
1.40	−0.25	0.05
0.75	−0.44	0.05
0.00	−0.17	0.04

Table 3.3: Eastbourne calcium-isotope data. Stratigraphic heights are relative to the base of the section. Values of $\delta^{44/42}$Ca are relative to the carbonate standard NIST SRM915a.

Eastbourne, Sussex, UK		
Height (m)	$\delta^{44/42}$Ca (‰)	2 SE
26.90	0.25	0.08
25.90	0.25	0.05
24.90	0.25	0.06
23.90	0.25	0.07
22.90	0.22	0.06
21.90	0.18	0.07
20.90	0.18	0.07
19.90	0.18	0.05
18.90	0.24	0.08
17.90	0.21	0.06
16.90	0.24	0.07
15.90	0.19	0.06
14.90	0.08	0.05
13.90	0.15	0.05
13.00	0.10	0.07
12.00	0.08	0.05
11.00	0.09	0.07
10.00	0.20	0.07
9.00	0.11	0.07
8.00	0.11	0.07
7.00	0.15	0.08
6.00	0.14	0.06
5.00	0.19	0.06
4.00	0.15	0.08
3.00	0.16	0.07
2.00	0.22	0.08
1.00	0.15	0.06
0.00	0.15	0.07

Figure 3.9: Photos of the Eastbourne chalk section covering the Cenomanian–Turonian OAE2. Photos by H.C. Jenkyns.

Table 3.4: South Ferriby calcium-isotope data. Stratigraphic heights are relative to the base of the section, with the base of the Black Band at 1.00 m. Values of $\delta^{44/42}$Ca are relative to the carbonate standard NIST SRM915a, and δ^{13}C are relative to VPDB.

South Ferriby, Lincolnshire, UK			
Height (m)	$\delta^{44/42}$Ca (‰)	2 SE	δ^{13}C (‰)
3.00	0.18	0.04	
2.50	0.15	0.04	3.36
2.00			3.33
1.95			3.28
1.90	0.06	0.05	3.18
1.85			3.20
1.80			3.23
1.75			3.19
1.70	0.24	0.09	3.26
1.65			3.16
1.60			3.23
1.55			3.16
1.50	−0.02	0.06	3.34
1.45			3.31
1.40			3.31
1.35			3.39
1.30	−0.04	0.06	3.34
1.25			3.48
1.20			3.61
1.15	−0.04	0.06	3.70
1.10			3.52
1.05			3.73
1.00	0.07	0.09	4.15
1.00*	−0.07	0.06	4.15
0.95			4.39
0.90	0.01	0.06	4.50
0.85	0.15	0.06	3.34
0.80			3.28
0.75			3.39
0.70			3.25
0.65	0.07	0.06	3.31
0.60			3.23
0.55			3.21
0.50			3.24
0.45	0.13	0.06	3.25
0.40			3.25
0.35			3.08
0.30			3.16
0.25	0.23	0.09	3.19
0.20			3.08
0.15			3.07
0.10			3.09
0.05	0.09	0.06	3.08
0.00			3.16

*duplicate measurement

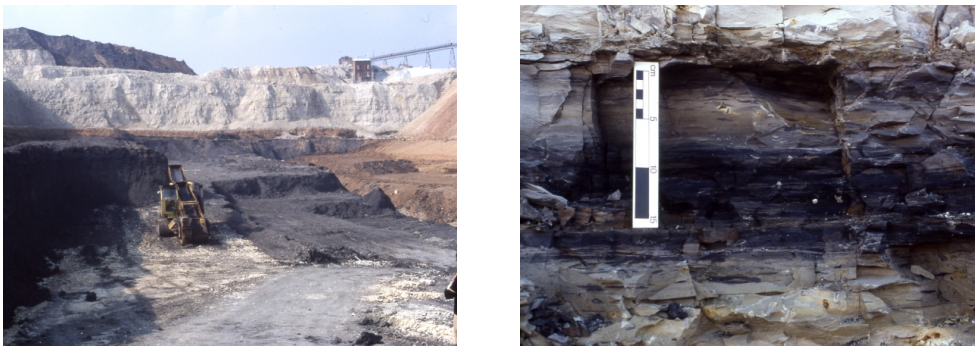

Figure 3.10: Photos of South Ferriby quarry (left) and the Black Band (right) representing the condensed Cenomanian–Turonian OAE2. Photos by H.C. Jenkyns.

Calcium-isotope records from additional sedimentary sections provide further information about how sedimentary carbonate records marine calcium-isotope ratios during the Cretaceous OAEs as well as other events. A shallow-water carbonate platform from Raia del Pedale, Italy, that records the characteristic two-step positive carbon-isotope excursion of OAE2 (Parente et al., 2008) has surprisingly invariant $\delta^{44/42}$Ca values throughout the OAE (Figure 3.11). The section consists of marly limestone with an ~8 m interval of yellow laminated shale at the Cenomanian–Turonian Boundary and thin dark laminated shale intervals interspersed at irregular intervals higher in the section. The lower part of the section is dolomitized, with dolomite rhombs present throughout the limestone, indicating that chemical alteration and recrystallization have significantly affected the section. The English Chalk, by contrast, sampled at Eastbourne and South Ferriby, has never been involved in an orogenic event and remains largely unlithified. The lack of a negative $\delta^{44/42}$Ca excursion at Raia del Pedale suggests that chemical alteration during the formation of the Southern Apennines has damped the small signal recorded from changing seawater calcium-isotope ratios. This result suggests that calcium-isotope ratios are best preserved in diagenetically immature sections, such as marine sediment cores and unlithified carbonate sediment.

In addition to OAE1a and OAE2, other abrupt climate perturbations in the geological record are expected to generate perturbations in the calcium cycle. Two of the largest such events in the Phanerozoic are the Toarcian OAE and the Paleocene–Eocene Thermal Maximum (PETM), from which preliminary calcium-isotope records have been measured.

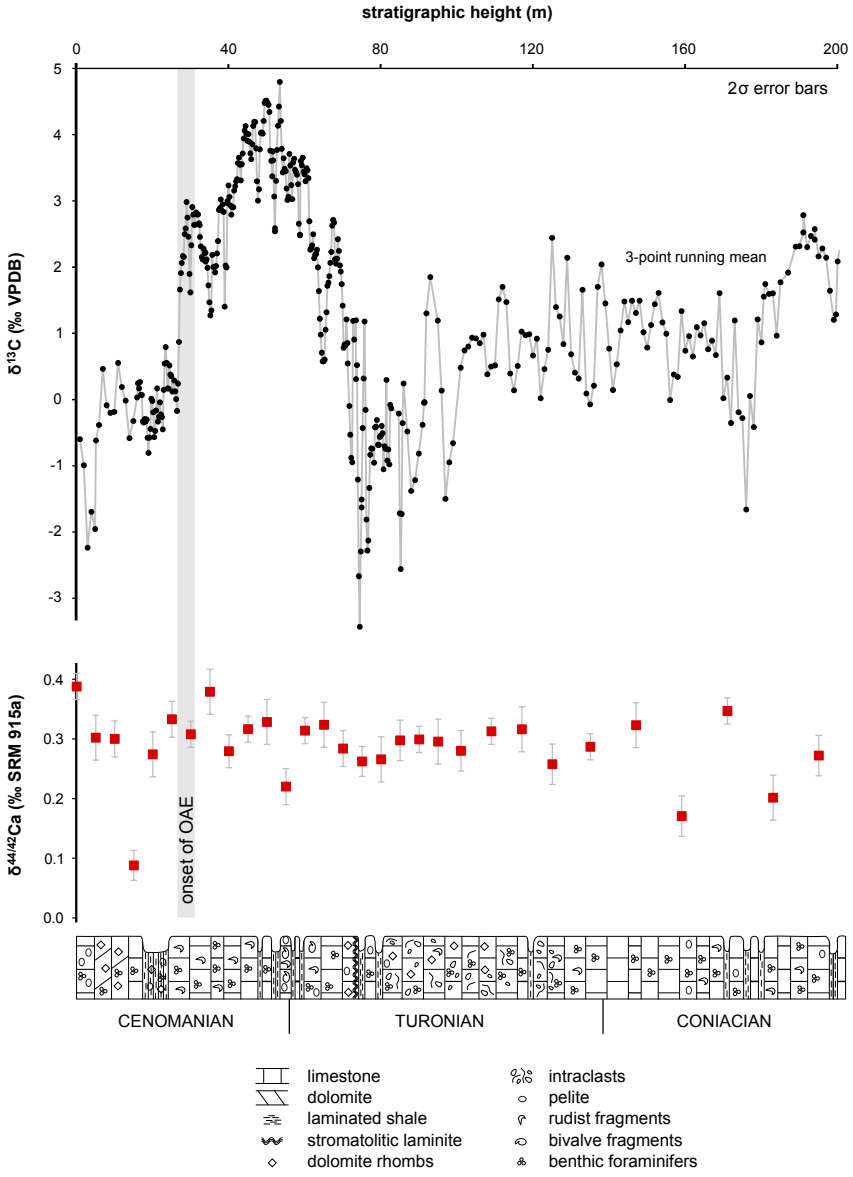

Figure 3.11: Calcium- and carbon-isotope ratios covering the OAE2 interval from Raia del Pedale, Italy. The stratigraphic log is adapted from H.C. Jenkyns. Values for $\delta^{13}C$ are from Parente et al. (2008) and unpublished data.

Table 3.5: Raia del Pedale calcium-isotope data. Stratigraphic heights are relative to the base of the section. Values of $\delta^{44/42}$Ca are relative to the carbonate standard NIST SRM915a.

Raia del Pedale, Italy		
Height (m)	$\delta^{44/42}$Ca (‰)	2 SE
195.00	0.76	0.03
183.00	0.68	0.04
171.00	0.83	0.02
159.00	0.66	0.03
147.00	0.80	0.04
135.00	0.77	0.02
125.00	0.75	0.03
117.00	0.79	0.04
109.00	0.80	0.02
101.00	0.77	0.03
95.00	0.77	0.04
90.00	0.78	0.02
85.00	0.79	0.03
80.00	0.74	0.04
75.00	0.74	0.03
70.00	0.77	0.03
65.00	0.80	0.04
60.00	0.80	0.02
55.00	0.71	0.03
50.00	0.81	0.04
45.00	0.80	0.02
40.00	0.77	0.03
35.00	0.86	0.04
30.00	0.79	0.02
25.00	0.82	0.03
20.00	0.75	0.04
15.00	0.57	0.03
10.00	0.79	0.03
5.00	0.78	0.04
0.00	0.87	0.02

The Port Mulgrave and Hawkser Bottoms sections in Yorkshire, England record the Toarcian OAE interval in geochemically well studied organic-rich mudrock, with perturbations observed in total organic carbon (TOC), organic matter $\delta^{13}C$, Mo-isotope ratios, and Os-isotope ratios (Cohen et al., 2004; Kemp et al., 2005; Pearce et al., 2008). The record of $\delta^{13}C$ in organic carbon contains a negative excursion of $-6.5‰$, with astronomical cyclicity revealed from high-resolution analyses (Kemp et al., 2005). Fossil belemnites collected throughout the section were analyzed for calcium-isotope ratios (Figure 3.12), but do not show a reliable trend. Multiple belemnites from the same stratigraphic level record values over a range of $\sim 0.3‰$, which would be inconsistent with globally uniform $\delta^{44/42}Ca$ values of seawater and a constant fractionation factor for belemnite fossils. The stratigraphic test performed with fossils from the Belemnite Bed (see section 2.4) suggests that belemnites are indeed a reliable archive for marine calcium-isotope ratios, so the non-reproducibility of the Yorkshire belemnites may be due to the effects of regional oceanography on local conditions or individual fossils. The organic-rich mudstones reflect deposition in a restricted anoxic basin, whose calcium-isotope composition may have deviated from that of global ocean seawater. Sedimentary carbonate derived from an environment that was clearly in communication with the world oceans would provide a more reliable record of calcium-isotope changes during the Toarcian OAE.

Another test for recording calcium-isotope ratios during the Toarcian OAE was performed with the lithologically unusual Junction Bed in Dorset, England. The sedimentology of this unit and its lateral variability is thoroughly described in Jenkyns and Senior (1991). The pinkish, fossiliferous limestone overlies a brown marlstone and represents a highly condensed sequence with stromatolitic textures, dark brown iron-rich intervals, and occasionally convoluted bedding. The bed is 40–70 cm thick at different localities and records a large negative excursion in $\delta^{13}C$ of $-7‰$, although this signal may be affected by diagenesis (see Figure 3.13). A close correlation between $\delta^{18}O$ and $\delta^{13}C$ values ($R^2 = 0.72$) could be due to kinetic isotope fractionation during chemical alteration, although correlation of primary carbon- and oxygen-isotope ratios in response to environmental conditions is also possible, and similar stable-isotope profiles have been mea-

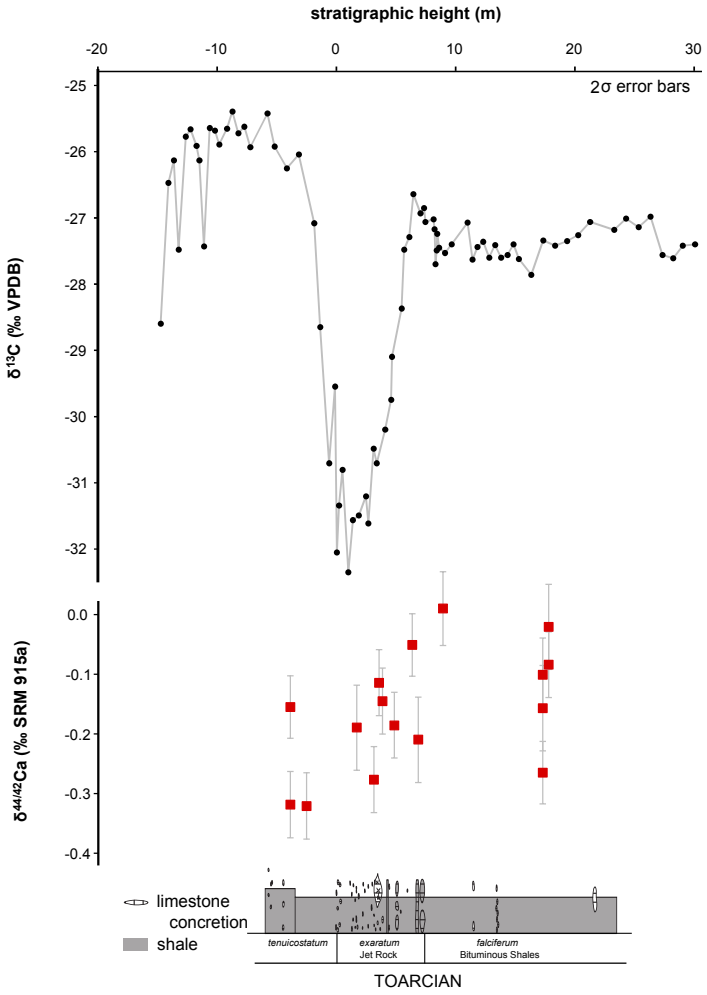

Figure 3.12: Calcium- and carbon-isotope ratios covering the Toarcian OAE interval from Port Mulgrave and Hawkser Bottoms, Yorkshire, England. Carbon isotopes of organic matter are from Cohen et al. (2004). The stratigraphic log is reproduced from that in Hesselbo and Jenkyns (1995).

Table 3.6: Yorkshire calcium-isotope data from Port Mulgrave and Hawkser Bottoms. Stratigraphic heights are relative to the base of the Jet Rock. Values of $\delta^{44/42}$Ca are relative to the carbonate standard NIST SRM915a.

Yorkshire, UK		
Height (m)	$\delta^{44/42}$Ca (‰)	2 SE
17.80	−0.08	0.06
17.80	−0.02	0.07
17.30	−0.27	0.05
17.30	−0.16	0.07
17.30	−0.10	0.06
8.93	0.01	0.06
6.86	−0.21	0.07
6.36	−0.05	0.05
4.86	−0.19	0.06
3.86	−0.15	0.06
3.57	−0.11	0.06
3.14	−0.28	0.06
1.70	−0.19	0.07
−2.50	−0.32	0.06
−3.86	−0.32	0.06
−3.86	−0.16	0.05

sured in the Junction Bed where sampled at other locations (Jenkyns and Clayton, 1997). Calcium-isotope ratios from both bulk carbonate and belemnite fossils were measured, including paired measurements of the two carbonate phases from the same stratigraphic level, where possible. Bulk carbonate $\delta^{44/42}$Ca values are generally within error or slightly higher than belemnite $\delta^{44/42}$Ca, suggesting that the fractionation factor between seawater and belemnite calcite is slightly larger than that for bulk carbonate in this setting. Although the Toarcian OAE was a more extreme and longer lasting event than OAE1a or OAE2, no comparable calcium-isotope excursion is evident in the Junction Bed in either carbonate phase. The condensed nature of the section and uncertainties in the interpretation of the carbon-isotope excursion and the stratigraphic location of the Toarcian OAE do not rule out the presence of a calcium-isotope response to this event. A suitable archive of sedimentary carbonate deposited during this interval, which is a challenging condition to meet due to the age of the event (~183 Ma) and the lack of undisturbed deep-ocean sediments, remains to be analyzed.

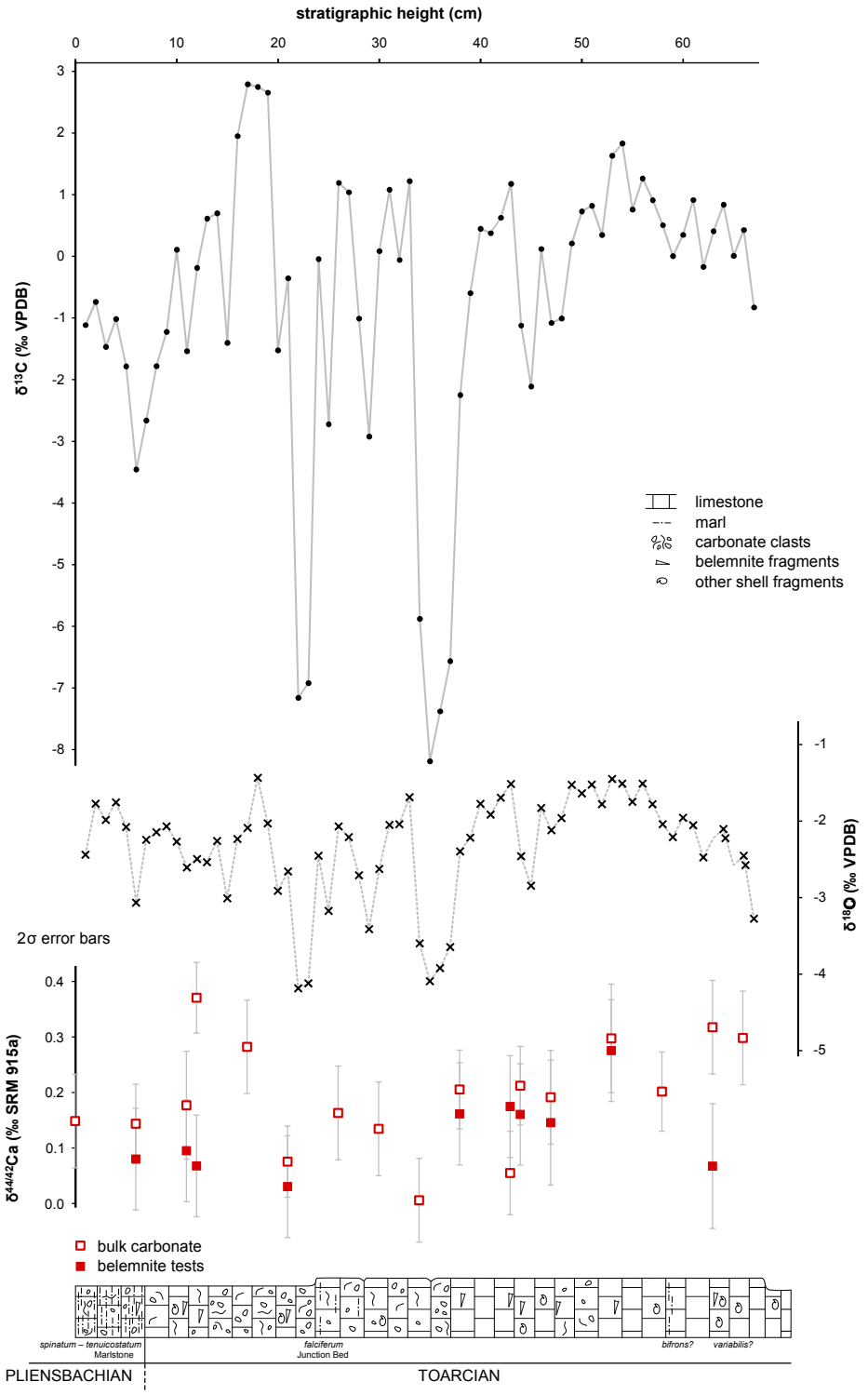

Figure 3.13: Calcium-, carbon-, and oxygen-isotope ratios covering the Toarcian OAE interval from the Junction Bed, Dorset, England. Values of $\delta^{13}C$ and $\delta^{18}O$, as well as $\delta^{44/42}Ca$ represented by open squares, are derived from powdered bulk carbonate samples, whereas $\delta^{44/42}Ca$ measurements represented by solid squares are from belemnite tests.

Table 3.7: Junction Bed calcium-isotope data. Stratigraphic heights are relative to the base of the limestone unit. Values of $\delta^{44/42}$Ca are relative to the carbonate standard NIST SRM915a, and δ^{13}C and δ^{18}O are relative to VPDB.

Junction Bed, Dorset, UK						
Height (cm)	$\delta^{44/42}$Ca (‰) belemnites	2 SE	$\delta^{44/42}$Ca (‰) bulk carbonate	2 SE	δ^{13}C (‰)	δ^{18}O (‰)
67					−0.83	−3.28
66			0.30	0.08	0.43	−2.45
65					0.01	−2.58
64					0.84	−2.10
63	0.07	0.11	0.32	0.08	0.41	−2.22
62					−0.17	−2.47
61					0.92	−2.05
60					0.35	−1.95
59					0.01	−2.21
58			0.20	0.07	0.51	−2.04
57					0.91	−1.78
56					1.26	−1.51
55					0.76	−1.75
54					1.83	−1.51
53	0.28	0.09	0.30	0.10	1.63	−1.45
52					0.35	−1.78
51					0.82	−1.52
50					0.73	−1.64
49					0.21	−1.52
48					−1.01	−1.96
47	0.15	0.11	0.19	0.08	−1.08	−2.12
46					0.12	−1.83
45					−2.11	−2.85
44	0.16	0.09	0.21	0.07	−1.12	−2.46
43	0.18	0.09	0.06	0.08	1.18	−1.51
42					0.63	−1.69
41					0.38	−1.91
40					0.45	−1.77
39					−0.59	−2.21
38	0.16	0.09	0.21	0.07	−2.25	−2.40
37					−6.56	−3.65
36					−7.37	−3.92
35					−8.18	−4.09
34			0.01	0.08	−5.87	−3.60
33					1.22	−1.69
32					−0.06	−2.04
31					1.08	−2.05
30			0.13	0.08	0.09	−2.63
29					−2.92	−3.41
28					−1.01	−2.71
27					1.04	−2.21
26			0.16	0.08	1.19	−2.07
25					−2.72	−3.18
24					−0.04	−2.45
23					−6.91	−4.12
22					−7.15	−4.19
21	0.03	0.09	0.08	0.06	−0.35	−2.66
20					−1.52	−2.91
19					2.66	−2.03

Continued on next page

Table 3.7: *Continued*

Height (cm)	$\delta^{44/42}$Ca (‰) belemnites	2 SE	$\delta^{44/42}$Ca (‰) bulk carbonate	2SE	δ^{13}C (‰)	δ^{18}O (‰)
18					2.75	−1.43
17			0.28	0.08	2.79	−2.09
16					1.95	−2.23
15					−1.40	−3.01
14					0.70	−2.26
13					0.61	−2.54
12	0.07	0.09	0.37	0.06	−0.19	−2.50
11	0.10	0.09	0.18	0.10	−1.53	−2.61
10					0.11	−2.27
9					−1.22	−2.07
8					−1.78	−2.15
7					−2.66	−2.24
6	0.08	0.09	0.14	0.07	−3.45	−3.07
5					−1.78	−2.08
4					−1.01	−1.75
3					−1.46	−1.98
2					−0.73	−1.77
1					−1.11	−2.44
0			0.15	0.08		

A geologically younger event with similar climatic implications to the Cretaceous OAEs, the PETM, is another possible candidate for identifying weathering feedbacks through measurement of calcium-isotope ratios. The Forada section of the Venetian pre-Alps represents a hemipelagic, near-continental depositional setting during the Early Cenozoic (Giusberti et al., 2007). The carbon-isotope excursion of the PETM begins at the base of a clay marl unit, with a 2–3 mm-thick laminated black clay layer, and the recovery continues into the limestone–marl couplets above (see Figure 3.14). Limited samples were available for calcium-isotope analysis, and the few $\delta^{44/42}$Ca values obtained do not definitively suggest any trend or lack thereof. The expected response for seawater calcium-isotope ratios can be modelled using constraints from studies of the carbon cycle during the PETM. Significant seafloor carbonate dissolution is evident from pelagic sediment cores (Zachos et al., 2005), although the model presented in section 3.6.2 above indicates that this additional source of calcium would not be large enough to modify oceanic $\delta^{44/42}$Ca significantly. Greenhouse warming during the PETM would be expected to produce a silicate weathering feedback and increased riverine calcium input, as during the Cretaceous OAEs, but the timescale of the PETM, estimated at ~10 ky for ocean acidi-

fication to begin reversing, ~50 ky for the main decrease in carbon-isotope values, and 120–220 ky for full recovery of the carbon cycle (Röhl et al., 2000; Farley and Eltgroth, 2003; Zachos et al., 2005), would be too short to influence seawater calcium-isotope ratios to a measurable degree. A modelled shutdown of the carbonate sink and increase in riverine calcium due to weathering over the timescale of the PETM generates a negative shift in $\delta^{44/40}$Ca of only 0.07‰. Further investigation of the PETM in reliable carbonate sections might confirm this behaviour and support the modelling of the calcium cycle as described in this chapter.

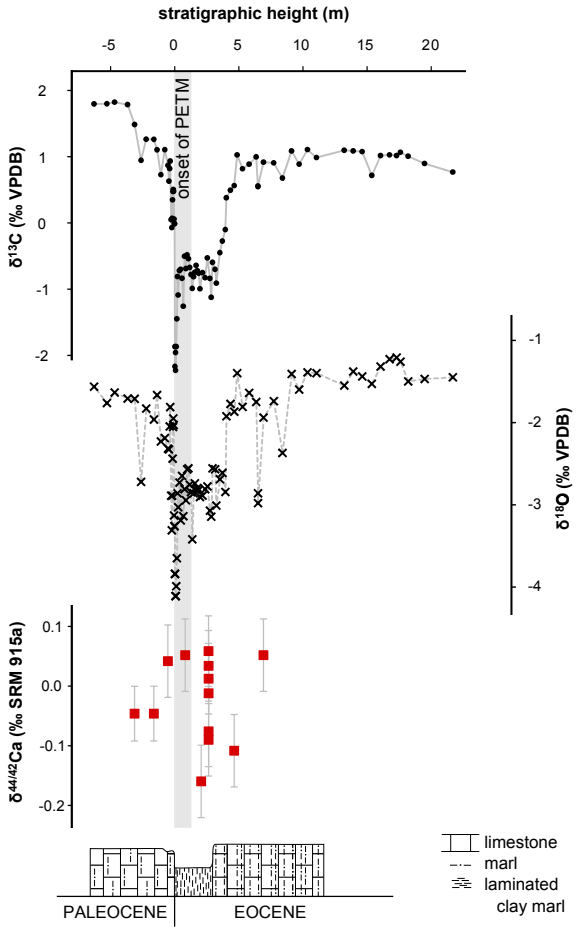

Figure 3.14: Calcium-, carbon-, and oxygen-isotope ratios covering the PETM interval from Forada, Italy. Stratigraphic information and values of δ^{13}C and δ^{18}O are from Giusberti et al. (2007).

The calcium-isotope data from these additional sedimentary sections do not change the interpretations of the calcium cycle and the Cretaceous OAEs presented in the above chapter. They signal the need for complete, diagenetically immature carbonate sections in

Table 3.8: Forada calcium-isotope data. Stratigraphic heights are relative to the onset of the PETM (at the Paleocene–Eocene boundary). Values of $\delta^{44/42}$Ca are relative to the carbonate standard NIST SRM915a.

Forada, Italy		
Height (m)	$\delta^{44/42}$Ca (‰)	2 SE
6.93	0.05	0.06
4.64	−0.11	0.06
2.65	0.01	0.05
2.65*	0.03	0.06
2.65*	−0.08	0.06
2.65*	0.06	0.06
2.65*	−0.09	0.06
2.65*	−0.01	0.06
2.08	−0.16	0.06
0.83	0.05	0.06
−0.52	0.04	0.06
−1.62	−0.05	0.05
−3.12	−0.05	0.05

*replicate measurement

order to record the small but significant variation in calcium-isotope ratios during extreme climate perturbations. Concerns about the reliability of carbon-isotope stratigraphy reflect similar reasoning, with the best preserved data originating from deep-ocean sediments which have not been uplifted in orogenic events. The small magnitude of calcium-isotope variation, relative to current measurement precision, makes $\delta^{44/42}$Ca excursions susceptible to significant damping, depending on the rates of deposition and recrystallization of carbonate sediment. For this reason, the strategic investigation of geological events correlated across several localities is important, both to confirm stratigraphic reproducibility of global ocean signals as well as to test the faithful preservation of isotopic signals in the sedimentary material.

Chapter 4

Explaining the Phanerozoic Ca-isotope history of seawater

This chapter will be published in very similar form in the journal *Geology* (Blättler et al., 2012). Supplementary information accompanying that version is provided below as an appendix.

4.1 Introduction

Measurements on fossil carbonates show that the Ca-isotope composition of seawater has varied throughout Phanerozoic time (Farkaš et al., 2007a). The dominant feature of the record is a shift toward higher Ca-isotope ratios in the Carboniferous, with a shift of comparable magnitude observed in the Mesozoic or Cenozoic (Figure 4.1). The differing ratio of aragonite to calcite precipitated during times of 'aragonite seas' and 'calcite seas' has been proposed as a mechanism for generating oscillations in seawater Ca-isotope ratios (Farkaš et al., 2007a), but the isotope data do not show a strong oscillatory response to intervals of changing seawater chemistry, particularly during the Cretaceous. To explain the single, large change in Ca-isotope composition observed in the Carboniferous, together with the lack of comparable shifts during the rest of the Phanerozoic, requires further consideration of the evolving carbonate sink over time to include various modes of carbonate secretion, precipitation and burial. This study presents a Ca-isotope budget

based on modern marine calcite and aragonite, which provides quantitative constraints with which to test the Ca-isotope response of ancient seawater to changing components of the carbonate sink.

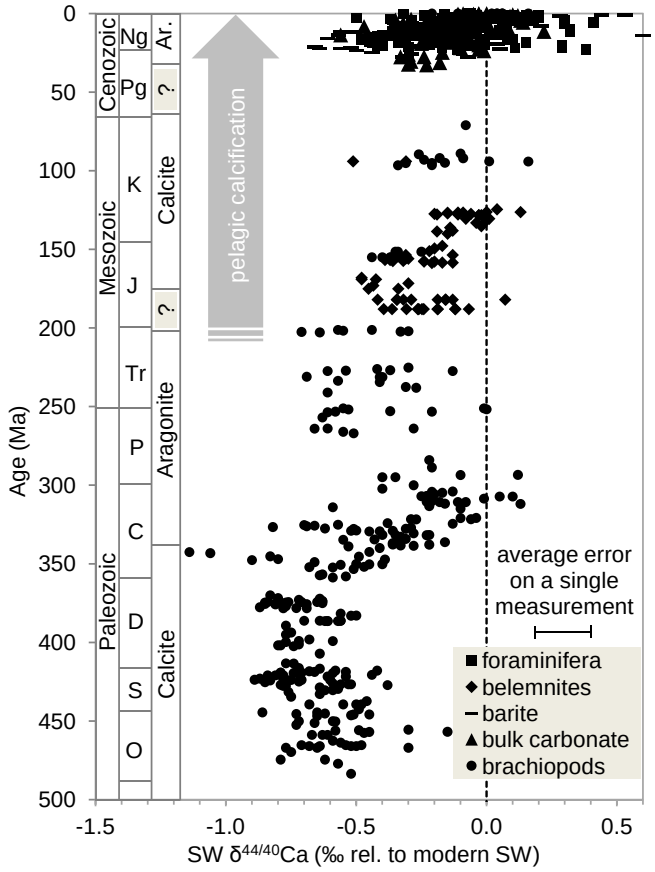

Figure 4.1: The Phanerozoic $\delta^{44/40}$Ca record of seawater from fossil carbonate and barite (details in Appendix). Measured $\delta^{44/40}$Ca values are corrected for expected species-dependent isotope fractionation from seawater in order to reconstruct the seawater value in which they formed. No corrections are made for temperature-dependent fractionation in this reconstruction. The majority of the data is reconstructed from diagenetically screened primary calcite of fossil brachiopods (fractionated from seawater by −0.9‰) or belemnites (fractionated by −1.4‰) published by Farkaš et al. (2007a), with additional contributions from Farkaš et al. (2007b) and this study. Cenozoic data include measurements of planktic foraminifera, deep-sea bulk carbonate, or marine barite, calibrated to modern samples (Fantle and DePaolo, 2005; Heuser et al., 2005; Fantle and DePaolo, 2007; Sime et al., 2007; Griffith et al., 2008a). Timescale for geological eras and periods from Ogg et al. (2008) and for aragonite sea and calcite sea intervals from Sandberg (1983).

Marine carbonates are enriched in the light isotopes of Ca relative to seawater, giving them a lower $\delta^{44/40}$Ca (isotopic ratios are reported relative to seawater throughout this study as $\delta^{44/40}\text{Ca} = [(^{44}\text{Ca}/^{40}\text{Ca})_{sample} / (^{44}\text{Ca}/^{40}\text{Ca})_{seawater} - 1] \cdot 1000$). Present-day seawater $\delta^{44/40}$Ca is uniform (Hippler et al., 2003), due to the large oceanic reservoir of

Ca (1.3×10^{19} mol) and its long residence time (0.5–1.0 My). Carbonate burial is the only major sink for oceanic Ca, so the isotopic fractionation between seawater and average marine carbonate determines how isotopically enriched is the world ocean relative to its sources. Although some studies have used changes in the input isotope ratio to explain Cenozoic seawater $\delta^{44/40}$Ca trends (e.g. Griffith et al., 2008a), Ca from riverine and groundwater discharge and from hydrothermal exchange reactions is expected to be isotopically stable through time (Schmitt et al., 2003a; Tipper et al., 2010) and is therefore unlikely to be a major cause of variation.

Large changes in the size of input fluxes may produce short-term (~1 My) excursions in seawater $\delta^{44/40}$Ca during periods of extreme environmental change before the system returns to steady state (Payne et al., 2010; Blättler et al., 2011), but long-term variation must be caused by changing isotope ratios of the inputs or outputs. Due to the relative homogeneity of the inputs, changes in fractionation of the carbonate sink are likely to have been the cause of major seawater $\delta^{44/40}$Ca variations over geological time.

In this study, the modern carbonate sink is characterized using a compilation of published $\delta^{44/40}$Ca data together with new measurements that extend the coverage of its quantitatively important components. Different types of carbonate show distinctive $\delta^{44/40}$Ca based on mineralogy and the process of biocalcification. Mass-balance models of the carbonate sink can use these isotopic signatures to test possible explanations for the $\delta^{44/40}$Ca record of Phanerozoic seawater.

4.2 Samples and methods

Ca-isotope ratios were measured in a range of modern carbonates, with a focus on taxa and environments not already widely sampled. In addition, several belemnites of Jurassic to Cretaceous age were analyzed. Over 50 measurements were made using MC-ICP-MS, following methods described in the Appendix and in Blättler et al. (2011). Measured values of $\delta^{44/42}$Ca relative to NIST SRM915a (with 2 SE analytical uncertainties of 0.06–0.08‰) were converted to $\delta^{44/40}$Ca relative to seawater using the difference between seawater and SRM915a of +1.88‰ (Hippler et al., 2003). New measurements are presented

along with literature values, which are also compiled and converted to $\delta^{44/40}$Ca relative to seawater (full details in Appendix).

To enable direct comparison of carbonates formed in different environments, all modern $\delta^{44/40}$Ca data were normalized to a theoretical temperature of formation of 15 °C using published data where provided or temperature estimates for the sample locality from the World Ocean Atlas 2005 (Locarnini et al., 2006). A $\delta^{44/40}$Ca–temperature relationship of 0.02‰ per °C was used, which is similar to that which has been established for many different types of carbonate, including inorganic precipitates, scleractinian corals, coccoliths, and most foraminifera (Gussone et al., 2003, 2005; Böhm et al., 2006), with the possible exception of certain foraminifera, e.g. *G. sacculifer* (Nägler et al., 2000; Hippler et al., 2006). It is assumed that this weak temperature relationship, observed across such a wide range of carbonates, holds for the entire marine carbonate sink, and extrapolations are continued even beyond the temperatures at which certain marine calcifiers might live in order to identify patterns across phylogenetic groups. An approximate mean oceanic temperature was used, although the choice is arbitrary for determining mineralogical or phylogenetic patterns, in order to minimize the magnitude of any single correction. The temperature normalization of 0.02‰ per °C resulted in an average correction of ~0.1‰ and a maximum correction of 0.3‰.

4.3 Results

Nine major calcifying phyla, as well as non-skeletal carbonate ooids, are represented in a compilation of nearly 400 $\delta^{44/40}$Ca values (Figure 4.2). New data significantly expand the dataset for aragonite-producers, particularly cnidarians (corals) and chlorophytes (green algae). Three major groups can be identified within the dataset (Figure 4.2):

- Group 1: Aragonitic samples with $\delta^{44/40}\text{Ca} \approx -1.5$‰. Within this group, chlorophytes, aragonitic poriferans (sponges), and ooids are more strongly fractionated (−1.6‰). Reef-building cnidarians, both scleractinians and hydrozoans, have a slightly higher average (−1.45‰), while their deep-sea relatives have significantly

higher values (−1.1‰).

- Group 2: Calcitic samples with $\delta^{44/40}$Ca ≈ −0.9‰. This group consists of rhodophytes (coralline red algae), calcitic poriferans, and brachiopods.

- Group 3: Calcitic samples with $\delta^{44/40}$Ca ≈ −1.3‰. This group includes measurements of bulk deep-sea carbonate as well as individual measurements of foraminifera, both planktonic and benthonic, haptophytes (coccolithophorids), and echinoderms.

Molluscan skeletons, which can be aragonite, calcite, or both, cover the whole range of values for marine carbonates and cannot be easily assigned to one of these groups.

The $\delta^{44/40}$Ca for inorganic aragonite (≈ −1.7‰) and calcite (≈ −0.8‰) precipitated at 15 °C and average growth rates (Gussone et al., 2003; Marriott et al., 2004; Tang et al., 2008) bracket the range determined for most marine carbonate (grey lines in Figure 4.2). Groups 1 and 2 are close to the values for aragonite and calcite, respectively, while Group 3 occupies an intermediate position. No systematic difference is observed between samples of low-Mg and high-Mg calcite within these groups.

4.4 Discussion

4.4.1 Patterns of biocalcification

The $\delta^{44/40}$Ca of biogenic calcite is close to that expected from inorganically precipitated calcite for Group 2 taxa, in which the mechanism of biocalcification is relatively simple (Stanley, 2006). Inorganic experiments show aragonite to be ∼0.9‰ lighter than calcite (Gussone et al., 2003; Marriott et al., 2004; Tang et al., 2008), which is similar to the offset between skeletons of biologically simple organisms, e.g. between aragonitic and calcitic sponges or green/red algae. Although the theoretical mechanism governing this mineralogical offset is not established, the experimental growth-rate dependence of $\delta^{44/40}$Ca in calcite shown by Tang et al. (2008) and the kinetic model for Ca-isotope fractionation described by DePaolo (2011) suggest that it may be linked to the energetics and rates of

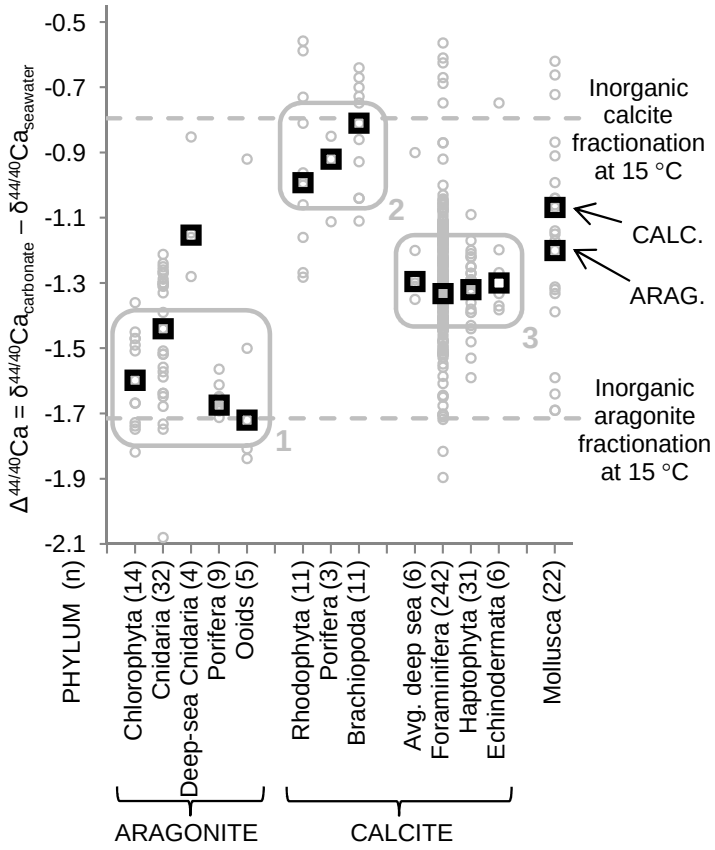

Figure 4.2: Ca-isotope measurements of modern carbonates, organized by phylum/division (details in Appendix). The vertical axis is presented in units of ‰ as the difference between carbonate $\delta^{44/40}$Ca and seawater (or experimental fluid) $\delta^{44/40}$Ca, which is equal to $\Delta^{44/40}$Ca or simply $\delta^{44/40}$Ca using seawater as the reference standard. All data are normalized to a temperature of 15 °C. Grey circles show individual samples; black squares are median values. Samples fall into three groups, identified by numbered boxes and discussed in the text.

ion attachment onto crystal growth surfaces. The preference for certain carbonate polymorphs at particular temperatures, e.g. higher temperatures favouring aragonite, would be consistent with inherent properties such as crystal structures and activation energies influencing mineral growth and kinetic Ca-isotope fractionation, as proposed by Gussone et al. (2005). The observation that simple biocalcifiers express to a large extent the inorganic offset between aragonite and calcite shows that unmoderated mineral growth kinetics are an essential component of these biogenic calcification mechanisms.

The $\delta^{44/40}$Ca of the more sophisticated biocalcifiers in Group 3 lies between those for inorganic calcite and aragonite. The specific biocalcification processes used by these taxa differ (Weiner and Dove, 2003), so the fact that their $\delta^{44/40}$Ca deviates similarly suggests that biological complexity has a first-order control on Ca-isotope fractionation, possibly due to active Ca^{2+}-transport. While higher $\delta^{44/40}$Ca values are characteristic of the high-Mg calcite produced by Group 1, the absence of any statistical difference between low-Mg and high-Mg calcite samples within Group 3 indicates that more detailed groupings based on mineralogy or biological control mechanisms would not have a discerning effect on the Ca-isotope budget developed below. In general, stronger control over biocalcification appears to produce skeletal $\delta^{44/40}$Ca intermediate between that of inorganic calcite and aragonite.

Mollusks are a good example of biological overprinting of the inorganic Ca-isotope signal. Heinemann et al. (2008) recorded an offset in $\delta^{44/40}$Ca of only ~0.25‰ between the aragonitic (nacreous) and calcitic (prismatic) portions of a blue mussel shell, noting the tightly controlled composition of the fluid from which the skeleton precipitates. Cnidarians also exhibit smaller fractionations than other types of biogenic aragonite, possibly due to controlled Ca^{2+}-transport effects (Böhm et al., 2006). The much higher $\delta^{44/40}$Ca of deep-sea corals may reflect a growth-rate effect, since they are known to grow much more slowly than reef-building corals (Adkins et al., 2004).

4.4.2 The modern Ca-isotope budget

A Ca-isotope budget for the modern ocean can be created using characteristic $\delta^{44/40}$Ca signatures of components of the carbonate sink. The carbonate budget of Milliman (1993) is taken as the basis for characterizing the Ca-isotope system. While significant uncertainty surrounds elements of this budget, and more recent assessments (e.g. Milliman and Droxler, 1996; Milliman et al., 1999; Berelson et al., 2007) are especially revisionary concerning pelagic production and dissolution fluxes and the relation between surface and deep-ocean carbon, the compartmentalization of the carbonate sink and environments of accumulation by Milliman (1993) is most illustrative of the compositional changes affecting the Ca-isotope budget. As a conservative estimate, deep-sea environments account for 55% of carbonate accumulation and are predominantly low-Mg calcite from planktic foraminifera and coccoliths (Milliman, 1993; Schiebel, 2002). These organisms have very similar $\delta^{44/40}$Ca, so deep-sea $\delta^{44/40}$Ca is effectively represented by the value for Group 3, with a fractionation from seawater of $-1.3‰$. Aragonite constitutes a small fraction of deep-sea carbonate, despite the existence of relatively large deep-water reefs, due to the very slow accumulation rate of asymbiotic corals (e.g. Fosså et al., 2002; Adkins et al., 2004). Pteropods may contribute ~10% of the pelagic carbonate flux (Berner and Honjo, 1981; Milliman, 1993), although the preferential dissolution of aragonite within sediments would cause it to have even less influence on deep-sea Ca-isotope ratios, since it is ultimately the burial and preservation of carbonate which determines the long-term, steady-state $\delta^{44/40}$Ca of seawater.

The remaining ~45% of carbonate accumulation occurs in a variety of shallow-water environments. These environments include significant contributions from the aragonitic producers of Group 1, such as reef corals (Hubbard et al., 1990; Riding, 2002; Vecsei, 2004) and carbonate sediment from ooids and chlorophytes (Neumann and Land, 1975; Wefer, 1980; Milliman et al., 1993). In particular, aragonitic *Halimeda* bioherms constitute a significant and previously underestimated contribution to shallow-water sediment (Rees et al., 2007). The shallow-water sink also includes smaller fractions of various Group 2 and Group 3 components, such as rhodophytes, benthic foraminifera, and echin-

oderms (Kiessling et al., 2003). Overall, Group 1 aragonite production is estimated to account for ~70% of the modern shallow-water sink, which translates to 30% of the total Ca removal (see compartmentalized estimates in Table 4.1).

The actual $\delta^{44/40}$Ca of the carbonate output flux must consider the temperature of precipitation of each type of carbonate, which can be approximated by the latitudinal distribution of relevant environments. For example, the tropical habitat of most corals means that the real $\delta^{44/40}$Ca measured is smaller than the temperature-normalized values used to compare different biocalcifiers. Accounting for this effect, the estimated average Ca-isotope fractionation during carbonate removal from seawater is -1.2 to $-1.3‰$, slightly lower than the value of $-1.12‰$ reported by Holmden et al. (2012), who utilized a smaller dataset and a single, tropical locality for the estimation of the shallow-water sink. These estimates agree with the analysis of Tipper et al. (2010), suggesting that the modern Ca cycle is within 10–15% of steady state.

4.4.3 The evolution of marine carbonate and Ca-isotope ratios

The isotopic differences between various types of carbonate suggest that their relative proportions are important for defining seawater $\delta^{44/40}$Ca. Intervals of calcite seas and aragonite seas, corresponding to the dominant mineralogy of non-skeletal carbonate as well as the composition of evaporites and fluid inclusions (Sandberg, 1983; Stanley and Hardie, 1998; Lowenstein et al., 2003), were initially proposed as a first-order explanation for variation in the Phanerozoic $\delta^{44/40}$Ca record of seawater (Farkaš et al., 2007a) without the support of a comprehensive dataset for modern marine calcifiers. Using the three groups of carbonate identified in this study, each with a characteristic $\delta^{44/40}$Ca, the effect of compositional changes in the carbonate sink can be assessed quantitatively with simple isotopic mass-balance models (see Figure 4.3).

In the modern aragonite sea, an estimated 70% of the shallow-water sink is aragonite, but during the last calcite sea of the mid-Jurassic to Paleogene, much smaller contributions would have been expected from Group 1 aragonitic biocalcifiers and ooids. The effect of this change on average global Ca-isotope fractionation would not have been

very large, however, due to the dominance in Jurassic to Recent carbonate production of deep-sea calcite with intermediate $\delta^{44/40}$Ca. The effect of changing from a Cretaceous calcite sea to a modern aragonite sea would have increased seawater $\delta^{44/40}$Ca by only 0.10–0.15‰, depending on the size of the deep-sea sink. The magnitude of this change would be smaller still if the modern fraction of carbonate production in the deep-sea is underestimated relative to the Pleistocene average (see dashed vs dotted lines, Figure 4.3). If lower sea level during glacial periods provided less area for shallow-water carbonate production than during the Holocene and other interglacials (e.g. Opdyke and Walker, 1992; Ryan et al., 2001), deep-sea calcite would have represented a larger proportion of the global sink and exerted more control on average Ca-isotope fractionation during the Pleistocene. In summary, during the Cenozoic, switching the dominant mineralogy of carbonate production in shallow seas is expected to have had little impact on the $\delta^{44/40}$Ca of seawater, due to the buffering effect of deep-sea calcite.

Prior to the development of pelagic calcification in the Mesozoic, however, carbonate removal operated very differently, with negligible deep-sea carbonate buried before the diversification and radiation of planktic foraminifera and coccolithophores in the Jurassic (Wilkinson and Algeo, 1989; Martin, 1995; Bown et al., 2004). Without the buffering effect of deep-sea carbonate, the shifts between aragonite seas and calcite seas would have had a much stronger effect on the global proportion of aragonite precipitated and thus on seawater $\delta^{44/40}$Ca. For example, during the Carboniferous transition from a calcite sea to an aragonite sea, if the aragonite portion of the carbonate sink grew from 10% to 80%, the average fractionation of carbonate and the steady-state $\delta^{44/40}$Ca of seawater would have increased by ~0.5‰ (solid line, Figure 4.3). Indeed, the largest step-change in Phanerozoic Ca-isotope history occurs during the Carboniferous and is consistent with the nature of the dominant mineralogy of marine carbonate.

This model can explain the single largest shift in seawater $\delta^{44/40}$Ca during the Paleozoic as due to a change from calcite to aragonite production, while also explaining the absence of large effects on $\delta^{44/40}$Ca at subsequent switches from calcite to aragonite seas. Observations about the composition of reefs and carbonate platforms over the Phanero-

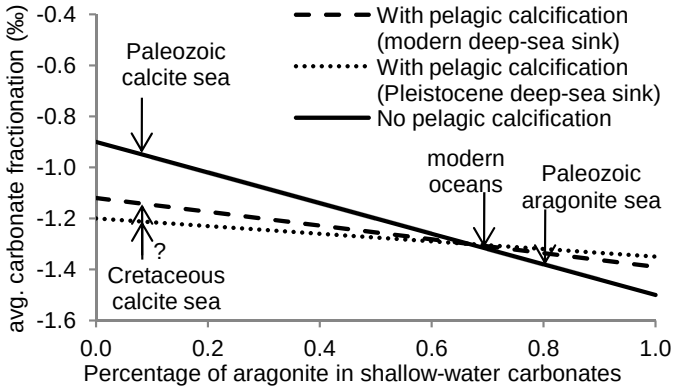

Figure 4.3: Model calculations of the effect of different states of the carbonate sink on the average fractionation of marine carbonate from seawater. As the fractionation becomes larger, i.e. toward more negative $\delta^{44/40}$Ca, seawater $\delta^{44/40}$Ca becomes higher by the same magnitude. The deep-sea sink has a fractionation of $-1.3‰$, and the shallow-water sink is a mixture between Group 1 aragonite (with a fractionation of $-1.5‰$) and Group 2 calcite ($-0.9‰$). The modern shallow-water sink (dashed line) represents 45% of global carbonate burial; the Pleistocene average shallow-water sink (dotted line) is reduced to 25% of global carbonate burial. With no pelagic calcification (solid line), shallow-water carbonates represent the entire global carbonate sink. Arrows show expected fractionations for various periods of Earth history, using estimates of the composition of the carbonate output (details in Appendix). Note the large change in fractionation predicted by the switch from calcite to aragonite seas in the Paleozoic, compared to the much smaller change between Cretaceous and younger oceans.

zoic are consistent with this basic model for controlling seawater $\delta^{44/40}$Ca, although the proportion of aragonite or calcite in ancient sediment is impossible to quantify fully.

In the calcite sea of the mid-Paleozoic, seawater $\delta^{44/40}$Ca was $\sim 0.7‰$ lower than today, suggesting that the fractionation between seawater and carbonate was significantly smaller. This hypothesis is supported by the dominant calcifiers of the fossil record, predominantly organisms with inferred weak Ca-isotope fractionation due to their simple biocalcification processes and likely members of Group 2: reefs were constructed by hypercalcifying bryozoans, perhaps with a similar $\delta^{44/40}$Ca to their lophophorate relatives the brachiopods, calcitic tabulate and rugose corals, calcitic sponges, and stromotoporoids (Hubbard et al., 1990; Wood, 1995; Stanley, 2006). Non-reefal platform carbonates were rich in microbial and oolitic calcite (Kiessling et al., 2003), whose $\delta^{44/40}$Ca would likely have resembled that of inorganic calcite. The transition to an aragonite sea in the Carboniferous, coincident with the pronounced shift in seawater $\delta^{44/40}$Ca, was also accompanied by a shift in the composition of reef and platform carbonates toward

Group 1 and Group 3 taxa. Aragonitic skeletons of phylloid algae, dasycladacean algae, chaetetid sponges, sphinctozoan and inozoan sponges, bivalve mollusks, and scleractinian corals were all important sediment contributors during this aragonite sea interval (Wood, 1995; Stanley, 2006), as were the more strongly fractionated calcite skeletons of benthic foraminifera (Kiessling et al., 2003). These observations suggest that an increased Ca-isotope fractionation of carbonate caused higher seawater $\delta^{44/40}$Ca during this period.

The transition back to a calcite sea in the Early Jurassic was accompanied by a shift toward calcitic taxa, with rudist bivalves, foraminifera, and coccolithophorids becoming major calcifiers (Martin, 1995; Wood, 1995; Bown et al., 2004). In contrast to the Group 2 taxa prevalent in the Paleozoic calcite sea, these organisms were the more sophisticated biomineralizers of Group 3 with lower $\delta^{44/40}$Ca that would not have produced as large a decrease in seawater $\delta^{44/40}$Ca. Aragonitic scleractinian corals also persisted throughout this calcite sea interval (Stanley, 2006) and may have contributed to maintaining higher seawater $\delta^{44/40}$Ca. Most importantly, the development of pelagic calcification, resulting in relatively decreased carbonate burial on shelves and continental margins and relatively increased burial in the deep oceans (Wilkinson and Algeo, 1989; Wallmann, 2001), began to buffer the effects of an isotopically variable shallow-water sink.

Besides the composition of the carbonate sink, global temperature and dolomitization rate may contribute significantly to seawater $\delta^{44/40}$Ca variability. Periods of global warmth would result in decreased average fractionation and lower seawater $\delta^{44/40}$Ca, although global mean temperature anomalies of 10 °C would be expected to affect this ratio by only ~0.2‰. Lowered global temperature may have been the cause of high $\delta^{44/40}$Ca in the Late Carboniferous 'icehouse' relative to the lower values of the Permo–Triassic 'greenhouse', there being no obvious change in proportions of aragonite to calcite sediment producers over this interval.

4.5 Conclusions

The carbonate system is a crucial component of both short-term and long-term climate stability, and the history of carbonate precipitation can now be linked to the Phanerozoic

Ca-isotope record of seawater. A modern Ca-isotope budget reveals that different groups of taxa exhibit distinctive $\delta^{44/40}$Ca values that reflect a combination of biological control and mineralogical effects on Ca-isotope fractionation. The changing proportions of these groups provide a mechanism for explaining the history of seawater $\delta^{44/40}$Ca values. Shifts between aragonite seas and calcite seas, most notably in the Carboniferous Period, significantly affected seawater $\delta^{44/40}$Ca before the mid-Mesozoic development of pelagic calcification. After this development, changes in the composition of shallow-water carbonates were buffered by a deep-sea carbonate sink (primarily coccoliths and planktic foraminifera), so that switches from calcite to aragonite seas had only minor impact on seawater $\delta^{44/40}$Ca values.

Acknowledgements

Thanks are due to T.J. Horner for Ca sample cuts and W.J. Kennedy for Cretaceous belemnite samples. The manuscript was improved by the suggestions of editor Ellen Thomas and two anonymous reviewers.

4.A Appendix

Supplementary Material for Blättler et al. (2012) provides additional information about analytical methods and data processing. An expanded methods description details sample preparation and mass spectrometry (not included here, see Chapter 2 for a more complete description). To clarify the reconstructed Phanerozoic seawater data shown in Figure 4.1, two supplementary figures are provided. Figure 4.4 shows an expanded view of the condensed upper Cenozoic data, where the different phase reconstructions can be more clearly distinguished. Figure 4.5 identifies the different phases used with different colours, showing the raw data where each phase is reported relative to the same standard, and then the seawater reconstruction where each phase has been offset by the species-specific fractionation factor. The datasets represented by the figures in this chapter are presented with full details and citations in Table 4.1, Table 4.2, Table 4.3, and Table 4.4.

In addition, photographs of several samples analyzed for this chapter are included here in Figure 4.6.

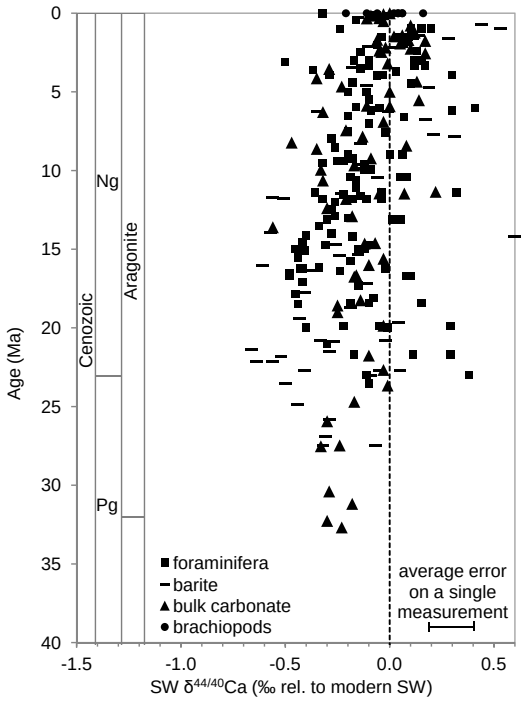

Figure 4.4: An expanded version of Figure 4.1, showing only data from 0–40Ma.

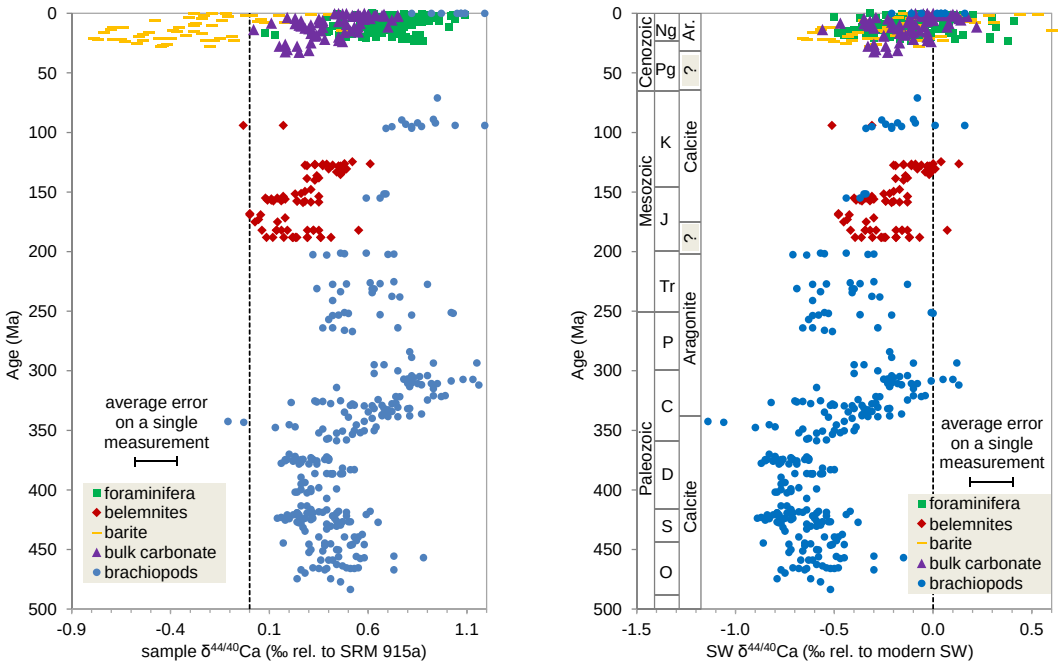

Figure 4.5: Data from Figure 4.1 shown as raw Ca-isotope values measured against the carbonate standard SRM915a (left), and seawater Ca-isotope values reconstructed by applying constant offsets for each fossil phase used (right).

Table 4.1: Model budget and calculations. Carbonate budget calculations for the modern ocean and estimates for past oceans. Habitats and percent carbonate removal are from Milliman (1993). Predominant types of carbonate and group percentages are estimated from several sources (Neumann and Land, 1975; Wefer, 1980; Hubbard et al., 1990; Milliman, 1993; Milliman et al., 1993; Riding, 2002; Schiebel, 2002; Kiessling et al., 2003). Proposed compositions of the carbonate sink for hypothetical past oceans are approximate and used to illustrate the mass-balance model.

Habitat	% carbonate removal	Predominant types of carbonate	% group 1, −1.5‰ (aragonite)	% group 2, −0.9‰ (calcite)	% group 3, −1.3‰ (calcite)	carbonate $\delta^{44/40}$Ca (‰)
MODERN OCEANS						
Shallow						
coral reef complex	22%	corals, red/green algae, forams, cement	90%	5%	5%	−1.46
banks/bays	6%	red/green algae, mollusks, forams, ooids	33%	33%	33%	−1.22
non-carbonate shelves	3%	forams, mollusks, echinoderms	10%	50%	40%	−1.12
carbonate shelves	9%	red algae, forams, echinoderms, mollusks	33%	33%	33%	−1.22
Halimeda bioherms	5%	green algae	95%	5%	0%	−1.47
Deep						
slopes	12%	forams, mollusks, echinoderms	0%	10%	90%	−1.26
imported to slopes	6%	detrital shelf material	10%	10%	80%	−1.28
enclosed basins	3%	coccoliths, planktic forams	10%	10%	80%	−1.28
deep sea	34%	coccoliths, planktic forams	0%	0%	100%	−1.30
Total	100%		30%	10%	60%	−1.32
accounting for temperature						−1.23
PAST OCEANS						
Pleistocene average		aragonitic shallow-water sink, larger deep-sea sink	15%	5%	80%	−1.31
Cretaceous calcite sea		calcitic shallow-water sink, larger deep-sea sink	5%	15%	80%	−1.25
Paleozoic aragonite sea		aragonitic shallow-water sink, no deep-sea sink	80%	20%	0%	−1.38
Paleozoic calcite sea		calcitic shallow-water sink, no deep-sea sink	10%	90%	0%	−0.96

Table 4.2: Reconstructed Ca-isotope ratios of seawater over time, including data from this study and compiled from the literature (Fantle and DePaolo, 2005; Heuser et al., 2005; Fantle and DePaolo, 2007; Farkaš et al., 2007a,b; Sime et al., 2007; Griffith et al., 2008a). Timescale is based on Ogg et al. (2008). Stratigraphy for Pliensbachian and Toarcian belemnites (this study) from Weedon and Jenkyns (1999) and Hesselbo and Jenkyns (1995). Seawater Ca-isotope values are reconstructed using calibrated fractionation factors for the analyzed fossil/phase. The calibration for fossil belemnites and brachiopods is from Farkaš et al. (2007b). For other phases, calibrations were performed by comparison with modern samples (see individual references). Data from phosphates are omitted due to poor calibrations. The difference in $\delta^{44/40}$Ca between SRM915a and modern seawater is taken to be 1.88‰ (Hippler et al., 2003).

Source	Location	Depth (m)	Age (Ma)	Material	Raw $\delta^{44/40}$Ca	±	Raw $\delta^{44/42}$Ca	±	Relative to standard	$\delta^{44/40}$Ca of ancient SW rel. to SRM 915a	$\delta^{44/40}$Ca of ancient SW rel. to modern SW
this study	Belemnite Bed, Dorset, UK	—	188	belemnite			0.15	0.08	SRM 915a	1.69	-0.19
	Belemnite Bed, Dorset, UK	—	188	belemnite			0.09	0.08	SRM 915a	1.57	−0.31
	Belemnite Bed, Dorset, UK	—	188	belemnite			0.15	0.08	SRM 915a	1.69	−0.19
	Belemnite Bed, Dorset, UK	—	188	belemnite			0.18	0.08	SRM 915a	1.76	−0.12
	Belemnite Bed, Dorset, UK	—	188	belemnite			0.11	0.08	SRM 915a	1.62	−0.26
	Belemnite Bed, Dorset, UK	—	188	belemnite			0.18	0.08	SRM 915a	1.76	−0.12
	Belemnite Bed, Dorset, UK	—	188	belemnite			0.06	0.08	SRM 915a	1.52	−0.36
	Belemnite Bed, Dorset, UK	—	188	belemnite			0.04	0.10	SRM 915a	1.49	−0.39
	Belemnite Bed, Dorset, UK	—	188	belemnite			0.21	0.10	SRM 915a	1.81	−0.07
	Belemnite Stone, Dorset, UK	—	188	belemnite			0.11	0.05	SRM 915a	1.62	−0.26
	Belemnite Stone, Dorset, UK	—	188	belemnite			0.12	0.05	SRM 915a	1.64	−0.24
	Belemnite Stone, Dorset, UK	—	188	belemnite			0.12	0.05	SRM 915a	1.63	−0.25
	Junction Bed, Dorset, UK	—	182	belemnite			0.08	0.09	SRM 915a	1.56	−0.32
	Junction Bed, Dorset, UK	—	182	belemnite			0.10	0.09	SRM 915a	1.59	−0.29
	Junction Bed, Dorset, UK	—	182	belemnite			0.07	0.09	SRM 915a	1.54	−0.34
	Junction Bed, Dorset, UK	—	182	belemnite			0.03	0.09	SRM 915a	1.46	−0.42
	Junction Bed, Dorset, UK	—	182	belemnite			0.16	0.09	SRM 915a	1.72	−0.16
	Junction Bed, Dorset, UK	—	182	belemnite			0.18	0.09	SRM 915a	1.75	−0.13
	Junction Bed, Dorset, UK	—	182	belemnite			0.16	0.09	SRM 915a	1.72	−0.16
	Junction Bed, Dorset, UK	—	182	belemnite			0.15	0.11	SRM 915a	1.69	−0.19
	Junction Bed, Dorset, UK	—	182	belemnite			0.28	0.09	SRM 915a	1.95	0.07
	Junction Bed, Dorset, UK	—	182	belemnite			0.07	0.11	SRM 915a	1.54	−0.34
	Burton Bradstock, Dorset, UK	—	175	belemnite			0.01	0.05	SRM 915a	1.43	−0.45
	Burton Bradstock, Dorset, UK	—	168	belemnite			0.00	0.05	SRM 915a	1.40	−0.48
	Burton Bradstock, Dorset, UK	—	169	belemnite			0.00	0.05	SRM 915a	1.40	−0.48
	Burton Bradstock, Dorset, UK	—	169	belemnite			0.03	0.05	SRM 915a	1.46	−0.42
	Burton Bradstock, Dorset, UK	—	173	belemnite			0.02	0.05	SRM 915a	1.45	−0.43

Continued on next page

Table 4.2: *Continued*

Source	Location	Depth (m)	Age (Ma)	Material	Raw $\delta^{44/40}Ca$	±	Raw $\delta^{44/42}Ca$	±	Relative to standard	$\delta^{44/40}Ca$ of ancient SW rel. to SRM 915a	$\delta^{44/40}Ca$ of ancient SW rel. to modern SW
	Burton Bradstock, Dorset, UK	—	171.6	belemnite			0.09	0.05	SRM 915a	1.58	−0.30
	Burton Bradstock, Dorset, UK	—	175	belemnite			0.07	0.06	SRM 915a	1.54	−0.34
	Mangyshlak Mts., W. Kazakhstan	—	94	belemnite			−0.02	0.04	SRM 915a	1.37	−0.51
	Holywell, Eastbourne, Sussex, UK	—	94	belemnite			0.09	0.04	SRM 915a	1.57	−0.31
Sime et al. (2007)	ODP Site 925, Ceara Rise (040N 043W)	1.83	0.02	*Globigerinoides trilobus*			0.31	0.04	SRM 915a	1.56	−0.32
	ODP Site 925, Ceara Rise (040N 043W)	16.04	0.45	*Globigerinoides trilobus*			0.39	0.02	SRM 915a	1.72	−0.16
	ODP Site 925, Ceara Rise (040N 043W)	32.03	1.01	*Globigerinoides trilobus*			0.35	0.03	SRM 915a	1.64	−0.24
	ODP Site 925, Ceara Rise (040N 043W)	45.93	1.50	*Globigerinoides trilobus*			0.45	0.04	SRM 915a	1.84	−0.04
	ODP Site 925, Ceara Rise (040N 043W)	60.29	2.01	*Globigerinoides trilobus*			0.44	0.03	SRM 915a	1.82	−0.06
	ODP Site 925, Ceara Rise (040N 043W)	74.28	2.49	*Globigerinoides trilobus*			0.40	0.03	SRM 915a	1.74	−0.14
	ODP Site 925, Ceara Rise (040N 043W)	89.34	2.98	*Globigerinoides trilobus*			0.42	0.04	SRM 915a	1.78	−0.10
	ODP Site 925, Ceara Rise (040N 043W)	103.93	3.52	*Globigerinoides trilobus*			0.40	0.04	SRM 915a	1.74	−0.14
	ODP Site 925, Ceara Rise (040N 043W)	115.63	3.97	*Globigerinoides trilobus*			0.44	0.03	SRM 915a	1.82	−0.06
	ODP Site 925, Ceara Rise (040N 043W)	128.14	4.48	*Globigerinoides trilobus*			0.52	0.02	SRM 915a	1.98	0.10
	ODP Site 925, Ceara Rise (040N 043W)	141.77	5.00	*Globigerinoides trilobus*			0.37	0.03	SRM 915a	1.68	−0.20
	ODP Site 925, Ceara Rise (040N 043W)	152.18	5.50	*Globigerinoides trilobus*			0.42	0.02	SRM 915a	1.78	−0.10
	ODP Site 925, Ceara Rise (040N 043W)	161.30	5.96	*Globigerinoides trilobus*			0.39	0.03	SRM 915a	1.72	−0.16
	ODP Site 925, Ceara Rise (040N 043W)	176.90	6.51	*Globigerinoides trilobus*			0.37	0.04	SRM 915a	1.68	−0.20
	ODP Site 925, Ceara Rise (040N 043W)	192.39	6.98	*Globigerinoides trilobus*			0.42	0.06	SRM 915a	1.78	−0.10
	ODP Site 925, Ceara Rise (040N 043W)	200.69	7.50	*Globigerinoides trilobus*			0.37	0.05	SRM 915a	1.68	−0.20
	ODP Site 925, Ceara Rise (040N 043W)	208.94	7.99	*Globigerinoides trilobus*			0.33	0.04	SRM 915a	1.60	−0.28
	ODP Site 925, Ceara Rise (040N 043W)	226.24	8.51	*Globigerinoides trilobus*			0.34	0.04	SRM 915a	1.62	−0.26
	ODP Site 925, Ceara Rise (040N 043W)	234.57	9.02	*Globigerinoides trilobus*			0.37	0.05	SRM 915a	1.68	−0.20
	ODP Site 925, Ceara Rise (040N 043W)	240.72	9.50	*Globigerinoides trilobus*			0.31	0.05	SRM 915a	1.56	−0.32
	ODP Site 925, Ceara Rise (040N 043W)	247.64	9.95	*Globigerinoides trilobus*			0.41	0.03	SRM 915a	1.76	−0.12
	ODP Site 925, Ceara Rise (040N 043W)	261.89	10.59	*Globigerinoides trilobus*			0.39	0.02	SRM 915a	1.72	−0.16
	ODP Site 925, Ceara Rise (040N 043W)	269.67	11.11	*Globigerinoides trilobus*			0.39	0.03	SRM 915a	1.72	−0.16
	ODP Site 925, Ceara Rise (040N 043W)	276.31	11.49	*Globigerinoides trilobus*			0.36	0.05	SRM 915a	1.66	−0.22
	ODP Site 925, Ceara Rise (040N 043W)	282.22	12.02	*Globigerinoides trilobus*			0.34	0.03	SRM 915a	1.62	−0.26
	ODP Site 925, Ceara Rise (040N 043W)	289.66	12.47	*Globigerinoides trilobus*			0.33	0.04	SRM 915a	1.60	−0.28
	ODP Site 925, Ceara Rise (040N 043W)	298.07	13.00	*Globigerinoides trilobus*			0.37	0.01	SRM 915a	1.68	−0.20
	ODP Site 925, Ceara Rise (040N 043W)	304.74	13.55	*Globigerinoides trilobus*			0.30	0.04	SRM 915a	1.54	−0.34
	ODP Site 925, Ceara Rise (040N 043W)	315.93	13.98	*Globigerinoides trilobus*			0.33	0.04	SRM 915a	1.60	−0.28

Continued on next page

Table 4.2: *Continued*

Source	Location	Depth (m)	Age (Ma)	Material	Raw $\delta^{44/40}$Ca	±	Raw $\delta^{44/42}$Ca	±	Relative to standard	$\delta^{44/40}$Ca of ancient SW rel. to SRM 915a	$\delta^{44/40}$Ca of ancient SW rel. to modern SW
	ODP Site 925, Ceara Rise (040N 043W)	314.69	14.14	*Globigerinoides trilobus*			0.27	0.03	SRM 915a	1.48	−0.40
	ODP Site 925, Ceara Rise (040N 043W)	323.36	14.56	*Globigerinoides trilobus*			0.26	0.01	SRM 915a	1.46	−0.42
	ODP Site 925, Ceara Rise (040N 043W)	342.84	15.51	*Globigerinoides trilobus*			0.25	0.03	SRM 915a	1.44	−0.44
	ODP Site 925, Ceara Rise (040N 043W)	357.85	16.15	*Globigerinoides trilobus*			0.30	0.02	SRM 915a	1.54	−0.34
	ODP Site 925, Ceara Rise (040N 043W)	369.39	16.52	*Globigerinoides trilobus*			0.23	0.05	SRM 915a	1.40	−0.48
	ODP Site 925, Ceara Rise (040N 043W)	381.69	17.06	*Globigerinoides trilobus*			0.26	0.03	SRM 915a	1.46	−0.42
	ODP Site 925, Ceara Rise (040N 043W)	411.03	18.11	*Globigerinoides trilobus*			0.43	0.03	SRM 915a	1.80	−0.08
Fantle and DePaolo (2007)	ODP Site 807, Ontong Java Plateau (040N 157E)	0.95	0.06	deep sea carbonate ooze	−0.49	0.11			bulk Earth	1.85	−0.03
	ODP Site 807, Ontong Java Plateau (040N 157E)	4.64	0.31	deep sea carbonate ooze	−0.51	0.13			bulk Earth	1.83	−0.05
	ODP Site 807, Ontong Java Plateau (040N 157E)	18.55	1.23	deep sea carbonate ooze	−0.34	0.08			bulk Earth	2.00	0.12
	ODP Site 807, Ontong Java Plateau (040N 157E)	78.73	3.54	deep sea carbonate ooze	−0.75	0.20			bulk Earth	1.59	−0.29
	ODP Site 807, Ontong Java Plateau (040N 157E)	104.97	4.35	deep sea carbonate ooze	−0.33	0.04			bulk Earth	2.01	0.13
	ODP Site 807, Ontong Java Plateau (040N 157E)	164.64	5.88	deep sea carbonate ooze	−0.57	0.18			bulk Earth	1.77	−0.11
	ODP Site 807, Ontong Java Plateau (040N 157E)	166.14	5.91	deep sea carbonate ooze	−0.46	0.28			bulk Earth	1.88	0.00
	ODP Site 807, Ontong Java Plateau (040N 157E)	209.49	6.90	deep sea carbonate ooze	−0.49	0.30			bulk Earth	1.85	−0.03
	ODP Site 807, Ontong Java Plateau (040N 157E)	250.49	7.84	deep sea carbonate ooze	−0.59	0.03			bulk Earth	1.75	−0.13
	ODP Site 807, Ontong Java Plateau (040N 157E)	275.86	8.42	deep sea carbonate ooze	−0.38	0.08			bulk Earth	1.96	0.08
	ODP Site 807, Ontong Java Plateau (040N 157E)	305.15	9.67	deep sea carbonate ooze	−0.63	0.06			bulk Earth	1.71	−0.17
	ODP Site 807, Ontong Java Plateau (040N 157E)	334.97	11.35	deep sea carbonate ooze	−0.24	0.16			bulk Earth	2.10	0.22
	ODP Site 807, Ontong Java Plateau (040N 157E)	336.75	11.46	deep sea carbonate ooze	−0.39	0.05			bulk Earth	1.95	0.07
	ODP Site 807, Ontong Java Plateau (040N 157E)	362.31	12.90	deep sea carbonate ooze	−0.64	0.08			bulk Earth	1.70	−0.18
	ODP Site 807, Ontong Java Plateau (040N 157E)	391.72	14.64	deep sea carbonate ooze	−0.58	0.07			bulk Earth	1.76	−0.12
	ODP Site 807, Ontong Java Plateau (040N 157E)	424.87	16.65	deep sea carbonate ooze	−0.62	0.13			bulk Earth	1.72	−0.16
	ODP Site 807, Ontong Java Plateau (040N 157E)	426.45	16.74	deep sea carbonate ooze	−0.63	0.07			bulk Earth	1.71	−0.17
	ODP Site 807, Ontong Java Plateau (040N 157E)	451.11	18.24	deep sea carbonate ooze	−0.60	0.21			bulk Earth	1.74	−0.14
	ODP Site 807, Ontong Java Plateau (040N 157E)	478.00	19.86	deep sea carbonate ooze	−0.49	0.10			bulk Earth	1.85	−0.03
	ODP Site 807, Ontong Java Plateau (040N 157E)	509.24	21.76	deep sea carbonate ooze	−0.56	0.16			bulk Earth	1.78	−0.10
	ODP Site 807, Ontong Java Plateau (040N 157E)	536.06	22.67	deep sea carbonate ooze	−0.49	0.04			bulk Earth	1.85	−0.03
	ODP Site 807, Ontong Java Plateau (040N 157E)	565.98	23.66	deep sea carbonate ooze	−0.47	0.08			bulk Earth	1.87	−0.01
	ODP Site 807, Ontong Java Plateau (040N 157E)	596.69	24.69	deep sea carbonate ooze	−0.63	0.08			bulk Earth	1.71	−0.17
	ODP Site 807, Ontong Java Plateau (040N 157E)	634.22	25.93	deep sea carbonate ooze	−0.76	0.07			bulk Earth	1.58	−0.30
	ODP Site 807, Ontong Java Plateau (040N 157E)	680.36	27.47	deep sea carbonate ooze	−0.70	0.04			bulk Earth	1.64	−0.24
	ODP Site 807, Ontong Java Plateau (040N 157E)	681.98	27.52	deep sea carbonate ooze	−0.79	0.03			bulk Earth	1.55	−0.33

Continued on next page

Table 4.2: *Continued*

Source	Location	Depth (m)	Age (Ma)	Material	Raw $\delta^{44/40}$Ca	±	Raw $\delta^{44/42}$Ca	±	Relative to standard	$\delta^{44/40}$Ca of ancient SW rel. to SRM 915a	$\delta^{44/40}$Ca of ancient SW rel. to modern SW
	ODP Site 807, Ontong Java Plateau (040N 157E)	709.56	30.39	deep sea carbonate ooze	−0.75	0.07			bulk Earth	1.59	−0.29
	ODP Site 807, Ontong Java Plateau (040N 157E)	738.58	31.18	deep sea carbonate ooze	−0.64	0.06			bulk Earth	1.70	−0.18
	ODP Site 807, Ontong Java Plateau (040N 157E)	778.59	32.26	deep sea carbonate ooze	−0.76	0.11			bulk Earth	1.58	−0.30
	ODP Site 807, Ontong Java Plateau (040N 157E)	794.38	32.68	deep sea carbonate ooze	−0.69	0.21			bulk Earth	1.65	−0.23
Fantle and DePaolo (2005)	Holocene average		0.00	carbonate sediment	−0.36	0.15			bulk Earth	1.88	0.00
	DSDP Site 590, Lord Howe Rise (031S 163 E)	0.08	0.15	carbonate sediment	−0.45	0.10			bulk Earth	1.79	−0.09
	DSDP Site 590, Lord Howe Rise (031S 163 E)	3.00	0.33	carbonate sediment	−0.47	0.10			bulk Earth	1.77	−0.11
	DSDP Site 590, Lord Howe Rise (031S 163 E)	5.80	0.50	carbonate sediment	−0.39	0.10			bulk Earth	1.85	−0.03
	DSDP Site 590, Lord Howe Rise (031S 163 E)	10.46	0.78	carbonate sediment	−0.26	0.10			bulk Earth	1.98	0.10
	DSDP Site 590, Lord Howe Rise (031S 163 E)	22.15	1.40	carbonate sediment	−0.30	0.10			bulk Earth	1.94	0.06
	DSDP Site 590, Lord Howe Rise (031S 163 E)	23.66	1.47	carbonate sediment	−0.34	0.20			bulk Earth	1.90	0.02
	DSDP Site 590, Lord Howe Rise (031S 163 E)	28.15	1.69	carbonate sediment	−0.42	0.23			bulk Earth	1.82	−0.06
	DSDP Site 590, Lord Howe Rise (031S 163 E)	28.40	1.70	carbonate sediment	−0.27	0.20			bulk Earth	1.97	0.09
	DSDP Site 590, Lord Howe Rise (031S 163 E)	29.65	1.76	carbonate sediment	−0.19	0.10			bulk Earth	2.05	0.17
	DSDP Site 590, Lord Howe Rise (031S 163 E)	33.25	1.92	carbonate sediment	−0.31	0.16			bulk Earth	1.93	0.05
	DSDP Site 590, Lord Howe Rise (031S 163 E)	39.25	2.18	carbonate sediment	−0.38	0.10			bulk Earth	1.86	−0.02
	DSDP Site 590, Lord Howe Rise (031S 163 E)	41.36	2.26	carbonate sediment	−0.26	0.10			bulk Earth	1.98	0.10
	DSDP Site 590, Lord Howe Rise (031S 163 E)	44.35	2.38	carbonate sediment	−0.41	0.10			bulk Earth	1.83	−0.05
	DSDP Site 590, Lord Howe Rise (031S 163 E)	46.30	2.46	carbonate sediment	−0.40	0.25			bulk Earth	1.84	−0.04
	DSDP Site 590, Lord Howe Rise (031S 163 E)	48.85	2.55	carbonate sediment	−0.19	0.10			bulk Earth	2.05	0.17
	DSDP Site 590, Lord Howe Rise (031S 163 E)	68.01	3.19	carbonate sediment	−0.37	0.40			bulk Earth	1.87	−0.01
	DSDP Site 590, Lord Howe Rise (031S 163 E)	106.45	4.14	carbonate sediment	−0.71	0.20			bulk Earth	1.53	−0.35
	DSDP Site 590, Lord Howe Rise (031S 163 E)	133.75	4.66	carbonate sediment	−0.59	0.13			bulk Earth	1.65	−0.23
	DSDP Site 590, Lord Howe Rise (031S 163 E)	152.96	4.99	carbonate sediment	−0.36	0.27			bulk Earth	1.88	0.00
	DSDP Site 590, Lord Howe Rise (031S 163 E)	152.96	4.99	foraminifera	−0.47	0.10			bulk Earth	1.77	−0.11
	DSDP Site 590, Lord Howe Rise (031S 163 E)	184.76	5.53	carbonate sediment	−0.22	0.10			bulk Earth	2.02	0.14
	DSDP Site 590, Lord Howe Rise (031S 163 E)	223.71	6.28	carbonate sediment	−0.68	0.16			bulk Earth	1.56	−0.32
	DSDP Site 590, Lord Howe Rise (031S 163 E)	272.52	7.44	carbonate sediment	−0.57	0.10			bulk Earth	1.67	−0.21
	DSDP Site 590, Lord Howe Rise (031S 163 E)	299.75	8.22	carbonate sediment	−0.83	0.13			bulk Earth	1.41	−0.47
	DSDP Site 590, Lord Howe Rise (031S 163 E)	313.00	8.62	carbonate sediment	−0.71	0.19			bulk Earth	1.53	−0.35
	DSDP Site 590, Lord Howe Rise (031S 163 E)	331.60	9.22	carbonate sediment	−0.45	0.10			bulk Earth	1.79	−0.09
	DSDP Site 590, Lord Howe Rise (031S 163 E)	353.60	9.95	carbonate sediment	−0.69	0.10			bulk Earth	1.55	−0.33
	DSDP Site 590, Lord Howe Rise (031S 163 E)	373.70	10.63	carbonate sediment	−0.68	0.10			bulk Earth	1.56	−0.32

Continued on next page

Table 4.2: *Continued*

Source	Location	Depth (m)	Age (Ma)	Material	Raw $\delta^{44/40}$Ca	±	Raw $\delta^{44/42}$Ca	±	Relative to standard	$\delta^{44/40}$Ca of ancient SW rel. to SRM 915a	$\delta^{44/40}$Ca of ancient SW rel. to modern SW
	DSDP Site 590, Lord Howe Rise (031S 163 E)	373.70	10.63	foraminifera	−0.52	0.16			bulk Earth	1.72	−0.16
	DSDP Site 590, Lord Howe Rise (031S 163 E)	398.80	11.45	carbonate sediment	−0.41	0.10			bulk Earth	1.83	−0.05
	DSDP Site 590, Lord Howe Rise (031S 163 E)	409.90	11.80	carbonate sediment	−0.57	0.48			bulk Earth	1.67	−0.21
	DSDP Site 590, Lord Howe Rise (031S 163 E)	430.60	12.39	carbonate sediment	−0.66	0.16			bulk Earth	1.58	−0.30
	DSDP Site 590, Lord Howe Rise (031S 163 E)	435.60	13.60	carbonate sediment	−0.92	0.21			bulk Earth	1.32	−0.56
	DSDP Site 590, Lord Howe Rise (031S 163 E)	448.30	14.61	carbonate sediment	−0.43	0.13			bulk Earth	1.81	−0.07
	DSDP Site 590, Lord Howe Rise (031S 163 E)	461.30	15.60	carbonate sediment	−0.39	0.10			bulk Earth	1.85	−0.03
	Graves Creek 15	—	15.75	foraminifera	-0.55	0.15			bulk Earth	1.69	−0.19
	DSDP Site 590, Lord Howe Rise (031S 163 E)	462.6	16.00	carbonate sediment	−0.46	0.19			bulk Earth	1.78	−0.10
	Graves Creek 14	—	17.85	foraminifera	-0.81	0.11			bulk Earth	1.43	−0.45
	DSDP Site 590, Lord Howe Rise (031S 163 E)	477	18.57	carbonate sediment	−0.61	0.10			bulk Earth	1.63	−0.25
	DSDP Site 590, Lord Howe Rise (031S 163 E)	487.3	19.00	carbonate sediment	−0.61	0.13			bulk Earth	1.63	−0.25
	DSDP Site 400	—	20.00	foraminifera	−0.37	0.15			bulk Earth	1.87	−0.01
Griffith et al. (2008a)	Holocene coretops		0.00	barite	−2.01	0.15			SW	1.89	0.01
	ODP Site 572 (001N 134W)	3.85	0.24	barite	−2.17	0.13			SW	1.73	−0.15
	ODP Site 572 (001N 134W)	6.30	0.41	barite	−2.08				SW	1.82	−0.06
	ODP Site 572 (001N 134W)	10.93	0.72	barite	−1.58	0.04			SW	2.32	0.44
	ODP Site 572 (001N 134W)	14.15	0.94	barite	−1.49	0.37			SW	2.41	0.53
	ODP Site 572 (001N 134W)	20.75	1.39	barite	−1.88				SW	2.02	0.14
	ODP Site 572 (001N 134W)	23.84	1.60	barite	−1.91	0.39			SW	1.99	0.11
	ODP Site 572 (001N 134W)	23.84	1.60	barite	−1.74				SW	2.16	0.28
	ODP Site 572 (001N 134W)	32.72	2.20	barite	−2.00				SW	1.90	0.02
	ODP Site 572 (001N 134W)	67.63	4.71	barite	−1.83	0.21			SW	2.07	0.19
	ODP Site 572 (001N 134W)	140.62	6.23	barite	−2.37	0.18			SW	1.53	−0.35
	ODP Site 572 (001N 134W)	209.92	7.84	barite	−1.71	0.29			SW	2.19	0.31
	ODP Site 572 (001N 134W)	229.55	8.26	barite	−2.16	0.09			SW	1.74	−0.14
	ODP Site 572 (001N 134W)	314.20	11.69	barite	−2.58	0.10			SW	1.32	−0.56
	ODP Site 573 (001N 133W)	170.77	9.86	barite	−2.17	0.18			SW	1.73	−0.15
	ODP Site 573 (001N 133W)	188.73	11.45	barite	−2.25	0.13			SW	1.65	−0.23
	ODP Site 573 (001N 133W)	303.50	21.47	barite	−2.31	0.00			SW	1.59	−0.29
	ODP Site 573 (001N 133W)	311.61	21.82	barite	−2.54				SW	1.36	−0.52
	ODP Site 574 (004N 113W)	10.30	2.12	barite	−2.12	0.22			SW	1.78	−0.10
	ODP Site 574 (004N 113W)	19.50	3.46	barite	−2.20				SW	1.70	−0.18

Continued on next page

Table 4.2: *Continued*

Source	Location	Depth (m)	Age (Ma)	Material	Raw $\delta^{44/40}$Ca	±	Raw $\delta^{44/42}$Ca	±	Relative to standard	$\delta^{44/40}$Ca of ancient SW rel. to SRM 915a	$\delta^{44/40}$Ca of ancient SW rel. to modern SW
	ODP Site 574 (004N 113W)	27.34	4.60	barite	−2.13				SW	1.77	−0.11
	ODP Site 574 (004N 113W)	39.92	6.25	barite	−2.03				SW	1.87	−0.01
	ODP Site 574 (004N 113W)	45.47	6.77	barite	−1.85				SW	2.05	0.17
	ODP Site 574 (004N 113W)	55.32	7.70	barite	−1.81				SW	2.09	0.21
	ODP Site 574 (004N 113W)	77.52	9.64	barite	−2.17	0.32			SW	1.73	−0.15
	ODP Site 574 (004N 113W)	150.55	13.94	barite	−2.59	0.21			SW	1.31	−0.57
	ODP Site 574 (004N 113W)	198.08	16.02	barite	−2.63				SW	1.27	−0.61
	ODP Site 574 (004N 113W)	224.00	17.15	barite	−2.13	0.19			SW	1.77	−0.11
	ODP Site 574 (004N 113W)	238.50	17.78	barite	−2.43	0.15			SW	1.47	−0.41
	ODP Site 574 (004N 113W)	260.45	18.68	barite	−2.21	0.10			SW	1.69	−0.19
	ODP Site 574 (004N 113W)	313.21	20.82	barite	−2.35				SW	1.55	−0.33
	ODP Site 574 (004N 113W)	313.21	20.82	barite	−2.04				SW	1.86	−0.02
	ODP Site 574 (004N 113W)	314.50	20.89	barite	−2.29				SW	1.61	−0.27
	ODP Site 574 (004N 113W)	336.45	22.13	barite	−2.66				SW	1.24	−0.64
	ODP Site 574 (004N 113W)	336.45	22.13	barite	−2.58				SW	1.32	−0.56
	ODP Site 574 (004N 113W)	346.80	22.71	barite	−2.43	0.52			SW	1.47	−0.41
	ODP Site 574 (004N 113W)	346.95	22.72	barite	−1.97				SW	1.93	0.05
	ODP Site 574 (004N 113W)	346.95	22.72	barite	−2.07				SW	1.83	−0.05
	ODP Site 574 (004N 113W)	349.80	23.05	barite	−2.11	0.15			SW	1.79	−0.09
	ODP Site 574 (004N 113W)	353.70	23.56	barite	−2.52	0.03			SW	1.38	−0.50
	ODP Site 574 (004N 113W)	367.02	24.89	barite	−2.46	0.01			SW	1.44	−0.44
	ODP Site 574 (004N 113W)	377.51	25.81	barite	−2.31	0.00			SW	1.59	−0.29
	ODP Site 574 (004N 113W)	390.00	26.88	barite	−2.33				SW	1.57	−0.31
	ODP Site 574 (004N 113W)	397.17	27.49	barite	−2.09	0.17			SW	1.81	−0.07
	ODP Site 574 (004N 113W)	417.70	27.49	barite	−2.34	0.09			SW	1.56	−0.32
	ODP Site 575 (006N 135W)	38.41	10.46	barite	−2.08				SW	1.82	−0.06
	ODP Site 575 (006N 135W)	47.20	11.77	barite	−2.53				SW	1.37	−0.51
	ODP Site 575 (006N 135W)	83.50	14.20	barite	−1.42	0.41			SW	2.48	0.60
	ODP Site 575 (006N 135W)	92.50	14.72	barite	−2.28				SW	1.62	−0.26
	ODP Site 575 (006N 135W)	102.04	15.36	barite	−2.17				SW	1.73	−0.15
	ODP Site 575 (006N 135W)	118.65	16.36	barite	−2.40				SW	1.50	−0.38
	ODP Site 575 (006N 135W)	167.20	19.39	barite	−2.45				SW	1.45	−0.43
	ODP Site 575 (006N 135W)	196.10	21.36	barite	−2.68				SW	1.22	−0.66
	ODP Site 1218 (009N 135W)	66.54	19.67	barite	−1.98				SW	1.92	0.04

Continued on next page

Table 4.2: *Continued*

Source	Location	Depth (m)	Age (Ma)	Material	Raw $\delta^{44/40}$Ca	±	Raw $\delta^{44/42}$Ca	±	Relative to standard	$\delta^{44/40}$Ca of ancient SW rel. to SRM 915a	$\delta^{44/40}$Ca of ancient SW rel. to modern SW
	ODP Site 1219 (008N 142W)	21.45	15.40	barite	−2.26	0.12			SW	1.64	−0.24
Heuser et al. (2005)	ODP Site 871, Limalok Guyot (006N 172E)	1H-1, 124–126	0.10	*Globigerinoides trilobus*	0.87	0.05			SRM 915a	1.81	−0.07
	ODP Site 871, Limalok Guyot (006N 172E)	2H-1, 59–61	1.00	*Globigerinoides trilobus*	1.09	0.03			SRM 915a	2.03	0.15
	ODP Site 871, Limalok Guyot (006N 172E)	2H-6, 59–61	1.50	*Globigerinoides trilobus*	1.03	0.11			SRM 915a	1.97	0.09
	ODP Site 871, Limalok Guyot (006N 172E)	3H-2, 123–125	3.00	*Globigerinoides trilobus*	0.77	0.13			SRM 915a	1.71	−0.17
	ODP Site 872, Lo-En Guyot (010N 163E)	3H02, 59–61	3.30	*Globigerinoides trilobus*	0.84	0.14			SRM 915a	1.78	−0.10
	ODP Site 872, Lo-En Guyot (010N 163E)	3H-5, 118–120	3.90	*Globigerinoides trilobus*	0.65	0.03			SRM 915a	1.59	−0.29
	ODP Site 871, Limalok Guyot (006N 172E)	3H-5, 60–62	6.00	*Globigerinoides trilobus*	0.89	0.10			SRM 915a	1.83	−0.05
	ODP Site 871, Limalok Guyot (006N 172E)	3H-5, 123–125	6.20	*Globigerinoides trilobus*	0.85	0.15			SRM 915a	1.79	−0.09
	ODP Site 872, Lo-En Guyot (010N 163E)	5H-2, 14–16	9.00	*Globigerinoides trilobus*	0.74	0.10			SRM 915a	1.68	−0.20
	ODP Site 872, Lo-En Guyot (010N 163E)	5H-6, 59–61	10.40	*Globigerinoides trilobus*	0.75	0.10			SRM 915a	1.69	−0.19
	ODP Site 872, Lo-En Guyot (010N 163E)	6H-5, 20–22	11.40	*Globigerinoides trilobus*	0.58	0.15			SRM 915a	1.52	−0.36
	ODP Site 871, Limalok Guyot (006N 172E)	4H-5, 59–61	11.80	*Globigerinoides trilobus*	0.62	0.15			SRM 915a	1.56	−0.32
	ODP Site 871, Limalok Guyot (006N 172E)	6H-6, 60–62	13.10	*Globigerinoides trilobus*	0.64	0.16			SRM 915a	1.58	−0.30
	ODP Site 871, Limalok Guyot (006N 172E)	7H-2, 124–126	14.70	*Globigerinoides trilobus*	0.63	0.14			SRM 915a	1.57	−0.31
	ODP Site 871, Limalok Guyot (006N 172E)	7H-5, 59–61	15.00	*Globigerinoides trilobus*	0.49	0.15			SRM 915a	1.43	−0.45
	ODP Site 871, Limalok Guyot (006N 172E)	8H-2, 59–63	16.20	*Globigerinoides trilobus*	0.51	0.18			SRM 915a	1.45	−0.43
	ODP Site 872, Lo-En Guyot (010N 163E)	11H-1, 20–22	16.70	*Globigerinoides trilobus*	0.46	0.19			SRM 915a	1.40	−0.48
	ODP Site 872, Lo-En Guyot (010N 163E)	11H-6, 20–22	18.40	*Globigerinoides trilobus*	0.84	0.07			SRM 915a	1.78	−0.10
	ODP Site 872, Lo-En Guyot (010N 163E)	12H-2, 78–80	19.90	*Globigerinoides trilobus*	0.72	0.18			SRM 915a	1.66	−0.22
	ODP Site 872, Lo-En Guyot (010N 163E)	13H-3, 20–22	21.70	*Globigerinoides trilobus*	0.77	0.09			SRM 915a	1.71	−0.17
	ODP Site 872, Lo-En Guyot (010N 163E)	13H-5, 20–22	23.00	*Globigerinoides trilobus*	0.83	0.22			SRM 915a	1.77	−0.11
	ODP Site 872, Lo-En Guyot (010N 163E)	14H-4, 20–22	23.50	*Globigerinoides trilobus*	0.84	0.17			SRM 915a	1.78	−0.10
Heuser et al. (2005)	ODP Site 871, Limalok Guyot (006N 172E)	1H-1, 124–126	0.10	*Globigerinoides ruber*	0.63	0.05			SRM 915a	1.82	−0.06
	ODP Site 871, Limalok Guyot (006N 172E)	2H-2, 59–61	1.00	*Globigerinoides ruber*	0.79	0.15			SRM 915a	1.98	0.10
	ODP Site 871, Limalok Guyot (006N 172E)	2H-6, 59–61	1.50	*Globigerinoides ruber*	0.73	0.19			SRM 915a	1.92	0.04
	ODP Site 871, Limalok Guyot (006N 172E)	3H-2, 123–125	3.00	*Globigerinoides ruber*	0.81	0.30			SRM 915a	2.00	0.12
	ODP Site 872, Lo-En Guyot (010N 163E)	3H-2,59–61	3.30	*Globigerinoides ruber*	0.86	0.16			SRM 915a	2.05	0.17
	ODP Site 872, Lo-En Guyot (010N 163E)	2H-5, 118–120	3.90	*Globigerinoides ruber*	0.66	0.19			SRM 915a	1.85	−0.03
	ODP Site 872, Lo-En Guyot (010N 163E)	5H-2, 14–16	9.00	*Globigerinoides ruber*	0.69	0.09			SRM 915a	1.88	0.00
	ODP Site 872, Lo-En Guyot (010N 163E)	5H-6, 59–61	10.40	*Globigerinoides ruber*	0.74	0.11			SRM 915a	1.93	0.05
	ODP Site 872, Lo-En Guyot (010N 163E)	6H-5, 20–22	11.40	*Globigerinoides ruber*	1.01	0.20			SRM 915a	2.20	0.32

Continued on next page

Table 4.2: *Continued*

Source	Location	Depth (m)	Age (Ma)	Material	Raw $\delta^{44/40}$Ca	±	Raw $\delta^{44/42}$Ca	±	Relative to standard	$\delta^{44/40}$Ca of ancient SW rel. to SRM 915a	$\delta^{44/40}$Ca of ancient SW rel. to modern SW
	ODP Site 871, Limalok Guyot (006N 172E)	4H-5, 59–61	11.80	*Globigerinoides ruber*	0.58	0.08			SRM 915a	1.77	−0.11
	ODP Site 871, Limalok Guyot (006N 172E)	6H-6, 60–62	13.10	*Globigerinoides ruber*	0.70	0.29			SRM 915a	1.89	0.01
	ODP Site 871, Limalok Guyot (006N 172E)	7H-5, 59–61	15.00	*Globigerinoides ruber*	0.54	0.20			SRM 915a	1.73	−0.15
	ODP Site 871, Limalok Guyot (006N 172E)	8H-2, 59–63	16.20	*Globigerinoides ruber*	0.67	0.12			SRM 915a	1.86	−0.02
	ODP Site 872, Lo-En Guyot (010N 163E)	11H-1, 20–22	16.70	*Globigerinoides ruber*	0.77	0.21			SRM 915a	1.96	0.08
	ODP Site 872, Lo-En Guyot (010N 163E)	11H-6, 20–22	18.40	*Globigerinoides ruber*	0.84	0.06			SRM 915a	2.03	0.15
	ODP Site 872, Lo-En Guyot (010N 163E)	12H-2, 78–80	19.90	*Globigerinoides ruber*	0.64	0.03			SRM 915a	1.83	−0.05
	ODP Site 872, Lo-En Guyot (010N 163E)	13H-3, 20–22	21.70	*Globigerinoides ruber*	0.80	0.20			SRM 915a	1.99	0.11
Heuser et al. (2005)	ODP Site 871, Limalok Guyot (006N 172E)	1H-1, 124–626	0.10	*Globigerinella* spp.	0.44	0.13			SRM 915a	1.82	−0.06
	ODP Site 871, Limalok Guyot (006N 172E)	2H-2, 59–61	1.00	*Globigerinella* spp.	0.70	0.23			SRM 915a	2.08	0.20
	ODP Site 871, Limalok Guyot (006N 172E)	2H-6, 59–61	1.50	*Globigerinella* spp.	0.54	0.27			SRM 915a	1.92	0.04
	ODP Site 871, Limalok Guyot (006N 172E)	3H-2, 123–125	3.00	*Globigerinella* spp.	0.65	0.10			SRM 915a	2.03	0.15
	ODP Site 872, Lo-En Guyot (010N 163E)	3H-2, 59–61	3.30	*Globigerinella* spp.	0.62	0.21			SRM 915a	2.00	0.12
	ODP Site 872, Lo-En Guyot (010N 163E)	3H-5, 118–120	3.90	*Globigerinella* spp.	0.80	0.14			SRM 915a	2.18	0.30
	ODP Site 871, Limalok Guyot (006N 172E)	3H-5, 60–62	6.00	*Globigerinella* spp.	0.91	0.13			SRM 915a	2.29	0.41
	ODP Site 871, Limalok Guyot (006N 172E)	3H-5, 123–125	6.20	*Globigerinella* spp.	0.80	0.25			SRM 915a	2.18	0.30
	ODP Site 872, Lo-En Guyot (010N 163E)	5H-2, 14–16	9.00	*Globigerinella* spp.	0.56	0.16			SRM 915a	1.94	0.06
	ODP Site 872, Lo-En Guyot (010N 163E)	5H-6, 59–61	10.40	*Globigerinella* spp.	0.58	0.21			SRM 915a	1.96	0.08
	ODP Site 872, Lo-En Guyot (010N 163E)	6H-5, 20–22	11.40	*Globigerinella* spp.	0.46	0.20			SRM 915a	1.84	−0.04
	ODP Site 871, Limalok Guyot (006N 172E)	4H-5, 59–61	11.80	*Globigerinella* spp.	0.46	0.16			SRM 915a	1.84	−0.04
	ODP Site 871, Limalok Guyot (006N 172E)	6H-6, 60–62	13.10	*Globigerinella* spp.	0.55	0.25			SRM 915a	1.93	0.05
	ODP Site 871, Limalok Guyot (006N 172E)	7H-2, 124–126	14.70	*Globigerinella* spp.	0.40	0.04			SRM 915a	1.78	−0.10
	ODP Site 871, Limalok Guyot (006N 172E)	7H-5, 59–61	15.00	*Globigerinella* spp.	0.38	0.24			SRM 915a	1.76	−0.12
	ODP Site 871, Limalok Guyot (006N 172E)	8H-2, 59–63	16.20	*Globigerinella* spp.	0.08	0.06			SRM 915a	1.46	−0.42
	ODP Site 872, Lo-En Guyot (010N 163E)	11H-1, 20–22	16.70	*Globigerinella* spp.	0.60	0.24			SRM 915a	1.98	0.10
	ODP Site 872, Lo-En Guyot (010N 163E)	11H-6, 20–22	18.40	*Globigerinella* spp.	0.31	0.10			SRM 915a	1.69	−0.19
	ODP Site 872, Lo-En Guyot (010N 163E)	12H-2, 78–80	19.90	*Globigerinella* spp.	0.79	0.10			SRM 915a	2.17	0.29
	ODP Site 872, Lo-En Guyot (010N 163E)	13H-3, 20–22	21.70	*Globigerinella* spp.	0.79	0.25			SRM 915a	2.17	0.29
	ODP Site 872, Lo-En Guyot (010N 163E)	13H-5, 20–22	23.00	*Globigerinella* spp.	0.88	0.29			SRM 915a	2.26	0.38
Heuser et al. (2005)	ODP Site 1138, S Indian Ocean (054S 076E)	57.67	1.90	*Globigerina bulloides*	0.96	0.04			SRM 915a	1.95	0.07
	ODP Site 1138, S Indian Ocean (054S 076E)	67.92	2.40	*Globigerina bulloides*	1.02	0.05			SRM 915a	2.01	0.13
	ODP Site 1138, S Indian Ocean (054S 076E)	76.00	3.10	*Globigerina bulloides*	0.39	0.11			SRM 915a	1.38	−0.50

Continued on next page

Table 4.2: *Continued*

Source	Location	Depth (m)	Age (Ma)	Material	Raw $\delta^{44/40}Ca$	±	Raw $\delta^{44/42}Ca$	±	Relative to standard	$\delta^{44/40}Ca$ of ancient SW rel. to SRM 915a	$\delta^{44/40}Ca$ of ancient SW rel. to modern SW
	ODP Site 1138, S Indian Ocean (054S 076E)	87.00	3.60	*Globigerina bulloides*	0.52	0.09			SRM 915a	1.51	−0.37
	ODP Site 1138, S Indian Ocean (054S 076E)	93.34	3.70	*Globigerina bulloides*	0.92	0.07			SRM 915a	1.91	0.03
	ODP Site 1138, S Indian Ocean (054S 076E)	104.10	4.40	*Globigerina bulloides*	0.71	0.13			SRM 915a	1.70	−0.18
	ODP Site 1138, S Indian Ocean (054S 076E)	112.94	6.60	*Globigerina bulloides*	0.96	0.13			SRM 915a	1.95	0.07
	ODP Site 1138, S Indian Ocean (054S 076E)	117.38	7.60	*Globigerina bulloides*	0.87	0.15			SRM 915a	1.86	−0.02
	ODP Site 1138, S Indian Ocean (054S 076E)	123.78	9.20	*Globigerina bulloides*	0.71	0.11			SRM 915a	1.70	−0.18
	ODP Site 1138, S Indian Ocean (054S 076E)	133.00	9.40	*Globigerina bulloides*	0.64	0.06			SRM 915a	1.63	−0.25
	ODP Site 1138, S Indian Ocean (054S 076E)	134.00	9.40	*Globigerina bulloides*	0.67	0.06			SRM 915a	1.66	−0.22
	ODP Site 1138, S Indian Ocean (054S 076E)	144.60	9.60	*Globigerina bulloides*	0.77	0.18			SRM 915a	1.76	−0.12
	ODP Site 1138, S Indian Ocean (054S 076E)	157.12	9.90	*Globigerina bulloides*	0.80	0.04			SRM 915a	1.79	−0.09
	ODP Site 1138, S Indian Ocean (054S 076E)	169.80	11.60	*Globigerina bulloides*	0.75	0.13			SRM 915a	1.74	−0.14
	ODP Site 1138, S Indian Ocean (054S 076E)	174.30	11.80	*Globigerina bulloides*	0.71	0.08			SRM 915a	1.70	−0.18
	ODP Site 1138, S Indian Ocean (054S 076E)	180.98	12.90	*Globigerina bulloides*	0.63	0.12			SRM 915a	1.62	−0.26
	ODP Site 1138, S Indian Ocean (054S 076E)	190.59	14.20	*Globigerina bulloides*	0.71	0.18			SRM 915a	1.70	−0.18
	ODP Site 1138, S Indian Ocean (054S 076E)	199.50	15.10	*Globigerina bulloides*	0.48	0.06			SRM 915a	1.47	−0.41
	ODP Site 1138, S Indian Ocean (054S 076E)	209.11	16.40	*Globigerina bulloides*	0.65	0.08			SRM 915a	1.64	−0.24
	ODP Site 1138, S Indian Ocean (054S 076E)	217.90	17.30	*Globigerina bulloides*	0.74	0.16			SRM 915a	1.73	−0.15
	ODP Site 1138, S Indian Ocean (054S 076E)	227.50	18.50	*Globigerina bulloides*	0.45	0.14			SRM 915a	1.44	−0.44
	ODP Site 1138, S Indian Ocean (054S 076E)	237.12	20.00	*Globigerina bulloides*	0.49	0.13			SRM 915a	1.48	−0.40
	ODP Site 1138, S Indian Ocean (054S 076E)	248.22	21.00	*Globigerina bulloides*	0.59	0.11			SRM 915a	1.58	−0.30
Farkaš et al. (2007b)	Russia		158.40	belemnite	0.35				SRM 915a	1.75	−0.13
	Russia		157.70	belemnite	0.28				SRM 915a	1.68	−0.20
	Russia		157.40	belemnite	0.12				SRM 915a	1.52	−0.36
	Russia		156.70	belemnite	0.09				SRM 915a	1.49	−0.39
	Russia		155.70	belemnite	0.11				SRM 915a	1.51	−0.37
	New Zealand		153.60	belemnite	0.17				SRM 915a	1.57	−0.31
	New Zealand		151.10	belemnite	0.26				SRM 915a	1.66	−0.22
	Russia		149.40	belemnite	0.28				SRM 915a	1.68	−0.20
	Russia		147.80	belemnite	0.31				SRM 915a	1.71	−0.17
	Germany		140.00	belemnite	0.33				SRM 915a	1.73	−0.15
	Germany		138.60	belemnite	0.29				SRM 915a	1.69	−0.19
	Germany		138.10	belemnite	0.35				SRM 915a	1.75	−0.13
	Germany		136.20	belemnite	0.34				SRM 915a	1.74	−0.14

Continued on next page

Table 4.2: *Continued*

Source	Location	Depth (m)	Age (Ma)	Material	Raw $\delta^{44/40}Ca$	±	Raw $\delta^{44/42}Ca$	±	Relative to standard	$\delta^{44/40}Ca$ of ancient SW rel. to SRM 915a	$\delta^{44/40}Ca$ of ancient SW rel. to modern SW
	Germany		135.20	belemnite	0.46				SRM 915a	1.86	−0.02
	Germany		133.10	belemnite	0.47				SRM 915a	1.87	−0.01
	Great Britain		130.50	belemnite	0.49				SRM 915a	1.89	0.01
	Great Britain		128.20	belemnite	0.46				SRM 915a	1.86	−0.02
	Germany		127.80	belemnite	0.37				SRM 915a	1.77	−0.11
	Great Britain		127.40	belemnite	0.42				SRM 915a	1.82	−0.06
	Germany		126.60	belemnite	0.37				SRM 915a	1.77	−0.11
	Great Britain		126.30	belemnite	0.61				SRM 915a	2.01	0.13
	Great Britain		126.20	belemnite	0.48				SRM 915a	1.88	0.00
	Germany		124.50	belemnite	0.52				SRM 915a	1.92	0.04
Farkaš et al. (2007b)	Russia		158.70	belemnite	0.27				SRM 915a	1.67	−0.21
	Russia		158.40	belemnite	0.31				SRM 915a	1.71	−0.17
	Russia		157.70	belemnite	0.24				SRM 915a	1.64	−0.24
	Russia		157.40	belemnite	0.24				SRM 915a	1.64	−0.24
	Russia		157.30	belemnite	0.16				SRM 915a	1.56	−0.32
	Russia		156.70	belemnite	0.11				SRM 915a	1.51	−0.37
	Russia		155.90	belemnite	0.18				SRM 915a	1.58	−0.30
	Russia		155.70	belemnite	0.17				SRM 915a	1.57	−0.31
	New Zealand		153.60	belemnite	0.35				SRM 915a	1.75	−0.13
	Germany		133.10	belemnite	0.44				SRM 915a	1.84	−0.04
	Great Britain		130.50	belemnite	0.40				SRM 915a	1.80	−0.08
	Germany		128.30	belemnite	0.45				SRM 915a	1.85	−0.03
	Great Britain		128.20	belemnite	0.45				SRM 915a	1.85	−0.03
	Germany		127.80	belemnite	0.29				SRM 915a	1.69	−0.19
	Great Britain		127.40	belemnite	0.28				SRM 915a	1.68	−0.20
	Germany		127.10	belemnite	0.33				SRM 915a	1.73	−0.15
	Germany		126.70	belemnite	0.33				SRM 915a	1.73	−0.15
	Germany		126.60	belemnite	0.39				SRM 915a	1.79	−0.09
Farkaš et al. (2007b)	San Juan Island, WA, USA		0.00	brachiopod	1.07				SRM 915a	1.92	0.04
	San Juan Island, WA, USA		0.00	brachiopod	1.09				SRM 915a	1.94	0.06
	Ursental, Germany		151.50	belemnite	0.23				SRM 915a	1.63	−0.25
	Geisingen, Germany		155.00	belemnite	0.14				SRM 915a	1.54	−0.34

Continued on next page

Table 4.2: *Continued*

Source	Location	Depth (m)	Age (Ma)	Material	Raw $\delta^{44/40}Ca$	±	Raw $\delta^{44/42}Ca$	±	Relative to standard	$\delta^{44/40}Ca$ of ancient SW rel. to SRM 915a	$\delta^{44/40}Ca$ of ancient SW rel. to modern SW
	Geisingen, Germany		155.00	belemnite	0.08				SRM 915a	1.48	−0.40
Farkaš et al. (2007a)	San Juan Island, WA, USA		0.00	brachiopod	1.07				SRM 915a	1.92	0.04
	San Juan Island, WA, USA		0.00	brachiopod	1.09				SRM 915a	1.94	0.06
	San Juan Island, WA, USA		0.00	brachiopod	0.92				SRM 915a	1.77	−0.11
	San Juan Island, WA, USA		0.00	brachiopod	0.97				SRM 915a	1.82	−0.06
	Madeira, Spain		0.00	brachiopod	1.05				SRM 915a	1.90	0.02
	South Island, New Zealand		0.00	brachiopod	0.82				SRM 915a	1.67	−0.21
	Osprey Reef, Coral Sea, Australia		0.00	brachiopod	1.19				SRM 915a	2.04	0.16
	Kronsmoor, Germany		71.00	brachiopod	0.95				SRM 915a	1.80	−0.08
	St. Margarets, Great Britain		89.00	brachiopod	0.93				SRM 915a	1.78	−0.10
	Lewes, Shoreham, Great Britain		89.50	brachiopod	0.77				SRM 915a	1.62	-0.26
	Lewes, New Pit, Great Britain		91.90	brachiopod	0.85				SRM 915a	1.70	−0.18
	Glyndebourne, Great Britain		92.00	brachiopod	0.94				SRM 915a	1.79	−0.09
	Eastbourne, Great Britain		93.00	brachiopod	0.79				SRM 915a	1.64	−0.24
	Eastbourne, Great Britain		94.00	brachiopod	1.04				SRM 915a	1.89	0.01
	Eastbourne, Great Britain		94.10	brachiopod	1.19				SRM 915a	2.04	0.16
	Dover, Great Britain		94.90	brachiopod	0.87				SRM 915a	1.72	−0.16
	Southerham, Great Britain		95.00	brachiopod	0.82				SRM 915a	1.67	−0.21
	Southerham, Great Britain		95.10	brachiopod	0.72				SRM 915a	1.57	−0.31
	Southerham, Great Britain		96.40	brachiopod	0.82				SRM 915a	1.67	−0.21
	Southerham, Great Britain		96.50	brachiopod	0.69				SRM 915a	1.54	−0.34
	Ursental, Germany		151.50	brachiopod	0.68				SRM 915a	1.53	−0.35
	Ursental, Germany		151.50	brachiopod	0.69				SRM 915a	1.54	−0.34
	Geisingen, Germany		155.00	brachiopod	0.66				SRM 915a	1.51	−0.37
	Geisingen, Germany		155.00	brachiopod	0.59				SRM 915a	1.44	−0.44
	Weissloferbach, Austria		201.20	brachiopod	0.46				SRM 915a	1.31	−0.57
	Weissloferbach, Austria		201.20	brachiopod	0.59				SRM 915a	1.44	−0.44
	Weissloferbach, Austria		201.70	brachiopod	0.48				SRM 915a	1.33	−0.55
	Weissloferbach, Austria		202.00	brachiopod	0.73				SRM 915a	1.58	−0.30
	Weissloferbach, Austria		202.30	brachiopod	0.70				SRM 915a	1.55	−0.33
	Weissloferbach, Austria		202.50	brachiopod	0.32				SRM 915a	1.17	−0.71
	Weissloferbach, Austria		202.80	brachiopod	0.39				SRM 915a	1.24	−0.64
	St. Cassian / Cortina d'Ampezzo, Italy		225.20	brachiopod	0.73				SRM 915a	1.58	−0.30

Continued on next page

Table 4.2: *Continued*

Source	Location	Depth (m)	Age (Ma)	Material	Raw $\delta^{44/40}Ca$	±	Raw $\delta^{44/42}Ca$	±	Relative to standard	$\delta^{44/40}Ca$ of ancient SW rel. to SRM 915a	$\delta^{44/40}Ca$ of ancient SW rel. to modern SW
	St. Cassian / Cortina d'Ampezzo, Italy		226.10	brachiopod	0.61				SRM 915a	1.46	−0.42
	St. Cassian / Cortina d'Ampezzo, Italy		226.80	brachiopod	0.66				SRM 915a	1.51	−0.37
	St. Cassian / Cortina d'Ampezzo, Italy		227.10	brachiopod	0.49				SRM 915a	1.34	−0.54
	Köveskál, Hungary		227.40	brachiopod	0.90				SRM 915a	1.75	−0.13
	St. Cassian / Cortina d'Ampezzo, Italy		227.40	brachiopod	0.42				SRM 915a	1.27	−0.61
	Gähnheim, Germany		231.00	brachiopod	0.34				SRM 915a	1.19	−0.69
	Gerichtstetten, Germany		231.20	brachiopod	0.62				SRM 915a	1.47	−0.41
	Gähnheim, Germany		231.20	brachiopod	0.63				SRM 915a	1.48	−0.40
	Zwingelhausen (Backnang), Germany		233.60	brachiopod	0.46				SRM 915a	1.31	−0.57
	Gähnheim, Germany		234.40	brachiopod	0.62				SRM 915a	1.47	−0.41
	Neidenfels, Germany		237.50	brachiopod	0.72				SRM 915a	1.57	−0.31
	Neidenfels, Germany		238.00	brachiopod	0.76				SRM 915a	1.61	−0.27
	Laibach, Germany		241.00	brachiopod	0.42				SRM 915a	1.27	−0.61
	Chongquing Zhongliang Section, China		251.10	brachiopod	1.02				SRM 915a	1.87	−0.01
	Chongquing Zhongliang Section, China		251.10	brachiopod	0.48				SRM 915a	1.33	−0.55
	Chejiaba near Guangyuan, China		251.70	brachiopod	1.03				SRM 915a	1.88	0.00
	Meishan D, China		251.80	brachiopod	0.50				SRM 915a	1.35	−0.53
	Chongquing Zhongliang Section, China		252.90	brachiopod	0.66				SRM 915a	1.51	−0.37
	Chongquing Zhongliang Section, China		253.20	brachiopod	0.45				SRM 915a	1.30	−0.58
	Chongquing Zhongliang Section, China		253.20	brachiopod	0.82				SRM 915a	1.67	−0.21
	Chongquing Zhongliang Section, China		253.60	brachiopod	0.42				SRM 915a	1.27	−0.61
	Shangsi Section near Guangyuan, China		256.90	brachiopod	0.40				SRM 915a	1.25	−0.63
	Laibin, Guanxi Province, China		263.90	brachiopod	0.75				SRM 915a	1.60	−0.28
	Tonkeng, Xinshao County / Hunan, China		263.90	brachiopod	0.42				SRM 915a	1.27	−0.61
	Laibin 4, China		264.00	brachiopod	0.37				SRM 915a	1.22	−0.66
	Xiangliangbei village, Jian county, China		266.00	brachiopod	0.48				SRM 915a	1.33	−0.55
	Laibin 3, China		267.00	brachiopod	0.52				SRM 915a	1.37	−0.51
	Longyin Puan Country / Guizhou, China		284.00	brachiopod	0.81				SRM 915a	1.66	−0.22
	Laibin, Guanxi Province, China		288.70	brachiopod	0.82				SRM 915a	1.67	−0.21
	Usolka, Russia		293.40	brachiopod	1.15				SRM 915a	2.00	0.12
	Guanjiayu, Dongshan, Taiyuan, China		293.50	brachiopod	0.93				SRM 915a	1.78	−0.10
	Longyin Puan Country / Guizhou, China		294.90	brachiopod	0.63				SRM 915a	1.48	−0.40
	Longyin Puan Country / Guizhou, China		294.90	brachiopod	0.68				SRM 915a	1.53	−0.35
	Moscow Basin, Russia		300.00	brachiopod	0.75				SRM 915a	1.60	−0.28

Continued on next page

Table 4.2: *Continued*

Source	Location	Depth (m)	Age (Ma)	Material	Raw $\delta^{44/40}Ca$	±	Raw $\delta^{44/42}Ca$	±	Relative to standard	$\delta^{44/40}Ca$ of ancient SW rel. to SRM 915a	$\delta^{44/40}Ca$ of ancient SW rel. to modern SW
	Moscow Basin, Russia		302.20	brachiopod	0.63				SRM 915a	1.48	−0.40
	Moscow Basin, Russia		304.00	brachiopod	0.90				SRM 915a	1.75	−0.13
	Moscow Basin, Russia		304.20	brachiopod	0.82				SRM 915a	1.67	−0.21
	Moscow Basin, Russia		304.80	brachiopod	0.86				SRM 915a	1.71	−0.17
	Moscow Basin, Russia		305.70	brachiopod	0.83				SRM 915a	1.68	−0.20
	Moscow Basin, Russia		306.80	brachiopod	0.80				SRM 915a	1.65	−0.23
	Moscow Basin, Russia		307.00	brachiopod	0.78				SRM 915a	1.63	−0.25
	Moscow Basin, Russia		307.20	brachiopod	1.08				SRM 915a	1.93	0.05
	Moscow Basin, Russia		307.20	brachiopod	1.13				SRM 915a	1.98	0.10
	Moscow Basin, Russia		307.50	brachiopod	0.80				SRM 915a	1.65	−0.23
	Moscow Basin, Russia		308.20	brachiopod	0.82				SRM 915a	1.67	−0.21
	Moscow Basin, Russia		308.50	brachiopod	1.02				SRM 915a	1.87	−0.01
	Moscow Basin, Russia		310.10	brachiopod	0.82				SRM 915a	1.67	−0.21
	Moscow Basin, Russia		310.50	brachiopod	0.80				SRM 915a	1.65	−0.23
	Moscow Basin, Russia		310.70	brachiopod	0.92				SRM 915a	1.77	−0.11
	Moscow Basin, Russia		310.70	brachiopod	0.85				SRM 915a	1.70	−0.18
	Moscow Basin, Russia		310.70	brachiopod	0.95				SRM 915a	1.80	−0.08
	Moscow Basin, Russia		311.70	brachiopod	0.87				SRM 915a	1.72	−0.16
	Donetsk Basin, Ukraine		311.90	brachiopod	1.16				SRM 915a	2.01	0.13
	Donetsk Basin, Ukraine		313.30	brachiopod	0.81				SRM 915a	1.66	−0.22
	Donetsk Basin, Ukraine		314.00	brachiopod	0.44				SRM 915a	1.29	−0.59
	Donetsk Basin, Ukraine		314.90	brachiopod	0.93				SRM 915a	1.78	−0.10
	Donetsk Basin, Ukraine		320.80	brachiopod	0.99				SRM 915a	1.84	−0.04
	Donetsk Basin, Ukraine		320.90	brachiopod	0.93				SRM 915a	1.78	−0.10
	Donetsk Basin, Ukraine		321.60	brachiopod	0.97				SRM 915a	1.82	−0.06
	Donetsk Basin, Ukraine		321.60	brachiopod	0.74				SRM 915a	1.59	−0.29
	Donetsk Basin, Ukraine		321.70	brachiopod	0.76				SRM 915a	1.61	−0.27
	Moscow Basin, Russia		324.10	brachiopod	0.65				SRM 915a	1.50	−0.38
	Donetsk Basin, Ukraine		324.50	brachiopod	0.90				SRM 915a	1.75	−0.13
	Moscow Basin, Russia		325.10	brachiopod	0.46				SRM 915a	1.31	−0.57
	Moscow Basin, Russia		325.30	brachiopod	0.33				SRM 915a	1.18	−0.70
	Donetsk Basin, Ukraine		325.70	brachiopod	0.37				SRM 915a	1.22	−0.66
	Donetsk Basin, Ukraine		326.10	brachiopod	0.34				SRM 915a	1.19	−0.69
	Donetsk Basin, Ukraine		326.60	brachiopod	0.21				SRM 915a	1.06	−0.82

Continued on next page

Table 4.2: *Continued*

Source	Location	Depth (m)	Age (Ma)	Material	Raw $\delta^{44/40}Ca$	±	Raw $\delta^{44/42}Ca$	±	Relative to standard	$\delta^{44/40}Ca$ of ancient SW rel. to SRM 915a	$\delta^{44/40}Ca$ of ancient SW rel. to modern SW
	Donetsk Basin, Ukraine		327.00	brachiopod	0.74				SRM 915a	1.59	−0.29
	Donetsk Basin, Ukraine		327.50	brachiopod	0.41				SRM 915a	1.26	−0.62
	Donetsk Basin, Ukraine		327.70	brachiopod	0.72				SRM 915a	1.57	−0.31
	Donetsk Basin, Ukraine		327.80	brachiopod	0.52				SRM 915a	1.37	−0.51
	Turnhout, Belgium		328.80	brachiopod	0.53				SRM 915a	1.38	−0.50
	Gravenvoeren, Belgium		329.00	brachiopod	0.67				SRM 915a	1.52	−0.36
	Moscow Basin, Russia		329.00	brachiopod	0.51				SRM 915a	1.36	−0.52
	Gravenvoeren, Belgium		329.30	brachiopod	0.62				SRM 915a	1.47	−0.41
	Halen, Belgium		329.40	brachiopod	0.58				SRM 915a	1.43	−0.45
	Turnhout, Belgium		330.60	brachiopod	0.75				SRM 915a	1.60	−0.28
	Gravenvoeren, Belgium		331.50	brachiopod	0.68				SRM 915a	1.53	−0.35
	Halen, Belgium		331.60	brachiopod	0.63				SRM 915a	1.48	−0.40
	Halen, Belgium		331.60	brachiopod	0.81				SRM 915a	1.66	−0.22
	Halen, Belgium		331.80	brachiopod	0.80				SRM 915a	1.65	−0.23
	Donetsk Basin, Ukraine		332.80	brachiopod	0.70				SRM 915a	1.55	−0.33
	Moscow Basin, Russia		333.40	brachiopod	0.69				SRM 915a	1.54	−0.34
	Sligo-Ireland, Ireland		334.10	brachiopod	0.72				SRM 915a	1.57	−0.31
	E Sagard 1/70, Belgium		334.50	brachiopod	0.60				SRM 915a	1.45	−0.43
	Gravenvoeren, Belgium		334.70	brachiopod	0.48				SRM 915a	1.33	−0.55
	Gravenvoeren, Belgium		336.20	brachiopod	0.87				SRM 915a	1.72	−0.16
	Lives, Belgium		336.80	brachiopod	0.67				SRM 915a	1.52	−0.36
	Halen, Belgium		337.70	brachiopod	0.67				SRM 915a	1.52	−0.36
	Halen, Belgium		337.80	brachiopod	0.81				SRM 915a	1.66	−0.22
	Gravenvoeren, Belgium		338.30	brachiopod	0.70				SRM 915a	1.55	−0.33
	Halen, Belgium		338.50	brachiopod	0.75				SRM 915a	1.60	−0.28
	Salet, Belgium		338.90	brachiopod	0.50				SRM 915a	1.35	−0.53
	Turnhout, Belgium		339.90	brachiopod	0.62				SRM 915a	1.47	−0.41
	Turnhout, Belgium		342.40	brachiopod	0.58				SRM 915a	1.43	−0.45
	E Sagard 1/70, Belgium		342.50	brachiopod	-0.11				SRM 915a	0.74	−1.14
	E Sagard 1/70, Belgium		343.20	brachiopod	-0.03				SRM 915a	0.82	−1.06
	E Sagard 1/70, Belgium		345.20	brachiopod	0.20				SRM 915a	1.05	−0.83
	Tournais 1, Belgium		345.40	brachiopod	0.54				SRM 915a	1.39	−0.49
	Tournais 2, Belgium		347.00	brachiopod	0.23				SRM 915a	1.08	−0.80
	Tournais 2, Belgium		347.20	brachiopod	0.64				SRM 915a	1.49	−0.39

Continued on next page

Table 4.2: *Continued*

Source	Location	Depth (m)	Age (Ma)	Material	Raw $\delta^{44/40}Ca$	±	Raw $\delta^{44/42}Ca$	±	Relative to standard	$\delta^{44/40}Ca$ of ancient SW rel. to SRM 915a	$\delta^{44/40}Ca$ of ancient SW rel. to modern SW
	Tournais 2, Belgium		347.60	brachiopod	0.13				SRM 915a	0.98	−0.90
	Yvoir, Belgium		348.90	brachiopod	0.37				SRM 915a	1.22	−0.66
	E Sagard 1/70, Belgium		350.10	brachiopod	0.53				SRM 915a	1.38	−0.50
	E Sagard 1/70, Belgium		350.20	brachiopod	0.63				SRM 915a	1.48	−0.40
	E Sagard 1/70, Belgium		350.30	brachiopod	0.58				SRM 915a	1.43	−0.45
	Yvoir, Belgium		350.60	brachiopod	0.47				SRM 915a	1.32	−0.56
	Rocher Bayard, Belgium		351.90	brachiopod	0.56				SRM 915a	1.41	−0.47
	Rocher Bayard, Belgium		352.10	brachiopod	0.35				SRM 915a	1.20	−0.68
	E Dranske 2/70, Germany		352.30	brachiopod	0.44				SRM 915a	1.29	−0.59
	Cardiff, Great Britain		353.30	brachiopod	0.52				SRM 915a	1.37	−0.51
	Aneseremme, Belgium		356.70	brachiopod	0.40				SRM 915a	1.25	-−0.63
	Aneseremme, Belgium		357.30	brachiopod	0.39				SRM 915a	1.24	−0.64
	Aneseremme, Belgium		358.00	brachiopod	0.49				SRM 915a	1.34	−0.54
	Aneseremme, Belgium		358.70	brachiopod	0.44				SRM 915a	1.29	−0.59
	Neuenkirchen, Germany		372.20	brachiopod	0.39				SRM 915a	1.24	−0.64
	Sagard, Germany		372.90	brachiopod	0.31				SRM 915a	1.16	−0.72
	Sagard, Germany		373.60	brachiopod	0.40				SRM 915a	1.25	−0.63
	Aachen, Germany		373.90	brachiopod	0.40				SRM 915a	1.25	−0.63
	Aachen, Germany		374.30	brachiopod	0.38				SRM 915a	1.23	−0.65
	Sagard, Germany		375.00	brachiopod	0.40				SRM 915a	1.25	−0.63
	Aachen, Germany		375.60	brachiopod	0.34				SRM 915a	1.19	−0.69
	Aachen, Germany		375.80	brachiopod	0.22				SRM 915a	1.07	−0.81
	Siberia, Russia		370.00	brachiopod	0.20				SRM 915a	1.05	−0.83
	South China		371.80	brachiopod	0.23				SRM 915a	1.08	−0.80
	Siberia, Russia		373.90	brachiopod	0.23				SRM 915a	1.08	−0.80
	Siberia, Russia		374.30	brachiopod	0.19				SRM 915a	1.04	−0.84
	Siberia, Russia		374.30	brachiopod	0.27				SRM 915a	1.12	−0.76
	Siberia, Russia		374.30	brachiopod	0.32				SRM 915a	1.17	−0.71
	Siberia, Russia		374.60	brachiopod	0.24				SRM 915a	1.09	−0.79
	Siberia, Russia		374.60	brachiopod	0.18				SRM 915a	1.03	−0.85
	Siberia, Russia		374.60	brachiopod	0.26				SRM 915a	1.11	−0.77
	Siberia, Russia		375.30	brachiopod	0.22				SRM 915a	1.07	−0.81
	Siberia, Russia		375.50	brachiopod	0.18				SRM 915a	1.03	−0.85
	Iowa, USA		376.90	brachiopod	0.26				SRM 915a	1.11	−0.77

Continued on next page

Table 4.2: *Continued*

Source	Location	Depth (m)	Age (Ma)	Material	Raw $\delta^{44/40}Ca$	±	Raw $\delta^{44/42}Ca$	±	Relative to standard	$\delta^{44/40}Ca$ of ancient SW rel. to SRM 915a	$\delta^{44/40}Ca$ of ancient SW rel. to modern SW
	Iowa, USA		377.60	brachiopod	0.16				SRM 915a	1.01	−0.87
	Iowa, USA		378.10	brachiopod	0.30				SRM 915a	1.15	−0.73
	Iowa, USA		378.20	brachiopod	0.34				SRM 915a	1.19	−0.69
	Iowa, USA		378.20	brachiopod	0.25				SRM 915a	1.10	−0.78
	Iowa, USA		381.60	brachiopod	0.47				SRM 915a	1.32	−0.56
	Iowa, USA		382.90	brachiopod	0.53				SRM 915a	1.38	−0.50
	Iowa, USA		383.00	brachiopod	0.51				SRM 915a	1.36	−0.52
	Iowa, USA		386.20	brachiopod	0.47				SRM 915a	1.32	−0.56
	Iowa, USA		386.20	brachiopod	0.47				SRM 915a	1.32	−0.56
	Iowa, USA		386.20	brachiopod	0.39				SRM 915a	1.24	−0.64
	Iowa, USA		386.20	brachiopod	0.33				SRM 915a	1.18	−0.70
	Iowa, USA		386.40	brachiopod	0.46				SRM 915a	1.31	−0.57
	Iowa, USA		386.40	brachiopod	0.42				SRM 915a	1.27	−0.61
	Iowa, USA		386.40	brachiopod	0.41				SRM 915a	1.26	−0.62
	Iowa, USA		386.40	brachiopod	0.42				SRM 915a	1.27	−0.61
	Anti-Atlas, Morocco		389.30	brachiopod	0.26				SRM 915a	1.11	−0.77
	Anti-Atlas, Morocco		393.70	brachiopod	0.28				SRM 915a	1.13	−0.75
	Eifel Mountains, Germany		395.00	brachiopod	0.26				SRM 915a	1.11	−0.77
	Cantabrian Mountains, Spain		398.10	brachiopod	0.35				SRM 915a	1.20	−0.68
	Anti-Atlas, Morocco		399.00	brachiopod	0.31				SRM 915a	1.16	−0.72
	Anti-Atlas, Morocco		399.10	brachiopod	0.44				SRM 915a	1.29	−0.59
	Anti-Atlas, Morocco		399.70	brachiopod	0.26				SRM 915a	1.11	−0.77
	Anti-Atlas, Morocco		401.20	brachiopod	0.31				SRM 915a	1.16	−0.72
	Anti-Atlas, Morocco		401.80	brachiopod	0.23				SRM 915a	1.08	−0.80
	Anti-Atlas, Morocco		401.80	brachiopod	0.24				SRM 915a	1.09	−0.79
	Anti-Atlas, Morocco		402.40	brachiopod	0.29				SRM 915a	1.14	−0.74
	Siberia, Russia		407.10	brachiopod	0.39				SRM 915a	1.24	−0.64
	Cantabrian Mountains, Spain		413.30	brachiopod	0.26				SRM 915a	1.11	−0.77
	Cantabrian Mountains, Spain		413.40	brachiopod	0.29				SRM 915a	1.14	−0.74
	Podolia, Ukraine		416.30	brachiopod	0.31				SRM 915a	1.16	−0.72
	Podolia, Ukraine		416.70	brachiopod	0.39				SRM 915a	1.24	−0.64
	Taurage-11, Lithuania		417.90	brachiopod	0.61				SRM 915a	1.46	−0.42
	Taurage-11, Lithuania		417.90	brachiopod	0.45				SRM 915a	1.30	−0.58
	Kolka 54, Latvia		418.30	brachiopod	0.35				SRM 915a	1.20	−0.68

Continued on next page

Table 4.2: *Continued*

Source	Location	Depth (m)	Age (Ma)	Material	Raw $\delta^{44/40}Ca$	±	Raw $\delta^{44/42}Ca$	±	Relative to standard	$\delta^{44/40}Ca$ of ancient SW rel. to SRM 915a	$\delta^{44/40}Ca$ of ancient SW rel. to modern SW
	Kolka 54, Latvia		418.70	brachiopod	0.37				SRM 915a	1.22	−0.66
	Podolia, Ukraine		418.70	brachiopod	0.49				SRM 915a	1.34	−0.54
	Gotland, Sweden		419.50	brachiopod	0.44				SRM 915a	1.29	−0.59
	Gotland, Sweden		420.20	brachiopod	0.31				SRM 915a	1.16	−0.72
	Gotland, Sweden		420.60	brachiopod	0.59				SRM 915a	1.44	−0.44
	Gotland, Sweden		421.70	brachiopod	0.42				SRM 915a	1.27	−0.61
	Gotland, Sweden		421.70	brachiopod	0.49				SRM 915a	1.34	−0.54
	Much Wenlock, Great Britain		423.80	brachiopod	0.43				SRM 915a	1.28	−0.60
	Gotland, Sweden		423.80	brachiopod	0.32				SRM 915a	1.17	−0.71
	Gotland, Sweden		423.80	brachiopod	0.28				SRM 915a	1.13	−0.75
	Gotland, Sweden		423.80	brachiopod	0.26				SRM 915a	1.11	−0.77
	Gotland, Sweden		424.90	brachiopod	0.31				SRM 915a	1.16	−0.72
	Grauzai-105, Lithuania		426.00	brachiopod	0.44				SRM 915a	1.29	−0.59
	Gotland, Sweden		426.60	brachiopod	0.50				SRM 915a	1.35	−0.53
	Gotland, Sweden		426.60	brachiopod	0.51				SRM 915a	1.36	−0.52
	Gotland, Sweden		426.60	brachiopod	0.47				SRM 915a	1.32	−0.56
	Gotland, Sweden		427.10	brachiopod	0.65				SRM 915a	1.50	−0.38
	Gotland, Sweden		428.60	brachiopod	0.39				SRM 915a	1.24	−0.64
	Anticosti Island, Canada		429.50	brachiopod	0.46				SRM 915a	1.31	−0.57
	Anticosti Island, Canada		430.40	brachiopod	0.44				SRM 915a	1.29	−0.59
	Anticosti Island, Canada		430.40	brachiopod	0.41				SRM 915a	1.26	−0.62
	Anticosti Island, Canada		431.50	brachiopod	0.27				SRM 915a	1.12	−0.76
	Anticosti Island, Canada		432.80	brachiopod	0.39				SRM 915a	1.24	−0.64
	Anticosti Island, Canada		434.50	brachiopod	0.28				SRM 915a	1.13	−0.75
	Anticosti Island, Canada		437.30	brachiopod	0.57				SRM 915a	1.42	−0.46
	Anticosti Island, Canada		439.40	brachiopod	0.48				SRM 915a	1.33	−0.55
	Anticosti Island, Canada		439.40	brachiopod	0.35				SRM 915a	1.20	−0.68
	Anticosti Island, Canada		439.40	brachiopod	0.53				SRM 915a	1.38	−0.50
	Anticosti Island, Canada		439.40	brachiopod	0.55				SRM 915a	1.40	−0.48
	Anticosti Island, Canada		442.50	brachiopod	0.54				SRM 915a	1.39	−0.49
	Gotland, Sweden		419.20	brachiopod	0.24				SRM 915a	1.09	−0.79
	Gotland, Sweden		419.20	brachiopod	0.32				SRM 915a	1.17	−0.71
	Gotland, Sweden		419.20	brachiopod	0.24				SRM 915a	1.09	−0.79
	Gotland, Sweden		419.40	brachiopod	0.29				SRM 915a	1.14	−0.74

Continued on next page

Table 4.2: *Continued*

Source	Location	Depth (m)	Age (Ma)	Material	Raw $\delta^{44/40}Ca$	±	Raw $\delta^{44/42}Ca$	±	Relative to standard	$\delta^{44/40}Ca$ of ancient SW rel. to SRM 915a	$\delta^{44/40}Ca$ of ancient SW rel. to modern SW
	Gotland, Sweden		420.90	brachiopod	0.24				SRM 915a	1.09	−0.79
	Gotland, Sweden		420.90	brachiopod	0.22				SRM 915a	1.07	−0.81
	Gotland, Sweden		420.90	brachiopod	0.25				SRM 915a	1.10	−0.78
	Gotland, Sweden		420.90	brachiopod	0.19				SRM 915a	1.04	−0.84
	Gotland, Sweden		423.00	brachiopod	0.16				SRM 915a	1.01	−0.87
	Gotland, Sweden		423.70	brachiopod	0.14				SRM 915a	0.99	−0.89
	Gotland, Sweden		424.10	brachiopod	0.20				SRM 915a	1.05	−0.83
	Gotland, Sweden		425.30	brachiopod	0.18				SRM 915a	1.03	−0.85
	Gotland, Sweden		425.30	brachiopod	0.25				SRM 915a	1.10	−0.78
	Gotland, Sweden		426.90	brachiopod	0.24				SRM 915a	1.09	−0.79
	Gotland, Sweden		427.60	brachiopod	0.26				SRM 915a	1.11	−0.77
	Gotland, Sweden		427.60	brachiopod	0.25				SRM 915a	1.10	−0.78
	South China		444.50	brachiopod	0.38				SRM 915a	1.23	−0.65
	South China		444.50	brachiopod	0.17				SRM 915a	1.02	−0.86
	Cincinnati, USA		445.20	brachiopod	0.41				SRM 915a	1.26	−0.62
	South China		445.50	brachiopod	0.30				SRM 915a	1.15	−0.73
	Cincinnati, USA		445.80	brachiopod	0.58				SRM 915a	1.43	−0.45
	Cincinnati, USA		445.80	brachiopod	0.52				SRM 915a	1.37	−0.51
	Cincinnati, USA		446.30	brachiopod	0.51				SRM 915a	1.36	−0.52
	Cincinnati, USA		446.70	brachiopod	0.38				SRM 915a	1.23	−0.65
	Cincinnati, USA		450.10	brachiopod	0.44				SRM 915a	1.29	−0.59
	Cincinnati, USA		450.10	brachiopod	0.31				SRM 915a	1.16	−0.72
	Cincinnati, USA		450.30	brachiopod	0.45				SRM 915a	1.30	−0.58
	Cincinnati, USA		451.20	brachiopod	0.37				SRM 915a	1.22	−0.66
	Lexington, USA		452.40	brachiopod	0.30				SRM 915a	1.15	−0.73
	St. Louis, USA		455.50	brachiopod	0.73				SRM 915a	1.58	−0.30
	St. Louis, USA		455.80	brachiopod	0.54				SRM 915a	1.39	−0.49
	St. Louis, USA		456.10	brachiopod	0.45				SRM 915a	1.30	−0.58
	Lexington, USA		456.80	brachiopod	0.88				SRM 915a	1.73	−0.15
	Lexington, USA		456.90	brachiopod	0.58				SRM 915a	1.43	−0.45
	St. Louis, USA		457.50	brachiopod	0.56				SRM 915a	1.41	−0.47
	Arbuckle Mountains, USA		458.80	brachiopod	0.36				SRM 915a	1.21	−0.67
	Arbuckle Mountains, USA		458.80	brachiopod	0.40				SRM 915a	1.25	−0.63
	Arbuckle Mountains, USA		458.80	brachiopod	0.42				SRM 915a	1.27	−0.61

Continued on next page

Table 4.2: *Continued*

Source	Location	Depth (m)	Age (Ma)	Material	Raw $\delta^{44/40}Ca$	±	Raw $\delta^{44/42}Ca$	±	Relative to standard	$\delta^{44/40}Ca$ of ancient SW rel. to SRM 915a	$\delta^{44/40}Ca$ of ancient SW rel. to modern SW
	Arbuckle Mountains, USA		462.50	brachiopod	0.44				SRM 915a	1.29	−0.59
	South China		463.70	brachiopod	0.47				SRM 915a	1.32	−0.56
	Arbuckle Mountains, USA		465.30	brachiopod	0.49				SRM 915a	1.34	−0.54
	Arbuckle Mountains, USA		465.30	brachiopod	0.32				SRM 915a	1.17	−0.71
	Arbuckle Mountains, USA		465.30	brachiopod	0.55				SRM 915a	1.40	−0.48
	South China		465.90	brachiopod	0.39				SRM 915a	1.24	−0.64
	South China		465.90	brachiopod	0.51				SRM 915a	1.36	−0.52
	South China		465.90	brachiopod	0.35				SRM 915a	1.20	−0.68
	South China		465.90	brachiopod	0.53				SRM 915a	1.38	−0.50
	Amadeus Basin, Australia		467.00	brachiopod	0.26				SRM 915a	1.11	−0.77
	Amadeus Basin, Australia		467.00	brachiopod	0.38				SRM 915a	1.23	−0.65
	St. Petersburg, Russia		467.00	brachiopod	0.73				SRM 915a	1.58	−0.30
	South China		469.70	brachiopod	0.28				SRM 915a	1.13	−0.75
	South China		474.50	brachiopod	0.24				SRM 915a	1.09	−0.79
	South China		474.50	brachiopod	0.41				SRM 915a	1.26	−0.62
	South China		477.10	brachiopod	0.46				SRM 915a	1.31	−0.57
	South China		483.50	brachiopod	0.51				SRM 915a	1.36	−0.52

Table 4.3: Measurements from this study of a range of modern carbonates. Temperature estimates are from the World Ocean Atlas 2005 (Locarnini et al., 2006). Conversions from $\delta^{44/42}$Ca to $\delta^{44/40}$Ca are performed as described in Chapter 1. Temperature normalizations used the relationship of +0.02‰ per °C (see Section 4.2).

Common name	Binomen	Phylum or division	Subtaxon	Location	Sample name	Mineralogy	$\delta^{44/42}$Ca rel. to SRM915a	2 SE	$\delta^{44/40}$Ca rel. to seawater	T (°C)	T-normalized $\delta^{44/40}$Ca (15 °C)
MODERN SAMPLES											
bivalve fragment	unknown	mollusca	bivalvia	Skye, Scotland	BIV1	possibly mixed	0.36	0.04	−1.16	10.4	−1.07
bivalve fragment	unknown	mollusca	bivalvia	Skye, Scotland	BIV2	possibly mixed	0.46	0.05	−0.96	10.4	−0.87
snail fragments	unknown	mollusca	gastropoda	Skye, Scotland	GAS1	possibly mixed	0.20	0.06	−1.48	10.4	−1.39
snail fragments	unknown	mollusca	gastropoda	Skye, Scotland	GAS2	possibly mixed	0.31	0.06	−1.26	10.4	−1.17
encrusting foram	*Homotrema*	protozoa	foraminiferida	Bermuda	HOM1A	high-Mg calcite	0.30	0.06	−1.28	23.1	−1.44
encrusting foram	*Homotrema*	protozoa	foraminiferida	Bermuda	HOM1B	high-Mg calcite	0.34	0.06	−1.21	23.1	−1.37
encrusting foram	*Homotrema*	protozoa	foraminiferida	Bermuda	HOM2A	high-Mg calcite	0.35	0.06	−1.17	23.1	−1.33
encrusting foram	*Homotrema*	protozoa	foraminiferida	Bermuda	HOM2B	high-Mg calcite	0.40	0.06	−1.08	23.1	−1.24
sea urchin	unknown	echinodermata	echinoidea	Arran, Scotland	X1A-S	high-Mg calcite	0.21	0.05	−1.47	10.6	−1.38
sea urchin	unknown	echinodermata	echinoidea	Arran, Scotland	X2A-S	high-Mg calcite	0.23	0.06	−1.42	10.6	−1.33
sea urchin	unknown	echinodermata	echinoidea	Skye, Scotland	X3A	high-Mg calcite	0.30	0.07	−1.29	10.4	−1.20
sea urchin	unknown	echinodermata	echinoidea	Skye, Scotland	X3B	high-Mg calcite	0.26	0.07	−1.36	10.4	−1.27
red algae fragments	unknown	rhodophyta	—	Abu Dhabi	CSAD1	high-Mg calcite	0.70	0.05	−0.47	28.0	−0.73
red algae fragments	unknown	rhodophyta	—	Abu Dhabi	CSAD2	high-Mg calcite	0.57	0.05	−0.74	28.0	−1.00
red algae nodule	unknown	rhodophyta	—	Bermuda	ALG	high-Mg calcite	0.38	0.07	−1.12	23.1	−1.28
red algae fragments	unknown	rhodophyta	—	Skye, Scotland	SKYE1	high-Mg calcite	0.62	0.05	−0.65	10.4	−0.56
red algae fragments	unknown	rhodophyta	—	Skye, Scotland	SKYE2	high-Mg calcite	0.60	0.05	−0.68	10.4	−0.59
thicket algae	*Galaxaura*	rhodophyta	—	Bahamas	TH ALG	high-Mg calcite	0.42	0.08	−1.04	26.4	−1.27
red algae	unknown	rhodophyta	—	Arran, Scotland	ARR1	high-Mg calcite	0.40	0.05	−1.08	10.6	−0.99
red algae	unknown	rhodophyta	—	Arran, Scotland	ARR2	high-Mg calcite	0.42	0.05	−1.05	10.6	−0.96
coral	*Acropora*	cnidaria	scleractinia	Bora Bora	ACR1-2	aragonite	0.44	0.07	−1.00	28.0	−1.26
coral	*Porites*	cnidaria	scleractinia	Bermuda	POR1-2	aragonite	0.42	0.05	−1.05	23.1	−1.21
coral	*Diploria*	cnidaria	scleractinia	Bermuda	DIP1-2	aragonite	0.23	0.06	−1.41	23.1	−1.57
coral	unknown (pebble)	cnidaria	scleractinia	Barbados	COR1	aragonite	0.31	0.07	−1.26	27.4	−1.51
coral	unknown (pebble)	cnidaria	scleractinia	Barbados	COR2	aragonite	0.24	0.07	−1.40	27.4	−1.65
coral	unknown (pebble)	cnidaria	scleractinia	Barbados	COR3	aragonite	0.27	0.07	−1.34	27.4	−1.59
staghorn coral	*Acropora cervicornis*	cnidaria	scleractinia	Bahamas	STAG	aragonite	0.23	0.08	−1.41	26.4	−1.64
staghorn coral	*Acropora cervicornis*	cnidaria	scleractinia	Bahamas	BAH B17	aragonite	0.40	0.05	−1.08	26.4	−1.31

Continued on next page

Table 4.3: *Continued*

Common name	Binomen	Phylum or division	Subtaxon	Location	Sample name	Mineralogy	$\delta^{44/42}$Ca rel. to SRM915a	2 SE	$\delta^{44/40}$Ca rel. to seawater	T (°C)	T-normalized $\delta^{44/40}$Ca (15 °C)
golfball coral	*Favia*	cnidaria	scleractinia	Bahamas	GOLF	aragonite	0.27	0.08	−1.33	26.4	−1.56
coral	*Acropora palmata*	cnidaria	scleractinia	Bahamas	ACR	aragonite	0.18	0.08	−1.52	26.4	−1.75
coral	*Porites*	cnidaria	scleractinia	Bahamas	POR4	aragonite	0.24	0.08	−1.41	26.4	−1.64
coral	*Porites*	cnidaria	scleractinia	Bahamas	POR5	aragonite	0.21	0.08	−1.45	26.4	−1.68
fire coral	*Millepora*	cnidaria	hydrozoa	Bermuda	MIL1,2	aragonite	0.15	0.06	−1.57	23.1	−1.73
fire coral	*Millepora*	cnidaria	hydrozoa	Bahamas	FIRE1	aragonite	0.30	0.08	−1.29	26.4	−1.52
fire coral	*Millepora*	cnidaria	hydrozoa	Bahamas	FIRE2	aragonite	0.30	0.08	−1.29	26.4	−1.52
fire coral	*Millepora*	cnidaria	hydrozoa	Bahamas	BAH B12	aragonite	0.41	0.05	−1.06	26.4	−1.29
deep sea coral	*Desmophyllum dianthus*	cnidaria	scleractinia	deep South Atlantic	DSC H1	aragonite	0.39	0.05	−1.09	3.1	−0.85
deep sea coral	*Desmophyllum dianthus*	cnidaria	scleractinia	deep North Atlantic	DSC H2	aragonite	0.24	0.05	−1.37	3.8	−1.15
deep sea coral	*Madrepora oculata*	cnidaria	scleractinia	deep sea, Queensland Trough	DSC 548	aragonite	0.25	0.05	−1.38	4.0	−1.16
deep sea coral	*Enallopsammia rostrata*	cnidaria	scleractinia	deep sea, Queensland Trough	DSC 549	aragonite	0.19	0.05	−1.50	4.0	−1.28
ooid	—	—	—	Norman Reef Cay, Bahamas	OOID1	aragonite	0.14	0.08	−1.61	26.4	−1.84
ooid	—	—	—	Norman Reef Cay, Bahamas	OOID2	aragonite	0.15	0.08	−1.58	26.4	−1.81
green algae	*Penicillus*	chlorophyta	—	Bahamas	PEN1	aragonite	0.18	0.07	−1.51	26.4	−1.74
green algae	*Penicillus*	chlorophyta	—	Bahamas	PEN2	aragonite	0.26	0.06	−1.37	26.4	−1.60
green algae	*Penicillus*	chlorophyta	—	Bahamas	PEN3	aragonite	0.14	0.07	−1.59	26.4	−1.82
green algae	*Halimeda monile*	chlorophyta	—	Bahamas	HMON	aragonite	0.30	0.07	−1.28	26.4	−1.51
green algae	*Halimeda tuna*	chlorophyta	—	Big Point, Bahamas	HTUN	aragonite	0.18	0.07	−1.52	26.4	−1.75
green algae	*Halimeda discoidea*	chlorophyta	—	Bahamas	HDIS1	aragonite	0.26	0.07	−1.37	26.4	−1.60
green algae	*Halimeda discoidea*	chlorophyta	—	Bahamas	HDIS2	aragonite	0.22	0.07	−1.44	26.4	−1.67
green algae	*Halimeda incrassata*	chlorophyta	—	Bahamas	HINC1	aragonite	0.19	0.07	−1.50	26.4	−1.73
green algae	*Halimeda incrassata*	chlorophyta	—	Bahamas	HINC2	aragonite	0.22	0.07	−1.44	26.4	−1.67
ANCIENT SAMPLES											
belemnite	unknown	mollusca	cephalopoda	Belemnite Bed, Dorset, UK	BB2	calcite	0.15	0.08	−1.59	—	—
belemnite	unknown	mollusca	cephalopoda	Belemnite Bed, Dorset, UK	BB3	calcite	0.09	0.08	−1.71	—	—
belemnite	unknown	mollusca	cephalopoda	Belemnite Bed, Dorset, UK	BB4	calcite	0.15	0.08	−1.59	—	—
belemnite	unknown	mollusca	cephalopoda	Belemnite Bed, Dorset, UK	BB5	calcite	0.18	0.08	−1.52	—	—
belemnite	unknown	mollusca	cephalopoda	Belemnite Bed, Dorset, UK	BB6	calcite	0.11	0.08	−1.66	—	—
belemnite	unknown	mollusca	cephalopoda	Belemnite Bed, Dorset, UK	BB7	calcite	0.18	0.08	−1.52	—	—
belemnite	unknown	mollusca	cephalopoda	Belemnite Bed, Dorset, UK	BB8	calcite	0.06	0.08	−1.76	—	—
belemnite	unknown	mollusca	cephalopoda	Belemnite Bed, Dorset, UK	BB9	calcite	0.04	0.10	−1.79	—	—

Continued on next page

Table 4.3: *Continued*

Common name	Binomen	Phylum or division	Subtaxon	Location	Sample name	Mineralogy	$\delta^{44/42}$Ca rel. to SRM915a	2 SE	$\delta^{44/40}$Ca rel. to seawater	T (°C)	T-normalized $\delta^{44/40}$Ca (15 °C)
belemnite	unknown	mollusca	cephalopoda	Belemnite Bed, Dorset, UK	BB10	calcite	0.21	0.10	−1.47	—	—
belemnite	unknown	mollusca	cephalopoda	Belemnite Stone, Dorset, UK	BS1	calcite	0.11	0.05	−1.66	—	—
belemnite	unknown	mollusca	cephalopoda	Belemnite Stone, Dorset, UK	BS3	calcite	0.12	0.05	−1.64	—	—
belemnite	unknown	mollusca	cephalopoda	Belemnite Stone, Dorset, UK	BS4	calcite	0.12	0.05	−1.65	—	—
belemnite	unknown	mollusca	cephalopoda	Junction Bed, Dorset, UK	JB2	calcite	0.08	0.09	−1.72	—	—
belemnite	unknown	mollusca	cephalopoda	Junction Bed, Dorset, UK	JB3	calcite	0.10	0.09	−1.69	—	—
belemnite	unknown	mollusca	cephalopoda	Junction Bed, Dorset, UK	JB4	calcite	0.07	0.09	−1.74	—	—
belemnite	unknown	mollusca	cephalopoda	Junction Bed, Dorset, UK	JB5	calcite	0.03	0.09	−1.82	—	—
belemnite	unknown	mollusca	cephalopoda	Junction Bed, Dorset, UK	JB6	calcite	0.16	0.09	−1.56	—	—
belemnite	unknown	mollusca	cephalopoda	Junction Bed, Dorset, UK	JB7	calcite	0.18	0.09	−1.53	—	—
belemnite	unknown	mollusca	cephalopoda	Junction Bed, Dorset, UK	JB8	calcite	0.16	0.09	−1.56	—	—
belemnite	unknown	mollusca	cephalopoda	Junction Bed, Dorset, UK	JB9	calcite	0.15	0.11	−1.59	—	—
belemnite	unknown	mollusca	cephalopoda	Junction Bed, Dorset, UK	JB10	calcite	0.28	0.09	−1.33	—	—
belemnite	unknown	mollusca	cephalopoda	Junction Bed, Dorset, UK	JB11	calcite	0.07	0.11	−1.74	—	—
belemnite	unknown	mollusca	cephalopoda	Burton Bradstock, Dorset, UK	BED1	calcite	0.01	0.05	−1.85	—	—
belemnite	unknown	mollusca	cephalopoda	Burton Bradstock, Dorset, UK	BED15	calcite	0.00	0.05	−1.88	—	—
belemnite	unknown	mollusca	cephalopoda	Burton Bradstock, Dorset, UK	BED12	calcite	0.00	0.05	−1.88	—	—
belemnite	unknown	mollusca	cephalopoda	Burton Bradstock, Dorset, UK	BED11	calcite	0.03	0.05	−1.82	—	—
belemnite	unknown	mollusca	cephalopoda	Burton Bradstock, Dorset, UK	BED6	calcite	0.02	0.05	−1.83	—	—
belemnite	unknown	mollusca	cephalopoda	Burton Bradstock, Dorset, UK	BED8	calcite	0.09	0.05	−1.70	—	—
belemnite	unknown	mollusca	cephalopoda	Burton Bradstock, Dorset, UK	BED1B	calcite	0.07	0.06	−1.74	—	—
belemnite	unknown	mollusca	cephalopoda	W. Kazakhstan	KAZ	calcite	-0.02	0.04	−1.91	—	—
belemnite	unknown	mollusca	cephalopoda	Eastbourne, Sussex, UK	HOL	calcite	0.09	0.04	−1.71	—	—

Table 4.4: Ca-isotope measurements of modern carbonates compiled from this study and several other sources (Russell et al., 1978; Skulan et al., 1997; Zhu and Macdougall, 1998; Gussone et al., 2003; Schmitt et al., 2003b; Fantle and DePaolo, 2005; Gussone et al., 2005; Heuser et al., 2005; Sime et al., 2005; Gussone et al., 2006; Steuber and Buhl, 2006; Fantle and DePaolo, 2007; Farkaš et al., 2007b; Langer et al., 2007; Sime et al., 2007; Griffith et al., 2008b; Heinemann et al., 2008; Kasemann et al., 2008; von Allmen et al., 2010; Holmden et al., 2012). Further details about the samples can be found in the respective sources; details of the deep sea corals analyzed in this study are from A. Thomas (personal communication) and Case et al. (2010). Temperature estimates are from the World Ocean Atlas 2005 (Locarnini et al., 2006) or measured data from the reference. Temperature normalizations used the relationship of +0.02‰ per °C (see Section 4.2).

Common name	Binomen	Phylum or division	Subtaxon	Location	Mineralogy	Source	$\delta^{44/40}$Ca rel. to seawater	T (°C)	T-normalized $\delta^{44/40}$Ca (15 °C)
Holocene ooze	—	deep-sea avg		DSDP 590B	deep-sea calcite	Skulan et al. (1997)	−0.90	21.5	−0.90
nannofossil ooze	—	deep-sea avg		DSDP 590	deep-sea calcite	Fantle and DePaolo (2005)	−1.31	21.5	−1.31
nannofossil ooze	—	deep-sea avg		ODP 807A	deep-sea calcite	Fantle and DePaolo (2007)	−1.29	29.2	−1.29
deep-sea bulk carbonate	—	deep-sea avg		various	deep-sea calcite	De La Rocha and DePaolo (2000)	−1.30	18.0	−1.30
deep-sea bulk carbonate	—	deep-sea avg		various	deep-sea calcite	Schmitt et al. (2003b)	−1.20	18.0	−1.20
non-foraminiferal bulk	—	deep-sea avg		various	deep-sea calcite	Sime et al. (2007)	−1.35	18.0	−1.35
blue mussel	*Mytilus edulis*	mollusca	bivalvia	North Sea	calcite (prismatic)	Heinemann et al. (2008)	−0.77	9.6	−0.66
blue mussel	*Mytilus edulis*	mollusca	bivalvia	North Sea	calcite (prismatic)	Heinemann et al. (2008)	−0.83	9.6	−0.72
blue mussel	*Mytilus edulis*	mollusca	bivalvia	North Sea	calcite (prismatic)	Heinemann et al. (2008)	−1.10	9.6	−0.99
blue mussel	*Mytilus edulis*	mollusca	bivalvia	San Fransisco Bay, USA	possibly mixed	Skulan and DePaolo (1999)	−0.66	13.0	−0.62
oyster	*Ostrea*	mollusca	bivalvia	San Fransisco Bay, USA	possibly mixed	Skulan and DePaolo (1999)	−1.19	13.0	−1.15
oyster	*Ostrea*	mollusca	bivalvia	North Sea	possibly mixed	Steuber and Buhl (2006)	−1.44	9.6	−1.33
oyster	*Ostrea*	mollusca	bivalvia	North Sea	possibly mixed	Steuber and Buhl (2006)	−1.42	9.6	−1.31
giant clam	*Tridacna*	mollusca	bivalvia	Enewetak, tropical Pacific	possibly mixed	Steuber and Buhl (2006)	−1.06	28.0	−1.32
bivalve fragment	—	mollusca	bivalvia	Skye, Scotland	possibly mixed	this study	−1.16	10.4	−1.07
bivalve fragment	—	mollusca	bivalvia	Skye, Scotland	possibly mixed	this study	−0.96	10.4	−0.87
chiton	*Polyplacophora*	mollusca	polyplacophora	North Atlantic	possibly mixed	Steuber and Buhl (2006)	−1.14	10.0	−1.04
cone snail	*Conus puncticulatus*	mollusca	gastropoda	unknown (shallow, tropical)	possibly mixed	Skulan et al. (1997)	−1.35	27.0	−1.59
limpet	*Bathyacmaea*	mollusca	gastropoda	unknown (deep ocean)	possibly mixed	Skulan et al. (1997)	−1.32	2.0	−1.06
sea snail fragment	unknown	mollusca	gastropoda	Skye, Scotland	possibly mixed	this study	−1.48	10.4	−1.39
sea snail fragment	unknown	mollusca	gastropoda	Skye, Scotland	possibly mixed	this study	−1.26	10.4	−1.17
brachiopod	*Anakinetica*	brachiopoda		Australian shelf	low-Mg calcite	Steuber and Buhl (2006)	−0.94	20.0	−1.04
brachiopod	*Terebratulina septentrionalis*	brachiopoda		Bay of Fundy	low-Mg calcite	von Allmen et al. (2010)	−0.80	7.0	−0.64
brachiopod	*Terebratulina septentrionalis*	brachiopoda		Bay of Fundy	low-Mg calcite	von Allmen et al. (2010)	−0.86	7.0	−0.70
brachiopod	*Gryphus vitreus*	brachiopoda		Mediterranean	low-Mg calcite	von Allmen et al. (2010)	−0.56	20.5	−0.67
brachiopod	*Thecidellina*	brachiopoda		Osprey Reef, Coral Sea	low-Mg calcite	Gussone et al. (2005)	−0.69	26.9	−0.93
brachiopod	unknown	brachiopoda		Madeira	low-Mg calcite	Gussone et al. (2005)	−0.83	29.0	−1.11

Continued on next page

Table 4.4: *Continued*

Common name	Binomen	Phylum or division	Subtaxon	Location	Mineralogy	Source	$\delta^{44/40}$Ca rel. to seawater	T (°C)	T-normalized $\delta^{44/40}$Ca (15 °C)
brachiopod	*Waltonoia inconspicua*	brachiopoda		South New Zealand	low-Mg calcite	Gussone et al. (2005)	−1.06	14.0	−1.04
brachiopod	*Terebratalia transversa*	brachiopoda		San Juan Islands, WA, USA	low-Mg calcite	Gussone et al. (2005)	−0.96	10.0	−0.86
brachiopod	*Terebratalia transversa*	brachiopoda		San Juan Islands, WA, USA	low-Mg calcite	Gussone et al. (2005)	−0.91	10.0	−0.81
brachiopod	*Terebratalia transversa*	brachiopoda		San Juan Islands, WA, USA	low-Mg calcite	Farkaš et al. (2007b)	−0.81	11.9	−0.75
brachiopod	*Terebratalia transversa*	brachiopoda		San Juan Islands, WA, USA	low-Mg calcite	Farkaš et al. (2007b)	−0.79	11.9	−0.73
coccolithophore	*Emiliania huxleyi*	haptophyta		laboratory culture	low-Mg calcite	De La Rocha and DePaolo (2000)	−1.30	16.0	−1.32
coccolithophore	*Emiliania huxleyi*	haptophyta		laboratory culture	low-Mg calcite	Langer et al. (2007)	−1.29	17.0	−1.33
coccolithophore	*Emiliania huxleyi*	haptophyta		laboratory culture	low-Mg calcite	Langer et al. (2007)	−1.23	17.0	−1.27
coccolithophore	*Emiliania huxleyi*	haptophyta		laboratory culture	low-Mg calcite	Langer et al. (2007)	−1.26	17.0	−1.30
coccolithophore	*Emiliania huxleyi*	haptophyta		laboratory culture	low-Mg calcite	Langer et al. (2007)	−1.29	17.0	−1.33
coccolithophore	*Emiliania huxleyi*	haptophyta		laboratory culture	low-Mg calcite	Langer et al. (2007)	−1.29	17.0	−1.33
coccolithophore	*Emiliania huxleyi*	haptophyta		laboratory culture	low-Mg calcite	Langer et al. (2007)	−1.05	17.0	−1.09
coccolithophore	*Emiliania huxleyi*	haptophyta		laboratory culture	low-Mg calcite	Langer et al. (2007)	−1.28	17.0	−1.32
coccolithophore	*Emiliania huxleyi*	haptophyta		laboratory culture	low-Mg calcite	Langer et al. (2007)	−1.35	17.0	−1.39
coccolithophore	*Emiliania huxleyi*	haptophyta		laboratory culture	low-Mg calcite	Langer et al. (2007)	−1.49	17.0	−1.53
coccolithophore	*Emiliania huxleyi*	haptophyta		laboratory culture	low-Mg calcite	Langer et al. (2007)	−1.55	17.0	−1.59
coccolithophore	*Emiliania huxleyi*	haptophyta		laboratory culture	low-Mg calcite	Langer et al. (2007)	−1.44	17.0	−1.48
coccolithophore	*Emiliania huxleyi*	haptophyta		laboratory culture	low-Mg calcite	Gussone et al. (2006)	−1.49	5	−1.29
coccolithophore	*Emiliania huxleyi*	haptophyta		laboratory culture	low-Mg calcite	Gussone et al. (2006)	−1.53	5	−1.33
coccolithophore	*Emiliania huxleyi*	haptophyta		laboratory culture	low-Mg calcite	Gussone et al. (2006)	−1.58	5	−1.38
coccolithophore	*Emiliania huxleyi*	haptophyta		laboratory culture	low-Mg calcite	Gussone et al. (2006)	−1.63	5	−1.43
coccolithophore	*Emiliania huxleyi*	haptophyta		laboratory culture	low-Mg calcite	Gussone et al. (2006)	−1.64	5	−1.44
coccolithophore	*Emiliania huxleyi*	haptophyta		laboratory culture	low-Mg calcite	Gussone et al. (2006)	−1.30	11	−1.22
coccolithophore	*Emiliania huxleyi*	haptophyta		laboratory culture	low-Mg calcite	Gussone et al. (2006)	−1.30	11	−1.22
coccolithophore	*Emiliania huxleyi*	haptophyta		laboratory culture	low-Mg calcite	Gussone et al. (2006)	−1.35	11	−1.27
coccolithophore	*Emiliania huxleyi*	haptophyta		laboratory culture	low-Mg calcite	Gussone et al. (2006)	−1.44	11	−1.36
coccolithophore	*Emiliania huxleyi*	haptophyta		laboratory culture	low-Mg calcite	Gussone et al. (2006)	−1.47	11	−1.39
coccolithophore	*Emiliania huxleyi*	haptophyta		laboratory culture	low-Mg calcite	Gussone et al. (2006)	−1.17	15	−1.17
coccolithophore	*Emiliania huxleyi*	haptophyta		laboratory culture	low-Mg calcite	Gussone et al. (2006)	−1.25	15	−1.25
coccolithophore	*Emiliania huxleyi*	haptophyta		laboratory culture	low-Mg calcite	Gussone et al. (2006)	−1.25	15	−1.25
coccolithophore	*Emiliania huxleyi*	haptophyta		laboratory culture	low-Mg calcite	Gussone et al. (2006)	−1.29	15	−1.29
coccolithophore	*Emiliania huxleyi*	haptophyta		laboratory culture	low-Mg calcite	Gussone et al. (2006)	−1.23	20	−1.33
coccolithophore	*Emiliania huxleyi*	haptophyta		laboratory culture	low-Mg calcite	Gussone et al. (2006)	−1.20	20	−1.30
coccolithophore	*Emiliania huxleyi*	haptophyta		laboratory culture	low-Mg calcite	Gussone et al. (2006)	−1.19	20	−1.29

Continued on next page

Table 4.4: *Continued*

Common name	Binomen	Phylum or division	Subtaxon	Location	Mineralogy	Source	$\delta^{44/40}$Ca rel. to seawater	T (°C)	T-normalized $\delta^{44/40}$Ca (15 °C)
coccolithophore	*Emiliania huxleyi*	haptophyta		laboratory culture	low-Mg calcite	Gussone et al. (2006)	−1.11	20	−1.21
coccolithophore	*Emiliania huxleyi*	haptophyta		laboratory culture	low-Mg calcite	Gussone et al. (2006)	−1.10	20	−1.20
planktic foraminifera	*Globigerina bulloides*	protozoa	foraminiferida	Guyamas Basin, Gulf of CA	calcite	Griffith et al. (2008b)	−1.75	18.3	−1.82
planktic foraminifera	*Globigerina bulloides*	protozoa	foraminiferida	Guyamas Basin, Gulf of CA	calcite	Griffith et al. (2008b)	−1.16	18.2	−1.22
planktic foraminifera	*Globigerina bulloides*	protozoa	foraminiferida	Guyamas Basin, Gulf of CA	calcite	Griffith et al. (2008b)	−1.34	18.6	−1.41
planktic foraminifera	*Globigerina bulloides*	protozoa	foraminiferida	Guyamas Basin, Gulf of CA	calcite	Griffith et al. (2008b)	−1.39	23.4	−1.56
planktic foraminifera	*Globigerina bulloides*	protozoa	foraminiferida	Guyamas Basin, Gulf of CA	calcite	Griffith et al. (2008b)	−1.26	24.3	−1.45
planktic foraminifera	*Globigerina bulloides*	protozoa	foraminiferida	Guyamas Basin, Gulf of CA	calcite	Griffith et al. (2008b)	−1.38	31.2	−1.70
planktic foraminifera	*Globigerina bulloides*	protozoa	foraminiferida	Guyamas Basin, Gulf of CA	calcite	Griffith et al. (2008b)	−1.28	31.4	−1.61
planktic foraminifera	*Globigerinoides ruber*	protozoa	foraminiferida	Guyamas Basin, Gulf of CA	calcite	Griffith et al. (2008b)	−0.98	24.4	−1.17
planktic foraminifera	*Globigerinoides ruber*	protozoa	foraminiferida	Guyamas Basin, Gulf of CA	calcite	Griffith et al. (2008b)	−1.23	28.3	−1.50
planktic foraminifera	*Globigerinoides ruber*	protozoa	foraminiferida	Guyamas Basin, Gulf of CA	calcite	Griffith et al. (2008b)	−1.13	26.8	−1.37
planktic foraminifera	*Globigerinoides ruber*	protozoa	foraminiferida	Guyamas Basin, Gulf of CA	calcite	Griffith et al. (2008b)	−1.43	25.7	−1.64
planktic foraminifera	*Globigerinoides ruber*	protozoa	foraminiferida	Guyamas Basin, Gulf of CA	calcite	Griffith et al. (2008b)	−1.28	30.3	−1.59
planktic foraminifera	*Globigerinoides ruber*	protozoa	foraminiferida	Guyamas Basin, Gulf of CA	calcite	Griffith et al. (2008b)	−1.58	30.8	−1.90
planktic foraminifera	*Globigerinoides ruber*	protozoa	foraminiferida	Guyamas Basin, Gulf of CA	calcite	Griffith et al. (2008b)	−1.41	30.4	−1.72
planktic foraminifera	*Globigerinoides ruber*	protozoa	foraminiferida	Guyamas Basin, Gulf of CA	calcite	Griffith et al. (2008b)	−1.38	31.1	−1.70
planktic foraminifera	*Globigerinoides sacculifer*	protozoa	foraminiferida	Guyamas Basin, Gulf of CA	calcite	Griffith et al. (2008b)	−0.98	27.8	−1.24
planktic foraminifera	*Globigerinoides sacculifer*	protozoa	foraminiferida	Guyamas Basin, Gulf of CA	calcite	Griffith et al. (2008b)	−1.02	28.8	−1.30
planktic foraminifera	*Globigerinoides sacculifer*	protozoa	foraminiferida	Guyamas Basin, Gulf of CA	calcite	Griffith et al. (2008b)	−0.81	30.4	−1.12
planktic foraminifera	*Globigerinoides sacculifer*	protozoa	foraminiferida	Guyamas Basin, Gulf of CA	calcite	Griffith et al. (2008b)	−1.16	30.8	−1.48
planktic foraminifera	*Globigerinoides sacculifer*	protozoa	foraminiferida	Guyamas Basin, Gulf of CA	calcite	Griffith et al. (2008b)	−1.38	31.1	−1.70
planktic foraminifera	*Neogloboquadrina dutertrei*	protozoa	foraminiferida	Guyamas Basin, Gulf of CA	calcite	Griffith et al. (2008b)	−1.30	18.3	−1.37
planktic foraminifera	*Neogloboquadrina dutertrei*	protozoa	foraminiferida	Guyamas Basin, Gulf of CA	calcite	Griffith et al. (2008b)	−1.37	18.6	−1.44
planktic foraminifera	*Neogloboquadrina dutertrei*	protozoa	foraminiferida	Guyamas Basin, Gulf of CA	calcite	Griffith et al. (2008b)	−1.37	20.6	−1.48
planktic foraminifera	*Neogloboquadrina dutertrei*	protozoa	foraminiferida	Guyamas Basin, Gulf of CA	calcite	Griffith et al. (2008b)	−1.52	21.3	−1.65
planktic foraminifera	*Neogloboquadrina dutertrei*	protozoa	foraminiferida	Guyamas Basin, Gulf of CA	calcite	Griffith et al. (2008b)	−1.43	27.3	−1.68
planktic foraminifera	*Neogloboquadrina dutertrei*	protozoa	foraminiferida	Guyamas Basin, Gulf of CA	calcite	Griffith et al. (2008b)	−1.24	28.8	−1.52
planktic foraminifera	*Globigerinoides ruber*	protozoa	foraminiferida	equatorial Atlantic	calcite	Griffith et al. (2008b)	−1.14	26.6	−1.37
planktic foraminifera	*Globigerinoides ruber*	protozoa	foraminiferida	equatorial Atlantic	calcite	Griffith et al. (2008b)	−1.16	27.2	−1.40
planktic foraminifera	*Globigerinoides ruber*	protozoa	foraminiferida	equatorial Atlantic	calcite	Griffith et al. (2008b)	−1.02	27.7	−1.27
planktic foraminifera	*Globigerinoides ruber*	protozoa	foraminiferida	equatorial Atlantic	calcite	Griffith et al. (2008b)	−1.04	28.3	−1.31
planktic foraminifera	*Globigerinoides ruber*	protozoa	foraminiferida	equatorial Atlantic	calcite	Griffith et al. (2008b)	−1.19	28.5	−1.46
planktic foraminifera	*Globigerinoides ruber*	protozoa	foraminiferida	equatorial Atlantic	calcite	Griffith et al. (2008b)	−1.24	28.9	−1.52

Continued on next page

Table 4.4: *Continued*

Common name	Binomen	Phylum or division	Subtaxon	Location	Mineralogy	Source	$\delta^{44/40}$Ca rel. to seawater	T (°C)	T-normalized $\delta^{44/40}$Ca (15 °C)
planktic foraminifera	*Globigerinoides ruber*	protozoa	foraminiferida	equatorial Atlantic	calcite	Griffith et al. (2008b)	−1.21	25.8	−1.43
planktic foraminifera	*Globigerinoides ruber*	protozoa	foraminiferida	equatorial Atlantic	calcite	Griffith et al. (2008b)	−1.14	25.9	−1.36
planktic foraminifera	*Globigerinoides ruber*	protozoa	foraminiferida	equatorial Atlantic	calcite	Griffith et al. (2008b)	−1.15	26.1	−1.37
planktic foraminifera	*Globigerinoides ruber*	protozoa	foraminiferida	equatorial Atlantic	calcite	Griffith et al. (2008b)	−1.21	26.8	−1.45
planktic foraminifera	*Globigerinoides ruber*	protozoa	foraminiferida	equatorial Atlantic	calcite	Griffith et al. (2008b)	−1.08	26.9	−1.32
planktic foraminifera	*Globigerinoides ruber*	protozoa	foraminiferida	equatorial Atlantic	calcite	Griffith et al. (2008b)	−1.08	27.1	−1.32
planktic foraminifera	*Globigerinoides sacculifer*	protozoa	foraminiferida	equatorial Atlantic	calcite	Griffith et al. (2008b)	−1.08	20.1	−1.18
planktic foraminifera	*Globigerinoides sacculifer*	protozoa	foraminiferida	equatorial Atlantic	calcite	Griffith et al. (2008b)	−1.15	23.9	−1.33
planktic foraminifera	*Globigerinoides sacculifer*	protozoa	foraminiferida	equatorial Atlantic	calcite	Griffith et al. (2008b)	−1.18	24.0	−1.36
planktic foraminifera	*Globigerinoides sacculifer*	protozoa	foraminiferida	equatorial Atlantic	calcite	Griffith et al. (2008b)	−0.98	24.9	−1.18
planktic foraminifera	*Globigerinoides sacculifer*	protozoa	foraminiferida	equatorial Atlantic	calcite	Griffith et al. (2008b)	−1.30	25.3	−1.51
planktic foraminifera	*Globigerinoides sacculifer*	protozoa	foraminiferida	equatorial Atlantic	calcite	Griffith et al. (2008b)	−1.13	18.6	−1.20
planktic foraminifera	*Globigerinoides sacculifer*	protozoa	foraminiferida	equatorial Atlantic	calcite	Griffith et al. (2008b)	−1.00	23.7	−1.17
planktic foraminifera	*Globigerinoides sacculifer*	protozoa	foraminiferida	equatorial Atlantic	calcite	Griffith et al. (2008b)	−0.97	24.1	−1.15
planktic foraminifera	*Globigerinoides sacculifer*	protozoa	foraminiferida	equatorial Atlantic	calcite	Griffith et al. (2008b)	−0.92	24.3	−1.11
planktic foraminifera	*Globigerinoides sacculifer*	protozoa	foraminiferida	equatorial Atlantic	calcite	Griffith et al. (2008b)	−1.25	24.6	−1.44
planktic foraminifera	*Globorotalia inflata*	protozoa	foraminiferida	equatorial Atlantic	calcite	Griffith et al. (2008b)	−1.28	15.3	−1.29
planktic foraminifera	*Globorotalia inflata*	protozoa	foraminiferida	equatorial Atlantic	calcite	Griffith et al. (2008b)	−1.21	20.9	−1.33
planktic foraminifera	*Globorotalia inflata*	protozoa	foraminiferida	equatorial Atlantic	calcite	Griffith et al. (2008b)	−1.04	21.1	−1.16
planktic foraminifera	*Globorotalia truncatulinoides*	protozoa	foraminiferida	equatorial Atlantic	calcite	Griffith et al. (2008b)	−1.51	11.0	−1.43
planktic foraminifera	*Globorotalia truncatulinoides*	protozoa	foraminiferida	equatorial Atlantic	calcite	Griffith et al. (2008b)	−0.92	12.5	−0.87
planktic foraminifera	*Globorotalia truncatulinoides*	protozoa	foraminiferida	equatorial Atlantic	calcite	Griffith et al. (2008b)	−1.56	14.4	−1.55
planktic foraminifera	*Globorotalia truncatulinoides*	protozoa	foraminiferida	equatorial Atlantic	calcite	Griffith et al. (2008b)	−1.42	14.8	−1.42
planktic foraminifera	*Globorotalia truncatulinoides*	protozoa	foraminiferida	equatorial Atlantic	calcite	Griffith et al. (2008b)	−1.16	18.4	−1.23
planktic foraminifera	*Globorotalia tumida*	protozoa	foraminiferida	equatorial Atlantic	calcite	Griffith et al. (2008b)	−1.21	14.4	−1.20
planktic foraminifera	*Globorotalia tumida*	protozoa	foraminiferida	equatorial Atlantic	calcite	Griffith et al. (2008b)	−1.25	17.0	−1.29
planktic foraminifera	*Globorotalia tumida*	protozoa	foraminiferida	equatorial Atlantic	calcite	Griffith et al. (2008b)	−1.34	18.2	−1.40
planktic foraminifera	*Globorotalia tumida*	protozoa	foraminiferida	equatorial Atlantic	calcite	Griffith et al. (2008b)	−1.28	26.4	−1.51
planktic foraminifera	*Globorotalia tumida*	protozoa	foraminiferida	equatorial Atlantic	calcite	Griffith et al. (2008b)	−1.30	26.4	−1.53
planktic foraminifera	*Globorotalia tumida*	protozoa	foraminiferida	equatorial Atlantic	calcite	Griffith et al. (2008b)	−1.29	26.4	−1.52
planktic foraminifera	*Neogloboquadrina dutertrei*	protozoa	foraminiferida	equatorial Atlantic	calcite	Griffith et al. (2008b)	−1.21	19.5	−1.30
planktic foraminifera	*Neogloboquadrina dutertrei*	protozoa	foraminiferida	equatorial Atlantic	calcite	Griffith et al. (2008b)	−1.34	20.0	−1.44
planktic foraminifera	*Neogloboquadrina dutertrei*	protozoa	foraminiferida	equatorial Atlantic	calcite	Griffith et al. (2008b)	−1.20	20.1	−1.30
planktic foraminifera	*Neogloboquadrina dutertrei*	protozoa	foraminiferida	equatorial Atlantic	calcite	Griffith et al. (2008b)	−1.22	21.4	−1.35
planktic foraminifera	*Neogloboquadrina dutertrei*	protozoa	foraminiferida	equatorial Atlantic	calcite	Griffith et al. (2008b)	−1.19	21.8	−1.33

Continued on next page

Table 4.4: *Continued*

Common name	Binomen	Phylum or division	Subtaxon	Location	Mineralogy	Source	$\delta^{44/40}$Ca rel. to seawater	T (°C)	T-normalized $\delta^{44/40}$Ca (15 °C)
planktic foraminifera	*Globigerina bulloides*	protozoa	foraminiferida	north Atlantic	calcite	Griffith et al. (2008b)	−1.39	2.3	−1.14
planktic foraminifera	*Globigerina bulloides*	protozoa	foraminiferida	north Atlantic	calcite	Griffith et al. (2008b)	−1.56	2.8	−1.32
planktic foraminifera	*Globigerina bulloides*	protozoa	foraminiferida	north Atlantic	calcite	Griffith et al. (2008b)	−1.47	7.3	−1.32
planktic foraminifera	*Globigerina bulloides*	protozoa	foraminiferida	north Atlantic	calcite	Griffith et al. (2008b)	−1.30	7.3	−1.15
planktic foraminifera	*Globigerina bulloides*	protozoa	foraminiferida	north Atlantic	calcite	Griffith et al. (2008b)	−1.34	8.9	−1.22
planktic foraminifera	*Turborotalia quinqueloba*	protozoa	foraminiferida	Norwegian Sea, N Atlantic	low-Mg calcite	Gussone et al. (2005)	−1.38	10.0	−1.28
planktic foraminifera	*Turborotalia quinqueloba*	protozoa	foraminiferida	Norwegian Sea, N Atlantic	low-Mg calcite	Gussone et al. (2005)	−1.44	10.0	−1.34
planktic foraminifera	*Turborotalia quinqueloba*	protozoa	foraminiferida	Norwegian Sea, N Atlantic	low-Mg calcite	Gussone et al. (2005)	−1.36	10.0	−1.26
planktic foraminifera	*Turborotalia quinqueloba*	protozoa	foraminiferida	Norwegian Sea, N Atlantic	low-Mg calcite	Gussone et al. (2005)	−1.47	10.0	−1.37
planktic foraminifera	*Orbulina universa*	protozoa	foraminiferida	North Atlantic	calcite	Sime et al. (2005)	−1.28	10.5	−1.19
planktic foraminifera	*Orbulina universa*	protozoa	foraminiferida	North Atlantic	calcite	Sime et al. (2005)	−1.06	12.0	−1.00
planktic foraminifera	*Orbulina universa*	protozoa	foraminiferida	North Atlantic	calcite	Sime et al. (2005)	−1.12	13.1	−1.08
planktic foraminifera	*Orbulina universa*	protozoa	foraminiferida	North Atlantic	calcite	Sime et al. (2005)	−1.22	13.6	−1.19
planktic foraminifera	*Orbulina universa*	protozoa	foraminiferida	West Indian Ocean	calcite	Sime et al. (2005)	−1.20	24.4	−1.39
planktic foraminifera	*Orbulina universa*	protozoa	foraminiferida	West Indian Ocean	calcite	Sime et al. (2005)	−1.18	21.6	−1.31
planktic foraminifera	*Globigerinoides ruber*	protozoa	foraminiferida	North Atlantic	calcite	Sime et al. (2005)	−1.24	15.4	−1.25
planktic foraminifera	*Globigerinoides ruber*	protozoa	foraminiferida	North Atlantic	calcite	Sime et al. (2005)	−1.46	15.6	−1.47
planktic foraminifera	*Globigerinoides ruber*	protozoa	foraminiferida	North Atlantic	calcite	Sime et al. (2005)	−1.16	15.5	−1.17
planktic foraminifera	*Globigerinoides ruber*	protozoa	foraminiferida	North Atlantic	calcite	Sime et al. (2005)	−1.28	17.2	−1.32
planktic foraminifera	*Globigerinoides ruber*	protozoa	foraminiferida	North Atlantic	calcite	Sime et al. (2005)	−1.16	18.1	−1.22
planktic foraminifera	*Globigerinoides ruber*	protozoa	foraminiferida	West Indian Ocean	calcite	Sime et al. (2005)	−1.20	21.2	−1.32
planktic foraminifera	*Globigerinoides ruber*	protozoa	foraminiferida	West Indian Ocean	calcite	Sime et al. (2005)	−1.10	28.0	−1.36
planktic foraminifera	*Globigerinoides ruber*	protozoa	foraminiferida	West Indian Ocean	calcite	Sime et al. (2005)	−1.16	25.1	−1.36
planktic foraminifera	*Globigerinoides sacculifer*	protozoa	foraminiferida	North Atlantic	calcite	Sime et al. (2005)	−1.20	16.7	−1.23
planktic foraminifera	*Globigerinoides sacculifer*	protozoa	foraminiferida	West Indian Ocean	calcite	Sime et al. (2005)	−1.32	19.3	−1.41
planktic foraminifera	*Globigerinoides sacculifer*	protozoa	foraminiferida	West Indian Ocean	calcite	Sime et al. (2005)	−1.16	25.1	−1.36
planktic foraminifera	*Globigerinoides trilobus*	protozoa	foraminiferida	North Atlantic	calcite	Sime et al. (2005)	−1.14	16.5	−1.17
planktic foraminifera	*Globigerinoides trilobus*	protozoa	foraminiferida	West Indian Ocean	calcite	Sime et al. (2005)	−1.22	20.6	−1.33
planktic foraminifera	*Globigerinoides trilobus*	protozoa	foraminiferida	West Indian Ocean	calcite	Sime et al. (2005)	−1.16	26.2	−1.38
planktic foraminifera	*Globigerinoides trilobus*	protozoa	foraminiferida	West Indian Ocean	calcite	Sime et al. (2005)	−1.24	24.0	−1.42
planktic foraminifera	*Globigerinella aequilateris*	protozoa	foraminiferida	North Atlantic	calcite	Sime et al. (2005)	−1.26	12.0	−1.20
planktic foraminifera	*Globigerinella aequilateris*	protozoa	foraminiferida	North Atlantic	calcite	Sime et al. (2005)	−1.32	12.1	−1.26
planktic foraminifera	*Globigerinella aequilateris*	protozoa	foraminiferida	North Atlantic	calcite	Sime et al. (2005)	−1.34	14.0	−1.32
planktic foraminifera	*Globigerinella aequilateris*	protozoa	foraminiferida	West Indian Ocean	calcite	Sime et al. (2005)	−1.22	23.3	−1.39
planktic foraminifera	*Globigerinella aequilateris*	protozoa	foraminiferida	West Indian Ocean	calcite	Sime et al. (2005)	−1.32	22.9	−1.48

Continued on next page

Table 4.4: *Continued*

Common name	Binomen	Phylum or division	Subtaxon	Location	Mineralogy	Source	$\delta^{44/40}$Ca rel. to seawater	T (°C)	T-normalized $\delta^{44/40}$Ca (15 °C)
planktic foraminifera	*Globigerina bulloides*	protozoa	foraminiferida	North Atlantic	calcite	Sime et al. (2005)	−1.24	11.8	−1.18
planktic foraminifera	*Globigerina bulloides*	protozoa	foraminiferida	North Atlantic	calcite	Sime et al. (2005)	−1.32	13.7	−1.29
planktic foraminifera	*Globigerina bulloides*	protozoa	foraminiferida	North Atlantic	calcite	Sime et al. (2005)	−1.20	13.6	−1.17
planktic foraminifera	*Globigerina bulloides*	protozoa	foraminiferida	West Indian Ocean	calcite	Sime et al. (2005)	−1.16	15.1	−1.16
planktic foraminifera	*Neogloboquadrina pachyderma*	protozoa	foraminiferida	North Atlantic	calcite	Sime et al. (2005)	−1.28	9.3	−1.17
planktic foraminifera	*Neogloboquadrina pachyderma*	protozoa	foraminiferida	North Atlantic	calcite	Sime et al. (2005)	−1.10	12.1	−1.04
planktic foraminifera	*Neogloboquadrina pachyderma*	protozoa	foraminiferida	North Atlantic	calcite	Sime et al. (2005)	−1.30	12.5	−1.25
planktic foraminifera	*Neogloboquadrina pachyderma*	protozoa	foraminiferida	North Atlantic	calcite	Sime et al. (2005)	−1.18	12.7	−1.13
planktic foraminifera	*Neogloboquadrina pachyderma*	protozoa	foraminiferida	North Atlantic	calcite	Sime et al. (2005)	−1.18	13.3	−1.15
planktic foraminifera	*Neogloboquadrina pachyderma*	protozoa	foraminiferida	North Atlantic	calcite	Sime et al. (2005)	−1.16	15.5	−1.17
planktic foraminifera	*Neogloboquadrina pachyderma*	protozoa	foraminiferida	North Atlantic	calcite	Sime et al. (2005)	−1.10	14.7	−1.09
planktic foraminifera	*Neogloboquadrina pachyderma*	protozoa	foraminiferida	West Indian Ocean	calcite	Sime et al. (2005)	−1.20	19.9	−1.30
planktic foraminifera	*Neogloboquadrina pachyderma*	protozoa	foraminiferida	West Indian Ocean	calcite	Sime et al. (2005)	−1.36	21.0	−1.48
planktic foraminifera	*Neogloboquadrina pachyderma*	protozoa	foraminiferida	West Indian Ocean	calcite	Sime et al. (2005)	−1.20	20.1	−1.30
planktic foraminifera	*Neogloboquadrina dutertrei*	protozoa	foraminiferida	West Indian Ocean	calcite	Sime et al. (2005)	−1.34	17.8	−1.40
planktic foraminifera	*Neogloboquadrina dutertrei*	protozoa	foraminiferida	West Indian Ocean	calcite	Sime et al. (2005)	−1.34	22.7	−1.49
planktic foraminifera	*Neogloboquadrina dutertrei*	protozoa	foraminiferida	West Indian Ocean	calcite	Sime et al. (2005)	−1.22	20.6	−1.33
planktic foraminifera	*Pulleniatina obliquiloculata*	protozoa	foraminiferida	West Indian Ocean	calcite	Sime et al. (2005)	−1.18	21.3	−1.31
planktic foraminifera	*Pulleniatina obliquiloculata*	protozoa	foraminiferida	West Indian Ocean	calcite	Sime et al. (2005)	−1.18	19.4	−1.27
planktic foraminifera	*Globorotalia inflata*	protozoa	foraminiferida	North Atlantic	calcite	Sime et al. (2005)	−1.24	11.8	−1.18
planktic foraminifera	*Globorotalia inflata*	protozoa	foraminiferida	North Atlantic	calcite	Sime et al. (2005)	−1.24	11.8	−1.18
planktic foraminifera	*Globorotalia inflata*	protozoa	foraminiferida	North Atlantic	calcite	Sime et al. (2005)	−1.24	11.8	−1.18
planktic foraminifera	*Globorotalia inflata*	protozoa	foraminiferida	North Atlantic	calcite	Sime et al. (2005)	−1.24	11.8	−1.18
planktic foraminifera	*Globorotalia inflata*	protozoa	foraminiferida	North Atlantic	calcite	Sime et al. (2005)	−1.24	11.8	−1.18
planktic foraminifera	*Globorotalia inflata*	protozoa	foraminiferida	West Indian Ocean	calcite	Sime et al. (2005)	−1.24	11.8	−1.18
planktic foraminifera	*Globorotalia truncatulinoides*	protozoa	foraminiferida	North Atlantic	calcite	Sime et al. (2005)	−1.30	9.4	−1.19
planktic foraminifera	*Globorotalia truncatulinoides*	protozoa	foraminiferida	North Atlantic	calcite	Sime et al. (2005)	−1.34	10.4	−1.25
planktic foraminifera	*Globorotalia truncatulinoides*	protozoa	foraminiferida	North Atlantic	calcite	Sime et al. (2005)	−0.80	9.4	−0.69
planktic foraminifera	*Globorotalia truncatulinoides*	protozoa	foraminiferida	North Atlantic	calcite	Sime et al. (2005)	−0.72	9.5	−0.61
planktic foraminifera	*Globorotalia truncatulinoides*	protozoa	foraminiferida	North Atlantic	calcite	Sime et al. (2005)	−0.64	11.2	−0.56
planktic foraminifera	*Globorotalia truncatulinoides*	protozoa	foraminiferida	West Indian Ocean	calcite	Sime et al. (2005)	−0.82	11.4	−0.75
planktic foraminifera	*Globorotalia truncatulinoides*	protozoa	foraminiferida	West Indian Ocean	calcite	Sime et al. (2005)	−1.26	16.3	−1.29
planktic foraminifera	*Globorotalia scitula*	protozoa	foraminiferida	West Indian Ocean	calcite	Sime et al. (2005)	−0.94	11.5	−0.87
planktic foraminifera	*Globorotalia scitula*	protozoa	foraminiferida	West Indian Ocean	calcite	Sime et al. (2005)	−1.36	7.3	−1.21
planktic foraminifera	*Globigerinoides trilobus*	protozoa	foraminiferida	ODP Site 925, equatorial Atlantic	calcite	Sime et al. (2007)	−1.26	27.4	−1.51

Continued on next page

Table 4.4: *Continued*

Common name	Binomen	Phylum or division	Subtaxon	Location	Mineralogy	Source	$\delta^{44/40}$Ca rel. to seawater	T (°C)	T-normalized $\delta^{44/40}$Ca (15 °C)
planktic foraminifera	*Globigerinoides sacculifer*	protozoa	foraminiferida	ODP Site 925, equatorial Atlantic	calcite	Sime et al. (2007)	−1.16	27.4	−1.41
planktic foraminifera	*Globigerinoides trilobus*	protozoa	foraminiferida	ODP Site 871, equatorial Pacific	calcite	Heuser et al. (2005)	−1.01	28.5	−1.28
planktic foraminifera	*Globigerinoides ruber*	protozoa	foraminiferida	ODP Site 871, equatorial Pacific	calcite	Heuser et al. (2005)	−1.25	28.5	−1.52
planktic foraminifera	*Globigerinella*	protozoa	foraminiferida	ODP Site 871, equatorial Pacific	calcite	Heuser et al. (2005)	−1.44	28.5	−1.71
benthic foraminifera	*Glabratella ornatissima*	protozoa	foraminiferida	Bodega Bay, CA, USA	calcite	De La Rocha and DePaolo (2000)	−1.20	12.7	−1.15
planktic foraminifera	*Globorotalia menardii*	protozoa	foraminiferida	W equatorial Pacific, intermediate	calcite	Kasemann et al. (2008)	−1.19	25.1	−1.39
planktic foraminifera	*Globorotalia tumida*	protozoa	foraminiferida	W equatorial Pacific, intermediate	calcite	Kasemann et al. (2008)	−1.12	17.6	−1.17
planktic foraminifera	*Sphaeroidinella dehiscens*	protozoa	foraminiferida	W equatorial Pacific, mixed layer	calcite	Kasemann et al. (2008)	−1.23	25.6	−1.44
planktic foraminifera	*Globigerinoides conglobatus*	protozoa	foraminiferida	W equatorial Pacific, mixed layer	calcite	Kasemann et al. (2008)	−1.19	26.0	−1.41
planktic foraminifera	*Pulleniatina obliquiloculata*	protozoa	foraminiferida	W equatorial Pacific, mixed layer	calcite	Kasemann et al. (2008)	−1.09	23.5	−1.26
planktic foraminifera	*Globigerinoides sacculifer*	protozoa	foraminiferida	W equatorial Pacific, mixed layer	calcite	Kasemann et al. (2008)	−1.09	29.2	−1.37
planktic foraminifera	*Globigerinella siphonifera*	protozoa	foraminiferida	W equatorial Pacific, mixed layer	calcite	Kasemann et al. (2008)	−1.02	25.8	−1.24
planktic foraminifera	*Globigerinoides ruber*	protozoa	foraminiferida	W equatorial Pacific, mixed layer	calcite	Kasemann et al. (2008)	−1.12	30.2	−1.42
planktic foraminifera	*Orbulina universa*	protozoa	foraminiferida	W equatorial Pacific, mixed layer	calcite	Kasemann et al. (2008)	−0.93	30.0	−1.23
planktic foraminifera	*Orbulina universa*	protozoa	foraminiferida	laboratory culture	calcite	Gussone et al. (2003)	−1.14	10.5	−1.05
planktic foraminifera	*Orbulina universa*	protozoa	foraminiferida	laboratory culture	calcite	Gussone et al. (2003)	−1.16	10.5	−1.07
planktic foraminifera	*Orbulina universa*	protozoa	foraminiferida	laboratory culture	calcite	Gussone et al. (2003)	−1.12	12.9	−1.08
planktic foraminifera	*Orbulina universa*	protozoa	foraminiferida	laboratory culture	calcite	Gussone et al. (2003)	−1.17	12.9	−1.13
planktic foraminifera	*Orbulina universa*	protozoa	foraminiferida	laboratory culture	calcite	Gussone et al. (2003)	−1.15	16.2	−1.17
planktic foraminifera	*Orbulina universa*	protozoa	foraminiferida	laboratory culture	calcite	Gussone et al. (2003)	−1.06	18.0	−1.12
planktic foraminifera	*Orbulina universa*	protozoa	foraminiferida	laboratory culture	calcite	Gussone et al. (2003)	−1.08	18.0	−1.14
planktic foraminifera	*Orbulina universa*	protozoa	foraminiferida	laboratory culture	calcite	Gussone et al. (2003)	−1.01	21.0	−1.13
planktic foraminifera	*Orbulina universa*	protozoa	foraminiferida	laboratory culture	calcite	Gussone et al. (2003)	−1.12	21.0	−1.24
planktic foraminifera	*Orbulina universa*	protozoa	foraminiferida	laboratory culture	calcite	Gussone et al. (2003)	−1.00	22.0	−1.14
planktic foraminifera	*Orbulina universa*	protozoa	foraminiferida	laboratory culture	calcite	Gussone et al. (2003)	−0.99	23.3	−1.16
planktic foraminifera	*Orbulina universa*	protozoa	foraminiferida	laboratory culture	calcite	Gussone et al. (2003)	−0.89	23.3	−1.06
planktic foraminifera	*Orbulina universa*	protozoa	foraminiferida	laboratory culture	calcite	Gussone et al. (2003)	−0.87	27.0	−1.11
planktic foraminifera	*Orbulina universa*	protozoa	foraminiferida	laboratory culture	calcite	Gussone et al. (2003)	−0.83	27.0	−1.07
planktic foraminifera	*Orbulina universa*	protozoa	foraminiferida	laboratory culture	calcite	Gussone et al. (2003)	−0.88	27.0	−1.12
planktic foraminifera	*Orbulina universa*	protozoa	foraminiferida	laboratory culture	calcite	Gussone et al. (2003)	−1.07	29.2	−1.35
planktic foraminifera	*Orbulina universa*	protozoa	foraminiferida	laboratory culture	calcite	Gussone et al. (2003)	−0.76	29.3	−1.05
planktic foraminifera	*Orbulina universa*	protozoa	foraminiferida	laboratory culture	calcite	Gussone et al. (2003)	−0.79	29.3	−1.08
planktic foraminifera	*Orbulina universa*	protozoa	foraminiferida	laboratory culture	calcite	Gussone et al. (2003)	−0.84	29.3	−1.13
planktic foraminifera	*Orbulina universa*	protozoa	foraminiferida	laboratory culture	calcite	Gussone et al. (2003)	−0.89	29.3	−1.18
planktic foraminifera	*Orbulina universa*	protozoa	foraminiferida	laboratory culture	calcite	Gussone et al. (2003)	−0.86	29.3	−1.15

Continued on next page

Table 4.4: *Continued*

Common name	Binomen	Phylum or division	Subtaxon	Location	Mineralogy	Source	$\delta^{44/40}$Ca rel. to seawater	T (°C)	T-normalized $\delta^{44/40}$Ca (15 °C)
planktic foraminifera	*Orbulina universa*	protozoa	foraminiferida	laboratory culture	calcite	Gussone et al. (2003)	−0.97	22.0	−1.11
planktic foraminifera	*Orbulina universa*	protozoa	foraminiferida	laboratory culture	calcite	Gussone et al. (2003)	−1.01	22.0	−1.15
planktic foraminifera	*Orbulina universa*	protozoa	foraminiferida	laboratory culture	calcite	Gussone et al. (2003)	−1.07	22.0	−1.21
planktic foraminifera	*Orbulina universa*	protozoa	foraminiferida	laboratory culture	calcite	Gussone et al. (2003)	−1.13	22.0	−1.27
planktic foraminifera	*Orbulina universa*	protozoa	foraminiferida	laboratory culture	calcite	Gussone et al. (2003)	−0.89	22.0	−1.03
planktic foraminifera	*Orbulina universa*	protozoa	foraminiferida	laboratory culture	calcite	Gussone et al. (2003)	−0.97	22.0	−1.11
planktic foraminifera	*Orbulina universa*	protozoa	foraminiferida	laboratory culture	calcite	Gussone et al. (2003)	−1.01	22.0	−1.15
planktic foraminifera	*Orbulina universa*	protozoa	foraminiferida	laboratory culture	calcite	Gussone et al. (2003)	−1.08	22.0	−1.22
planktic foraminifera	*Orbulina universa*	protozoa	foraminiferida	laboratory culture	calcite	Gussone et al. (2003)	−0.98	22.0	−1.12
planktic foraminifera	*Globigerinoides sacculifer*	protozoa	foraminiferida	Western equatorial Pacific	calcite	Zhu and Macdougall (1998)	−0.86	25.0	−1.06
planktic foraminifera	*Globigerinoides sacculifer*	protozoa	foraminiferida	Western equatorial Pacific	calcite	Zhu and Macdougall (1998)	−1.45	25.0	−1.65
planktic foraminifera	*Neogloboquadrina pachyderma*	protozoa	foraminiferida	South Atlantic	calcite	Zhu and Macdougall (1998)	−0.86	18.0	−0.92
planktic foraminifera	*Neogloboquadrina pachyderma*	protozoa	foraminiferida	South Atlantic	calcite	Zhu and Macdougall (1998)	−1.37	18.0	−1.43
benthic foraminifera	*Cibicides kullenbergi*	protozoa	foraminiferida	South Pacific	calcite	Zhu and Macdougall (1998)	−0.57	18.0	−0.63
benthic foraminifera	*Cibicides kullenbergi*	protozoa	foraminiferida	South Pacific	calcite	Zhu and Macdougall (1998)	−1.00	18.0	−1.06
benthic foraminifera	*Alveolinella*	protozoa	foraminiferida	unknown (shalllow, warm water)	calcite	Skulan et al. (1997)	−0.43	27.0	−0.67
perforate foraminifera	various	protozoa	foraminiferida	various	calcite	Chang et al. (2004)*	−1.20	21.6	−1.33
perforate foraminifera	various	protozoa	foraminiferida	various	calcite	Chang et al. (2004)*	−1.20	21.6	−1.33
perforate foraminifera	various	protozoa	foraminiferida	various	calcite	Chang et al. (2004)*	−1.20	21.6	−1.33
perforate foraminifera	various	protozoa	foraminiferida	various	calcite	Chang et al. (2004)*	−1.20	21.6	−1.33
perforate foraminifera	various	protozoa	foraminiferida	various	calcite	Chang et al. (2004)*	−1.20	21.6	−1.33
perforate foraminifera	various	protozoa	foraminiferida	various	calcite	Chang et al. (2004)*	−1.20	21.6	−1.33
perforate foraminifera	various	protozoa	foraminiferida	various	calcite	Chang et al. (2004)*	−1.20	21.6	−1.33
perforate foraminifera	various	protozoa	foraminiferida	various	calcite	Chang et al. (2004)*	−1.20	21.6	−1.33
perforate foraminifera	various	protozoa	foraminiferida	various	calcite	Chang et al. (2004)*	−1.20	21.6	−1.33
perforate foraminifera	various	protozoa	foraminiferida	various	calcite	Chang et al. (2004)*	−1.20	21.6	−1.33
perforate foraminifera	various	protozoa	foraminiferida	various	calcite	Chang et al. (2004)*	−1.20	21.6	−1.33
perforate foraminifera	various	protozoa	foraminiferida	various	calcite	Chang et al. (2004)*	−1.20	21.6	−1.33
perforate foraminifera	various	protozoa	foraminiferida	various	calcite	Chang et al. (2004)*	−1.20	21.6	−1.33
perforate foraminifera	various	protozoa	foraminiferida	various	calcite	Chang et al. (2004)*	−1.20	21.6	−1.33
perforate foraminifera	various	protozoa	foraminiferida	various	calcite	Chang et al. (2004)*	−1.20	21.6	−1.33
perforate foraminifera	various	protozoa	foraminiferida	various	calcite	Chang et al. (2004)*	−1.20	21.6	−1.33
perforate foraminifera	various	protozoa	foraminiferida	various	calcite	Chang et al. (2004)*	−1.20	21.6	−1.33
perforate foraminifera	various	protozoa	foraminiferida	various	calcite	Chang et al. (2004)*	−1.20	21.6	−1.33
perforate foraminifera	various	protozoa	foraminiferida	various	calcite	Chang et al. (2004)*	−1.20	21.6	−1.33

Continued on next page

Table 4.4: *Continued*

Common name	Binomen	Phylum or division	Subtaxon	Location	Mineralogy	Source	$\delta^{44/40}$Ca rel. to seawater	T (°C)	T-normalized $\delta^{44/40}$Ca (15 °C)
perforate foraminifera	various	protozoa	foraminiferida	various	calcite	Chang et al. (2004)*	−1.20	21.6	−1.33
perforate foraminifera	various	protozoa	foraminiferida	various	calcite	Chang et al. (2004)*	−1.20	21.6	−1.33
perforate foraminifera	various	protozoa	foraminiferida	various	calcite	Chang et al. (2004)*	−1.20	21.6	−1.33
perforate foraminifera	various	protozoa	foraminiferida	various	calcite	CChang et al. (2004)*	−1.20	21.6	−1.33
perforate foraminifera	various	protozoa	foraminiferida	various	calcite	Chang et al. (2004)*	−1.20	21.6	−1.33
perforate foraminifera	various	protozoa	foraminiferida	various	calcite	Chang et al. (2004)*	−1.20	21.6	−1.33
perforate foraminifera	various	protozoa	foraminiferida	various	calcite	Chang et al. (2004)*	−1.20	21.6	−1.33
perforate foraminifera	various	protozoa	foraminiferida	various	calcite	Chang et al. (2004)*	−1.20	21.6	−1.33
perforate foraminifera	various	protozoa	foraminiferida	various	calcite	Chang et al. (2004)*	−1.20	21.6	−1.33
perforate foraminifera	various	protozoa	foraminiferida	various	calcite	Chang et al. (2004)*	−1.20	21.6	−1.33
perforate foraminifera	various	protozoa	foraminiferida	various	calcite	Chang et al. (2004)*	−1.20	21.6	−1.33
perforate foraminifera	various	protozoa	foraminiferida	various	calcite	Chang et al. (2004)*	−1.20	21.6	−1.33
perforate foraminifera	various	protozoa	foraminiferida	various	calcite	Chang et al. (2004)*	−1.20	21.6	−1.33
perforate foraminifera	various	protozoa	foraminiferida	various	calcite	Chang et al. (2004)*	−1.20	21.6	−1.33
perforate foraminifera	various	protozoa	foraminiferida	various	calcite	Chang et al. (2004)*	−1.20	21.6	−1.33
perforate foraminifera	various	protozoa	foraminiferida	various	calcite	Chang et al. (2004)*	−1.20	21.6	−1.33
perforate foraminifera	various	protozoa	foraminiferida	various	calcite	Chang et al. (2004)*	−1.20	21.6	−1.33
perforate foraminifera	various	protozoa	foraminiferida	various	calcite	Chang et al. (2004)*	−1.20	21.6	−1.33
perforate foraminifera	various	protozoa	foraminiferida	various	calcite	Chang et al. (2004)*	−1.20	21.6	−1.33
perforate foraminifera	various	protozoa	foraminiferida	various	calcite	Chang et al. (2004)*	−1.20	21.6	−1.33
perforate foraminifera	various	protozoa	foraminiferida	various	calcite	Chang et al. (2004)*	−1.20	21.6	−1.33
perforate foraminifera	various	protozoa	foraminiferida	various	calcite	Chang et al. (2004)*	−1.20	21.6	−1.33
perforate foraminifera	various	protozoa	foraminiferida	various	calcite	Chang et al. (2004)*	−1.20	21.6	−1.33
perforate foraminifera	various	protozoa	foraminiferida	various	calcite	Chang et al. (2004)*	−1.20	21.6	−1.33
perforate foraminifera	various	protozoa	foraminiferida	various	calcite	Chang et al. (2004)*	−1.20	21.6	−1.33
perforate foraminifera	various	protozoa	foraminiferida	various	calcite	Chang et al. (2004)*	−1.20	21.6	−1.33
perforate foraminifera	various	protozoa	foraminiferida	various	calcite	Chang et al. (2004)*	−1.20	21.6	−1.33
perforate foraminifera	various	protozoa	foraminiferida	various	calcite	Chang et al. (2004)*	−1.20	21.6	−1.33
perforate foraminifera	various	protozoa	foraminiferida	various	calcite	Chang et al. (2004)*	−1.20	21.6	−1.33
perforate foraminifera	various	protozoa	foraminiferida	various	calcite	Chang et al. (2004)*	−1.20	21.6	−1.33
planktic foraminifera	unknown	protozoa	foraminiferida	Punta Maroma, Mexico	calcite	Holmden et al. (2012)	−1.09	27.5	−1.34
encrusting foraminifera	*Homotrema*	protozoa	foraminiferida	Bermuda	high-Mg calcite	this study	−1.28	23.1	−1.44
encrusting foraminifera	*Homotrema*	protozoa	foraminiferida	Bermuda	high-Mg calcite	this study	−1.21	23.1	−1.37
encrusting foraminifera	*Homotrema*	protozoa	foraminiferida	Bermuda	high-Mg calcite	this study	−1.17	23.1	−1.33

Continued on next page

Table 4.4: *Continued*

Common name	Binomen	Phylum or division	Subtaxon	Location	Mineralogy	Source	$\delta^{44/40}$Ca rel. to seawater	T (°C)	T-normalized $\delta^{44/40}$Ca (15 °C)
encrusting foraminifera	*Homotrema*	protozoa	foraminiferida	Bermuda	high-Mg calcite	this study	−1.08	23.1	−1.24
sea urchin	unknown	echinodermata	echinoid	Arran, Scotland	high-Mg calcite	this study	−1.47	10.6	−1.38
sea urchin	unknown	echinodermata	echinoid	Arran, Scotland	high-Mg calcite	this study	−1.42	10.6	−1.33
sea urchin	unknown	echinodermata	echinoid	Skye, Scotland	high-Mg calcite	this study	−1.29	10.4	−1.20
sea urchin	unknown	echinodermata	echinoid	Skye, Scotland	high-Mg calcite	this study	−1.36	10.4	−1.27
echinoid spine	unknown	echinodermata	echinoid	Punta Maroma, Mexico	high-Mg calcite	Holmden et al. (2012)	−1.12	27.5	−1.37
starfish	*Pisaster ochraceus*	echinodermata	asteroid	Big Sur, CA, USA	high-Mg calcite	Skulan et al. (1997)	−0.79	12.9	−0.75
sclerosponge	*Acanthochaetetes wellsi*	porifera		Mactan, Cebu	high-Mg calcite	Gussone et al. (2005)	−0.86	27.6	−1.11
sclerosponge	*Acanthochaetetes wellsi*	porifera		New Caledonia, Coral Sea	high-Mg calcite	Gussone et al. (2005)	−0.67	24.0	−0.85
sclerosponge	*Acanthochaetetes wellsi*	porifera		Lizard Island, Great Barrier Reef	high-Mg calcite	Gussone et al. (2005)	−0.70	26.0	−0.92
coralline red algae	unknown	rhodophyta		Monterey Bay, CA, USA	high-Mg calcite	Gussone et al. (2005)	−0.83	14.0	−0.81
red algae	*Amphiroa tribulus*	rhodophyta		Punta Maroma, Mexico	high-Mg calcite	Holmden et al. (2012)	−0.81	27.5	−1.06
red algae	*Porolithon pachydermum*	rhodophyta		Punta Maroma, Mexico	high-Mg calcite	Holmden et al. (2012)	−0.91	27.5	−1.16
red algae	unknown	rhodophyta		Abu Dhabi	high-Mg calcite	this study	−0.47	28.0	−0.73
red algae	unknown	rhodophyta		Abu Dhabi	high-Mg calcite	this study	−0.74	28.0	−1.00
red algae nodule	unknown	rhodophyta		Bermuda	high-Mg calcite	this study	−1.12	23.1	−1.28
red algae	unknown	rhodophyta		Skye, Scotland	high-Mg calcite	this study	−0.65	10.4	−0.56
red algae	unknown	rhodophyta		Skye, Scotland	high-Mg calcite	this study	−0.68	10.4	−0.59
thicket algae	*Galaxaura*	rhodophyta		Bahamas	high-Mg calcite	this study	-1.04	26.4	−1.27
red algae	unknown	rhodophyta		Arran, Scotland	high-Mg calcite	this study	−1.08	10.6	−0.99
red algae	unknown	rhodophyta		Arran, Scotland	high-Mg calcite	this study	−1.05	10.6	−0.96
coral	unknown	cnidaria	scleractinia	unknown (tropical)	aragonite	Zhu and Macdougall (1998)	−1.84	27.0	−2.08
coral	*Acropora*, *Pocillopora*	cnidaria	scleractinia	Barbados, Mauritius, Red Sea	aragonite	Chang et al. (2004)**	−1.24	25.0	−1.44
coral	*Acropora*, *Pocillopora*	cnidaria	scleractinia	Barbados, Mauritius, Red Sea	aragonite	Chang et al. (2004)**	−1.24	25.0	−1.44
coral	*Acropora*, *Pocillopora*	cnidaria	scleractinia	Barbados, Mauritius, Red Sea	aragonite	Chang et al. (2004)**	−1.24	25.0	−1.44
coral	*Acropora*, *Pocillopora*	cnidaria	scleractinia	Barbados, Mauritius, Red Sea	aragonite	Chang et al. (2004)**	−1.24	25.0	−1.44
coral	*Acropora*, *Pocillopora*	cnidaria	scleractinia	Barbados, Mauritius, Red Sea	aragonite	Chang et al. (2004)**	−1.24	25.0	−1.44
coral	*Pavona clavus*	cnidaria	scleractinia	Galapagos Islands	aragonite	Böhm et al. (2006)	−1.08	24.4	−1.27
coral	*Porites*	cnidaria	scleractinia	Red Sea	aragonite	Böhm et al. (2006)	−1.03	26.0	−1.25
coral	*Porites*	cnidaria	scleractinia	Red Sea	aragonite	Böhm et al. (2006)	−0.98	28.0	−1.24
coral	*Porites*	cnidaria	scleractinia	Red Sea	aragonite	Böhm et al. (2006)	−1.02	29.0	−1.30
coral	*Dendrogyra cylindricus*	cnidaria	scleractinia	Punta Maroma, Mexico	aragonite	Holmden et al. (2012)	−1.05	27.5	−1.30

Continued on next page

Table 4.4: *Continued*

Common name	Binomen	Phylum or division	Subtaxon	Location	Mineralogy	Source	$\delta^{44/40}$Ca rel. to seawater	T (°C)	T-normalized $\delta^{44/40}$Ca (15 °C)
coral	*Monastrea annularis*	cnidaria	scleractinia	Punta Maroma, Mexico	aragonite	Holmden et al. (2012)	−1.06	27.5	−1.31
coral	*Colpophylia natans*	cnidaria	scleractinia	Punta Maroma, Mexico	aragonite	Holmden et al. (2012)	−1.14	27.5	−1.39
coral	*Porites furcata*	cnidaria	scleractinia	Punta Maroma, Mexico	aragonite	Holmden et al. (2012)	−1.05	27.5	−1.30
coral	*Porites astreoides*	cnidaria	scleractinia	Punta Maroma, Mexico	aragonite	Holmden et al. (2012)	−1.08	27.5	−1.33
coral	*Acropora*	cnidaria	scleractinia	Bora Bora	aragonite	this study	−1.00	28.0	−1.26
coral	*Porites*	cnidaria	scleractinia	Bermuda	aragonite	this study	−1.05	23.1	−1.21
coral	*Diploria*	cnidaria	scleractinia	Bermuda	aragonite	this study	−1.41	23.1	−1.57
coral	unknown (pebble)	cnidaria	scleractinia	Barbados	aragonite	this study	−1.26	27.4	−1.51
coral	unknown (pebble)	cnidaria	scleractinia	Barbados	aragonite	this study	−1.40	27.4	−1.65
coral	unknown (pebble)	cnidaria	scleractinia	Barbados	aragonite	this study	−1.34	27.4	−1.59
coral	*Acropora palmata*	cnidaria	scleractinia	Bahamas	aragonite	this study	−1.52	26.4	−1.75
coral	*Porites*	cnidaria	scleractinia	Bahamas	aragonite	this study	−1.41	26.4	−1.64
coral	*Porites*	cnidaria	scleractinia	Bahamas	aragonite	this study	−1.45	26.4	−1.68
staghorn coral	*Acropora cervicornis*	cnidaria	scleractinia	Bahamas	aragonite	this study	−1.41	26.4	−1.64
staghorn coral	*Acropora cervicornis*	cnidaria	scleractinia	Bahamas	aragonite	this study	−1.08	26.4	−1.31
golfball coral	*Favia*	cnidaria	scleractinia	Bahamas	aragonite	this study	−1.33	26.4	−1.56
fire coral	*Millepora complanata*	cnidaria	hydrozoa	Punta Maroma, Mexico	aragonite	Holmden et al. (2012)	−1.02	27.5	−1.27
fire coral	*Millepora*	cnidaria	hydrozoa	Bermuda	aragonite	this study	−1.57	23.1	−1.73
fire coral	*Millepora*	cnidaria	hydrozoa	Bahamas	aragonite	this study	−1.29	26.4	−1.52
fire coral	*Millepora*	cnidaria	hydrozoa	Bahamas	aragonite	this study	−1.29	26.4	−1.52
fire coral	*Millepora*	cnidaria	hydrozoa	Bahamas	aragonite	this study	−1.06	26.4	−1.29
deep sea coral	*Desmophyllum dianthus*	cnidaria	scleractinia	deep South Atlantic	aragonite	this study***	−1.09	3.1	−0.85
deep sea coral	*Desmophyllum dianthus*	cnidaria	scleractinia	deep North Atlantic	aragonite	this study***	−1.37	3.8	−1.15
deep sea coral	*Madrepora oculata*	cnidaria	scleractinia	deep sea, Queensland Trough	aragonite	this study****	−1.38	4.0	−1.16
deep sea coral	*Enallopsammia rostrata*	cnidaria	scleractinia	deep sea, Queensland Trough	aragonite	this study****	−1.50	4.0	−1.28
ooid	—	—		Norman Reef Cay, Bahamas	aragonite	this study	−1.61	26.4	−1.84
ooid	—	—		Norman Reef Cay, Bahamas	aragonite	this study	−1.58	26.4	−1.81
ooid	—	—		Joulters Cay, Bahamas	aragonite	Steuber and Buhl (2006)	−1.48	27.0	−1.72
ooid	—	—		Tolon, Greece	aragonite	Steuber and Buhl (2006)	−1.42	19.0	−1.50
ooid	—	—		Neapolis, Greece	aragonite	Steuber and Buhl (2006)	−0.84	19.0	−0.92
sclerosponge	*Vacelatia*	porifera		Lifou, New Caledonia	aragonite	Gussone et al. (2005)	−1.54	16.2	−1.56
sclerosponge	*Vacelatia*	porifera		Wallis and Futuma, South Pacific	aragonite	Gussone et al. (2005)	−1.49	23.0	−1.65
sclerosponge	*Vacelatia*	porifera		Norfolk Ridge, New Caledonia	aragonite	Gussone et al. (2005)	−1.65	17.1	−1.69

Continued on next page

Table 4.4: *Continued*

Common name	Binomen	Phylum or division	Subtaxon	Location	Mineralogy	Source	$\delta^{44/40}$Ca rel. to seawater	T (°C)	T-normalized $\delta^{44/40}$Ca (15 °C)
sclerosponge	*Vacelatia crypta*	porifera		Astrolabe Reef, Fiji	aragonite	Gussone et al. (2005)	−1.42	26.4	−1.65
sclerosponge	*Vacelatia crypta*	porifera		Lizard Island, Great Barrier Reef	aragonite	Gussone et al. (2005)	−1.45	26.8	−1.69
sclerosponge	*Ceratoporella nicholsonia*	porifera		Jamaica	aragonite	Gussone et al. (2005)	−1.37	27.1	−1.61
sclerosponge	*Ceratoporella nicholsonia*	porifera		Jamaica	aragonite	Gussone et al. (2005)	−1.47	27.1	−1.71
sclerosponge	*Ceratoporella nicholsonia*	porifera		Pedro Bank, Caribbean	aragonite	Gussone et al. (2005)	−1.46	25.7	−1.67
sclerosponge	*Astrosclera willeyana*	porifera		Gulf of Aqaba, Red Sea	aragonite	Gussone et al. (2005)	−1.46	26.1	−1.68
green algae	*Penicillus*	chlorophyta		Bahamas	aragonite	this study	−1.51	26.4	−1.74
green algae	*Penicillus*	chlorophyta		Bahamas	aragonite	this study	−1.37	26.4	−1.60
green algae	*Penicillus*	chlorophyta		Bahamas	aragonite	this study	−1.59	26.4	−1.82
green algae	*Rhipocephalus phoenix*	chlorophyta		Punta Maroma, Mexico	aragonite	Holmden et al. (2012)	−1.24	27.5	−1.49
green algae	*Udotea flabellum*	chlorophyta		Punta Maroma, Mexico	aragonite	Holmden et al. (2012)	−1.20	27.5	−1.45
green algae	*Halimeda opuntia*	chlorophyta		Punta Maroma, Mexico	aragonite	Holmden et al. (2012)	−1.22	27.5	−1.47
green algae	*Halimeda tuna*	chlorophyta		Punta Maroma, Mexico	aragonite	Holmden et al. (2012)	−1.22	27.5	−1.47
green algae	*Halimeda incrassata*	chlorophyta		Punta Maroma, Mexico	aragonite	Holmden et al. (2012)	−1.11	27.5	−1.36
green algae	*Halimeda monile*	chlorophyta		Bahamas	aragonite	this study	−1.28	26.4	−1.51
green algae	*Halimeda tuna*	chlorophyta		Big Point, Bahamas	aragonite	this study	−1.52	26.4	−1.75
green algae	*Halimeda discoidea*	chlorophyta		Bahamas	aragonite	this study	−1.37	26.4	−1.60
green algae	*Halimeda discoidea*	chlorophyta		Bahamas	aragonite	this study	−1.44	26.4	−1.67
green algae	*Halimeda incrassata*	chlorophyta		Bahamas	aragonite	this study	−1.50	26.4	−1.73
green algae	*Halimeda incrassata*	chlorophyta		Bahamas	aragonite	this study	−1.44	26.4	−1.67
pteropod	unknown	mollusca	gastropoda	Caribbean	aragonite	Gussone et al. (2005)	−1.39	27.5	−1.64
pteropod	unknown	mollusca	gastropoda	Caribbean	aragonite	Gussone et al. (2005)	−1.44	27.5	−1.69
pteropod	unknown	mollusca	gastropoda	Caribbean	aragonite	Gussone et al. (2005)	−1.44	27.5	−1.69
conch	*Strombus*	mollusca	gastropoda	unknown	aragonite	Russell et al. (1978)	−1.20	15.0	−1.20
blue mussel	*Mytilus edulis*	mollusca	bivalvia	North Sea	aragonite (nacre)	Heinemann et al. (2008)	−1.01	10.0	−0.91
blue mussel	*Mytilus edulis*	mollusca	bivalvia	North Sea	aragonite (nacre)	Heinemann et al. (2008)	−1.14	10.0	−1.04
blue mussel	*Mytilus edulis*	mollusca	bivalvia	North Sea	aragonite (nacre)	Heinemann et al. (2008)	−1.24	10.0	−1.14

* average of 49 individual measurements, planktonic and benthonic foraminifera

** average of 5 individual measurements

*** sample details from Case et al. (2010)

**** samples from A. Thomas

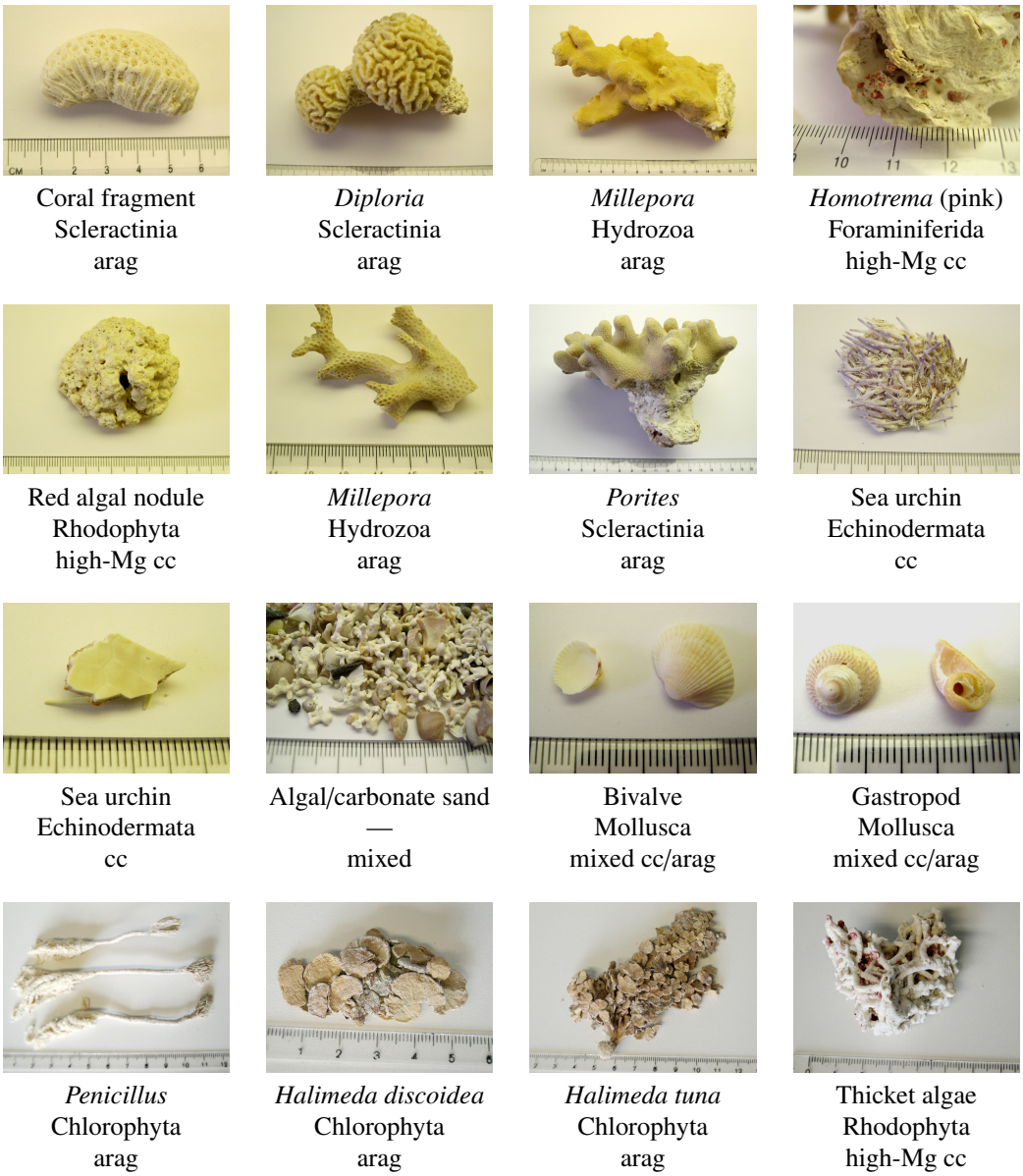

Figure 4.6: Photographs of a selection of modern carbonate samples which were analyzed for Ca-isotope ratios to help constrain the modern Ca-isotope budget. Identifying names are shown below along with phylum/division/subtaxon name and mineralogy (arag = aragonite, cc = calcite).

Chapter 5

Calcium isotopes and biomineralization processes in *Halimeda* algae and *Porites* corals

This chapter includes analyses of samples from growth experiments conducted by David I. Kline, Ove Hoegh-Guldberg, and Steven M. Stanley.

5.1 Introduction

The elemental and isotopic composition of mineral phases precipitated by biogenic systems deviate from those observed during inorganic mineral formation and expected from thermodynamics. These differences, sometimes referred to as 'vital effects', complicate the application of geochemical proxies to the geological past. Metal cation ratios in biogenic carbonate, such as Mg/Ca or Sr/Ca, can be empirically calibrated against environmental parameters, but varied responses to experimental conditions suggest that multiple factors may affect these ratios (e.g. Gagnon et al., 2007; Reynaud et al., 2007). Ca-isotope ratios may provide a useful tool to help understand these varied environmental influences and improve the use of trace-metal data in carbonates to assess past conditions. Ca is the dominant cation in most biogenic carbonates and plays a central role in skeletal growth, but its isotopic behaviour during biomineralization is still poorly understood. This work

investigates the mechanism of Ca-isotope fractionation in two aragonite-producers with contrasting styles of biomineralization, *Halimeda* algae and *Porites* corals. These sample organisms isolate biological processes that may generate vital effects and therefore allow models of biomineralization in geologically important aragonite systems to be tested.

Skeletal growth can be divided broadly into two categories, 'biologically induced' and 'biologically controlled', depending on the location of biomineralization and on the extent of environmental influence on and transport mechanisms of chemical species (Weiner and Dove, 2003). The green alga and major sediment producer, *Halimeda* spp., is recognized as an example of a biologically induced system, based on the crystallography and organization of its aragonite needles (Borowitzka and Larkum, 1987) and confirmed by changes in skeletal mineralogy observed under experimental conditions (Stanley et al., 2010). Its simplicity provides an ideal starting point for addressing the multiple potential mechanisms of cation fractionation during biogenic aragonite precipitation. In contrast, coral polyps have a relatively simple structure, basically a 'double-walled sack', but their calcification process appears to be tightly controlled, based on complex and species-specific crystal morphology, geochemical vital effects, and high precipitation rates (Cohen and McConnaughey, 2003). Coral aragonite undoubtedly incorporates more complex vital effects than *Halimeda*, and understanding these effects is critical for interpreting this valuable geological archive of high-resolution, dateable material from both the surface and deep oceans.

Two sets of experiments provide unique samples with which to constrain Ca-isotope behaviour during aragonite biomineralization. *Halimeda* algae, green plants which are normally pure aragonite producers under modern ocean conditions, were grown in seawater with Mg/Ca ratios mimicking hypothetical Cretaceous–Eocene values, and formed a mixture of calcite and aragonite (Stanley et al., 2010). The growth of two different carbonate minerals from the same fluid composition presents a test case for the isotopic effect of mineral growth on an organic substrate. Hermatypic corals, which are animals with photosynthetic symbionts, were obtained from the Free Ocean Carbon Enrichment (FOCE) system, which simulates ocean acidification conditions within a natural coral reef

environment (technical details in Marker et al., 2010). FOCE is a new technology for capturing the *in situ* ecological response of marine systems to increased atmospheric CO_2, and provides a closer analogue to marine coral archives than aquarium-grown coral experiments. Using these two sets of samples, the behaviour of Ca-isotope ratios can be used to indicate the sources of Ca and chemical processes occurring during biomineralization, with implications for other metal cation proxies.

5.2 Background to Ca-isotope fractionation

5.2.1 Inorganic Ca-isotope fractionation

Ca isotopes have previously been explored in a variety of inorganic precipitation experiments, with all calcium carbonate minerals exhibiting fractionation in favour of the lighter isotopes of Ca (i.e. $\alpha < 1$, where α is the ratio of precipitate $^{44}Ca/^{40}Ca$ to solution $^{44}Ca/^{40}Ca$). The only published Ca-isotope data for laboratory-grown aragonite, expressed as $\Delta^{44/40}Ca = \delta^{44/40}Ca_{carbonate} - \delta^{44/40}Ca_{solution}$, show a small temperature dependence of 0.015 ± 0.002‰ per °C (Gussone et al., 2003), with the average fractionation at 15 °C equal to −1.7‰. Smaller fractionations are generally observed during calcite growth, with a similar temperature dependence of 0.015 ± 0.011‰ per °C and an average fractionation of −0.8‰ at 15 °C for samples precipitated in a beaker (Marriott et al., 2004). Much greater fractionations have been observed in laboratory-generated speleothem-like calcite growth (Reynard et al., 2011), and relationships between $\delta^{44/40}Ca$, growth rate, and $[CO_3^{2-}]$ have also been identified (Lemarchand et al., 2004; Tang et al., 2008). Gussone et al. (2011) showed that the metastable $CaCO_3$ polymorph ikaite expresses smaller fractionations of −0.55‰ and −0.62‰ for experimental and natural samples, respectively, while laboratory-grown vaterite has an even smaller average fractionation of −0.36‰. Measured fractionations of less than −0.2‰ for synthetic amorphous calcium carbonate (ACC) suggest that Ca-isotope ratios are not strongly affected in the absence of a mineral structure (Gagnon et al., 2011).

Models of Ca-isotope fractionation suggest that the preference for light isotopes in

the solid phase (negative $\Delta^{44/40}$Ca, or $\alpha < 1$) is due to a kinetic effect associated with ion dehydration and attachment onto a mineral surface, moderated by the backwards reaction of ion rehydration and detachment with a kinetic isotope effect of a similar magnitude (Gussone et al., 2003; DePaolo, 2011). Evidence from deep-sea pore fluids (Fantle and DePaolo, 2007) and a carbonate aquifer (Jacobson and Holmden, 2008) indicate that the isotopic fractionation between fluid and carbonate in equilibrium is close to zero. This observation suggests that maximum fractionation is expected at intermediate growth rates when fractionated surface-layer ions are incorporated into the crystal, and ion transport in the fluid is rapid enough to allow this attachment fractionation to be expressed (DePaolo, 2011). This model can explain the majority of relationships between Ca isotopes and growth rate or temperature observed during inorganic calcite precipitation experiments.

5.2.2 Organic Ca-isotope fractionation

In biological calcification systems, carbonate skeletons are also lighter than the fluid (usually seawater) from which they precipitate. Several variables have been shown to affect skeletal Ca-isotope ratios, sometimes in ways that mimic inorganic behaviour, and sometimes with more complex relationships that reflect vital effects. Temperature changes induce a range of responses in different organisms. Many forms of biogenic carbonate, including scleractinian corals, exhibit a similar temperature dependence to inorganic precipitates of 0.01–0.03‰ per °C (Gussone et al., 2003, 2005; Böhm et al., 2006; Gussone et al., 2006), although there are significant exceptions to this trend. The planktic foraminifera *G. sacculifer* has been shown to have a much greater sensitivity of $\delta^{44/40}$Ca to temperature of 0.22–0.24‰ per °C (Nägler et al., 2000; Hippler et al., 2006), while other species and experiments show a negligible temperature dependence (Chang et al., 2004; Sime et al., 2005; Griffith et al., 2008b; Kasemann et al., 2008). A study of benthic foraminifera has revealed changes in $\delta^{44/40}$Ca of ~0.02‰ per °C for shells formed at temperatures > 5 °C, but deviate significantly at temperatures < 5 °C (Gussone and Filipsson, 2010). These different temperature trends suggest that metabolic or physiological processes are also contributing to foraminiferal $\delta^{44/40}$Ca.

Differences in Ca-isotope fractionation with changing carbonate-ion concentrations, or carbonate saturation state, and growth rates are also observed between inorganic and biogenic calcification. A strong correlation with both [CO_3^{2-}] and growth rate was observed for inorganic calcite (Lemarchand et al., 2004), but a lack of correlation with [CO_3^{2-}] was demonstrated for *O. universa* (Gussone et al., 2005) and several coccolithophore species (Gussone et al., 2006, 2007; Langer et al., 2007). Growth rate did have an effect on $\delta^{44/40}$Ca in *G. siphonifera* (Kısakürek et al., 2011), but not for *E. huxleyi* (Langer et al., 2007). These studies suggest that Ca-isotope responses to [CO_3^{2-}] and growth rate are determined by biological control over internal pH and carbonate chemistry, and are likely to vary according to the mechanism of biocalcification being employed. Variations in skeletal $\delta^{44/40}$Ca in response to salinity may also be related to changes in growth rate, when assemblages that are optimally adapted to local conditions become stressed (Gussone et al., 2009; Kısakürek et al., 2011).

The composition of the fluid from which Ca is supplied, and the degree of utilization of Ca in that fluid, are also important for explaining the effects of different environmental variables on biogenic $\delta^{44/40}$Ca. Foraminifera may precipitate carbonate from an internal pool of Ca, derived from seawater, modified by ion pumps, and subject to Rayleigh distillation effects as calcite forms (Erez, 2003; Gussone et al., 2009). Griffith et al. (2008b) developed a Ca-isotope model (α = 0.9985, 85% utilization) suggesting that this internal reservoir could be offset by −0.8 to −0.9‰ from seawater, whereas Kısakürek et al. (2011) proposed that utilization of only 10–40% of the reservoir indicates a smaller offset of −0.2 to −0.4‰, with additional fractionation originating from active Ca-pumping. Ca for coccolith formation may be supplied through a series of intracellular transport mechanisms with potential isotope effects (Gussone et al., 2006). Multicellular animals can also utilize separate extracellular reservoirs for biomineralization, such as the extra-pallial fluid of a blue mussel, which has higher $\delta^{44/40}$Ca than the surrounding seawater (Heinemann et al., 2008). Due to control over the composition of this fluid and the mineralogy of its skeletal components, blue mussels have been shown to express a small difference in $\delta^{44/40}$Ca of only 0.25‰ between calcite and aragonite, clear evidence of strong vital effects in their

biocalcification (Heinemann et al., 2008). Coral skeletal growth also occurs in spaces that are isolated from seawater by tissue and the underlying substrate, and the calcifying fluid composition may be subject to Rayleigh distillation and transport effects (Böhm et al., 2006).

Numerous studies on biocalcifiers have shown that temperature, carbonate-ion concentration, growth rate, salinity, internal Ca transport, and Rayleigh distillation can all introduce vital effects in skeletal carbonate in addition to the expected mineralogical $\delta^{44/40}$Ca behaviour. While the direction of the Ca-isotope effects can usually be predicted, the magnitude and relative contribution of each effect for a particular organism is not often clear. The two case studies presented here attempt to describe the balance of these isotopic fractionations in two sample organisms, separating the competing biological and physico-chemical responses.

5.3 Samples and methods

5.3.1 *Halimeda* experiment

The calcification of *Halimeda* algae, which normally produces aragonite within intercellular spaces, was manipulated by growth in simulated Cretaceous–Eocene seawater by Dr Steven Stanley at the University of Hawai‘i. Modern seawater chemistry favours the precipitation of aragonite and high-Mg calcite (cation composition > 4 mol% Mg), but changes in the Mg/Ca ratio of seawater may have favoured the precipitation of low-Mg calcite (cation composition < 4 mol% Mg) during periods such as the Cretaceous (Sandberg, 1983). Several lines of evidence, including the composition of nonskeletal carbonates, evaporite sequences, fluid inclusions, and echinoderm ossicles, support Mg/Ca variation from the modern value of 5.2 to ratios as low as 1.0–1.5 (Hardie, 1996; Stanley and Hardie, 1998; Lowenstein et al., 2001; Horita et al., 2002; Dickson, 2004). Growth experiments on different biocalcifiers under these low Mg/Ca conditions have produced changes in calcification rate and skeletal geochemistry (e.g. Stanley et al., 2002, 2005; Ries et al., 2006) and, in the case of *Halimeda incrassata*, a change in the carbonate

mineral produced from aragonite to calcite (Stanley et al., 2010). Similar experiments were performed with a close relative, *Halimeda discoidea*, to produce the unusual case of aragonite and calcite grown simultaneously by the same organism from the same fluid for Ca-isotope analysis.

Individual specimens of *Halimeda discoidea*, collected from offshore Hawai'i, were grown in an aquarium with molar Mg/Ca = 1.5 and $[Ca^{2+}]$ = 25.3 mM, while the sum of ($[Mg^{2+}]$ + $[Ca^{2+}]$) remained equal to that of modern seawater. After approximately six weeks of growth, eight individuals were harvested, and 4–5 of their terminal segments were sampled, bleached, and crushed (see section 5.3.3 below). X-ray diffraction (XRD) was used to quantify the percentage of calcite and aragonite in each sample using a PANalytical X'Pert Pro diffractometer in the Department of Chemistry, University of Oxford. Approximately 10 mg of sample powder was sprinkled onto a frosted glass slide, to randomize particle orientation. Aragonite produces prominent peaks at 2θ = 26.2° (3.40Å, [111]), 27.2° (3.27Å, [021]), and 33.0° (2.70Å, [012]), whereas calcite produces a much stronger signal at 2θ = 29.4° (3.04Å, [104]) with a greater magnitude than that of any aragonite peak for a mass contribution of only 10% calcite. A calibration curve was generated using mixtures of aragonite (*Millepora*, fire coral, from the Bahamas) and calcite (mineral spar) standards, using areas under the aragonite peak at 2θ = 26.2° and the calcite peak at 2θ = 29.4° (see Figure 5.1).

5.3.2 Coral FOCE experiment

Fragments of the coral *Porites cylindrica* from the FOCE experimental system provide the opportunity to test the effect of ocean pH on Ca-isotope ratios in hermatypic corals. Modelled after the Free Air Carbon Enrichment (FACE) experiments that simulated elevated atmospheric CO_2 in terrestrial environments (McLeod and Long, 1999), the FOCE system achieves the complexity of a natural marine setting under controlled pH and $[CO_2]$ (Marker et al., 2010). Aquarium studies often lack the cyclic variations in flow, light, temperature, and water chemistry that could affect the geochemical signals in coral skeletal records. In addition, coral colonies in laboratory experiments are often grown on im-

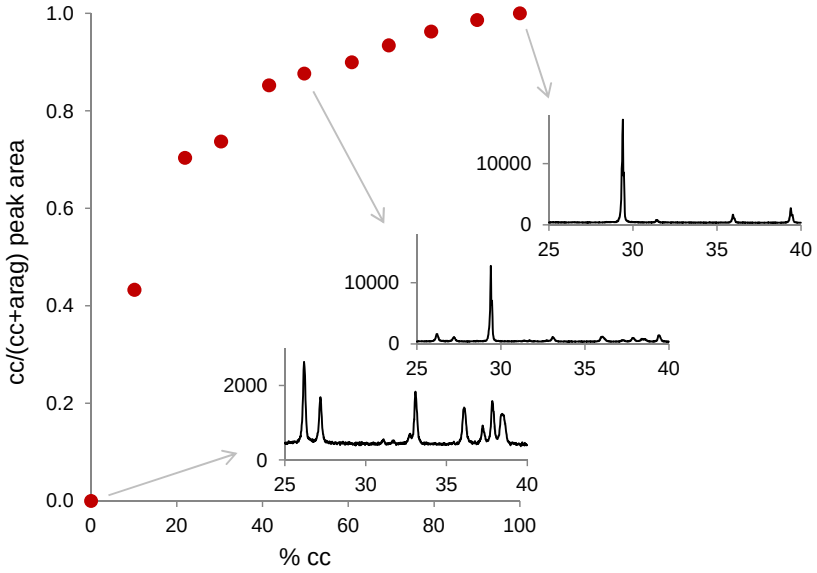

Figure 5.1: Standard calibration curve for quantifying the proportions of calcite and aragonite using XRD. Analyses used a Cu-Kα X-ray source (40 mA and 40 kV) with the sample loaded on a fixed stage while 2θ varied through 25–40° with a 0.004° step size (0.05°/sec). Areas under the calcite (cc) peak at 29.4° and the aragonite (arag) peak at 26.2° were used to calculate the proportional intensity of calcite as cc/(cc + arag). Insets show standard intensity vs 2θ-angle XRD spectra for 0% (pure aragonite), 49.7%, and 100% calcite (note the relative change in the vertical axis for the 0% calcite/pure aragonite standard).

permeable substrates such as glass plates, sealing the calcifying environment from fluid that might diffuse in from the porous reef structure below. The FOCE environment allows experiments to be conducted within a natural reef, which is of great value for the interpretation of samples from similar natural environments.

The FOCE experiment was performed at the Heron Island Marine Station off the coast of Queensland, Australia during June to December, 2010, led by Drs Davey Kline and Ove Hoegh-Guldberg. CO_2-enriched seawater was pumped in from onshore holding tanks to experimental and control chambers on the reef flat. Feedback control systems maintained pH levels at -0.2 below ambient seawater, despite the challenges of high tidal-current flow rates. This offset was superimposed on the natural diurnal cycle of pH and calcification, where the interaction of the reef with stagnant water at low tides can cause pH changes of up to 0.4 over the course of a day (Marker et al., 2010). Multiple coral fragments were analyzed from the two control settings (ambient oceanic pH) and two experimental settings (pH = -0.2 below ambient).

5.3.3 Ca-isotope analysis

Skeletal samples were bleached in ~15% NaClO to remove organic matter and powdered by low-speed handheld drill (corals) or mortar and pestle (*Halimeda*). Between 0.5 and 2.0 mg of carbonate was used for Ca-isotope analysis by multi-collector inductively coupled plasma mass spectrometry (MC-ICP-MS), following methods described in Blättler et al. (2011). For the *Halimeda* samples, the same homogenized powders used for mineral quantification by XRD were recollected and used for Ca-isotope analysis. Sample Ca was isolated using ion-exchange chromatographic columns and prepared as 10 ppm Ca solutions in 2% HNO_3, with blanks contributing < 5 ng Ca to the total sample. Ratios of $^{44}Ca/^{42}Ca$ were measured on a Nu Instruments MC-ICP-MS, with the international carbonate standard NIST SRM915a used as a reference. Mass-dependent fractionation was confirmed by measuring ^{44}Ca, ^{43}Ca, and ^{42}Ca beams, correcting for the interference of double-charged Sr by monitoring the beam at mass 43.5. Multiple internal standard measurements and replicate analyses of samples generate standard errors of ~0.05‰. Values

of $\delta^{44/40}Ca$ (= $[(^{44}Ca/^{40}Ca)_{sample}/(^{44}Ca/^{40}Ca)_{standard} - 1] \cdot 1000$) relative to modern seawater and $\Delta^{44/40}Ca$ (= $\delta^{44/40}Ca_{carbonate} - \delta^{44/40}Ca_{fluid}$) were calculated and are presented in Tables 5.1 and 5.2.

5.4 Results

XRD analysis of *Halimeda* algae and comparison with the calibration curve (Figure 5.3) revealed that natural samples contained 0–5% calcite. Seven of the experimental samples had, on average, slightly increased levels of 2.8–8.8% calcite, while the eighth experimental individual had > 85% calcite (see Table 5.1 and Figure 5.3). These data are supported by the morphologies of the experimental *Halimeda* (see Figure 5.2), with the lowest amounts of calcite (within the range of normal *Halimeda*) present in thick, well calcified segments, whereas higher levels (up to 8.8%) were present in flimsier, malformed samples. The most calcite-rich sample was particularly shriveled and yielded < 10% carbonate by mass, in comparison to the 45–75% carbonate by mass from other experimental and natural algae. The low mass of carbonate retrieved from this sample generated a very poor XRD spectrum, with a high background, a small calcite peak, and no identifiable aragonite peaks, so the calculated value of 88% calcite should be treated as a rough minimum.

Ca-isotope ratios were measured for various materials and stages of the experiment, including the calcium chloride salt added to the aquarium water, the aquarium water from both before and after the growth period, terminal algal samples which grew entirely in artificial Cretaceous seawater (eight individual *Halimeda*), and basal algal samples whose calcification commenced in natural seawater and may have continued in experimental seawater after transplanting (three individuals). The Ca in the Cretaceous seawater was a mixture of modern seawater Ca and added calcium chloride salt in a proportion of approximately 1:3, based on the $\delta^{44/40}Ca$ of seawater (0‰, as the reference standard), the salt (−1.19‰), and the resulting solution (−0.87‰). The Ca-isotope ratio in the aquarium rose slightly (by +0.1‰) during the course of the experiment, likely due to the preferential uptake of light Ca isotopes by algal calcification.

wild *Halimeda discoidea*

Sample #1, 2.8% cc

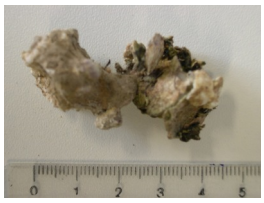

Sample #2, 4.9% cc

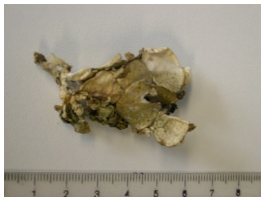

Sample #3, 7.6% cc

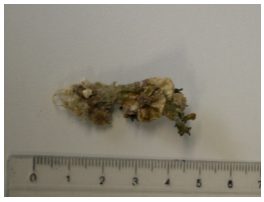

Sample #4, 8.8% cc

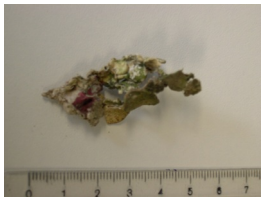

Sample #5, 3.7% cc

Sample #6, >88% cc

Sample #7, 8.5% cc

Sample #8, 4.0% cc*

*offshoot, grown entirely in aquarium

Figure 5.2: Photographs of the eight individual *Halimeda* samples from the experimental Cretaceous seawater. Note that Sample #6, which contained mostly calcite rather than aragonite, appears particularly malformed.

Table 5.1: Ca-isotope data for natural and experimental *Halimeda* algae, along with other materials from the experiment. Percent calcite (% cc) determined by quantifying calcite (cc) and aragonite (arag) by X-ray diffractometry and calculating % cc = cc/(cc+arag), with errors of ± 5% (except for sample HAL-6 for which they are ± 15%).

Sample name	$\delta^{44/42}$Ca (‰) rel. to SRM915a	n	$\delta^{44/40}$Ca (‰) rel. to seawater	2 SE	avg. $\delta^{44/40}$Ca	$\Delta^{44/40}$Ca (difference)	% cc	wt.% carbonate
Ca salt used for Cretaceous "seawater"								
$CaCl_2$-A	0.40	4	−1.08	0.07	−1.19			
$CaCl_2$-B	0.38	4	−1.13	0.07				
$CaCl_2$-C	0.33	4	−1.23	0.10				
$CaCl_2$-D	0.27	3	−1.34	0.11				
Pre-experimental Cretaceous "seawater"								
PRE-A	0.54	4	−0.80	0.07	−0.87	0.00		
PRE-B	0.51	4	−0.86	0.07				
PRE-C	0.49	4	−0.91	0.10				
PRE-D	0.49	3	−0.91	0.11				
Post-experimental Cretaceous "seawater"								
EXP-A	0.58	4	−0.72	0.07	−0.77	0.10		
EXP-B	0.55	4	−0.77	0.07				
EXP-C	0.54	3	−0.81	0.10				
EXP-D	0.54	4	−0.79	0.11				
Experimental *Halimeda* samples, post-XRD analysis (terminal segments only)								
HAL-1	−0.30	5	−2.49	0.10	−2.20	−1.62	2.8	73
HAL-2	−0.19	4	−2.25	0.11		−1.38	4.9	70
HAL-3	−0.21	4	−2.31	0.11		−1.44	7.6	63
HAL-4	−0.21	4	−2.31	0.11		−1.44	8.8	49
HAL-5	−0.15	4	−2.17	0.11		−1.30	3.7	57
HAL-6*	0.20	4	−1.47	0.09		−0.61	88.3	4
HAL-7	−0.15	4	−2.19	0.11		−1.32	8.5	45
HAL-8**	−0.27	5	−2.42	0.10		−1.56	4.0	50
Transplanted *Halimeda* samples (basal samples)								
HAL-2X	0.14	5	−1.59	0.09	−1.65	−1.59		
HAL-4X	0.01	5	−1.85	0.09		−1.85		
HAL-6X	0.19	5	−1.50	0.09		−1.50		
Wild *Halimeda* samples (from the Bahamas)								
H. monile	0.30	4	−1.28	0.13	−1.42	−1.28		
H. tuna	0.18	4	−1.52	0.13		−1.52		
H. discoidea	0.26	4	−1.36	0.13		−1.36		
H. discoidea	0.22	4	−1.44	0.13		−1.44		
H. incrassata	0.19	4	−1.50	0.13		−1.50		
H. incrassata	0.22	4	−1.44	0.13		−1.44		

* poorly calcified sample

** offshot of another individual, entirely grown in aquarium

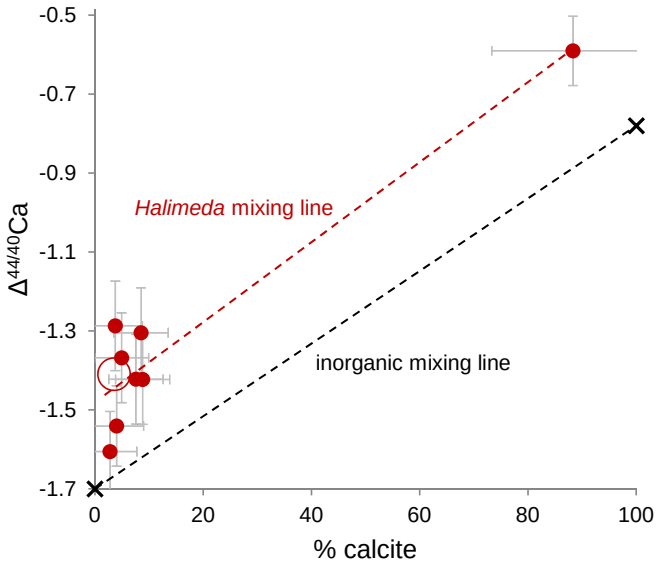

Figure 5.3: Ca-isotope ratios for *Halimeda* grown in experimental Cretaceous seawater, plotted against the percentage of calcite determined by XRD analysis. The open circle represents the average value for natural, ocean-grown *Halimeda*. The black line represents a mixing relationship between the inorganic calcite and aragonite end-members from Marriott et al. (2004) and Gussone et al. (2005) at 15 °C. The *Halimeda* data define a best-fit line with similar slope and approximately 0.25‰ heavier values than inorganic carbonate.

The seven experimental algae with < 10% calcite had an average $\delta^{44/40}Ca = -2.31‰$ relative to the modern seawater standard, or $\Delta^{44/40}Ca = -1.44‰$ relative to the original experimental seawater. This fractionation is in good agreement with six natural *Halimeda* samples which were offset from seawater by −1.42‰. Three samples taken from the base of the experimental algae, rather than the terminal segments which grew entirely in the aquarium, had an average $\delta^{44/40}Ca = -1.65‰$ relative to natural seawater, reflecting a mixture of carbonate precipitated before transfer to the aquarium, and the isotopically lighter product of continued calcification during the experimental period. The anomalous, calcite-rich sample had a much smaller fractionation than the other *Halimeda*, with $\delta^{44/40}Ca = -1.47‰$ and $\Delta^{44/40}Ca = -0.61‰$. This sample allows a relationship to be defined for the fractionation of *Halimeda* skeletal carbonate with differing proportions of calcite (see Table 5.2 and Figure 5.3).

The *Porites* coral fragments from the FOCE system represent two experimental settings (pH lowered by −0.2) and two control settings (normal oceanic pH). External and internal sections of some corals were sampled to capture the most recent growth under

acidified conditions as well as prior growth under pre-acidification conditions for the same coral. No statistical difference was found for bulk samples, external, or internal sections, for either the experimental or control environments (see Table 5.2 and Figure 5.4). The means for the two datasets are identical to two decimal places (−1.40‰) with similar individual variability within each group (standard deviation = 0.072 for acidified conditions and 0.079 for normal pH).

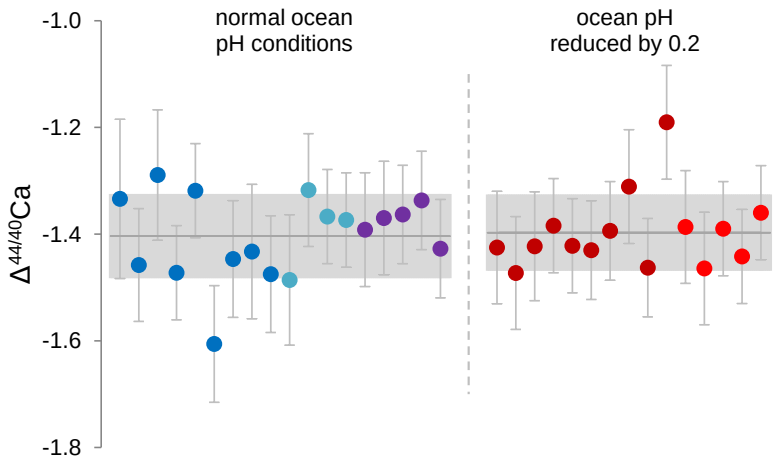

Figure 5.4: Ca-isotope ratios for coral fragments from the FOCE system, with colours representing different experimental settings. Dark blue represents FOCE 1, at normal pH; light blue represents FOCE 3, at normal pH; purple represents from FOCE 2, at decreased pH, but sampling only the inner portions of coral fragments that grew in normal seawater before the experiment commenced. Dark red represents FOCE 2, at decreased pH, sampling both bulk and outermost layers; bright red represents FOCE 4, at decreased pH, using bulk samples only. Grey bars indicate 2σ standard deviations of each dataset.

5.5 Discussion

The two datasets analyzed in this study provide new information about how biological and mineralogical influences affect skeletal Ca-isotope ratios. The following discussion first explores how Ca isotopes behave during the simple, biologically induced calcification of *Halimeda*, and then how additional isotope effects are involved in the more complex system of coral biocalcification.

Table 5.2: Ca-isotope data for FOCE coral samples, relative to modern seawater.

Sample name	Component	$\delta^{44/40}$Ca (‰)	2 SE
Normal oceanic pH			
F1-B0951	bulk	−1.33	0.15
F1-G1722	bulk	−1.46	0.11
F1-R0215	bulk	−1.29	0.12
F1-B1383	bulk	−1.47	0.09
F1-W2424	bulk	−1.32	0.09
F1-R0215	inner	−1.61	0.11
F1-R0215	outer	−1.45	0.11
F1-B1383	inner	−1.43	0.13
F1-B1383	outer	−1.48	0.11
F3-R0220	bulk	−1.49	0.12
F3-B1379	bulk	−1.32	0.11
F3-W2425	bulk	−1.37	0.09
F3-B0947	bulk	−1.37	0.09
F2-B0948	inner	−1.39	0.11
F2-R0219	inner	−1.37	0.11
F2-G1715	inner	−1.36	0.09
F2-B1377	inner	−1.34	0.09
F2-W2427	inner	−1.43	0.09
Acidified pH (0.2 lower)			
F2-B0948	bulk	−1.43	0.11
F2-R0219	bulk	−1.47	0.11
F2-G1715	bulk	−1.42	0.10
F2-B1377	bulk	−1.38	0.09
F2-W2427	bulk	−1.42	0.09
F2-B0948	outer	−1.43	0.09
F2-R0219	outer	−1.39	0.09
F2-G1715	outer	−1.31	0.11
F2-B1377	outer	−1.46	0.09
F2-W2427	outer	−1.19	0.11
F4-R0216	bulk	−1.39	0.11
F4-B1380	bulk	−1.46	0.11
F4-W2422	bulk	−1.39	0.09
F4-G1716	bulk	−1.44	0.09
F4-B0950	bulk	−1.36	0.09

5.5.1 Ca isotopes in *Halimeda*

The experimental conditions that promoted both calcite and aragonite growth in *Halimeda* show how inorganic isotope fractionation due to mineral surface attachment is expressed in a biologically induced calcification system. *Halimeda* exert minimal control on the process and environment in which calcification takes place. Cell walls provide surfaces on which carbonate precipitates due to oversaturation from the consumption of CO_2 by photosynthesis and subsequent local elevation of CO_3^{2-} (Borowitzka and Larkum, 1987). Aragonite needles fill the intercellular space, and their morphology suggests that the algae do not further control the crystallography of the precipitate (Borowitzka and Larkum, 1987; Macintyre and Reid, 1995). Insensitivity to Ca-channel blocking drugs indicates that algal tissue has no influence on the supply of Ca, leaving diffusion of seawater as the only uptake mechanism (de Beer and Larkum, 2001). This lack of biological transport is consistent with the observation that Mg incorporation into *Halimeda* mimics the response of inorganic precipitates under different Mg/Ca seawater treatments (Stanley et al., 2010).

In this context, the precipitation of both calcite and aragonite from the same fluid and under the same conditions isolates the effect of mineral kinetics on a biological surface from other complicating factors such as active transport mechanisms. The Mg/Ca of the experimental seawater would favour inorganic calcite growth, so the presence of aragonite in most samples indicates the effect of the biological substrate in determining skeletal mineralogy. The different proportions of calcite produced during experimental growth, especially the single, calcite-rich specimen, allow construction of a mixing line representing the Ca-isotope ratio of theoretical mixtures of the two minerals within *Halimeda*. The difference between the end-members with 100% aragonite and > 88% calcite is ~0.9‰ (see Figure 5.3), the same as the offset between the inorganic experiments of Gussone et al. (2003) and Marriott et al. (2004). This suggests that biological substrates have no additional influence on Ca-isotope fractionation besides promoting a particular mineral structure. In contrast, the aragonitic (nacreous) and calcitic (prismatic) portions of a blue mussel shell that have a $\delta^{44/40}$Ca difference of only ~0.25‰ (Heinemann et al., 2008) show that isotopic effects from more complex biological transport and control mecha-

nisms are active during mollusk biocalcification, preventing the difference in $\delta^{44/40}$Ca between carbonate minerals from being fully expressed.

In *Halimeda*, the aragonitic and calcitic end-members express the same difference as inorganic precipitates, but are less fractionated from the fluid by ~0.25‰ relative to the average fractionation in the experiments of Gussone et al. (2003) and Marriott et al. (2004). A range of $\delta^{44/40}$Ca values in inorganic precipitates can be generated in response to experimental variables, but the mechanism of calcification in *Halimeda* suggests that two primary effects could explain this difference. Rayleigh distillation is expected to increase $\delta^{44/40}$Ca values and decrease the apparent fractionation from the external fluid ($\delta^{44/40}$Ca) due to the removal of light isotopes of Ca into carbonate and the accumulation of heavier Ca isotopes in the intercellular fluid. The rate of calcification relative to the recharge of Ca ions into the calcifying space by diffusion would determine the magnitude of this effect. This mechanism could also be responsible for the slightly higher $\delta^{44/40}$Ca of aragonitic sclerosponges, which have a similarly simple system of induced biocalcification, relative to inorganic precipitates (Gussone et al., 2005). The increased carbonate saturation state within the intercellular space of *Halimeda*, which is a function of the carbonate ion concentration and therefore the photosynthetic activity of the algae, is also expected to produce a vital effect for skeletal $\delta^{44/40}$Ca. The stunted growth of the calcite-rich sample may express a smaller contribution from this isotope effect.

By comparing inorganic precipitation with a biologically induced system where calcite and aragonite are produced in the same environment, the effect of mineral surface control on Ca-isotope fractionation can be distinguished. Mineral surfaces, and not biological substrates, appear to control Ca-isotope ratios by expressing the fractionation factor associated with the respective carbonate polymorph. Differences from the expected $\delta^{44/40}$Ca must therefore be due to additional biological transport effects or modification of the fluid (e.g. Rayleigh distillation).

5.5.2 Ca isotopes in corals

The skeletal biocalcification of corals is much more complex than that of *Halimeda* algae, providing additional possibilities for generating Ca-isotope fractionation. However, Ca-isotope data for corals under a range of experimental conditions are surprisingly invariant. The FOCE system, providing the closest experimental analogue to natural coral growth, produced no difference in $\delta^{44/40}$Ca under acidified growth conditions. Aquarium-based acidification experiments, which do not permit diffusion from below or diurnal seawater chemistry changes, also show no variation in coral $\delta^{44/40}$Ca (Taubner et al., 2011). Changes in coral growth rate and other measures of skeletal geochemistry do take place in response to ocean acidification (e.g. Cohen et al., 2009), so the lack of a strong $\delta^{44/40}$Ca response in corals to pH suggests that multiple sources of Ca and isotopic effects are important for determining skeletal geochemistry. Ca-isotope ratios in corals tend to be higher than those for inorganic aragonite precipitates (Gussone et al., 2003; Chang et al., 2004; Böhm et al., 2006; Blättler et al., 2012; Holmden et al., 2012), implying additional levels of biological control on ion transport and incorporation that are associated with Ca-isotope fractionation. These processes and their predicted impacts on $\delta^{44/40}$Ca are examined below.

Coral growth and physiology are summarized in several reviews (Gattuso et al., 1999; Cohen and McConnaughey, 2003; Allemand et al., 2004). Calcification occurs in an extracellular space adjacent to a cell layer known as the calicoblastic epithelium, or alternatively, the aboral ectoderm (see Figure 5.5). A second cell layer, the aboral endoderm, is in contact with an internal cavity, the coelenteron. This cavity is then separated from external seawater by two cell layers, the oral endoderm and ectoderm. Calcification requires transport of inorganic carbon and Ca^{2+} through these cell layers into the calcifying space. Active Ca transport is effectively required to support high observed precipitation rates while maintaining cellular [Ca^{2+}] at low levels of < 0.1 μM (Gattuso et al., 1999; Allemand et al., 2004). The supply of Ca to the coelenteron appears to occur through passive ion channels as well as by diffusive/advective transport, and at a rate an order of magnitude greater than transport across the calicoblastic epithelium (Bénazet-Tambutté

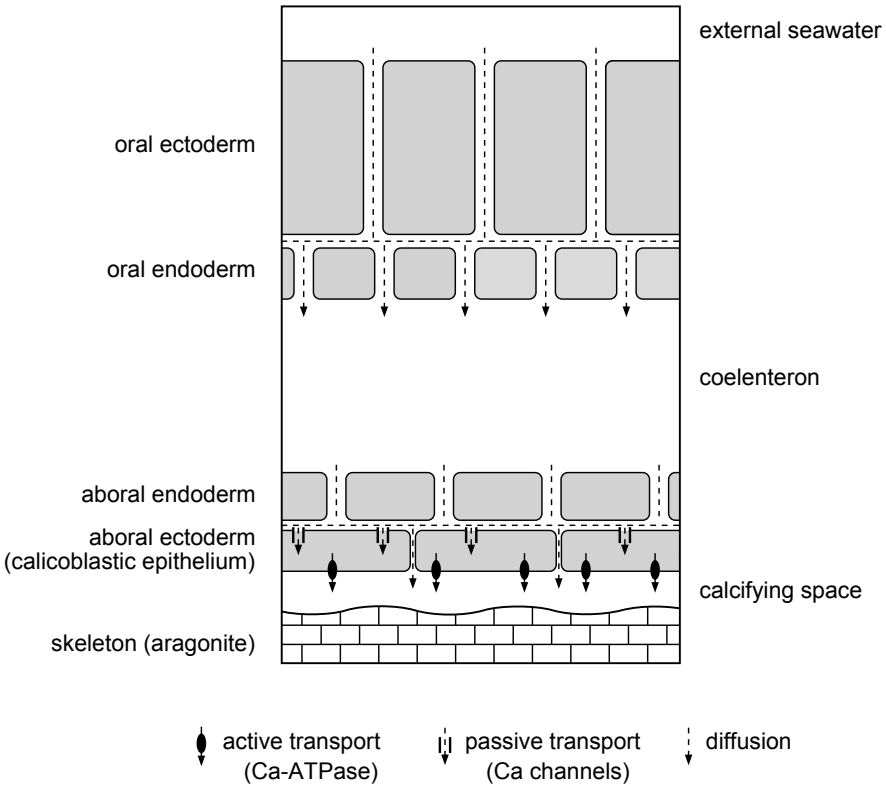

Figure 5.5: Schematic of coral physiology and ion transport pathways for Ca and other cations incorporated in calcification, modified from Tambutté et al. (1996) to reflect additional pathways for seawater to reach the calcifying space.

et al., 1996; Tambutté et al., 1996). Transport into the coelenteron is therefore not expected to be rate-limiting or to introduce fractionation to metal cation ratios, in contrast to mechanisms of transport into the calcifying space.

Ca-ATPase, an active ion pump, was identified specifically in the calicoblastic layer (Zoccola et al., 2004), and its involvement in coral skeletal growth is supported by several lines of evidence. A model of Ca-ATPase functioning is described in McConnaughey and Whelan (1997), involving exchange of two H^+ ions out of the calcifying space for one Ca^{2+} ion into the region, and measurements of Ca^{2+} uptake (calcification) in the light and excretion (dissolution) in the dark suggest that activity of the pump is linked to photosynthesis in symbiotic corals (de Beer et al., 2000). Within the calcifying space, pH has been measured at elevated levels up to ~9.3 (Al-Horani et al., 2003b), with the ion pump allowing skeletal growth even at significantly undersaturated external conditions while supplying H^+ ions and therefore CO_2 to the tissues that host photosynthesis (Cohen et al., 2009). The importance of this active transport mechanism is also demonstrated by significantly reduced calcification in response to inhibiting drugs (Tambutté et al., 1996). The selectivity of this ion pump to metal cations may be one source of geochemical fractionation, with a predicted preference for the light isotopes of Ca, as with all biological kinetic isotope effects.

Another source of Ca, in addition to that provided by Ca-ATPase through pH control of the extracellular space, is unmodified seawater, either from vesicular transport or diffusive leaking (Cohen and McConnaughey, 2003). The contribution of vesicles to calcification has been questioned, as previous observations of their involvement possibly represent artefacts of sample preparation methods (Clode and Marshall, 2002). Diffusive leaking was originally discounted, due to the observed insensitivity of radioactive ^{45}Ca uptake rate to the concentration of the radiotracer (Tambutté et al., 1996), but recent experiments show that paracellular pathways of a characteristic size do provide access to the calcification space (Tambutté et al., 2012). The effect of seawater transport can be shown by the incorporation of membrane-impermeable dyes (Tambutté et al., 2012) and trace elements such as U and Tb, with no known biological use or transport mechanism (Allison

et al., 2011; Gagnon et al., 2012). Diffusion of seawater through the porous skeleton and underlying reef is another possible source for natural corals, although not represented in laboratory-grown specimens. Given these pathways, the degree of mixing between seawater and actively pumped Ca^{2+} ions may respond to environmental parameters to generate a reservoir of Ca isotopes with a dependence on external conditions.

Rayleigh distillation could also affect the composition of the calcifying space and the geochemistry of coral aragonite. This mechanism has been proposed to explain Mg/Ca and Sr/Ca variability in both hermatypic and deep-sea corals (Cohen et al., 2006; Gaetani and Cohen, 2006; Gagnon et al., 2007) and possibly Ca-isotope data from deep-sea corals as well (Gagnon et al., 2012). Rayleigh distillation cannot be the only source of geochemical fractionation, however, due to experimental conditions inducing dissimilar responses across different elemental ratios, e.g. Mg/Ca but not Sr/Ca responding as predicted for a Rayleigh effect (Reynaud et al., 2007; Allison et al., 2011). With respect to Ca isotopes, partial removal of Ca from the calcifying space would be expected to enrich the remaining fluid in heavy isotopes and reduce Ca-isotope fractionation relative to that for inorganic aragonite precipitation. A decrease in calcification rate or utilization, due to acidified conditions or other external stress, might weaken this effect and result in lower values of $\delta^{44/40}$Ca. The observation that the FOCE experiment (Figure 5.4) as well as laboratory-based acidification experiments (Taubner et al., 2011) show no Ca-isotope effects suggests that Rayleigh distillation is only partially responsible for geochemical fractionation in corals.

Multiple sources of Ca-isotope fractionation, including temperature, carbonate saturation state, Rayleigh distillation, and mixing of seawater and actively transported Ca, must balance to explain the observed $\delta^{44/40}$Ca as well as other geochemical data for scleractinian corals. The relative importance of these factors for elemental or isotopic ratios can vary depending on the element, which explains how acidification experiments can affect Mg/Ca and Sr/Ca as for a Rayleigh model (Cohen et al., 2009), while allowing invariant $\delta^{44/40}$Ca. The expected decrease in $\delta^{44/40}$Ca from reduced utilization under ocean acidification may be offset by an increased proportion of seawater Ca relative to biologically

transported Ca, for example. This mixing model differs from previous assessments of Ca-isotope fractionation in corals, which ruled out any Rayleigh distillation effect due to complete utilization of Ca transported into the calcifying space and no contribution from seawater ions (Böhm et al., 2006). Based on the relationship between precipitation rate and inorganic precipitation experiments, Böhm et al. (2006) considered coral $\delta^{44/40}$Ca to be too low to permit any Rayleigh distillation, but the combination of additional sources of isotopic fractionation, such as a negative fractionation associated with dehydration of Ca^{2+} at cell membranes, as in *E. huxleyi* (Gussone et al., 2006), combined with a negative kinetic isotope effect by Ca-ATPase, could complement the positive isotope effect of Rayleigh fractionation to produce the observed coral Ca-isotope ratios.

5.6 Conclusions

Developing a mechanistic understanding of biogenic carbonate formation and associated vital effects is necessary for linking skeletal proxy measurements to past marine conditions. The processes that affect cation elemental and isotope ratios can be studied with Ca isotopes, whose behaviour is examined here in two case studies. Representing a biologically induced system of biomineralization, *Halimeda* algae that were stimulated to precipitate both calcite and aragonite demonstrate how inorganic mineral fractionation influences Ca-isotope ratios in biominerals. Rayleigh distillation and saturation state effects also appear to have possible influences on this simple system. Additional vital effects likely contribute to the skeletal geochemistry of *Porites* corals, which represent a biologically controlled system of biomineralization. Mechanisms that have been proposed for controlling coral skeletal composition, such as Rayleigh distillation or ion pump selectivity, are consistent with some datasets, but contradicted by others, such as the invariant $\delta^{44/40}$Ca of coral acidification experiments. This apparent paradox can be resolved by considering the balance of several sources of geochemical fractionation, such as mixing between seawater-derived and actively pumped Ca, temperature and saturation-state dependencies, and Rayleigh distillation. This model of coral calcification suggests that empirical calibrations of coral geochemical proxies cannot be extended to unknown ele-

mental or isotopic ratios without determining the variables to which a geochemical proxy is most sensitive. Further examination of the behaviour of cations in biogenic systems is required to resolve these specific vital effects and fully exploit the valuable geological archive of skeletal carbonate.

Acknowledgements

Thanks are due to Jennifer Engels and Olga Pantos for harvesting and shipping experimental samples to Oxford, Phil Holdship for analyzing cation concentrations in experimental seawater, and Phil Wiseman for generously accommodating XRD analyses in the Department of Chemistry, University of Oxford.

Chapter 6

Conclusions

Several geological problems over a variety of timescales have been addressed by the applications of Ca isotopes in the marine environment. In Chapter 3, Ca isotopes in bulk carbonate were used to reconstruct the isotopic composition of seawater, which records a negative isotope excursion during periods of global warmth and environmental change due to a large increase in the weathering flux of Ca. The modern Ca-isotope budget is described quantitatively in Chapter 4, which reveals patterns in carbonate mineralogy and depositional environment that help to explain the major features of the Phanerozoic Ca-isotope record. Chapter 5 presents the results of experiments probing the source of isotopic fractionation in biomineralization, which could lead to a better understanding of carbonate-based proxies for reconstructing environments of the geological past.

The natural variation in Ca-isotope ratios is relatively small, which restricts the possible uses of isotopic fractionation as a tracers for chemical reactions or ion sources. The long residence time of Ca in the oceans also constrains the timescale of questions that can be resolved with Ca isotopes. However, with appropriate consideration of these inherent qualities of the Ca cycle, the benefits of its abundance and importance in many global processes can be utilized. If isotopic variation can be resolved, understanding the Ca cycle has the potential to contribute to oceanographic, sedimentological, biochemical, diagenetic, and ecological problems in unique ways. As a tracer of major processes that can be difficult to observe directly, Ca-isotope ratios can be valuable for quantifying or verifying models of Earth system processes.

Ca isotopes hold the most potential when applied in combination with other geochemical tools. Other isotopic or chemical systems can provide constraints on issues which Ca isotopes cannot address on their own, and Ca-isotope ratios can in turn often quantify processes that are only more qualitatively addressed by other geochemical systems. For example, Sr- and Os-isotope evidence suggests the existence of an imbalance between weathering and hydrothermal fluxes of cations to seawater during the Cretaceous OAEs, but the difficulties of quantifying this imbalance given multiple unknown parameters in the Sr-isotope system, and the limited availability of organic-rich black shales suitable for Os-isotope analysis, show the importance of the small but significant excursion in seawater Ca-isotope ratios that can be directly related to weathering fluxes. The Phanerozoic Ca-isotope curve of seawater could be theoretically explained by combinations of several variables, but the composition of the marine carbonate budget and the proportion of aragonite to calcite sedimentation is found to be crucial due to supporting data on changes in seawater Mg/Ca ratios and the favoured carbonate polymorph over time. In the field of biomineralization, multi-proxy approaches to understanding skeletal geochemistry and revealing the mechanisms underlying geochemical fractionation are absolutely essential. Theoretical models may predict the magnitude and direction of fractionation for elemental ratios such as Mg/Ca, Sr/Ca, or U/Ca, as well as isotopic ratios such as $\delta^{44/40}$Ca, but empirical correlations or lack thereof between multiple proxies can determine the viability of biomineralization models. Only by showing that Ca-isotope data are consistent with the mechanisms used to justify other proxy records, particularly other cation ratios from the same carbonate samples, can vital effects be properly understood and utilized in reconstructions of ancient environmental conditions.

Extensions of the Ca-isotope work presented here could introduce the approaches and conclusions from these studies to other intervals and questions in Earth history. The weathering signal recorded in marine Ca-isotope ratios during OAE1a and OAE2 may reflect a fundamental feedback in the climate system, and investigating other intervals throughout the stratigraphic record could reveal the true importance of this mechanism. It remains difficult to generate large changes in seawater Ca-isotope ratios, and requires

rather extreme environmental forcing according to current modelling results. Observations of transient changes in Ca-isotope ratios therefore signal particularly dynamic intervals of Earth history, and the relationship between the Ca cycle and the C cycle throughout such intervals should continue to be developed through additional stratigraphic studies of Ca-isotope ratios. More extreme climate perturbations are known from more ancient sediments, such as the catastrophic Neoproterozoic glaciations, where further documentation and quantification of the linked Ca- and C-cycle responses could aid interpretation of how the surface environment responded to such dramatic change. Finding faithful sedimentary records to record seawater Ca-isotope ratios becomes a greater challenge with the increasing age of samples, however, and extensive work on the preservational issues and diagenetic effects for Ca isotopes will also need to be performed. In particular, the non-skeletal record of Ca isotopes in the Precambrian could yield valuable information about ancient oceans and carbonate precipitates, if mechanisms of Ca-isotope fractionation in such samples can be understood and their environments of formation appropriately interpreted.

The sources of smaller variation in the Phanerozoic record of seawater Ca-isotope ratios, which cannot be explained through a steady-state consideration of the composition of the carbonate sink, still remain to be resolved. A record with higher temporal resolution will need to be established in order to distinguish noise from real isotopic signals, which could arise from changes in global temperature, dolomitization rates, carbonate burial fluxes, or other factors. Analysis of additional primary calcite fossils would be necessary for such detailed interpretation of the Phanerozoic record, especially in intervals where belemnites or brachiopods are lacking, and characteristic fractionation factors associated with each type of fossil must be well established. Non-skeletal and non-carbonate mineral phases, such as phosphate and barite, can also record seawater Ca-isotope ratios, but more work needs to be done to establish how and to what degree Ca-isotopes are fractionated in these phases and how environmental conditions may influence these records. Ideally, multiple contemporaneous phases should be used to confirm the accuracy of reconstructed $\delta^{44/40}$Ca values and compile a more complete Ca-isotope history of seawater. Such de-

tailed analysis could lead to further understanding of the connections between seawater chemistry, sea level, global temperature, weathering fluxes, and carbonate burial during the dynamic Phanerozoic.

The contribution of Ca isotopes towards understanding mechanisms of mineralization and biological vital effects has just barely been scratched in the current literature and with the contribution of the case studies presented here for *Halimeda* algae and *Porites* corals. Analysis of a range of biocalcifiers under both experimental and natural conditions should continue to help develop models for geochemical fractionation that are empirically consistent with multiple proxy records. Understanding coral aragonite formation further will be particularly useful for extracting high-resolution, dateable records from both the surface and the deep sea, and extending this work to other biomineralizers could contribute greatly to environmental reconstructions over different timescales. Ca-isotope analysis in speleothems could also clarify the precipitation conditions for these valuable terrestrial climate records and therefore guide the interpretation of carbon-isotope, oxygen-isotope, and trace-metal data from their carbonate lattices. The recent extension of Ca-isotope analysis to monitor bone loss in humans, for example, suggests that further applications in the biomedical sciences may also be developed. A thorough mechanistic understanding of Ca-isotope fractionation in various minerals, both inorganic precipitates and biominerals, will be useful for these and other applications of Ca isotopes towards geological and biomedical questions.

The work presented here shows that Ca-isotope analysis is a useful tool that can and should be applied to a wide variety of problems. In marine carbonates, Ca-isotope ratios provide insight into a range of geological questions, and remain to be further exploited over new time intervals and in new mineral phases. Aided by the more widespread use of high-precision mass spectrometry, these results hopefully contribute to the diverse, creative, and fruitful continued application of Ca isotopes.

Bibliography

Adkins, J. F., Henderson, G. M., Wang, S.-L., O'Shea, S., and Mokadem, F., 2004. Growth rates of the deep-sea scleractinia *Desmophyllum cristagalli* and *Enallopsammia rostrata*. *Earth and Planetary Science Letters*, 227: 481–490. doi:10.1016/j.epsl.2004.08.022.

Al-Horani, F. A., Al-Moghrabi, S. M., and de Beer, D., 2003a. Microsensor study of photosynthesis and calcification in the scleractinian coral, *Galaxea fascicularis*: active internal carbon cycle. *Journal of Experimental Marine Biology and Ecology*, 288: 1–15. doi:10.1016/S0022-0981(02)00578-6.

Al-Horani, F. A., Al-Moghrabi, S. M., and de Beer, D., 2003b. The mechanism of calcification and its relation to photosynthesis and respiration in the scleractinian coral *Galaxea fascicularis*. *Marine Biology*, 142: 419–426. doi:10.1007/s00227-002-0981-8.

Allemand, D., Ferrier-Pagès, C., Furla, P., Houlbrèque, F., Puverel, S., Reynaud, S., Tambutté, E., Tambutté, S., and Zoccola, D., 2004. Biomineralisation in reef-building corals: from molecular mechanisms to environmental control. *Comptes Rendus Palevol*, 3: 453–467. doi:10.1016/j.crpv.2004.07.011.

Allison, N., Cohen, I., Finch, A. A., Erez, J., and EMIF, 2011. Controls on Sr/Ca and Mg/Ca in scleractinian corals: The effects of Ca-ATPase and transcellular Ca channels on skeletal chemistry. *Geochimica et Cosmochimica Acta*, 75: 6350–6360. doi:10.1016/j.gca.2011.08.012.

Amini, M., Eisenhauer, A., Böhm, F., Fietzke, J., Bach, W., Garbe-Schönberg, D., Rosner, M., Bock, B., Lackschewitz, K. S., and Hauff, F., 2008. Calcium isotope ($\delta^{44/40}$Ca) fractionation along hydrothermal pathways, Logatchev field (Mid-Atlantic Ridge, 14°45'N). *Geochimica et Cosmochimica Acta*, 72: 4107–4122. doi:10.1016/j.gca.2008.05.055.

Ando, A., Kaiho, K., Kawahata, H., and Kakegawa, T., 2008. Timing and magnitude of early Aptian extreme warming: Unraveling primary δ^{18}O variation in indurated pelagic carbonates at Deep Sea Drilling Project Site 463, central Pacific Ocean. *Palaeogeography, Palaeoclimatology, Palaeoecology*, 260: 463–476. doi:10.1016/j.palaeo.2007.12.007.

Archer, D., Kheshgi, H., and Maier-Reimer, E., 1997. Multiple timescales for neutralization of fossil fuel CO_2. *Geophysical Research Letters*, 24: 405–408. doi:10.1029/97GL00168.

Archer, D. E., 1996. An atlas of the distribution of calcium carbonate in sediments of the deep sea. *Global Biogeochemical Cycles*, 10: 159–174. doi:10.1029/95GB03016.

Arnaud, H. M., Flood, P. G., and Strasser, A., 1995. Resolution Guyot (Hole 866A, Mid-Pacific Mountains): facies evolution and sequence stratigraphy. In Winterer, E. L., Sager, W. W., Firth, J. V., and Sinton, J. M., editors, *Proceedings of the Ocean Drilling Program, Scientific Results*, 143: 133–159. Ocean Drilling Program, College Station, TX. doi:10.2973/odp.proc.sr.143.230.1995.

Arnaud-Vanneau, A. and Sliter, W. V., 1995. Early Cretaceous shallow-water benthic foraminifers and fecal pellets from Leg 143 compared with coeval faunas from the Pacific Basin, Central America, and the Tethys. In Winterer, E. L., Sager, W. W., Firth, J. V., and Sinton, J. M., editors, *Proceedings of the Ocean Drilling Program, Scientific Results*, 143: 537–564. Ocean Drilling Program, College Station, TX. doi:10.2973/odp.proc.sr.143.252.1995.

Arthur, M. A. and Sageman, B. B., 1994. Marine black shales: depositional mechanisms and environments of ancient deposits. *Annual Review of Earth and Planetary Sciences*, 22: 499–551. doi:10.1146/annurev.ea.22.050194.002435.

Beerling, D. J., Lomas, M. R., and Gröcke, D. R., 2002. On the nature of methane gas-hydrate dissociation during the Toarcian and Aptian oceanic anoxic events. *American Journal of Science*, 302: 28–49. doi:10.2475/ajs.302.1.28.

Belshaw, N. S., Freedman, P. A., O'Nions, R. K., Frank, M., and Guo, Y., 1998. A new variable dispersion double-focusing plasma mass spectrometer with performance illustrated for Pb isotopes. *International Journal of Mass Spectrometry*, 181: 51–58. doi:10.1016/S1387-3806(98)14150-7.

Bénazet-Tambutté, S., Allemand, D., and Jaubert, J., 1996. Permeability of the oral epithelial layers in cnidarians. *Marine Biology*, 126: 43–53. doi:10.1007/BF00571376.

Berelson, W. M., Balch, W. M., Najjar, R., Feely, R. A., Sabine, C., and Lee, K., 2007. Relating estimates of $CaCO_3$ production, export, and dissolution in the water column to measurements of $CaCO_3$ rain into sediment traps and dissolution on the sea floor: A revised global carbonate budget. *Global Biogeochemical Cycles*, 21: GB1024. doi:10.1029/2006GB002803.

Berner, R. A. and Honjo, S., 1981. Pelagic sedimentation of aragonite: its geochemical significance. *Science*, 211: 940–942. doi:10.1126/science.211.4485.940.

Blakey, R., 2010. *Global Paleogeography*. NAU Geology. http://jan.ucc.nau.edu/~rcb7/globaltext2.html.

Blättler, C. L., Jenkyns, H. C., Reynard, L. M., and Henderson, G. M., 2011. Significant increases in global weathering during Oceanic Anoxic Events 1a and 2 indicated by calcium isotopes. *Earth and Planetary Science Letters*, 309: 77–88. doi:10.1016/j.epsl.2011.06.029.

Blättler, C. L., Henderson, G. M., and Jenkyns, H. C., 2012. Explaining the Phanerozoic Ca-isotope history of seawater. *Geology*, in press. doi:10.1130/G33191.1.

Böhm, F., Eisenhauer, A., Fietzke, J., Rausch, S., Klügel, A., and Bach, W., 2011. Calcium isotope fractionation during dolomite formation. In *Goldschmidt Conference Abstracts, Mineralogical Magazine*, 75: 544.

Böhm, F., Gussone, N., Eisenhauer, A., Dullo, W.-C., Reynaud, S., and Paytan, A., 2006. Calcium isotope fractionation in modern scleractinian corals. *Geochimica et Cosmochimica Acta*, 70: 4452–4462. doi:10.1016/j.gca.2006.06.1546.

Borowitzka, M. A. and Larkum, A. W. D., 1987. Calcification in algae: mechanisms and the role of metabolism. *Critical Reviews in Plant Sciences*, 6: 1–45. doi:10.1080/07352688709382246.

Boulyga, S. F., 2010. Calcium isotope analysis by mass spectrometry. *Mass Spectrometry Reviews*, 29: 685–716. doi:10.1002/mas.20244.

Bown, P. R., Lees, J. A., and Young, J. R., 2004. Calcareous nannoplankton evolution and diversity through time. In Thierstein, H. R. and Young, J. R., editors, *Coccolithophores: from molecular processes to global impact*, pages 481–508. Springer, Berlin.

Boyle, E. A., 1981. Cadmium, zinc, copper, and barium in foraminifera tests. *Earth and Planetary Science Letters*, 53: 11–35. doi:10.1016/0012-821X(81)90022-4.

Bralower, T. J., Arthur, M. A., Leckie, R. M., Sliter, W. V., Allard, D. J., and Schlanger, S. O., 1994. Timing and paleoceanography of oceanic dysoxia/anoxia in the Late Barremian to Early Aptian (Early Cretaceous). *Palaios*, 9: 335–369. doi:10.2307/3515055.

Bralower, T. J., Fullagar, P. D., Paull, C. K., Dwyer, G. S., and Leckie, R. M., 1997. Mid-Cretaceous strontium-isotope stratigraphy of deep-sea sections. *Geological Society of America Bulletin*, 109: 1421–1442. doi:10.1130/0016-7606(1997)109<1421:MCSISO>2.3.CO;2.

Brennan, S. T. and Lowenstein, T. K., 2002. The major-ion composition of Silurian seawater. *Geochimica et Cosmochimica Acta*, 66: 2683–2700. doi:10.1016/S0016-7037(02)00870-0.

Brennan, S. T., Lowenstein, T. K., and Horita, J., 2004. Seawater chemistry and the advent of biocalcification. *Geology*, 32: 473–476. doi:10.1130/G20251.1.

Broecker, W. S., 1971. A kinetic model for the chemical composition of sea water. *Quaternary Research*, 1: 188–207. doi:10.1016/0033-5894(71)90041-X.

Cardinal, D., Hamelin, B., Bard, E., and Pätzold, J., 2001. Sr/Ca, U/Ca and $\delta^{18}O$ records in recent massive corals from Bermuda: relationships with sea surface temperature. *Chemical Geology*, 176: 213–233. doi:10.1016/S0009-2541(00)00396-X.

Caro, G., Papanastassiou, D. A., and Wasserburg, G. J., 2010. ^{40}K–^{40}Ca isotopic constraints on the oceanic calcium cycle. *Earth and Planetary Science Letters*, 296: 124–132. doi:10.1016/j.epsl.2010.05.001.

Case, D. H., Robinson, L. F., Auro, M. E., and Gagnon, A. C., 2010. Environmental and biological controls on Mg and Li in deep-sea scleractinian corals. *Earth and Planetary Science Letters*, 300: 215–225. doi:10.1016/j.epsl.2010.09.029.

Cenki-Tok, B., Chabaux, F., Lemarchand, D., Schmitt, A.-D., Pierret, M.-C., Viville, D., Bagard, M.-L., and Stille, P., 2009. The impact of water–rock interaction and vegetation on calcium isotope fractionation in soil- and stream waters of a small, forested catchment (the Strengbach case). *Geochimica et Cosmochimica Acta*, 73: 2215–2228. doi:10.1016/j.gca.2009.01.023.

Chang, V. T.-C., Williams, R. J. P., Makishima, A., Belshaw, N. S., and O'Nions, R. K., 2004. Mg and Ca isotope fractionation during $CaCO_3$ biomineralisation. *Biochemical and Biophysical Research Communications*, 323: 79–85. doi:10.1016/j.bbrc.2004.08.053.

Chu, N.-C., Henderson, G. M., Belshaw, N. S., and Hedges, R. E. M., 2006. Establishing the potential of Ca isotopes as proxy for consumption of dairy products. *Applied Geochemistry*, 21: 1656–1667. doi:10.1016/j.apgeochem.2006.07.003.

Clode, P. L. and Marshall, A. T., 2002. Low temperature FESEM of the calcifying interface of a scleractinian coral. *Tissue and Cell*, 34: 187–198. doi:10.1016/S0040-8166(02)00031-9.

Cobert, F., Schmitt, A.-D., Bourgeade, P., Labolle, F., Badot, P.-M., Chabaux, F., and Stille, P., 2011. Experimental identification of Ca isotopic fractionations in higher plants. *Geochimica et Cosmochimica Acta*, 75: 5467–5482. doi:10.1016/j.gca.2011.06.032.

Cobianchi, M., Luciani, V., and Menegatti, A., 1999. The Selli Level of the Gargano Promontory, Apulia, southern Italy: foraminiferal and calcareous nannofossil data. *Cretaceous Research*, 20: 255–269. doi:10.1006/cres.1999.0155.

Cohen, A. L., Gaetani, G. A., Lundälv, T., Corliss, B. H., and George, R. Y., 2006. Compositional variability in a cold-water scleractinian, *Lophelia pertusa*: New insights into "vital effects". *Geochemistry Geophysics Geosystems*, 7: Q12004. doi:10.1029/2006GC001354.

Cohen, A. L., Layne, G. D., Hart, S. R., and Lobel, P. S., 2001. Kinetic control of skeletal Sr/Ca in a symbiotic coral: Implications for the paleotemperature proxy. *Paleoceanography*, 16: 20–26. doi:10.1029/1999PA000478.

Cohen, A. L. and McConnaughey, T. A., 2003. Geochemical perspectives on coral mineralization. *Reviews in Mineralogy and Geochemistry*, 54: 151–187. doi:10.2113/0540151.

Cohen, A. L., McCorkle, D. C., de Putron, S., Gaetani, G. A., and Rose, K. A., 2009. Morphological and compositional changes in the skeletons of new coral recruits reared in acidified seawater: Insights into the biomineralization response to ocean acidification. *Geochemistry Geophysics Geosystems*, 10: Q07005. doi:10.1029/2009GC002411.

Cohen, A. S., Coe, A. L., Harding, S. M., and Schwark, L., 2004. Osmium isotope evidence for the regulation of atmospheric CO_2 by continental weathering. *Geology*, 32: 157–160. doi:10.1130/G20158.1.

Cohen, A. S., Coe, A. L., and Kemp, D. B., 2007. The Late Palaeocene Early Eocene and Toarcian (Early Jurassic) carbon isotope excursions: a comparison of their time scales, associated environmental changes, causes and consequences. *Journal of the Geological Society, London*, 164: 1093–1108. doi:10.1144/0016-76492006-123.

Davies, T. A. and Worsley, T. R., 1981. Paleoenvironmental implications of oceanic carbonate sedimentation rates. In Warme, J. E., Douglas, R. G., and Winterer, E. L., editors, *The Deep Sea Drilling Project: A Decade of Progress, Society of Economic Paleontologists and Mineralogists Special Publications*, 32: 169–179.

de Beer, D., Kühl, M., Stambler, N., and Vaki, L., 2000. A microsensor study of light enhanced Ca^{2+} uptake and photosynthesis in the reef-building hermatypic coral *Favia* sp. *Marine Ecology Progress Series*, 194: 75–85. doi:10.3354/meps194075.

de Beer, D. and Larkum, A. W. D., 2001. Photosynthesis and calcification in the calcifying algae *Halimeda discoidea* studied with microsensors. *Plant, Cell and Environment*, 24: 1209–1217. doi:10.1046/j.1365-3040.2001.00772.x.

De La Rocha, C. L. and DePaolo, D. J., 2000. Isotopic evidence for variations in the marine calcium cycle over the Cenozoic. *Science*, 289: 1176–1178. doi:10.1126/science.289.5482.1176.

de Laeter, J. R., Böhlke, J. K., de Bièvre, P., Hidaka, H., Peiser, H. S., Rosman, K. J. R., and Taylor, P. D. P., 2003. Atomic weights of the elements: Review 2000 (IUPAC Technical Report). *Pure and Applied Chemistry*, 75: 683–800. doi:10.1351/pac200375060683.

DePaolo, D. J., 2004. Calcium isotopic variations produced by biological, kinetic, radiogenic and nucleosynthetic processes. *Reviews in Mineralogy and Geochemistry*, 55: 255–288. doi:10.2138/gsrmg.55.1.255.

DePaolo, D. J., 2011. Surface kinetic model for isotopic and trace element fractionation during precipitation of calcite from aqueous solutions. *Geochimica et Cosmochimica Acta*, 75: 1039–1056. doi:10.1016/j.gca.2010.11.020.

Dickens, G. R., Castillo, M. M., and Walker, J. C. G., 1997. A blast of gas in the latest Paleocene: Simulating first-order effects of massive dissociation of oceanic methane hydrate. *Geology*, 25: 259–262. doi:10.1130/0091-7613(1997)025<0259:ABOGIT>2.3.CO;2.

Dickson, J. A. D., 2002. Fossil echinoderms as monitor of the Mg/Ca ratio of Phanerozoic oceans. *Science*, 298: 1222–1224. doi:10.1126/science.1075882.

Dickson, J. A. D., 2004. Echinoderm skeletal preservation: calcite–aragonite seas and the Mg/Ca ratio of Phanerozoic oceans. *Journal of Sedimentary Research*, 74: 355–365. doi:10.1306/112203740355.

Dumitrescu, M. and Brassell, S. C., 2005. Biogeochemical assessment of sources of organic matter and paleoproductivity during the early Aptian Oceanic Anoxic Event at Shatsky Rise, ODP Leg 198. *Organic Geochemistry*, 36: 1002–1022. doi:10.1016/j.orggeochem.2005.03.001.

Dumitrescu, M., Brassell, S. C., Schouten, S., Hopmans, E. C., and Sinninghe Damsté, J. S., 2006. Instability in tropical Pacific sea-surface temperatures during the early Aptian. *Geology*, 34: 833–836. doi:10.1130/G22882.1.

Eisenhauer, A., Nägler, T. F., Stille, P., Kramers, J., Gussone, N., Bock, B., Fietzke, J., Hippler, D., and Schmitt, A. D., 2004. Proposal for International Agreement on Ca Notation Resulting from Discussions at Workshops on Stable Isotope Measurements Held in Davos (Goldschmidt 2002) and Nice (EGS-AGU-EUG 2003). *Geostandards and Geoanalytical Research*, 28: 149–151. doi:10.1111/j.1751-908X.2004.tb01051.x.

Elderfield, H. and Ganssen, G., 2000. Past temperature and $\delta^{18}O$ of surface ocean waters inferred from foraminiferal Mg/Ca ratios. *Nature*, 405: 442–445. doi:10.1038/35013033.

Erba, E., 2004. Calcareous nannofossils and Mesozoic oceanic anoxic events. *Marine Micropaleontology*, 52: 85–106. doi:10.1016/j.marmicro.2004.04.007.

Erba, E., Channell, J. E. T., Claps, M., Jones, C., Larson, R., Opdyke, B., Premoli Silva, I., Riva, A., Salvini, G., and Torricelli, S., 1999. Integrated stratigraphy of the Cismon Apticore (southern Alps, Italy): a "reference section" for the Barremian–Aptian interval at low latitudes. *The Journal of Foraminiferal Research*, 29: 371–391.

Erbacher, J., Thurow, J., and Littke, R., 1996. Evolution patterns of radiolaria and organic matter variations: A new approach to identify sea-level changes in mid-Cretaceous pelagic environments. *Geology*, 24: 499–502. doi:10.1130/0091-7613(1996)024<0499:EPORAO>2.3.CO;2.

Erez, J., 2003. The source of ions for biomineralization in foraminifera and their implications for paleoceanographic proxies. *Reviews in Mineralogy and Geochemistry*, 54: 115–149. doi:10.2113/0540115.

Ewing, S. A., Yang, W., DePaolo, D. J., Michalski, G., Kendall, C., Stewart, B. W., Thiemens, M., and Amundson, R., 2008. Non-biological fractionation of stable Ca isotopes in soils of the Atacama Desert, Chile. *Geochimica et Cosmochimica Acta*, 72: 1096–1110. doi:10.1016/j.gca.2007.10.029.

Fantle, M. S., 2010. Evaluating the Ca isotope proxy. *American Journal of Science*, 310: 194–230. doi:10.2475/03.2010.03.

Fantle, M. S. and DePaolo, D. J., 2005. Variations in the marine Ca cycle over the past 20 million years. *Earth and Planetary Science Letters*, 237: 102–117. doi:10.1016/j.epsl.2005.06.024.

Fantle, M. S. and DePaolo, D. J., 2007. Ca isotopes in carbonate sediment and pore fluid from ODP Site 807A: The Ca^{2+}(aq)–calcite equilibrium fractionation factor and calcite recrystallization rates in Pleistocene sediments. *Geochimica et Cosmochimica Acta*, 71: 2524–2546. doi:10.1016/j.gca.2007.03.006.

Farkaš, J., Böhm, F., Wallmann, K., Blenkinsop, J., Eisenhauer, A., van Geldern, R., Munnecke, A., Voigt, S., and Veizer, J., 2007a. Calcium isotope record of Phanerozoic oceans: Implications for chemical evolution of seawater and its causative mechanisms. *Geochimica et Cosmochimica Acta*, 71: 5117–5134. doi:10.1016/j.gca.2007.09.004.

Farkaš, J., Buhl, D., Blenkinsop, J., and Veizer, J., 2007b. Evolution of the oceanic calcium cycle during the late Mesozoic: Evidence from $\delta^{44/40}$Ca of marine skeletal carbonates. *Earth and Planetary Science Letters*, 253: 96–111. doi:10.1016/j.epsl.2006.10.015.

Farkaš, J., Déjeant, A., Novák, M., and Jacobsen, S. B., 2011. Calcium isotope constraints on the uptake and sources of Ca^{2+} in a base-poor forest: A new concept of combining stable ($\delta^{44/42}$Ca) and radiogenic (ε_{Ca}) signals. *Geochimica et Cosmochimica Acta*, 75: 7031–7046. doi:10.1016/j.gca.2011.09.021.

Farley, K. A. and Eltgroth, S. F., 2003. An alternative age model for the Paleocene–Eocene thermal maximum using extraterrestrial ^{3}He. *Earth and Planetary Science Letters*, 208: 135–148. doi:10.1016/S0012-821X(03)00017-7.

Fietzke, J., Eisenhauer, A., Gussone, N., Bock, B., Liebetrau, V., Nägler, T. F., Spero, H. J., Bijma, J., and Dullo, C., 2004. Direct measurement of ^{44}Ca/^{40}Ca ratios by MC–ICP–MS using the cool plasma technique. *Chemical Geology*, 206: 11–20. doi:10.1016/j.chemgeo.2004.01.014.

Flood, P. G. and Chivas, A. R., 1995. Origin of massive dolomite, Leg 143, Hole 866A, Resolution Guyot, Mid-Pacific Mountains. In Winterer, E. L., Sager, W. W., Firth, J. V., and Sinton, J. M., editors, *Proceedings of the Ocean Drilling Program, Scientific Results*, 143: 161–169. Ocean Drilling Program, College Station, TX. doi:10.2973/odp.proc.sr.143.229.1995.

Forster, A., Schouten, S., Moriya, K., Wilson, P. A., and Sinninghe Damsté, J. S., 2007. Tropical warming and intermittent cooling during the Cenomanian/Turonian oceanic anoxic event 2: Sea surface temperature records from the equatorial Atlantic. *Paleoceanography*, 22: PA1219. doi:10.1029/2006PA001349.

Fosså, J. H., Mortensen, P. B., and Furevik, D. M., 2002. The deep-water coral *Lophelia pertusa* in Norwegian waters: distribution and fishery impacts. *Hydrobiologia*, 471: 1–12. doi:10.1023/A:1016504430684.

Frijia, G. and Parente, M., 2008. Strontium isotope stratigraphy in the upper Cenomanian shallow-water carbonates of the southern Apennines: Short-term perturbations of marine ^{87}Sr/^{86}Sr during the oceanic anoxic event 2. *Palaeogeography, Palaeoclimatology, Palaeoecology*, 261: 15–29. doi:10.1016/j.palaeo.2008.01.003.

Gaetani, G. A. and Cohen, A. L., 2006. Element partitioning during precipitation of aragonite from seawater: A framework for understanding paleoproxies. *Geochimica et Cosmochimica Acta*, 70: 4617–4634. doi:10.1016/j.gca.2006.07.008.

Gagnon, A. C., Adkins, J. F., and Erez, J., 2012. Seawater transport during coral biomineralization. *Earth and Planetary Science Letters*, 329–330: 150–161. doi:10.1016/j.epsl.2012.03.005.

Gagnon, A. C., Adkins, J. F., Fernandez, D. P., and Robinson, L. F., 2007. Sr/Ca and Mg/Ca vital effects correlated with skeletal architecture in a scleractinian deep-sea coral and the role of Rayleigh fractionation. *Earth and Planetary Science Letters*, 261: 280–295. doi:10.1016/j.epsl.2007.07.013.

Gagnon, A. C., DePaolo, D. J., Adkins, J. F., and De Yoreo, J. J., 2011. Calcium isotopes during coral biomineralization. In *Goldschmidt Conference Abstracts, Mineralogical Magazine*, 75: 880.

Gaillardet, J., Dupré, B., Louvat, P., and Allègre, C. J., 1999. Global silicate weathering and CO_2 consumption rates deduced from the chemistry of large rivers. *Chemical Geology*, 159: 3–30. doi:10.1016/S0009-2541(99)00031-5.

Gale, A. S., Jenkyns, H. C., Kennedy, W. J., and Corfield, R. M., 1993. Chemostratigraphy versus biostratigraphy: data from around the Cenomanian–Turonian boundary. *Journal of the Geological Society, London*, 150: 29–32. doi:10.1144/gsjgs.150.1.0029.

Gale, A. S., Kennedy, W. J., Voigt, S., and Walaszczyk, I., 2005. Stratigraphy of the Upper Cenomanian–Lower Turonian Chalk succession at Eastbourne, Sussex, UK: ammonites, inoceramid bivalves and stable carbon isotopes. *Cretaceous Research*, 26: 460–487. doi:10.1016/j.cretres.2005.01.006.

Gattuso, J.-P., Allemand, D., and Frankignoulle, M., 1999. Photosynthesis and calcification at cellular, organismal and community levels in coral reefs: a review on interactions and control by carbonate chemistry. *American Zoologist*, 39: 160–183. doi:10.1093/icb/39.1.160.

Giusberti, L., Rio, D., Agnini, C., Backman, J., Fornaciari, E., Tateo, F., and Oddone, M., 2007. Mode and tempo of the Paleocene–Eocene thermal maximum in an expanded section from the Venetian pre-Alps. *Geological Society of America Bulletin*, 119: 391–412. doi:10.1130/B25994.1.

Griffith, E. M., Paytan, A., Caldeira, K., Bullen, T. D., and Thomas, E., 2008a. A dynamic marine calcium cycle during the past 28 million years. *Science*, 322: 1671–1674. doi:10.1126/science.1163614.

Griffith, E. M., Paytan, A., Eisenhauer, A., Bullen, T. D., and Thomas, E., 2011. Seawater calcium isotope ratios across the Eocene–Oligocene transition. *Geology*, 39: 683–686. doi:10.1130/G31872.1.

Griffith, E. M., Paytan, A., Kozdon, R., Eisenhauer, A., and Ravelo, A. C., 2008b. Influences on the fractionation of calcium isotopes in planktonic foraminifera. *Earth and Planetary Science Letters*, 268: 124–136. doi:10.1016/j.epsl.2008.01.006.

Gröcke, D. R., Hesselbo, S. P., and Jenkyns, H. C., 1999. Carbon-isotope composition of Lower Cretaceous fossil wood: Ocean-atmosphere chemistry and relation to sea-level change. *Geology*, 27: 155–158. doi:10.1130/0091-7613(1999)027<0155:CICOLC>2.3.CO;2.

Gussone, N., Böhm, F., Eisenhauer, A., Dietzel, M., Heuser, A., Teichert, B. M. A., Reitner, J., Wörheide, G., and Dullo, W.-C., 2005. Calcium isotope fractionation in calcite and aragonite. *Geochimica et Cosmochimica Acta*, 69: 4485–4494. doi:10.1016/j.gca.2005.06.003.

Gussone, N., Eisenhauer, A., Heuser, A., Dietzel, M., Bock, B., Böhm, F., Spero, H. J., Lea, D. W., Bijma, J., and Nägler, T. F., 2003. Model for kinetic effects on calcium isotope fractionation (δ^{44}Ca) in inorganic aragonite and cultured planktonic foraminifera. *Geochimica et Cosmochimica Acta*, 67: 1375–1382. doi:10.1016/S0016-7037(02)01296-6.

Gussone, N. and Filipsson, H. L., 2010. Calcium isotope ratios in calcitic tests of benthic foraminifers. *Earth and Planetary Science Letters*, 290: 108–117. doi:10.1016/j.epsl.2009.12.010.

Gussone, N., Hönisch, B., Heuser, A., Eisenhauer, A., Spindler, M., and Hemleben, C., 2009. A critical evaluation of calcium isotope ratios in tests of planktonic foraminifers. *Geochimica et Cosmochimica Acta*, 73: 7241–7255. doi:10.1016/j.gca.2009.08.035.

Gussone, N., Langer, G., Geisen, M., Steel, B. A., and Riebesell, U., 2007. Calcium isotope fractionation in coccoliths of cultured *Calcidiscus leptoporus*, *Helicosphaera carteri*, *Syracosphaera pulchra* and *Umbilicosphaera foliosa*. *Earth and Planetary Science Letters*, 260: 505–515. doi:10.1016/j.epsl.2007.06.001.

Gussone, N., Langer, G., Thoms, S., Nehrke, G., Eisenhauer, A., Riebesell, U., and Wefer, G., 2006. Cellular calcium pathways and isotope fractionation in *Emiliania huxleyi*. *Geology*, 34: 625–628. doi:10.1130/G22733.1.

Gussone, N., Nehrke, G., and Teichert, B. M. A., 2011. Calcium isotope fractionation in ikaite and vaterite. *Chemical Geology*, 285: 194–202. doi:10.1016/j.chemgeo.2011.04.002.

Gussone, N., Zonneveld, K., and Kuhnert, H., 2010. Minor element and Ca isotope composition of calcareous dinoflagellate cysts of cultured *Thoracosphaera heimii*. *Earth and Planetary Science Letters*, 289: 180–188. doi:10.1016/j.epsl.2009.11.006.

Halicz, L., Galy, A., Belshaw, N. S., and O'Nions, R. K., 1999. High-precision measurement of calcium isotopes in carbonates and related materials by multiple collector inductively coupled plasma mass spectrometry (MC-ICP-MS). *Journal of Analytical Atomic Spectrometry*, 14: 1835–1838. doi:10.1039/A906422B.

Hardie, L. A., 1996. Secular variation in seawater chemistry: An explanation for the coupled secular variation in the mineralogies of marine limestones and potash evaporites over the past 600 m.y. *Geology*, 24: 279–283. doi:10.1130/0091-7613(1996)024<0279:SVISCA>2.3.CO;2.

Hart, M. B., Dodsworth, P., Ditchfield, P. W., Duane, A. M., and Orth, C. J., 1991. The late Cenomanian event in eastern England. *Historical Biology*, 5: 339–354. doi:10.1080/10292389109380411.

Hay, W. W., 1985. Potential errors in estimates of carbonate rock accumulating through geologic time. In Sundquist, E. T. and Broecker, W. S., editors, *The Carbon Cycle and Atmospheric CO_2: Natural Variations Archean to Present, Geophysical Monograph Series*, 32: 573–583. American Geophysical Union, Washington, D.C. doi:10.1029/GM032p0573.

Haynes, W. M., editor, 2011. *CRC Handbook of Chemistry and Physics*. CRC Press, Boca Raton, FL, 92nd edition.

Heinemann, A., Fietzke, J., Eisenhauer, A., and Zumholz, K., 2008. Modification of Ca isotope and trace metal composition of the major matrices involved in shell formation of *Mytilus edulis*. *Geochemistry Geophysics Geosystems*, 9: Q01006. doi:10.1029/2007GC001777.

Herrle, J. O., Kößler, P., Friedrich, O., Erlenkeuser, H., and Hemleben, C., 2004. High-resolution carbon isotope records of the Aptian to Lower Albian from SE France and the Mazagan Plateau (DSDP Site 545): a stratigraphic tool for paleoceanographic and paleobiologic reconstruction. *Earth and Planetary Science Letters*, 218: 149–161. doi:10.1016/S0012-821X(03)00646-0.

Hesselbo, S. P. and Jenkyns, H. C., 1995. A comparison of the Hettangian to Bajocian successions of Dorset and Yorkshire. In Taylor, P. D., editor, *Field Geology of the British Jurassic*, pages 105–150. Geological Society, London.

Hetzel, A., Böttcher, M. E., Wortmann, U. G., and Brumsack, H.-J., 2009. Paleo-redox conditions during OAE 2 reflected in Demerara Rise sediment geochemistry (ODP Leg 207). *Palaeogeography, Palaeoclimatology, Palaeoecology*, 273: 302–328. doi:10.1016/j.palaeo.2008.11.005.

Heuser, A. and Eisenhauer, A., 2008. The calcium isotope composition ($\delta^{44/40}$Ca) of NIST SRM 915b and NIST SRM 1486. *Geostandards and Geoanalytical Research*, 32: 311–315. doi:10.1111/j.1751-908X.2008.00877.x.

Heuser, A. and Eisenhauer, A., 2010. A pilot study on the use of natural calcium isotope (^{44}Ca/^{40}Ca) fractionation in urine as a proxy for the human body calcium balance. *Bone*, 46: 889–896. doi:10.1016/j.bone.2009.11.037.

Heuser, A., Eisenhauer, A., Böhm, F., Wallmann, K., Gussone, N., Pearson, P. N., Nägler, T. F., and Dullo, W.-C., 2005. Calcium isotope ($\delta^{44/40}$Ca) variations of Neogene planktonic foraminifera. *Paleoceanography*, 20: PA2013. doi:10.1029/2004PA001048.

Hindshaw, R. S., Reynolds, B. C., Wiederhold, J. G., Kretzschmar, R., and Bourdon, B., 2011. Calcium isotopes in a proglacial weathering environment: Damma glacier, Switzerland. *Geochimica et Cosmochimica Acta*, 75: 106–118. doi:10.1016/j.gca.2010.09.038.

Hippler, D., Eisenhauer, A., and Nägler, T. F., 2006. Tropical Atlantic SST history inferred from Ca isotope thermometry over the last 140ka. *Geochimica et Cosmochimica Acta*, 70: 90–100. doi:10.1016/j.gca.2005.07.022.

Hippler, D., Kozdon, R., Darling, K. F., Eisenhauer, A., and Nägler, T. F., 2009. Calcium isotopic composition of high-latitude proxy carrier *Neogloboquadrina pachyderma* (sin.). *Biogeosciences*, 6: 1–14. doi:10.5194/bg-6-1-2009.

Hippler, D., Schmitt, A.-D., Gussone, N., Heuser, A., Stille, P., Eisenhauer, A., and Nägler, T. F., 2003. Calcium isotopic composition of various reference materials and seawater. *Geostandards Newsletter*, 27: 13–19. doi:10.1111/j.1751-908X.2003.tb00709.x.

Hirata, T., Tanoshima, M., Suga, A., Tanaka, Y., Nagata, Y., Shinohara, A., and Chiba, M., 2008. Isotopic analysis of calcium in blood plasma and bone from mouse samples by multiple collector-ICP-mass spectrometry. *Analytical Sciences*, 24: 1501–1507. doi:10.2116/analsci.24.1501.

Holland, H. D., 1972. The geologic history of sea water—an attempt to solve the problem. *Geochimica et Cosmochimica Acta*, 36: 637–651. doi:10.1016/0016-7037(72)90108-1.

Holland, H. D., 2005. Sea level, sediments and the composition of seawater. *American Journal of Science*, 305: 220–239. doi:10.2475/ajs.305.3.220.

Holland, H. D., Horita, J., and Seyfried, Jr., W. E., 1996. On the secular variations in the composition of Phanerozoic marine potash evaporites. *Geology*, 24: 993–996. doi:10.1130/0091-7613(1996)024<0993:OTSVIT>2.3.CO;2.

Holmden, C., 2009. Ca isotope study of Ordovician dolomite, limestone, and anhydrite in the Williston Basin: Implications for subsurface dolomitization and local Ca cycling. *Chemical Geology*, 268: 180–188. doi:10.1016/j.chemgeo.2009.08.009.

Holmden, C. and Bélanger, N., 2010. Ca isotope cycling in a forested ecosystem. *Geochimica et Cosmochimica Acta*, 74: 995–1015. doi:10.1016/j.gca.2009.10.020.

Holmden, C., Papanastassiou, D. A., Blanchon, P., and Evans, S., 2012. $\delta^{44/40}$Ca variability in shallow water carbonates and the impact of submarine groundwater discharge on Ca-cycling in marine environments. *Geochimica et Cosmochimica Acta*, 83: 179–194. doi:10.1016/j.gca.2011.12.031.

Horita, J., Weinberg, A., Das, N., and Holland, H. D., 1996. Brine inclusions in halite and the origin of the Middle Devonian Prairie evaporites of western Canada. *Journal of Sedimentary Research*, 66: 956–964. doi:10.1306/D4268450-2B26-11D7-8648000102C1865D.

Horita, J., Zimmermann, H., and Holland, H. D., 2002. Chemical evolution of seawater during the Phanerozoic: Implications from the record of marine evaporites. *Geochimica et Cosmochimica Acta*, 66: 3733–3756. doi:10.1016/S0016-7037(01)00884-5.

Hubbard, D. K., Miller, A. I., and Scaturo, D., 1990. Production and cycling of calcium carbonate in a shelf-edge reef system (St. Croix, US Virgin Islands): applications to the nature of reef systems in the fossil record. *Journal of Sedimentary Research*, 60: 335–360. doi:10.1306/212F9197-2B24-11D7-8648000102C1865D.

Immenhauser, A., Nägler, T. F., Steuber, T., and Hippler, D., 2005. A critical assessment of mollusk $^{18}O/^{16}O$, Mg/Ca, and $^{44}Ca/^{40}Ca$ ratios as proxies for Cretaceous seawater temperature seasonality. *Palaeogeography, Palaeoclimatology, Palaeoecology*, 215: 221–237. doi:10.1016/j.palaeo.2004.09.005.

Isozaki, Y., 1997. Permo–Triassic boundary superanoxia and stratified superocean: records from lost deep sea. *Science*, 276: 235–238. doi:10.1126/science.276.5310.235.

Jacobson, A. D. and Holmden, C., 2008. δ^{44}Ca evolution in a carbonate aquifer and its bearing on the equilibrium isotope fractionation factor for calcite. *Earth and Planetary Science Letters*, 270: 349–353. doi:10.1016/j.epsl.2008.03.039.

Jahren, A. H., Arens, N. C., Sarmiento, G., Guerrero, J., and Amundson, R., 2001. Terrestrial record of methane hydrate dissociation in the Early Cretaceous. *Geology*, 29: 159–162. doi:10.1130/0091-7613(2001)029<0159:TROMHD>2.0.CO;2.

Jarvis, I., Gale, A. S., Jenkyns, H. C., and Pearce, M. A., 2006. Secular variation in Late Cretaceous carbon isotopes: a new δ^{13}C carbonate reference curve for the Cenomanian–Campanian (99.6–70.6 Ma). *Geological Magazine*, 143: 561–608. doi:10.1017/S0016756806002421.

Jenkyns, H. C., 1995. Carbon-isotope stratigraphy and paleoceanographic significance of the Lower Cretaceous shallow-water carbonates of Resolution Guyot, Mid-Pacific Mountains. In Winterer, E. L., Sager, W. W., Firth, J. V., and Sinton, J. M., editors, *Proceedings of the Ocean Drilling Program, Scientific Results*, 143: 99–104. Ocean Drilling Program, College Station, TX. doi:10.2973/odp.proc.sr.143.213.1995.

Jenkyns, H. C., 2003. Evidence for rapid climate change in the Mesozoic–Palaeogene greenhouse world. *Philosophical Transactions of the Royal Society A*, 361: 1885–1916. doi:10.1098/rsta.2003.1240.

Jenkyns, H. C., 2010. Geochemistry of oceanic anoxic events. *Geochemistry Geophysics Geosystems*, 11: Q03004. doi:10.1029/2009GC002788.

Jenkyns, H. C. and Clayton, C. J., 1997. Lower Jurassic epicontinental carbonates and mudstones from England and Wales: chemostratigraphic signals and the early Toarcian anoxic event. *Sedimentology*, 44: 687–706. doi:10.1046/j.1365-3091.1997.d01-43.x.

Jenkyns, H. C., Gale, A. S., and Corfield, R. M., 1994. Carbon- and oxygen-isotope stratigraphy of the English Chalk and Italian Scaglia and its palaeoclimatic significance. *Geological Magazine*, 131: 1–34. doi:10.1017/S0016756800010451.

Jenkyns, H. C., Matthews, A., Tsikos, H., and Erel, Y., 2007. Nitrate reduction, sulfate reduction, and sedimentary iron isotope evolution during the Cenomanian–Turonian oceanic anoxic event. *Paleoceanography*, 22: PA3208. doi:10.1029/2006PA001355.

Jenkyns, H. C., Paull, C. K., Cummins, D. I., and Fullagar, P. D., 1995. Strontium-isotope stratigraphy of lower Cretaceous atoll carbonates in the Mid-Pacific Mountains. In Winterer, E. L., Sager, W. W., Firth, J. V., and Sinton, J. M., editors, *Proceedings of the Ocean Drilling Program, Scientific Results*, 143: 89–97. Ocean Drilling Program, College Station, TX. doi:10.2973/odp.proc.sr.143.212.1995.

Jenkyns, H. C. and Senior, J. R., 1991. Geological evidence for intra-Jurassic faulting in the Wessex Basin and its margins. *Journal of the Geological Society, London*, 148: 245–260. doi:10.1144/gsjgs.148.2.0245.

Jenkyns, H. C. and Strasser, A., 1995. Lower Cretaceous oolites from the Mid-Pacific Mountains (Resolution Guyot, Site 866). In Winterer, E. L., Sager, W. W., Firth, J. V., and Sinton, J. M., editors, *Proceedings of the Ocean Drilling Program, Scientific Results*, 143: 111–118. Ocean Drilling Program, College Station, TX. doi:10.2973/odp.proc.sr.143.211.1995.

Jenkyns, H. C. and Wilson, P. A., 1999. Stratigraphy, paleoceanography, and evolution of Cretaceous Pacific guyots: relics from a greenhouse Earth. *American Journal of Science*, 299: 341–392. doi:10.2475/ajs.299.5.341.

Jones, C. E. and Jenkyns, H. C., 2001. Seawater strontium isotopes, oceanic anoxic events, and seafloor hydrothermal activity in the Jurassic and Cretaceous. *American Journal of Science*, 301: 112–149. doi:10.2475/ajs.301.2.112.

Jones, C. E., Jenkyns, H. C., and Hesselbo, S. P., 1994. Strontium isotopes in Early Jurassic seawater. *Geochimica et Cosmochimica Acta*, 58: 1285–1301. doi:10.1016/0016-7037(94)90382-4.

Kasemann, S. A., Hawkesworth, C. J., Prave, A. R., Fallick, A. E., and Pearson, P. N., 2005. Boron and calcium isotope composition in Neoproterozoic carbonate rocks from Namibia: evidence for extreme environmental change. *Earth and Planetary Science Letters*, 231: 73–86. doi:10.1016/j.epsl.2004.12.006.

Kasemann, S. A., Schmidt, D. N., Pearson, P. N., and Hawkesworth, C. J., 2008. Biological and ecological insights into Ca isotopes in planktic foraminifers as a palaeotemperature proxy. *Earth and Planetary Science Letters*, 271: 292–302. doi:10.1016/j.epsl.2008.04.007.

Kemp, D. B., Coe, A. L., Cohen, A. S., and Schwark, L., 2005. Astronomical pacing of methane release in the Early Jurassic period. *Nature*, 437: 396–399. doi:10.1038/nature04037.

Kennedy, W. J., Walaszczyk, I., and Cobban, W. A., 2005. The Global Boundary Stratotype Section and Point for the base of the Turonian Stage of the Cretaceous: Pueblo, Colorado, USA. *Episodes*, 28: 93–104.

Kerr, A. C., 1998. Oceanic plateau formation: a cause of mass extinction and black shale deposition around the Cenomanian–Turonian boundary? *Journal of the Geological Society, London*, 155: 619–626. doi:10.1144/gsjgs.155.4.0619.

Kiessling, W., Flügel, E., and Golonka, J., 2003. Patterns of Phanerozoic carbonate platform sedimentation. *Lethaia*, 36: 195–225. doi:10.1080/00241160310004648.

Kısakürek, B., Eisenhauer, A., Böhm, F., Hathorne, E. C., and Erez, J., 2011. Controls on calcium isotope fractionation in cultured planktic foraminifera, *Globigerinoides ruber* and *Globigerinella siphonifera*. *Geochimica et Cosmochimica Acta*, 75: 427–443. doi:10.1016/j.gca.2010.10.015.

Kovalevich, V. M., Peryt, T. M., and Petrichenko, O. I., 1998. Secular variation in seawater chemistry during the Phanerozoic as indicated by brine inclusions in halite. *The Journal of Geology*, 106: 695–712. doi:10.1086/516054.

Kuroda, J., Ogawa, N. O., Tanimizu, M., Coffin, M. F., Tokuyama, H., Kitazato, H., and Ohkouchi, N., 2007. Contemporaneous massive subaerial volcanism and late Cretaceous Oceanic Anoxic Event 2. *Earth and Planetary Science Letters*, 256: 211–223. doi:10.1016/j.epsl.2007.01.027.

Kuypers, M. M. M., Pancost, R. D., Nijenhuis, I. A., and Sinninghe Damsté, J. S., 2002. Enhanced productivity led to increased organic carbon burial in the euxinic North Atlantic basin during the late Cenomanian oceanic anoxic event. *Paleoceanography*, 17: 1051. doi:10.1029/2000PA000569.

Langer, G., Gussone, N., Nehrke, G., Riebesell, U., Eisenhauer, A., and Thoms, S., 2007. Calcium isotope fractionation during coccolith formation in *Emiliania huxleyi*: Independence of growth and calcification rate. *Geochemistry Geophysics Geosystems*, 8: Q05007. doi:10.1029/2006GC001422.

Larson, R. L. and Erba, E., 1999. Onset of the mid-Cretaceous greenhouse in the Barremian–Aptian: Igneous events and the biological, sedimentary, and geochemical responses. *Paleoceanography*, 14: 663–678. doi:10.1029/1999PA900040.

Lea, D. W., 1993. Constraints on the alkalinity and circulation of glacial circumpolar deep water from benthic foraminiferal barium. *Global Biogeochemical Cycles*, 7: 695–710. doi:10.1029/93GB01536.

Leckie, R. M., Bralower, T. J., and Cashman, R., 2002. Oceanic anoxic events and plankton evolution: Biotic response to tectonic forcing during the mid-Cretaceous. *Paleoceanography*, 17: 1041. doi:10.1029/2001PA000623.

Lemarchand, D., Wasserburg, G. J., and Papanastassiou, D. A., 2004. Rate-controlled calcium isotope fractionation in synthetic calcite. *Geochimica et Cosmochimica Acta*, 68: 4665–4678. doi:10.1016/j.gca.2004.05.029.

Li, Y.-X., Bralower, T. J., Montañez, I. P., Osleger, D. A., Arthur, M. A., Bice, D. M., Herbert, T. D., Erba, E., and Premoli Silva, I., 2008. Toward an orbital chronology for the early Aptian Oceanic Anoxic Event (OAE1a, ~120 Ma). *Earth and Planetary Science Letters*, 271: 88–100. doi:10.1016/j.epsl.2008.03.055.

Linnert, C., Mutterlose, J., and Mortimore, R., 2011. Calcareous nannofossils from Eastbourne (Southeastern England) and the paleoceanography of the Cenomanian–Turonian Boundary Interval. *Palaios*, 26: 298–313. doi:10.2110/palo.2010.p10-130r.

Locarnini, R. A., Mishonov, A. V., Antonov, J. I., Boyer, T. P., and Garcia, H. E., 2006. *World Ocean Atlas 2005, Volume 1: Temperature*. Levitus, S., editor, NOAA Atlas NESDIS 61. U.S. Government Printing Office, Washington D.C.

Lowenstam, H. A. and Weiner, S., 1989. *On Biomineralization*. Oxford University Press, New York.

Lowenstein, T. K., Hardie, L. A., Timofeeff, M. N., and Demicco, R. V., 2003. Secular variation in seawater chemistry and the origin of calcium chloride basinal brines. *Geology*, 31: 857–860. doi:10.1130/G19728R.1.

Lowenstein, T. K., Timofeeff, M. N., Brennan, S. T., Hardie, L. A., and Demicco, R. V., 2001. Oscillations in Phanerozoic seawater chemistry: evidence from fluid inclusions. *Science*, 294: 1086–1088. doi:10.1126/science.1064280.

Luciani, V., Cobianchi, M., and Jenkyns, H. C., 2001. Biotic and geochemical response to anoxic events: the Aptian pelagic succession of the Gargano Promontory (southern Italy). *Geological Magazine*, 138: 277–298. doi:10.1017/S0016756801005301.

Lynch-Stieglitz, J., van Geen, A., and Fairbanks, R. G., 1996. Interocean exchange of glacial North Atlantic Intermediate Water: Evidence from subantarctic Cd/Ca and carbon isotope measurements. *Paleoceanography*, 11: 191–201. doi:10.1029/95PA03772.

Macintyre, I. G. and Reid, R. P., 1995. Crystal alteration in a living calcareous alga (*Halimeda*): implications for studies in skeletal diagenesis. *Journal of Sedimentary Research*, 65: 143–153. doi:10.1306/D4268054-2B26-11D7-8648000102C1865D.

Mackenzie, F. T. and Garrels, R. M., 1966. Chemical mass balance between rivers and oceans. *American Journal of Science*, 264: 507–525. doi:10.2475/ajs.264.7.507.

Malinverno, A., Erba, E., and Herbert, T. D., 2010. Orbital tuning as an inverse problem: Chronology of the early Aptian oceanic anoxic event 1a (Selli Level) in the Cismon APTICORE. *Paleoceanography*, 25: PA2203. doi:10.1029/2009PA001769.

Marchitto, Jr., T. M., Curry, W. B., and Oppo, D. W., 2000. Zinc concentrations in benthic foraminifera reflect seawater chemistry. *Paleoceanography*, 15: 299–306. doi:10.1029/1999PA000420.

Marker, M., Kline, D. I., Kirkwood, W. J., Headley, K., Brewer, P. G., Peltzer, E. T., Miard, T., Chai, A., James, M., Schneider, K., Silverman, J., Caldeira, K., Koseff, J. R., Monismith, S., Opdyke, B., Dunbar, R., White, R., Dove, S., and Hoegh-Guldberg, O., 2010. The Coral Proto - Free Ocean Carbon Enrichment system (CP–FOCE): Engineering and development. In *Oceans 2010 IEEE*, pages 1–10, Sydney. doi:10.1109/OCEANSSYD.2010.5603603.

Marriott, C. S., Henderson, G. M., Belshaw, N. S., and Tudhope, A. W., 2004. Temperature dependence of δ^7Li, δ^{44}Ca and Li/Ca during growth of calcium carbonate. *Earth and Planetary Science Letters*, 222: 615–624. doi:10.1016/j.epsl.2004.02.031.

Martin, R. E., 1995. Cyclic and secular variation in microfossil biomineralization: clues to the biogeochemical evolution of Phanerozoic oceans. *Global and Planetary Change*, 11: 1–23. doi:10.1016/0921-8181(94)00011-2.

Maynard, J. B., 1976. The long-term buffering of the oceans. *Geochimica et Cosmochimica Acta*, 40: 1523–1532. doi:10.1016/0016-7037(76)90091-0.

McArthur, J. M., Howarth, R. J., and Bailey, T. R., 2001. Strontium Isotope Stratigraphy: LOWESS Version 3: Best Fit to the Marine Sr-Isotope Curve for 0–509 Ma and Accompanying Look-up Table for Deriving Numerical Age. *The Journal of Geology*, 109: 155–170. doi:10.1086/319243.

McArthur, J. M., Thirlwall, M. F., Gale, A. S., Kennedy, W. J., Burnett, J. A., Mattey, D., and Lord, A. R., 1993. Strontium isotope stratigraphy for the Late Cretaceous: a new curve, based on the English Chalk. In Hailwood, E. A. and Kidd, R. B., editors, *High Resolution Stratigraphy, Geological Society, London, Special Publications*, 70: 195–209. doi:10.1144/GSL.SP.1993.070.01.14.

McConnaughey, T. A. and Whelan, J. F., 1997. Calcification generates protons for nutrient and bicarbonate uptake. *Earth-Science Reviews*, 42: 95–117. doi:10.1016/S0012-8252(96)00036-0.

McLeod, A. R. and Long, S. P., 1999. Free-air Carbon Dioxide Enrichment (FACE) in global change research: a review. *Advances in Ecological Research*, 28: 1–56. doi:10.1016/S0065-2504(08)60028-8.

Méhay, S., Keller, C. E., Bernasconi, S. M., Weissert, H., Erba, E., Bottini, C., and Hochuli, P. A., 2009. A volcanic CO_2 pulse triggered the Cretaceous Oceanic Anoxic Event 1a and a biocalcification crisis. *Geology*, 37: 819–822. doi:10.1130/G30100A.1.

Menegatti, A. P., Weissert, H., Brown, R. S., Tyson, R. V., Farrimond, P., Strasser, A., and Caron, M., 1998. High-resolution $\delta^{13}C$ stratigraphy through the Early Aptian "Livello Selli" of the Alpine Tethys. *Paleoceanography*, 13: 530–545. doi:10.1029/98PA01793.

Meybeck, M., 1987. Global chemical weathering of surficial rocks estimated from river dissolved loads. *American Journal of Science*, 287: 401–428. doi:10.2475/ajs.287.5.401.

Meyer, K. M. and Kump, L. R., 2008. Oceanic euxinia in Earth history: Causes and consequences. *Annual Review of Earth and Planetary Sciences*, 36: 251–288. doi:10.1146/annurev.earth.36.031207.124256.

Millán, M. I., Weissert, H. J., Fernández-Mendiola, P. A., and García-Mondéjar, J., 2009. Impact of Early Aptian carbon cycle perturbations on evolution of a marine shelf system in the Basque–Cantabrian Basin (Aralar, N Spain). *Earth and Planetary Science Letters*, 287: 392–401. doi:10.1016/j.epsl.2009.08.023.

Milliman, J. D., 1993. Production and accumulation of calcium carbonate in the ocean: Budget of a nonsteady state. *Global Biogeochemical Cycles*, 7: 927–957. doi:10.1029/93GB02524.

Milliman, J. D. and Droxler, A. W., 1996. Neritic and pelagic carbonate sedimentation in the marine environment: ignorance is not bliss. *Geologische Rundschau*, 85: 496–504. doi:10.1007/BF02369004.

Milliman, J. D., Freile, D., Steinen, R. P., and Wilber, R. J., 1993. Great Bahama Bank aragonitic muds: mostly inorganically precipitated, mostly exported. *Journal of Sedimentary Research*, 63: 589–595. doi:10.1306/D4267B81-2B26-11D7-8648000102C1865D.

Milliman, J. D., Troy, P. J., Balch, W. M., Adams, A. K., Li, Y.-H., and Mackenzie, F. T., 1999. Biologically mediated dissolution of calcium carbonate above the chemical lysocline? *Deep Sea Research I*, 46: 1653–1669. doi:10.1016/S0967-0637(99)00034-5.

Misumi, K., Yamanaka, Y., and Tajika, E., 2009. Numerical simulation of atmospheric and oceanic biogeochemical cycles to an episodic CO_2 release event: Implications for the cause of mid-Cretaceous Ocean Anoxic Event-1a. *Earth and Planetary Science Letters*, 286: 316–323. doi:10.1016/j.epsl.2009.06.045.

Montoya-Pino, C., Weyer, S., Anbar, A. D., Pross, J., Oschmann, W., van de Schootbrugge, B., and Arz, H. W., 2010. Global enhancement of ocean anoxia during Oceanic Anoxic Event 2: A quantitative approach using U isotopes. *Geology*, 38: 315–318. doi:10.1130/G30652.1.

Mort, H. P., Adatte, T., Föllmi, K. B., Keller, G., Steinmann, P., Matera, V., Berner, Z., and Stüben, D., 2007. Phosphorus and the roles of productivity and nutrient recycling during oceanic anoxic event 2. *Geology*, 35: 483–486. doi:10.1130/G23475A.1.

Nägler, T. F., Eisenhauer, A., Müller, A., Hemleben, C., and Kramers, J., 2000. The δ^{44}Ca-temperature calibration on fossil and cultured *Globigerinoides sacculifer*: New tool for reconstruction of past sea surface temperatures. *Geochemistry Geophysics Geosystems*, 1: 1052. doi:10.1029/2000GC000091.

Najarro, M., Rosales, I., and Martín-Chivelet, J., 2011. Major palaeoenvironmental perturbation in an Early Aptian carbonate platform: Prelude of the Oceanic Anoxic Event 1a? *Sedimentary Geology*, 235: 50–71. doi:10.1016/j.sedgeo.2010.03.011.

Neumann, A. C. and Land, L. S., 1975. Lime mud deposition and calcareous algae in the Bight of Abaco, Bahamas: a budget. *Journal of Sedimentary Research*, 45: 763–786. doi:10.1306/212F6E3D-2B24-11D7-8648000102C1865D.

Ogg, J. G., Ogg, G., and Gradstein, F. M., 2008. *The Concise Geologic Time Scale*. Cambridge University Press, Cambridge.

Opdyke, B. N. and Walker, J. C. G., 1992. Return of the coral reef hypothesis: Basin to shelf partitioning of $CaCO_3$ and its effect on atmospheric CO_2. *Geology*, 20: 733–736. doi:10.1130/0091-7613(1992)020<0733:ROTCRH>2.3.CO;2.

Opdyke, B. N. and Wilkinson, B. H., 1988. Surface area control of shallow cratonic to deep marine carbonate accumulation. *Paleoceanography*, 3: 685–703. doi:10.1029/PA003i006p00685.

Page, B. D., Bullen, T. D., and Mitchell, M. J., 2008. Influences of calcium availability and tree species on Ca isotope fractionation in soil and vegetation. *Biogeochemistry*, 88: 1–13. doi:10.1007/s10533-008-9188-5.

Palmer, M. R. and Edmond, J. M., 1989. The strontium isotope budget of the modern ocean. *Earth and Planetary Science Letters*, 92: 11–26. doi:10.1016/0012-821X(89)90017-4.

Panchuk, K., Ridgwell, A., and Kump, L. R., 2008. Sedimentary response to Paleocene–Eocene Thermal Maximum carbon release: A model–data comparison. *Geology*, 36: 315–318. doi:10.1130/G24474A.1.

Parente, M., Frijia, G., Di Lucia, M., Jenkyns, H. C., Woodfine, R. G., and Baroncini, F., 2008. Stepwise extinction of larger foraminifers at the Cenomanian–Turonian boundary: A shallow-water perspective on nutrient fluctuations during Oceanic Anoxic Event 2 (Bonarelli Event). *Geology*, 36: 715–718. doi:10.1130/G24893A.1.

Paul, C. R. C., Lamolda, M. A., Mitchell, S. F., Vaziri, M. R., Gorostidi, A., and Marshall, J. D., 1999. The Cenomanian–Turonian boundary at Eastbourne (Sussex, UK): a proposed European reference section. *Palaeogeography, Palaeoclimatology, Palaeoecology*, 150: 83–121. doi:10.1016/S0031-0182(99)00009-7.

Payne, J. L., Turchyn, A. V., Paytan, A., DePaolo, D. J., Lehrmann, D. J., Yu, M., and Wei, J., 2010. Calcium isotope constraints on the end-Permian mass extinction. *Proceedings of the National Academy of Sciences*, 107: 8543–8548. doi:10.1073/pnas.0914065107.

Pearce, C. R., Cohen, A. S., Coe, A. L., and Burton, K. W., 2008. Molybdenum isotope evidence for global ocean anoxia coupled with perturbations to the carbon cycle during the Early Jurassic. *Geology*, 36: 231–234. doi:10.1130/G24446A.1.

Pearce, M. A., Jarvis, I., and Tocher, B. A., 2009. The Cenomanian–Turonian boundary event, OAE2 and palaeoenvironmental change in epicontinental seas: New insights from the dinocyst and geochemical records. *Palaeogeography, Palaeoclimatology, Palaeoecology*, 280: 207–234. doi:10.1016/j.palaeo.2009.06.012.

Perakis, S. S., Maguire, D. A., Bullen, T. D., Cromack, K., Waring, R. H., and Boyle, J. R., 2006. Coupled nitrogen and calcium cycles in forests of the Oregon Coast Range. *Ecosystems*, 9: 63–74. doi:10.1007/s10021-004-0039-5.

Premoli Silva, I., Erba, E., Salvini, G., Locatelli, C., and Verga, D., 1999. Biotic changes in Cretaceous oceanic anoxic events of the Tethys. *The Journal of Foraminiferal Research*, 29: 352–370.

R Development Core Team, 2009. *R: A language and environment for statistical computing*. R Foundation for Statistical Computing, Vienna.

Ravizza, G., Norris, R. N., Blusztajn, J., and Aubry, M.-P., 2001. An osmium isotope excursion associated with the late Paleocene thermal maximum: Evidence of intensified chemical weathering. *Paleoceanography*, 16: 155–163. doi:10.1029/2000PA000541.

Rees, S. A., Opdyke, B. N., Wilson, P. A., and Henstock, T. J., 2007. Significance of *Halimeda* bioherms to the global carbonate budget based on a geological sediment budget for the Northern Great Barrier Reef, Australia. *Coral Reefs*, 26: 177–188. doi:10.1007/s00338-006-0166-x.

Reynard, L. M., Day, C. C., and Henderson, G. M., 2011. Large fractionation of calcium isotopes during cave-analogue calcium carbonate growth. *Geochimica et Cosmochimica Acta*, 75: 3726–3740. doi:10.1016/j.gca.2011.04.010.

Reynard, L. M., Henderson, G. M., and Hedges, R. E. M., 2010. Calcium isotope ratios in animal and human bone. *Geochimica et Cosmochimica Acta*, 74: 3735–3750. doi:10.1016/j.gca.2010.04.002.

Reynaud, S., Ferrier-Pagès, C., Meibom, A., Mostefaoui, S., Mortlock, R., Fairbanks, R., and Allemand, D., 2007. Light and temperature effects on Sr/Ca and Mg/Ca ratios in the scleractinian coral *Acropora* sp. *Geochimica et Cosmochimica acta*, 71: 354–362. doi:10.1016/j.gca.2006.09.009.

Riding, R., 2002. Structure and composition of organic reefs and carbonate mud mounds: concepts and categories. *Earth-Science Reviews*, 58: 163–231. doi:10.1016/S0012-8252(01)00089-7.

Ries, J. B., Stanley, S. M., and Hardie, L. A., 2006. Scleractinian corals produce calcite, and grow more slowly, in artificial Cretaceous seawater. *Geology*, 34: 525–528. doi:10.1130/G22600.1.

Robinson, S. A., Clarke, L. J., Nederbragt, A., and Wood, I. G., 2008. Mid-Cretaceous oceanic anoxic events in the Pacific Ocean revealed by carbon-isotope stratigraphy of the Calera Limestone, California, USA. *Geological Society of America Bulletin*, 120: 1416–1427. doi:10.1130/B26350.1.

Röhl, U., Bralower, T. J., Norris, R. D., and Wefer, G., 2000. New chronology for the late Paleocene thermal maximum and its environmental implications. *Geology*, 28: 927–930. doi:10.1130/0091-7613(2000)28<927:NCFTLP>2.0.CO;2.

Rollion-Bard, C., Vigier, N., and Spezzaferri, S., 2007. In situ measurements of calcium isotopes by ion microprobe in carbonates and application to foraminifera. *Chemical Geology*, 244: 679–690. doi:10.1016/j.chemgeo.2007.07.021.

Ronov, A. B., 1982. The Earth's sedimentary shell (quantitative patterns of its structure, compositions, and evolution): The 20th V. I. Vernadskiy Lecture, March 12, 1978. *International Geology Review*, 24: 1313–1363. doi:10.1080/00206818209451075.

Russell, W. A., Papanastassiou, D. A., and Tombrello, T. A., 1978. Ca isotope fractionation on the Earth and other solar system materials. *Geochimica et Cosmochimica Acta*, 42: 1075–1090. doi:10.1016/0016-7037(78)90105-9.

Rustad, J. R., Casey, W. H., Yin, Q.-Z., Bylaska, E. J., Felmy, A. R., Bogatko, S. A., Jackson, V. E., and Dixon, D. A., 2010. Isotopic fractionation of Mg^{2+}(aq), Ca^{2+}(aq), and Fe^{2+}(aq) with carbonate minerals. *Geochimica et Cosmochimica Acta*, 74: 6301–6323. doi:10.1016/j.gca.2010.08.018.

Ryan, D. A., Opdyke, B. N., and Jell, J. S., 2001. Holocene sediments of Wistari Reef: towards a global quantification of coral reef related neritic sedimentation in the Holocene. *Palaeogeography, Palaeoclimatology, Palaeoecology*, 175: 173–184. doi:10.1016/S0031-0182(01)00370-4.

Sageman, B. B., Meyers, S. R., and Arthur, M. A., 2006. Orbital time scale and new C-isotope record for Cenomanian–Turonian boundary stratotype. *Geology*, 34: 125–128. doi:10.1130/G22074.1.

Sandberg, P. A., 1983. An oscillating trend in Phanerozoic non-skeletal carbonate mineralogy. *Nature*, 305: 19–22. doi:10.1038/305019a0.

Sarmiento, J. L., Herbert, T. D., and Toggweiler, J. R., 1988. Causes of anoxia in the world ocean. *Global Biogeochemical Cycles*, 2: 115–128. doi:10.1029/GB002i002p00115.

Schiebel, R., 2002. Planktic foraminiferal sedimentation and the marine calcite budget. *Global Biogeochemical Cycles*, 16: 1065. doi:10.1029/2001GB001459.

Schlanger, S. O., Arthur, M. A., Jenkyns, H. C., and Scholle, P. A., 1987. The Cenomanian–Turonian Oceanic Anoxic Event, I. Stratigraphy and distribution of organic carbon-rich beds and the marine $\delta^{13}C$ excursion. In Brooks, J. and Fleet, A. J., editors, *Marine Petroleum Source Rocks, Geological Society, London, Special Publications*, 26: 371–399. doi:10.1144/GSL.SP.1987.026.01.24.

Schlanger, S. O. and Jenkyns, H. C., 1976. Cretaceous oceanic anoxic events: causes and consequences. *Geologie en Mijnbouw*, 55: 179–184.

Schmitt, A.-D., Chabaux, F., and Stille, P., 2003a. The calcium riverine and hydrothermal isotopic fluxes and the oceanic calcium mass balance. *Earth and Planetary Science Letters*, 213: 503–518. doi:10.1016/S0012-821X(03)00341-8.

Schmitt, A.-D., Stille, P., and Vennemann, T., 2003b. Variations of the $^{44}Ca/^{40}Ca$ ratio in seawater during the past 24 million years: Evidence from $\delta^{44}Ca$ and $\delta^{18}O$ values of Miocene phosphates. *Geochimica et Cosmochimica Acta*, 67: 2607–2614. doi:10.1016/S0016-7037(03)00100-5.

Scholle, P. A. and Arthur, M. A., 1980. Carbon isotope fluctuations in Cretaceous pelagic limestones: potential stratigraphic and petroleum exploration tool. *American Association of Petroleum Geologists Bulletin*, 64: 67–87. doi:10.1306/2F91892D-16CE-11D7-8645000102C1865D.

Sime, N. G., De La Rocha, C. L., and Galy, A., 2005. Negligible temperature dependence of calcium isotope fractionation in 12 species of planktonic foraminifera. *Earth and Planetary Science Letters*, 232: 51–66. doi:10.1016/j.epsl.2005.01.011.

Sime, N. G., De La Rocha, C. L., Tipper, E. T., Tripati, A., Galy, A., and Bickle, M. J., 2007. Interpreting the Ca isotope record of marine biogenic carbonates. *Geochimica et Cosmochimica Acta*, 71: 3979–3989. doi:10.1016/j.gca.2007.06.009.

Sinninghe Damsté, J. S., van Bentum, E. C., Reichart, G.-J., Pross, J., and Schouten, S., 2010. A CO_2 decrease-driven cooling and increased latitudinal temperature gradient during the mid-Cretaceous Oceanic Anoxic Event 2. *Earth and Planetary Science Letters*, 293: 97–103. doi:10.1016/j.epsl.2010.02.027.

Skulan, J., Bullen, T., Anbar, A. D., Puzas, J. E., Shackelford, L., LeBlanc, A., and Smith, S. M., 2007. Natural calcium isotopic composition of urine as a marker of bone mineral balance. *Clinical Chemistry*, 53: 1155–1158. doi:10.1373/clinchem.2006.080143.

Skulan, J. and DePaolo, D. J., 1999. Calcium isotope fractionation between soft and mineralized tissues as a monitor of calcium use in vertebrates. *Proceedings of the National Academy of Sciences*, 96: 13709–13713. doi:10.1073/pnas.96.24.13709.

Skulan, J., DePaolo, D. J., and Owens, T. L., 1997. Biological control of calcium isotopic abundances in the global calcium cycle. *Geochimica et Cosmochimica Acta*, 61: 2505–2510. doi:10.1016/S0016-7037(97)00047-1.

Sliter, W. V., 1989. Aptian anoxia in the Pacific Basin. *Geology*, 17: 909–912. doi:10.1130/0091-7613(1989)017<0909:AAITPB>2.3.CO;2.

Snow, L. J., Duncan, R. A., and Bralower, T. J., 2005. Trace element abundances in the Rock Canyon Anticline, Pueblo, Colorado, marine sedimentary section and their relationship to Caribbean plateau construction and oxygen anoxic event 2. *Paleoceanography*, 20: PA3005. doi:10.1029/2004PA001093.

Soudry, D., Glenn, C. R., Nathan, Y., Segal, I., and VonderHaar, D., 2006. Evolution of Tethyan phosphogenesis along the northern edges of the Arabian–African shield during the Cretaceous–Eocene as deduced from temporal variations of Ca and Nd isotopes and rates of P accumulation. *Earth-Science Reviews*, 78: 27–57. doi:10.1016/j.earscirev.2006.03.005.

Stanley, S. M., 2006. Influence of seawater chemistry on biomineralization throughout Phanerozoic time: Paleontological and experimental evidence. *Palaeogeography, Palaeoclimatology, Palaeoecology*, 232: 214–236. doi:10.1016/j.palaeo.2005.12.010.

Stanley, S. M. and Hardie, L. A., 1998. Secular oscillations in the carbonate mineralogy of reef-building and sediment-producing organisms driven by tectonically forced shifts in seawater chemistry. *Palaeogeography, Palaeoclimatology, Palaeoecology*, 144: 3–19. doi:10.1016/S0031-0182(98)00109-6.

Stanley, S. M., Ries, J. B., and Hardie, L. A., 2002. Low-magnesium calcite produced by coralline algae in seawater of Late Cretaceous composition. *Proceedings of the National Academy of Sciences*, 99: 15323–15326. doi:10.1073/pnas.232569499.

Stanley, S. M., Ries, J. B., and Hardie, L. A., 2005. Seawater chemistry, coccolithophore population growth, and the origin of Cretaceous chalk. *Geology*, 33: 593–596. doi:10.1130/G21405.1.

Stanley, S. M., Ries, J. B., and Hardie, L. A., 2010. Increased production of calcite and slower growth for the major sediment-producing alga *Halimeda* as the Mg/Ca ratio of seawater is lowered to a "calcite sea" level. *Journal of Sedimentary Research*, 80: 6–16. doi:10.2110/jsr.2010.011.

Steuber, T. and Buhl, D., 2006. Calcium-isotope fractionation in selected modern and ancient marine carbonates. *Geochimica et Cosmochimica Acta*, 70: 5507–5521. doi:10.1016/j.gca.2006.08.028.

Strasser, A., Arnaud, H., Baudin, F., and Röhl, U., 1995. Small-scale shallow-water carbonate sequences of Resolution Guyot (Sites 866, 867, and 868). In Winterer, E. L., Sager, W. W., Firth, J. V., and Sinton, J. M., editors, *Proceedings of the Ocean Drilling Program, Scientific Results*, 143: 119–131. Ocean Drilling Program, College Station, TX. doi:10.2973/odp.proc.sr.143.228.1995.

Tambutté, E., Allemand, D., Mueller, E., and Jaubert, J., 1996. A compartmental approach to the mechanism of calcification in hermatypic corals. *The Journal of Experimental Biology*, 199: 1029–1041.

Tambutté, E., Tambutté, S., Segonds, N., Zoccola, D., Venn, A., Erez, J., and Allemand, D., 2012. Calcein labelling and electrophysiology: insights on coral tissue permeability and calcification. *Proceedings of the Royal Society B: Biological Sciences*, 279: 19–27. doi:10.1098/rspb.2011.0733.

Tang, J., Dietzel, M., Böhm, F., Köhler, S. J., and Eisenhauer, A., 2008. Sr^{2+}/Ca^{2+} and $^{44}Ca/^{40}Ca$ fractionation during inorganic calcite formation: II. Ca isotopes. *Geochimica et Cosmochimica Acta*, 72: 3733–3745. doi:10.1016/j.gca.2008.05.033.

Tarduno, J. A., Sliter, W. V., Kroenke, L., Leckie, M., Mayer, H., Mahoney, J. J., Musgrave, R., Storey, M., and Winterer, E. L., 1991. Rapid formation of Ontong Java Plateau by Aptian mantle plume volcanism. *Science*, 254: 399–403. doi:10.1126/science.254.5030.399.

Taubner, I., Böhm, F., Fietzke, J., Eisenhauer, A., Garbe-Schönberg, D., and Erez, J., 2011. Elemental and isotopic composition of cultured scleractinian corals. In *Goldschmidt Conference Abstracts, Mineralogical Magazine*, 75: 1989.

Tejada, M. L. G., Suzuki, K., Kuroda, J., Coccioni, R., Mahoney, J. J., Ohkouchi, N., Sakamoto, T., and Tatsumi, Y., 2009. Ontong Java Plateau eruption as a trigger for the early Aptian oceanic anoxic event. *Geology*, 37: 855–858. doi:10.1130/G25763A.1.

Tipper, E. T., Gaillardet, J., Galy, A., Louvat, P., Bickle, M. J., and Capmas, F., 2010. Calcium isotope ratios in the world's largest rivers: A constraint on the maximum imbalance of oceanic calcium fluxes. *Global Biogeochemical Cycles*, 24. doi:10.1029/2009GB003574.

Tipper, E. T., Galy, A., and Bickle, M. J., 2006. Riverine evidence for a fractionated reservoir of Ca and Mg on the continents: Implications for the oceanic Ca cycle. *Earth and Planetary Science Letters*, 247: 267–279. doi:10.1016/j.epsl.2006.04.033.

Tipper, E. T., Galy, A., and Bickle, M. J., 2008. Calcium and magnesium isotope systematics in rivers draining the Himalaya-Tibetan-Plateau region: Lithological or fractionation control? *Geochimica et Cosmochimica Acta*, 72: 1057–1075. doi:10.1016/j.gca.2007.11.029.

Tsandev, I. and Slomp, C. P., 2009. Modeling phosphorus cycling and carbon burial during Cretaceous Oceanic Anoxic Events. *Earth and Planetary Science Letters*, 286: 71–79. doi:10.1016/j.epsl.2009.06.016.

Tsikos, H., Jenkyns, H. C., Walsworth-Bell, B., Petrizzo, M. R., Forster, A., Kolonic, S., Erba, E., Premoli Silva, I., Baas, M., Wagner, T., and Sinninghe Damsté, J. S., 2004. Carbon-isotope stratigraphy recorded by the Cenomanian–Turonian Oceanic Anoxic Event: correlation and implications based on three key localities. *Journal of the Geological Society, London*, 161: 711–719. doi:10.1144/0016-764903-077.

Turgeon, S. and Brumsack, H.-J., 2006. Anoxic vs dysoxic events reflected in sediment geochemistry during the Cenomanian–Turonian Boundary Event (Cretaceous) in the Umbria–Marche Basin of central Italy. *Chemical Geology*, 234: 321–339. doi:10.1016/j.chemgeo.2006.05.008.

Turgeon, S. C. and Creaser, R. A., 2008. Cretaceous oceanic anoxic event 2 triggered by a massive magmatic episode. *Nature*, 454: 323–326. doi:10.1038/nature07076.

Vahrenkamp, V. C., 2010. Chemostratigraphy of the Lower Cretaceous Shu'aiba Formation: A $\delta^{13}C$ reference profile for the Aptian Stage from the southern Neo-Tethys Ocean. *GeoArabia Special Publication*, 4: 107–137.

Vecsei, A., 2004. A new estimate of global reefal carbonate production including the fore-reefs. *Global and Planetary Change*, 43: 1–18. doi:10.1016/j.gloplacha.2003.12.002.

Voigt, S., Erbacher, J., Mutterlose, J., Weiss, W., Westerhold, T., Wiese, F., Wilmsen, M., and Wonik, T., 2008. The Cenomanian–Turonian of the Wunstorf section (North Germany): global stratigraphic reference section and new orbital time scale for Oceanic Anoxic Event 2. *Newsletters on Stratigraphy*, 43: 65–89. doi:10.1127/0078-0421/2008/0043-0065.

von Allmen, K., Nägler, T. F., Pettke, T., Hippler, D., Griesshaber, E., Logan, A., Eisenhauer, A., and Samankassou, E., 2010. Stable isotope profiles (Ca, O, C) through modern brachiopod shells of *T. septentrionalis* and *G. vitreus*: Implications for calcium isotope paleo-ocean chemistry. *Chemical Geology*, 269: 210–219. doi:10.1016/j.chemgeo.2009.09.019.

Walker, J. C. G., Hays, P. B., and Kasting, J. F., 1981. A negative feedback mechanism for the long-term stabilization of the Earth's surface temperature. *Journal of Geophysical Research*, 86: 9776–9782. doi:10.1029/JC086iC10p09776.

Wallmann, K., 2001. Controls on the Cretaceous and Cenozoic evolution of seawater composition, atmospheric CO_2 and climate. *Geochimica et Cosmochimica Acta*, 65: 3005–3025. doi:10.1016/S0016-7037(01)00638-X.

Weedon, G. P. and Jenkyns, H. C., 1999. Cyclostratigraphy and the Early Jurassic timescale: Data from the Belemnite Marls, Dorset, southern England. *Geological Society of America Bulletin*, 111: 1823–1840. doi:10.1130/0016-7606(1999)111<1823:CATEJT>2.3.CO;2.

Wefer, G., 1980. Carbonate production by algae *Halimeda*, *Penicillus* and *Padina*. *Nature*, 285: 323–324. doi:10.1038/285323a0.

Weiner, S. and Dove, P. M., 2003. An overview of biomineralization processes and the problem of the vital effect. *Reviews in Mineralogy and Geochemistry*, 54: 1–29. doi:10.2113/0540001.

Weissert, H., Lini, A., Föllmi, K. B., and Kuhn, O., 1998. Correlation of Early Cretaceous carbon isotope stratigraphy and platform drowning events: a possible link? *Palaeogeography, Palaeoclimatology, Palaeoecology*, 137: 189–203. doi:10.1016/S0031-0182(97)00109-0.

Wiegand, B. A., Chadwick, O. A., Vitousek, P. M., and Wooden, J. L., 2005. Ca cycling and isotopic fluxes in forested ecosystems in Hawaii. *Geophysical Research Letters*, 32: L11404. doi:10.1029/2005GL022746.

Wignall, P. B. and Hallam, A., 1992. Anoxia as a cause of the Permian/Triassic mass extinction: facies evidence from northern Italy and the western United States. *Palaeogeography, Palaeoclimatology, Palaeoecology*, 93: 21–46. doi:10.1016/0031-0182(92)90182-5.

Wilkinson, B. H. and Algeo, T. J., 1989. Sedimentary carbonate record of calcium–magnesium cycling. *American Journal of Science*, 289: 1158–1194. doi:10.2475/ajs.289.10.1158.

Wilkinson, B. H. and Walker, J. C. G., 1989. Phanerozoic cycling of sedimentary carbonate. *American Journal of Science*, 289: 525–548. doi:10.2475/ajs.289.4.525.

Wilson, P. A., Jenkyns, H. C., Elderfield, H., and Larson, R. L., 1998. The paradox of drowned carbonate platforms and the origin of Cretaceous Pacific guyots. *Nature*, 392: 889–894. doi:10.1038/31865.

Wombacher, F., Eisenhauer, A., Heuser, A., and Weyer, S., 2009. Separation of Mg, Ca and Fe from geological reference materials for stable isotope ratio analyses by MC-ICP-MS and double-spike TIMS. *Journal of Analytical Atomic Spectrometry*, 24: 627–636. doi:10.1039/b820154d.

Wood, R., 1995. The changing biology of reef-building. *Palaios*, 10: 517–529. doi:10.2307/3515091.

Young, E. D., Galy, A., and Nagahara, H., 2002. Kinetic and equilibrium mass-dependent isotope fractionation laws in nature and their geochemical and cosmochemical significance. *Geochimica et Cosmochimica Acta*, 66: 1095–1104. doi:10.1016/S0016-7037(01)00832-8.

Zachos, J. C., Röhl, U., Schellenberg, S. A., Sluijs, A., Hodell, D. A., Kelly, D. C., Thomas, E., Nicolo, M., Raffi, I., Lourens, L. J., McCarren, H., and Kroon, D., 2005. Rapid acidification of the ocean during the Paleocene–Eocene Thermal Maximum. *Science*, 308: 1611–1615. doi:10.1126/science.1109004.

Zhu, P. and Macdougall, J. D., 1998. Calcium isotopes in the marine environment and the oceanic calcium cycle. *Geochimica et Cosmochimica Acta*, 62: 1691–1698. doi:10.1016/S0016-7037(98)00110-0.

Zoccola, D., Tambutté, E., Kulhanek, E., Puverel, S., Scimeca, J.-C., Allemand, D., and Tambutté, S., 2004. Molecular cloning and localization of a PMCA P-type calcium ATPase from the coral *Stylophora pistillata*. *Biochimica et Biophysica Acta*, 1663: 117–126. doi:10.1016/j.bbamem.2004.02.010.